

Lehrstuhl für Steuerungs- und Regelungstechnik
Technische Universität München
Prof. Dr.-Ing./Univ. Tokio Martin Buss

Design and Control of Admittance-Type Telemanipulation Systems

Angelika Peer

Dissertation

Lehrstuhl für Steuerungs- und Regelungstechnik
Technische Universität München
Univ.-Prof. Dr.-Ing./Univ. Tokio Martin Buss

Design and Control of Admittance-Type Telemanipulation Systems

Angelika Peer

Vollständiger Abdruck der von der Fakultät für Elektrotechnik und Informationstechnik
der Technischen Universität München zur Erlangung des akademischen Grades eines

Doktor-Ingenieurs (Dr.-Ing.)

genehmigten Dissertation.

Vorsitzender: Univ.-Prof. Dr.-Ing. Eckehard Steinbach

Prüfer der Dissertation:

1. Univ.-Prof. Dr.-Ing./Univ. Tokio Martin Buss
2. Prof. Dr. Bruno Siciliano,
Università degli Studi di Napoli Federico II
Italien

Die Dissertation wurde am 15.05.2008 bei der Technischen Universität München eingereicht und durch die Fakultät für Elektrotechnik und Informationstechnik am 14.07.2008 angenommen.

Foreword

This thesis summarizes four years of my research carried out at the Institute of Automatic Control Engineering (LSR) of the Technische Universität München. Herewith, I would like to take the opportunity to thank all the people who supported me during this phase and helped me to successfully conclude this work.

First of all, I would like to thank my advisor Prof. Dr.-Ing./Univ. Tokio Martin Buss, who gave me the opportunity to conduct research in a very international environment at one of the undoubtedly best established German robotics institutes. He always supported me with his immense experience and invaluable advice and allowed me enough freedom for own creativity.

Special thanks go to Dr. Franz Freyberger who encouraged me to take up a position as research assistant and helped me in all administrative issues in the first years of my research activities.

A considerable contribution to the success of this thesis was also made by all my colleagues. I would like to thank them for their fruitful discussions and immense assistance they provided me in all the phases of my work. Special thanks go hereby to Bartłomiej Stanczyk, Ulrich Unterhinninghofen, Kwang-Kyu Lee, Nikolay Stefanov, Marc Ueberle, Helena Pongrac and Sandra Hirche with whom I collaborated in a large number of experiments and to Thomas Pröll, Michael Fritschi, Jan Wolff and Jens Hölldampf for their extraordinary assistance in all network issues. Furthermore, I would also like to thank all my colleagues in the SFB453 “Collaborative Research Center on Telepresence and Teleaction”, who allowed me to extend my horizon to other research fields. In particular I would like to mention here all members of the multi-modal multi-user telepresence and teleaction demonstrator research group. Finally, thanks go to Prof. Abderrahmane Kheddar, Prof. Kazuhito Yokoi, Sylvain Miossec, Paul Evrard, Olivier Stasse and Ee Sian Neo of the AIST/CNRS institute in Tsukuba/Japan who made also long distance teleoperation experiments possible.

The numerous hardware developments would not have been possible without the active support of people in the mechanical and electronic workshop, who always shared their experience with me and tried to realize all my extraordinary wishes. Special thanks go to Josef Gradl, Horst Kubick, Tobias Stoeber, and Thomas Lowitz for all their valuable contributions in the development of mechanical and electronic systems and their repeated efforts in the maintenance of them. Thanks go also to Wolfgang Jaschik who provided me with an excellent computer infrastructure.

I would also like to thank all students who contributed to this thesis. Particularly I would like to thank Alexander Mörtl for his contribution in the design of ViSHARD7, Nico Mock, Yuta Komoguchi and Andreas Froschermeier for their work in the implementation of different control architectures for ViSHARD7 and ViSHARD10, Stephan Eienkel for his effort in developing a multi-fingered telemanipulation system as well as Inga Krause and Carolina Weber for their engagement in the intercontinental teleoperation experiment with Japan. Thanks go also to my working students Alexander Prah, Daniel Wiedemann,

and Byron-Lim Steffan for their assistance in many hardware and software issues and all students of the practical lab course who contributed to this thesis.

Finally, I would like to thank also my family and my boyfriend Thomas who always stood behind my decisions and supported me particularly in critical phases. Without their understanding and love this thesis would not have been possible.

Munich, May 2008.

Angelika Peer

to Thomas

...

Abstract

This thesis summarizes guidelines for the design and control of a highly integrated, multi-modal, and intuitive teleoperation system that can be used to perform a variety of different manipulation tasks requiring bimanual and multi-fingered interactions as well as the collaboration of multiple operators. Hereby, exclusively teleoperation systems using admittance-type devices are investigated. Bimanual 6 DOF manipulations with high interaction forces are realized by newly developed admittance-type haptic interfaces, which are mounted on a mobile platform and thus also allow performance of manipulations in large remote environments. Taking into account a large number of mechatronic requirements, a novel, enhanced, and highly integrated teleoperation system consisting of redundant haptic interfaces and telemanipulators as well as a stereo-vision-system is developed. Dextrous fine manipulations are realized by a multi-fingered telemanipulation system, whereby efficient position and force mapping algorithms are used to map human hand motions to gripper motions and to provide a realistic force feedback. The usage of admittance-type devices instead of classical impedance-type devices poses new challenges on the control concepts. Different types of bilateral control algorithms suitable for admittance-type devices are proposed and robust stability of them is analyzed by using the parameter space approach. Further improvements are achieved by incorporating human factors in the development process. Effects of varied human movement control on task performance and feeling of telepresence are analyzed by means of experimental evaluation and new design guidelines for a user-friendly teleoperation system are derived. Finally, different types of collaborative teleoperation architectures are proposed, application scenarios are described, and challenges on the control of these systems are formulated. In particular, robust stability of a bimanual, a multi-user, and a cooperative teleoperation system is investigated in detail. A variety of laboratory experiments, characterized particularly by their very high complexity, serve for the evaluation and validation of all proposed software and hardware developments.

Zusammenfassung

In der vorliegenden Dissertationsschrift werden Richtlinien zum Entwurf und zur Regelung eines hoch integrierten, multi-modalen und intuitiven Teleoperationssystems zusammengefasst, welches zur Durchführung von Tele-Manipulationsaufgaben herangezogen werden kann, die sowohl beidhändiger als auch mehrfingriger Interaktion, sowie der Kollaboration mehrerer Operatoren bedürfen. Dabei werden ausschließlich Teleoperationssysteme näher untersucht, die Manipulatoren vom Admittanz-Typ verwenden. Beidhändige Manipulationen in sechs Freiheitsgraden bei denen zudem hohe Interaktionskräfte auftreten werden dabei mit Hilfe von neu entwickelten haptischen Eingabegeräten vom Admittanz-Typ realisiert. Diese sind ihrerseits auf einer mobilen Plattform montiert, um auch Manipulationen in ausgedehnten entfernten Umgebungen zu ermöglichen. Unter Berücksichtigung einer Vielzahl mechatronischer Anforderungen, wird ein neuartiges, weiterentwickeltes und hoch integriertes Teleoperationssystem, bestehend aus redundanten haptischen Eingabegeräten und Telemanipulatoren, sowie einem Stereo-Sichtsystem entwickelt. Feinmotorische Manipulationen werden mit Hilfe eines mehrfingrigen Telemanipulationssystems durchgeführt, wobei effiziente Algorithmen zum Positions- und Kraftmapping herangezogen werden, um menschliche Handbewegungen auf einen Greifer abzubilden sowie einen realistischen Krafteindruck zu vermitteln. Die Verwendung von Manipulatoren des Admittanz-Typs im Gegensatz zu klassischen Geräten des Impedanz-Typs bringt hierbei neue Herausforderungen an die Regelung dieser Systeme mit sich. Verschiedene Arten von bilateralen Regelalgorithmen, welche sich speziell für Manipulatoren des Admittanz-Typs eignen, werden vorgeschlagen und deren Robustheit mit Hilfe des Parameterraumverfahrens untersucht. Zusätzliche Verbesserungen werden erzielt, indem auch menschliche Faktoren in den Entwurfsprozess einbezogen werden. Effekte variabler menschlicher Bewegungssteuerung auf die Aufgabenperformanz und das Telepräsenzempfinden werden mit Hilfe experimenteller Evaluation analysiert und neue Entwurfsrichtlinien für ein benutzerfreundliches Teleoperationssystem davon abgeleitet. Schließlich werden unterschiedliche Arten kollaborativer Teleoperationssysteme vorgeschlagen, entsprechende Anwendungsfelder beschrieben, sowie Herausforderungen an die Regelung dieser Systeme formuliert. Insbesondere wird die robuste Stabilität eines beidhändigen, eines Multi-User, sowie eines kooperativen Teleoperationssystems näher untersucht. Eine Vielzahl an Laborexperimenten, welche sich insbesondere durch ihre hohe Komplexität auszeichnen, dienen zur Evaluation und Validierung der vorgeschlagenen Soft- und Hardwareentwicklungen.

Contents

1	Introduction	1
1.1	Problem Definitions and Challenges	3
1.2	Main Contributions and Outline of the Dissertation	5
2	Design, Control, and Evaluation of an Admittance-Type Haptic Interface	8
2.1	State-of-the-Art	9
2.2	Design of New Haptic Interface	10
2.2.1	Requirements	10
2.2.2	Design Description	12
2.3	Control	14
2.3.1	Master Dynamics	15
2.3.2	Motion Controller	16
2.3.3	Inverse Kinematics	17
2.4	Stability Analysis	19
2.4.1	Models for Haptic Interface and Human Operator	19
2.4.2	Actuator and Sensor Dynamics	21
2.4.3	Simulation Results	21
2.5	Performance Measures	24
2.6	Performance Evaluation	25
2.6.1	Model-based Performance Evaluation	25
2.6.2	Measurement-Based Performance Evaluation	29
2.7	Discussion	37
3	Development of Integrated Teleoperation Systems	39
3.1	Bimanual Teleoperation System with 6 DOF	39
3.1.1	Requirements on Teleoperation System	40
3.1.2	State-of-the-Art Teleoperation Systems	41
3.1.3	System Description	42
3.2	Multi-Fingered Teleoperation System	43
3.2.1	System Description	43
3.2.2	Position Mapping	45
3.2.3	Force Mapping	54
3.2.4	Experimental Evaluation	54
3.3	Integration of Single Components	56
3.4	Linear one DOF Teleoperation System	57
3.5	Discussion	58
4	Bilateral Control of Teleoperation Systems using Admittance-Type Devices	59
4.1	Bilateral Teleoperation Systems	59

4.2	Bilateral Control Architectures for Admittance-Type Devices	60
4.3	Parameter Space Approach	64
4.4	Modelling of Teleoperation System	67
4.4.1	Models for Telemanipulator and Remote Environment	67
4.5	Stability Analysis of Bilateral Teleoperation Systems	68
4.5.1	Linear one DOF Device	68
4.5.2	ViSHaRD10 - Dual Arm Telemanipulator	79
4.5.3	Summary	84
4.6	Experimental Evaluation	85
4.6.1	Quaternion-based Admittance Control	85
4.6.2	Redundancy Resolution	86
4.6.3	Overall Control Structure	86
4.6.4	Experimental Setup	87
4.6.5	Experimental Results	88
4.7	Discussion	96
5	Experimental Evaluation: Effects of Varied Human Movement Control	97
5.1	Definitions	97
5.2	State-of-the-Art	98
5.3	Hypotheses	100
5.4	Method	100
5.4.1	Measures for Performance, Rotation, and Feeling of Telepresence	100
5.4.2	Experimental Setup	102
5.4.3	Procedure	103
5.4.4	Experimental Design	104
5.4.5	Participants	105
5.5	Results	105
5.5.1	Task Execution Strategy	105
5.5.2	Analysis of Variance	106
5.6	Discussion	108
6	Collaborative Teleoperation Systems	110
6.1	Collaborative Teleoperation Architectures	110
6.2	Control Approaches for Collaborative Teleoperation Systems	113
6.2.1	Unconstrained Teleoperation Systems	113
6.2.2	Constrained Teleoperation Systems	113
6.2.3	Summary	118
6.3	Bimanual Teleoperation	119
6.3.1	Modelling of Bimanual Teleoperation System	120
6.3.2	Stability Analysis	121
6.3.3	Experimental Results	122
6.4	Multi-user Teleoperation	123
6.5	Intercontinental Cooperative Teleoperation	129
6.5.1	Stability Analysis	130
6.5.2	Numerical Stability Test	133
6.5.3	Experimental Evaluation	134

6.6	Discussion	138
7	Conclusions and Future Directions	141
7.1	Concluding Remarks	141
7.2	Outlook	143
A	Hardware Specifications of ViSHaRD7	145
A.1	Specification of Gears	145
A.2	Specifications of Motors and Encoders	146
B	Dynamic Device Models	147
B.1	ViSHaRD7 Right Arm	147
B.2	ViSHaRD7 Left Arm	153
B.3	ViSHaRD10	159
B.4	Dual Arm Telemanipulator	165
C	Parameters of Simulation Models	170
C.1	Haptic Interface ViSHaRD7	170
C.2	Linear one DOF Teleoperation System	170
C.3	Teleoperation System Vishard10 - Dual Arm Telemanipulator	171
C.4	Human Operator Model	171
D	Descriptive Statistics and Results of the Analysis of Variance	172
D.1	Descriptive Statistics	172
	D.1.1 Efficiency Measures	172
	D.1.2 Rotation Measures	173
	D.1.3 Telepresence Measures	173
D.2	Results of the Analysis of Variance	174
	D.2.1 Factor freed DOF during Experimental Session	174
	D.2.2 Factor Visual Feedback	174
	D.2.3 Factor Task Phase	175
	D.2.4 Factor Hand	175
	D.2.5 Factor Number of Freed DOF during Training	176
	D.2.6 Factor Repetition	176
E	Presence and Immersive Tendence Questionnaire	177
	Bibliography	181

Notations

Abbreviations

DOF	degrees of freedom
FK	forward kinematics
IK	inverse kinematics
IJC	independent joint control
CT	computed torque
CAD	computer aided design
RPY	roll, pitch, yaw
RRB	real root boundary
CRB	complex root boundary
IRB	infinite root boundary
UDP	user datagram protocol
HSI	human-system interface
TOP	teleoperator
HMD	head-mounted display
LED	light emitting diode
PaFa	position-based admittance control with force-position exchange
FaPa	position-based admittance control with position-force exchange
FaFa	position-based admittance control with force-force exchange
SOSR	single operator, single robot system
MOMR	multiple operator, multiple robot system
MOSR	multiple operator, single robot system
SOMR	single operator, multiple robot system
ViSHARD7	Virtual Scenario Haptic Rendering Device with 7 actuated DOF
ViSHARD10	Virtual Scenario Haptic Rendering Device with 10 actuated DOF

Conventions

Scalars, Vectors, and Matrices

Scalars are denoted by upper and lower case letters in italic type. *Vectors* are denoted by lower case letters in boldface type, as the vector \mathbf{x} is composed of elements x_i . *Matrices* are denoted by upper case letters in boldface type, as the matrix \mathbf{M} is composed of elements M_{ij} (i -th row, j -th column).

x	scalar
\mathbf{x}	vector
\mathbf{X}	matrix
$f(\cdot)$	scalar function
$\mathbf{f}(\cdot)$	vector function
\dot{x}, \ddot{x}	equivalent to $\frac{d}{dt}x$ and $\frac{d^2}{dt^2}x$
\tilde{x}	estimate of x
x_{rms}	root mean square of x
$\ \cdot\ $	Euclidean norm

Subscripts and Superscripts

x_d	desired value of x
x_t	target value of x
x_a	value x associated with actuator
x_{ct}	value x associated with the computed torque controller
x_e	value x associated with end-effector or environment
x_E	value x associated with the extended kinematics formulation
x_f	value x associated with force
x_h	value x associated with the human operator
x_j	value x associated with the independent joint controller
x_m	value x associated with master device
x_o	value x associated with rotational coordinates
x_p	value x associated with translational coordinates or position
x_{rot}	value x associated with rotations
x_s	value x associated with slave device
x_x	value x associated with task coordinates
Sx	value x expressed in coordinate frame S

Symbols and Abbreviations

A	system matrix
<i>a</i>	polynomial coefficient
α	scaling variable
α, β, γ	Euler angles
B	input matrix
<i>b</i>	damping
C	output matrix, stiffness matrix
<i>c</i>	stiffness
D	feedthrough matrix, matrix of derivative control coefficients
<i>d</i>	damping coefficient
E	unity matrix
<i>e</i>	error
ε	vector part of Quaternion
<i>f</i>	force
<i>g</i>	scaling factor
Γ	Γ -stability
γ	rotation angle
H	performance criterion
<i>h</i>	height
h	wrench including forces and torques
h_N	vector of coriolis, friction and gravity forces
η	scalar part of Quaternion
θ	elbow angle, rotation angle
Θ	BarrettHand motor angle
J	Jacobian
K	matrix of proportional control coefficients
<i>k</i>	control parameter
<i>l</i>	link length
λ	eigenvalue, generalized frequency
M	mass matrix
<i>m</i>	mass
μ	step length of gradient
$\boldsymbol{\mu}$	torque vector
<i>P</i>	operating domain
p	parameter vector
Φ	offset angle
Q	Quaternion
q	vector of joint coordinates
R	rotation matrix
<i>r</i>	radius
r	offset vector, axis of rotation
S	coordinate system
<i>s</i>	covered distance
<i>T</i>	time constant
<i>t</i>	time
t	translation vector

$\boldsymbol{\tau}$	joint space torque
\boldsymbol{u}	control input vector
\boldsymbol{W}	weighting matrix
$\boldsymbol{\omega}$	angular velocity
\boldsymbol{x}	position, state
$\dot{\boldsymbol{x}}$	velocity
\boldsymbol{y}	control output vector
ζ	fidelity factor

1 Introduction

Nowadays more and more tasks and functions which some time ago were exclusively reserved to humans, are passed to robots. Especially in the field of manufacturing many tasks are by now executed by robots. This is mainly due to the fact, that in contrast to humans, robots are able to operate over a long time period with constant precision and velocity and thus guaranteeing constantly high quality at low costs. Moreover, robots are able to carry heavy objects and operate with a precision which is below the range of human hand tremor. Both are necessary in many assembling tasks. Other applications again require the operation in human-unfriendly or hazardous environments. Thus, at present, typical application fields for robots can be found in areas where human physical abilities are exceeded or the usage in human-inaccessible or unfriendly environments is necessary.

As long as the tasks are characterized by very structured and repeated motion sequences in well known environments, fully automated robots can be used to interact with the environment in a pre-programmed manner. But if the task requires to operate in variable, unstructured, unknown, and dynamic working environments, the robot has to adapt to sudden changes by taking decisions and adapting plans appropriately. Researchers have been trying to provide robots with cognitive facilities already for a long time. Especially in recent years, this field enjoys great popularity, which might be partly ascribed to the continuously increasing computational power that allows realization of complex programs not implementable at an earlier stage. But nevertheless, human reasoning and decision-making ability is to date by far not reached by any technical system.

On this account, so called telepresence and teleaction systems have been developed, which combine skills as human adaptability and decision-making ability with the advantages of robotic manipulation. Using such a teleoperation system the human operator is not any more in direct contact with the environment, but interacts with it by means of technical systems. In doing so, the human operator uses a human-system interface, which allows her/him to control a robot, the teleoperator, that interacts in her/his place with the environment, see Fig. 1.1. Hereby, the human-system interface provides multi-modal feedback in form of visual, auditory, and haptic information and is used as control input for the teleoperator, which executes the commands. All command signals and sensory information is hereby transmitted over an appropriate communication channel. Different barriers, like distance and scaling, can be overcome in that way by still preserving the cognitive abilities of a human being.

In the past years several application areas for such telerobotic systems have been presented, see [110, 116]: space and underwater exploration, surgery, plant maintenance, micro-assembly, toxic waste cleanup, telemanufacturing, training as well as entertainment. In the following some of these applications are explained in more detail: Using a teleoperation system for space or underwater exploration, see e.g. [102, 103], prevents exposing humans to dangerous environments such as outer space and the deep sea. Dangerous repairs on spacecrafts can for example, be performed by teleoperating a robot from the inside the space-shuttle or from earth. Barriers typically exist hereby in the hazardous

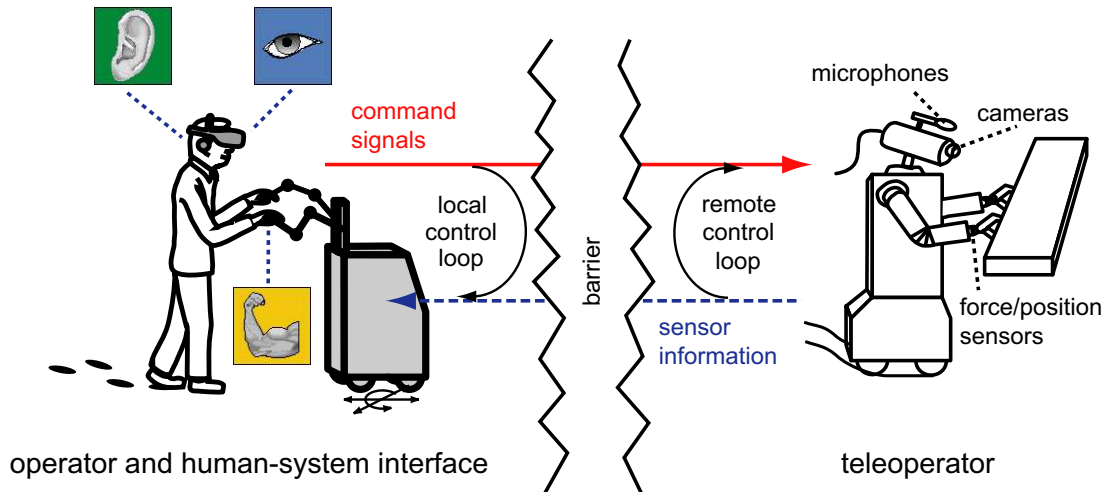


Figure 1.1: Multi-modal telepresence and teleaction system

environmental conditions or/and the large distances to the remote location. Large distances also play an important role in surgery or plant-maintenance, when a specialist is not located at the site of the patient or plant. In this case, a teleoperation system allows transference of the specialist's knowledge and facilities to the required location without need to travel. In the field of minimal-invasive surgery the barrier exists in the skin of the human body, which restricts the available space and degrees of motion available for the surgeon. Also in this case a teleoperation system can help to overcome this barrier, see [23, 97] for some examples. Finally, an application area should be mentioned, where the scaling causes severe difficulties: In micro-assembly really precise and small scale manipulations are needed, which a human cannot perform without further technical assistance. A teleoperation system like [101] can help in performing these small scale manipulations.

What all applications have in common is the demand of a very realistic display of the remote environment not being affected by technical systems. Ideally, the human operator should not perceive any difference between direct interaction with the remote environment and interaction via a teleoperation system. In this ideal case, the system is called transparent and the corresponding measure transparency [77, 139]. If the system is transparent and thus the human operator is not restricted by the telerobotic system in any sense, an intuitive interaction with the remote environment is possible. In order to achieve such a high-quality teleoperation, appropriate design and control concepts must be developed and human factors must be incorporated in the development process. Providing multi-modal feedback is hereby of special importance. While the visual and auditory modality are already rather advanced and several high quality devices are available on the market, the haptic modality needs further attention.

Although research in the field of telerobotics dates back to the early nineteenth century, the design and analysis of haptic feedback systems became popular only in recent years. As a result, a huge variety of haptic interfaces designed for and adapted to specific application scenarios has been developed, see [19, 87] for an overview. Hereby, basic devices of so called impedance and admittance type can be distinguished. While impedance-type devices are characterized by a very lightweight design, which ensures low friction and inertia as well as a high backdrivability and bandwidth, admittance-type devices are featured by a large

workspace and high force capability [29]. Most telerobotics literature focuses hereby on the usage of impedance-type devices, which allows the implementation of high-quality force controllers. The usage of admittance-type devices is only rarely studied, although these kind of devices are characterized by completely different properties and approaches developed for impedance-type devices cannot be simply transferred to them. As will be shown in this thesis, the high inertia and friction of admittance-type devices requires different control approaches to realize a high degree of transparency.

This thesis aims to design and control a highly integrated, multi-modal, and intuitive teleoperation system using admittance-type devices, which can be used for different kind of tele-assembling tasks, ranging from very simple to more complicated manipulations requiring both hands and multiple fingers. Fixing of a broken tube is hereby used as benchmark scenario throughout this work. As not all tasks can be carried out by a single person, typically multiple users share their facilities and capabilities to achieve a common goal. On this account, also different types of collaborative teleoperation architectures are analyzed in detail.

1.1 Problem Definitions and Challenges

The development of an intuitive admittance-type teleoperation system as described above requires solving different design and control problems, which should be shortly addressed in the following:

A teleoperation system typically consists of devices used as a human-system interface as well as a teleoperator. Focusing first on the human-system interface, devices for visual, auditory and haptic feedback can be distinguished. While for the visual and auditory feedback off-the-shelf devices such as a head-mounted display or stereo-projection system can be used, only a few haptic feedback systems are available on the market. Since most of them are limited in their degrees of freedom (DOF) and have only a small workspace or a low output capability, they do not enable an intuitive interaction with the remote environment. Moreover, most haptic interfaces are fixed to the ground and thus do not allow any locomotion of the human operator. This thesis aims to face these problems by developing a new bimanual admittance-type haptic interface, which fulfills the aforementioned requirements. The presented concept foresees mounting of two haptic interfaces (with a workspace size of the human arm reach) on a mobile platform. In doing so, the workspace of the haptic interfaces can be extended to nearly arbitrary large remote environments. The realization of such a device requires the design of appropriate haptic interfaces and control algorithms that realize the required behavior.

In order to extend this system to a telemanipulation system, further design requirements must be taken into account which concern the single devices as well as the whole telemanipulation system. Looking at the telemanipulator, it is known that an anthropomorphic kinematic structure significantly enhances the feeling of telepresence. This reveals a redundant kinematic design with link lengths adapted to the human arm reach. As these requirements differ significantly from the requirements formulated on the haptic interface, also different kinematic designs result. But, when coupling two manipulators with different kinematics, new complications arise. One of the reasons is the different location of kinematic and algebraic singularities in the workspace of the single devices. To not restrict the overall workspace, measures to avoid kinematic and algebraic singularities must be

adopted. In addition, both workspace sizes have to be matched to avoid fatiguing indexing and shifting techniques, which would deteriorate the feeling of immersion.

If further dextrous manipulation tasks are required, systems for multi-fingered telemanipulation must be installed. Since anthropomorphic hands, see e.g. [31, 62, 106], are mostly very bulky, they cannot be mounted at the end-effector of the telemanipulator. At the development stage only simple three-finger grippers were available on the market [1], which had an acceptable weight and package size. Using such a three-finger gripper in a telemanipulation setup requires an appropriate motion and force mapping between human and gripper fingers. Hereby, human finger motions have to be measured and mapped to gripper finger motions and measured interaction forces have to be fed back to the human operator. Despite of the non-anthropomorphic structure of the robotic grippers the to be developed mappings have to be intuitive, easy to predict and understand. To be further able to perform a variety of manipulation tasks a number of different grasp types ranging from precision to power grasps [32] must be covered.

A typical attribute of a telemanipulation system is the coupling of single components and the corresponding energy exchange. In order to avoid instabilities caused by this energy exchange, an adequate control architecture has to be selected and implemented. While the literature provides many possible solutions for impedance-type devices, coupling of two admittance-type devices is typically not considered. Usage of classical two-channel force-position or position-force architectures, see [57], requires the implementation of force control on either haptic interface or telemanipulator. But as a consequence of the high inertia and friction of admittance-type devices, force control can only be realized with a very poor performance and thus other types of controllers, so called admittance-type controllers, have to be implemented. Coupling of different admittance-type controllers has to be investigated and stabilizing control parameter sets have to be determined. As the human operator can behave in very different ways and possible remote environments range from free space to hard contact, special attention must therefore be paid on robust stability of the implemented controllers. Controllers have to be selected in such a way that they provide a high degree of transparency and simultaneously guarantee stable interaction despite changing human operator and environment impedances.

Beside optimization of the mechatronic design and control architectures, a teleoperation system can also be improved by incorporating human factors in the development process. Having developed a telemanipulation system which allows manipulation of objects in all 6 DOF it is of interest whether the number of freed DOF should be varied depending on the actual task to be performed to increase e.g. task performance and feeling of telepresence. Such behavior can be simply achieved by freezing certain motion axis by control. Current statements in the literature do not provide a clear answer to this question. Thus, it is investigated whether human movement control is driven by intuition or task performance, and how varied human movement control influences efficiency and feeling of telepresence. Depending on the findings of this analysis, the control of haptic interface and telemanipulator has to be modified in an appropriate manner to simultaneously increase task performance and the feeling of telepresence and consequently increase the intuitiveness of the interaction with the teleoperation system.

If the task to be performed requires more than one person, some people have to collaborate to achieve the required result. As a teleoperation system separates the human operator from the environment she/he interacts with, different structures of collaboration can be realized. The following combinations, for example, are possible: each person controls a

corresponding teleoperator, multiple persons control only one teleoperator, or a teleoperated robot interacts with collocated humans. Depending on the architecture, different challenges on the control can be formulated. Stability of the overall system, which has to be guaranteed despite changing kinematic configurations, is hereby of special interest. Interactions of one manipulator arm with the remote environment as well as the interaction of two or multiple arms over an object, for example, must be considered. In this context, especially closed kinematic chains between single entities play an important role, since they may cause instability. On this account robustly stabilizing controllers that are able to deal with different kind of kinematic configurations must be selected and implemented.

1.2 Main Contributions and Outline of the Dissertation

The main goal of this thesis is the design and control of an integrated, multi-modal, and intuitive teleoperation system using admittance-type devices, which can be used for the execution of different kind of tele-assembling tasks. Depending on the complexity of the task to be performed, only one or multiple users are hereby considered. While teleoperation systems composed of impedance-type devices are intensively studied in the literature, this thesis is dedicated to the design and analysis of teleoperation systems using admittance-type devices.

The thesis is organized in seven chapters. Chapter 2 and 3 are related to research issues concerning the design of the teleoperation system. Chapter 4 deals with control problems of bilateral teleoperation systems with special focus on admittance-type devices. Chapter 5 analyzes effects of varied human movement control on task performance and feeling of telepresence. Finally, chapter 6 concentrates on different types of collaborative teleoperation systems. The thesis concludes with chapter 7, which summarizes the most important results and formulates directions of future research.

In chapter 2 the concept of a new bimanual mobile haptic interface which enables a proprioceptive perception of locomotion is presented. In contrast to already existing haptic interfaces, it is characterized by its large workspace and its high output capability. The large workspace is hereby achieved by mounting two haptic interfaces on a mobile platform and by controlling these components in a coordinated manner. In this thesis, the design and control concepts of the manipulator arms mounted on the mobile platform are intensively discussed. After formulating requirements on the design of them, a detailed description of the chosen kinematic structure is given. To simplify the interaction between mobile platform and manipulator arms, a special kinematic structure has been chosen, which enables decoupling of translational from rotational movements. No similar approach has been reported to date in the literature. Also different types of inverse functions and motion controllers are analyzed and compared with each other. Depending on the results design guidelines for the implementation of them are formulated. Further, the effects of different human arm impedances as well as actuator and sensor dynamics on the stability of the haptic interface are investigated and reasons for unstable behavior of admittance-type haptic interfaces are reported. These results lead to a deeper understanding of the implemented control architectures and explain effects visible in the real hardware experiment. Finally, an extensive evaluation of the developed device has been carried out concerning the Cartesian position tracking performance and the impedance display fidelity. To determine the specifications of the device the following performance

measures are analyzed: dexterous workspace, output capability, and backdrivability. All these specification data are typically not available for haptic interfaces developed by other research groups.

Chapter 3 deals with the development of a multi-modal teleoperation system, which integrates components for visual and auditory feedback, as well as haptic interaction. In the first step, mechatronic design requirements for this system are formulated. While state-of-the-art teleoperation systems cannot meet all presented requirements at the same time, the newly developed system is of superior performance. The single components the system is composed of are presented in detail, and their integration into one high-fidelity teleoperation system is described. Dexterous telemanipulation is further made possible by using a multi-fingered teleoperation system. Special mapping algorithms are developed, which map the human hand configuration to the robotic gripper and provide adequate force information.

One of the main challenges in telerobotics is the selection of control architectures and control parameters, which are able to robustly stabilize the overall teleoperation system despite of changing human operator and environment impedances. In chapter 4 robust stability of different types of bilateral control algorithms is analyzed. While other works mostly deal with teleoperation systems composed of impedance-type devices, the main focus of this chapter is on the analysis of different types of bilateral control architectures using admittance-type devices. Hereby stability of the system is investigated by using the parameter space approach, which allows the analysis of uncertain systems with varying plant parameters. Simple linear models are assumed for human operator, human-system interface, teleoperator as well as remote environment. The parameter space method is used for controller design as well as for robustness analysis. Stability of the presented architectures is evaluated for two different types of mechatronic teleoperation systems. Finally, some experimental results are reported, which show the validity of the presented simulations.

Chapter 5 analyzes the effects of varied human movement control on task performance and feeling of telepresence by using the developed integrated teleoperation system. While it is well known that humans are able to coordinate and integrate multiple degrees of freedom, the focus of this chapter is on how humans utilize rotational degrees of freedom provided by a human-system interface. For the analysis, a telemanipulation experiment with varying freed degrees of freedom has been conducted and analyzed. The main aim hereby is to improve the interaction with the teleoperation system by incorporating also human factors into the development process.

Chapter 6 is devoted to collaborative teleoperation systems. After giving a definition, a classification of possible collaborative teleoperation systems is presented and five different architectures are derived. Out of these five architectures three of them are analyzed in more detail: a bimanual, a multi-user, and a cooperative teleoperation system. In the stability analysis different types of interactions between the single components are considered. Simulation results are verified by real hardware experiments using the developed integrated teleoperation systems. These multi-user teleoperation experiments are world-wide unique as no similar experiments have been conducted and presented before.

Finally chapter 7 summarizes the main results of this thesis and elaborates directions of future research.

Supplementary information in form of videos and publications can be found at the institute's web page <http://www.lsr.ei.tum.de>.

2 Design, Control, and Evaluation of an Admittance-Type Haptic Interface

The design of an integrated, multi-modal teleoperation system, which does not restrict the human operator in the execution of tasks, begins with the design of an appropriate human-system interface. Typically, such a human-system interface consists of devices for visual, auditory, and haptic feedback systems. In contrast to visual and auditory devices which are unidirectional and transfer information only from the remote environment to the human operator, haptic interfaces can be described as bidirectional devices. On the one hand they provide the operator with force/torque information from virtual or remote environments, and on the other hand they are used to read the operator's motion/force input. This input is used to manipulate the remote environment.

While visual and auditory devices are relatively advanced and commercially available, the design and analysis of haptic feedback systems became popular only in recent years: They found their way into applications such as medical training, rehabilitation, virtual prototyping, telesurgery, telemaintenance as well as micromanipulation. However, most existing haptic interfaces are limited in their degrees of freedom (DOF), have only a small workspace and/or a low output capability (velocity, acceleration, and/or force/torque capability). Thus, tasks which require 6 DOF manipulations with high interaction forces (high output capability) in extended remote or virtual environments (large workspace) cannot be carried out with them.

In order to increase the workspace of such devices, usually hand controlled input devices, such as a joystick or a mouse, are used [80] or some indexing technique is applied. If control by the operator's hand is not possible, as in the case of bimanual manipulation, these devices are also substituted by a special kind of foot pedal [21, 162].

Since the operator cannot move around, none of these approaches provides a proprioceptive perception of locomotion. As shown in [33], such incomplete or false proprioceptive cues result in a deterioration of the natural orientation and navigation capabilities of a human operator.

More realistic locomotion interfaces, such as treadmills and tracking systems for human operator locomotion, can be found in the field of virtual reality applications [58, 113]. These systems allow the human operator to freely move around in the remote environment, but do not provide any force feedback information. Thus, simultaneous manipulation and locomotion is not possible.

A known approach to circumvent this problem is to use body grounded haptic interfaces, such as exoskeletons. However, as reported in [109], working with exoskeletons is very fatiguing since the range of human arm movements is restricted and/or long time operations are not possible because of the high weight of the system. In addition, mounting application specific end-effectors is extremely difficult.

A much more advanced locomotion interface has been proposed in preceding works at our institute, see [95, 96], and later adapted by [45]. Hereby a haptic interface is mounted on a mobile platform. Since in this case the weight of the haptic interface is fully supported

by the platform, the operator fatigue can be significantly reduced. However, these systems allow only one-handed manipulations and their haptic interfaces are limited to either 3 or 4 DOFs. The first bimanual mobile haptic interface for haptic grasping in large virtual environments has been presented in [99], but again haptic interfaces with only 3 DOFs were used. Moreover, due to the small workspace of the haptic interfaces, the platform has to move even for very small size manipulations. This again means that the maximum manipulation velocity is restricted by the maximum platform velocity.

In order to overcome all these limitations, this work aims to develop new haptic interfaces which are mountable on a mobile platform, allowing bimanual manipulations in a workspace of the human arm reach and providing high interaction forces. In the following sections, the design and control concepts of these new haptic interfaces are intensively discussed.

This chapter is structured as follows: Sec. 2.2 addresses the design concepts of the haptic interfaces, whereby requirements on the design are formulated and a detailed description of the selected kinematics is given. Sec. 2.3 deals with control issues. The admittance control architecture is introduced and different kind of inverse kinematics and motion controllers are presented and compared. Stability of the haptic interfaces is analyzed in Sec. 2.4 by evaluating asymptotic stability. Hereby, the effects of different human arm impedances as well as actuator and sensor dynamics are investigated. The second part of this chapter is devoted to the evaluation of the newly developed devices. Different performance measures are listed in Sec. 2.5. While for most haptic interfaces only very few specifications are available, Sec. 2.6 provides a variety of evaluation results concerning the Cartesian position tracking performance and the impedance display fidelity. In addition, the following performance measures are analyzed: dextrous workspace, output capability, and backdrivability. In order to reduce the measurement effort, some of these measures are determined by model-based, others by measurement-based performance evaluation.

2.1 State-of-the-Art

Haptic interfaces that achieved a sufficient development status are mostly characterized by highly lightweight mechanical designs requiring no active force feedback control to provide a good backdrivability, e.g., the PHANToM family [89] belongs to that kind of system. Only a few devices, e.g., the PHANToM Premium, as well as, the DELTA haptic device [49] show an improved, yet still moderate, output capability. If the device size increases, friction and inertia also increase and thus force sensing is necessary to compensate for these effects. The HapticMASTER [131] is an example for such a haptic device which provides 100 N continuous force, but is limited to 3 DOF. The 6 DOF device Mirage F3D-35 haptic system satisfies the force requirements (peak forces of about 100 N), but is limited to a quite small workspace. More advanced haptic interfaces are the Virtuose 6D40-40 with 30 N continuous force and a workspace of the human arm reach, as well as the INCA 6D of Haption with 40 N continuous force and an almost unlimited operational workspace. While the former is very bulky, and thus cannot be mounted on a mobile platform, the latter seems to be only suitable for one handed operations. A broader overview of existing haptic interfaces can be found in [19, 87].

Summarizing, it can be stated that at the moment no adequate haptic interface with 6 DOF, a large workspace, and a high output capability, which is furthermore suited to be

mounted on a mobile platform, is available on the market. In order to bridge this gap, a new bimanual admittance-type haptic interface called *ViSHARD7* has been developed. As it is mountable on a mobile platform, this device is not restricted only to desktop applications but also enables bimanual manipulation tasks with high interaction forces in extended remote or virtual environments.

2.2 Design of New Haptic Interface

2.2.1 Requirements

The new haptic interface should be used to perform bimanual 6 DOF tele-assembling and tele-manipulation tasks in large remote environments. Hereby, stiff objects such as tubes, handwheels, and metal parts of several kinds should be handled and mounted by using tools like screwdrivers and pincers. The following design objectives of this new haptic interface were chosen in accordance with this application scenario: workspace of the human arm reach free of singularities, high payload to accommodate various application-specific end-effectors as, e.g., an exoskeleton or data glove system for the human hand, high output capability, redundancy to avoid user interferences and kinematical singularities, and possible dual-arm haptic interaction with full 6 DOF capability.

To compensate for different dynamic properties of the haptic interface and the mobile platform, the workspace of the haptic interfaces should be of the size of the human arm reach. On this account, manipulation tasks which require only a small workspace can be performed without moving the platform. Fig. 2.1 visualizes a typical human arm reachable workspace based on the physiological model presented in [73]. Since most manipulations take place in front of the human operator, only this part of the workspace which can be approximated by two intersecting hemispheres is considered as design criteria.

To achieve the aim of allowing also bimanual manipulation tasks, the workspace of the haptic interfaces must overlap. Fig. 2.1 clearly shows the overlapping areas of left and right hand, which must be covered by the haptic interface.

To be able to extend the manipulation capabilities to a large remote environment, in addition the following requirements must be fulfilled: First, the device must be compact and lightweight so that it can be mounted on a mobile platform, and second, the kinematical design must be chosen in such a way that the interaction of the mobile platform and the haptic interfaces becomes feasible.

Extending the workspace of the haptic interfaces to very large scale environments requires coupling of haptic interfaces and mobile platform. Different optimization strategies can be used to position the platform in such a way that the manipulability of the haptic interfaces is maximized. This optimization is simplified when using a special design concept to decouple translational from rotational movements of the haptic interfaces. The advantage of such a design is the possibility to compute an offline manipulability measure for the bimanual setup. This again significantly simplifies the control algorithms that manage the interaction between mobile platform and haptic interfaces, but as a drawback, a redundant kinematical design of the haptic interfaces is necessary.

In the following section, a more detailed description of the new haptic interfaces is given.

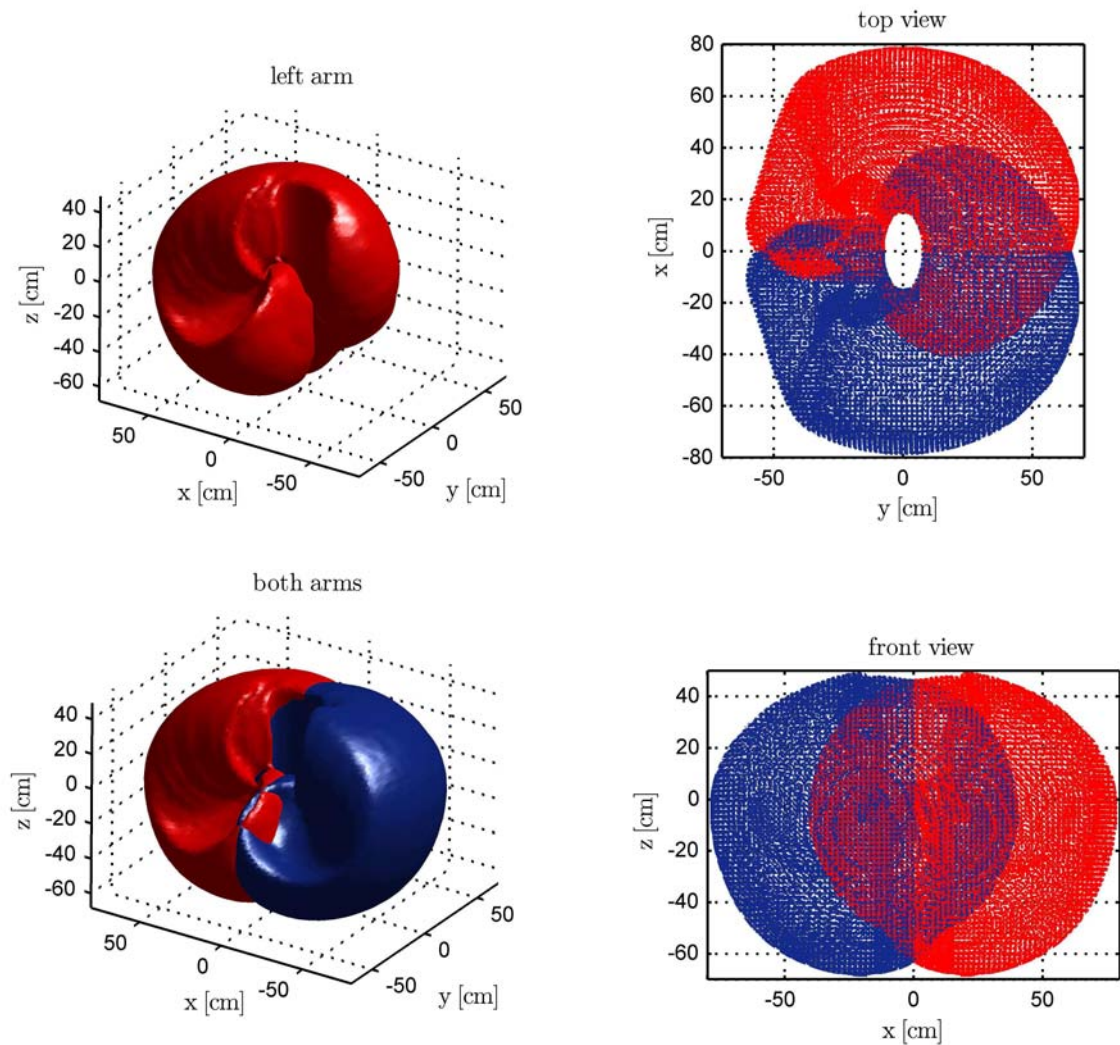


Figure 2.1: Reachable workspace of a typical human arm [73, 107], top-left: reachable workspace of left arm, down-left: reachable workspace of both arms, right: side and front view of reachable workspace of both arms

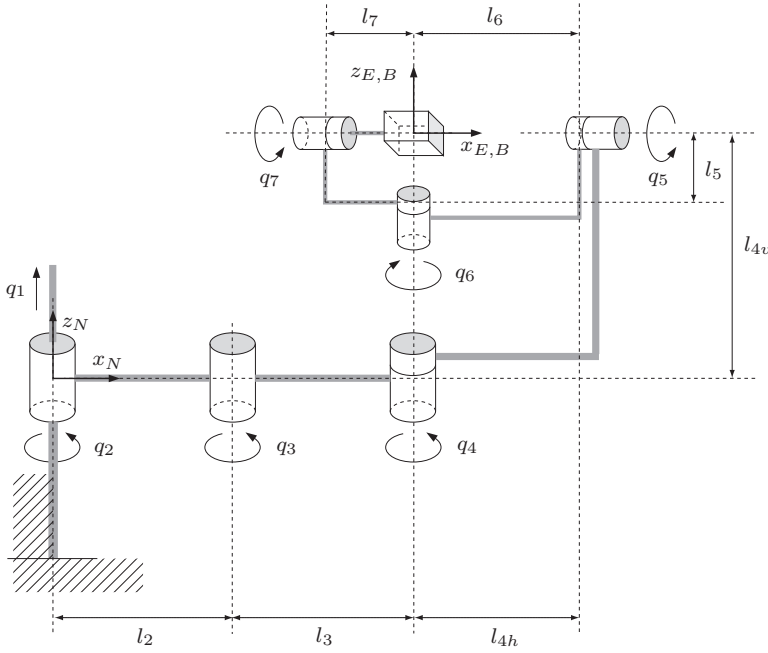


Figure 2.2: Kinematic model of ViSHARD7

Table 2.1: Link length design of ViSHARD7

Link i	Length
l_1	0.6 m
$l_2 = l_3$	0.35 m
$l_{4h} = l_6$	0.2155 m
l_{4v}	0.3411 m
l_5	0.082 m
l_7	0.0654 m

2.2.2 Design Description

The kinematic structure of one of the haptic interfaces, called Virtual Scenario Haptic Rendering Device with 7 actuated DOF (ViSHARD7), is illustrated in Fig. 2.2. It shows the reference configuration with all joint angles q_i ($i = 1 \dots 7$) defined to be zero. The corresponding link length design is summarised in Tab. 2.1 and a typical operational configuration is shown in Fig. 2.4.

The first joint has been designed as linear axis and enables vertical motions in z_N -direction. Joint 2 and 3 are arranged in a selective compliance assembly robot arm (SCARA) configuration and allow positioning in the x_N - y_N plane. As known from literature, see e.g. [141], the maximum manipulability of such a two-link planar arm can be achieved for a construction with equal joint lengths. Thus, the link lengths two and three have been set to $l_2 = l_3 = 0.35$ m.

The SCARA part is in a singular configuration when link 2 and 3 are collinear. Hence, configurations near the base have to be omitted. Since the device would collide with itself, this can be easily realized. Joint 4 is used to prevent singular configurations in the wrist formed by joints 5, 6, and 7. Singularities in the wrist arise when the axes of joint 5 and 7 are collinear, which can be avoided by a rotation of joints 4 and 6. An adequate inverse kinematics algorithm must be implemented to guarantee singularity-free operation.

ViSHARD7 has been designed in such a way that joint 4, 5, 6, 7 intersect in a single point, where the angular DOFs are mechanically decoupled from the translational ones. As mentioned already in [169], such a mechanical decoupling of the angular from the translational DOF has several advantages: The natural dynamics of the orientational DOFs is reduced and the torque capability of the rotational actuators can be chosen to match the capability of a human wrist so that no additional safety mechanisms are required. In the case of designing a mobile haptic interface consisting of two independently working components (haptic interface and mobile platform) such a construction can furthermore

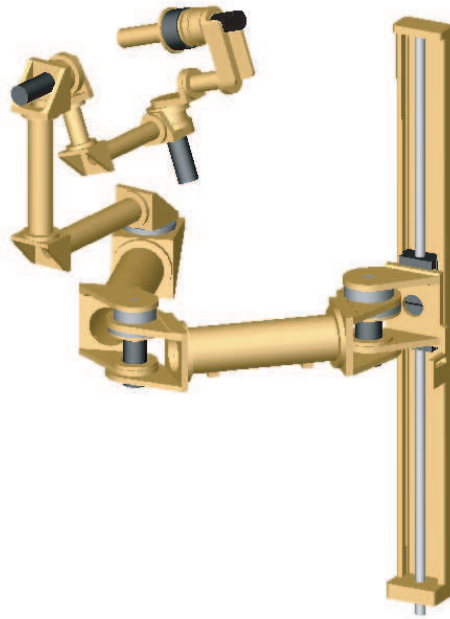


Figure 2.3: 3D-CAD model of ViSHARD7

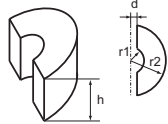
significantly simplify the algorithms that take care of the interaction between these two components as the complexity of the before mentioned optimization task is reduced.

The link length design guarantees a reachable workspace of almost a half cylinder with radius and height of 0.7 m. Thereby, possible collisions with the arm itself and the platform have to be considered. In contrast to this reachable workspace, the specifications of the dextrous workspace of the device are given in Table 2.2.

The haptic interface is built using commercially available components combined with aluminum construction elements. The actuation torque of all rotational joints is provided by dc motors coupled with harmonic drive gears offering zero backlash. The motors and gears have been selected to meet the specifications summarised in Table 2.2. The corresponding motor, power amplifier, and gear specification data can be found in appendix A. For the linear axis, an *LM Guide Actuator* of THK has been chosen, which guarantees high rigidity and high accuracy. A brushless dc motor, which carries the whole weight of all movable parts, is used to drive this linear axis. Since brushless dc motors usually have better thermal properties than comparable dc motors, this results in a more compact design [19]. An additional brake holds the haptic interface in a fixed position when no motor currents are provided. While all dc motors of the rotational joints are supplied by Copley amplifiers configured in torque mode, the brushless dc motor is driven by a 4QEC servo amplifier DES 70/10 of Maxon motor with sinusoidal commutation and digital current control.

In order to provide force feedback, the device is equipped with a six-axis JR3 force-torque sensor mounted at the tip of the end-effector with a bandwidth of 8 kHz. The joint angles of the rotational joints are measured by digital MR-encoders with a resolution of 4096 counts per revolution, resulting in a high position resolution when multiplied with the gear ratio. The position of the linear axis is measured at the drive end by using a Scancon Encoder with a resolution of 30 000 counts per revolution (quadrature encoder).

Table 2.2: Specifications of VISHARD7

Property	Value
transl. workspace	$h = 0.6$ m $d = 0.1$ m $r_1 = 0.2$ m $r_2 = 0.6$ m 
rot. workspace*	pitch, roll: $\pm 360^\circ$ yaw: $\pm 60^\circ$
peak force	vertical: 533 N horizontal: 155 N
peak torque	pitch, yaw: 11 Nm roll: 4.8 Nm
trans. velocity	vertical: 0.895 m/s horizontal: 1.1 m/s
rot. velocity*	pitch, yaw: 4.3 rad/s roll: 8.9 rad/s
trans. acceleration	vertical: 9.2 m/s ² horizontal: 13.5 m/s ²
rot. acceleration*	pitch, yaw: 183 rad/s ² roll: 318 rad/s ²
maximum payload**	34 kg
mass of moving parts	≈ 13 kg

* numbers refer to a device controlled by inverse function, see Sec. 2.3.3

** calculated for zero steady state human operator input force

The combination of a slope of 10 mm/round of the linear axis and a maximum motor speed of 5370 rpm allows translational velocities of up to 0.895 m/s. The maximum payload of the linear axis is 340 N and is calculated considering the limit of the average torque of the motor, the slope of the linear axis, and the mass of all moving parts.

Matlab/Simulink Real-Time-Workshop is used to automatically generate code from Simulink models (representing the control of the haptic interface), which is then executed on a RTAI real-time operating system. All models run with a sampling rate of 1 kHz. Data acquisition is performed by using Sensoray S626 PCI-I/O boards.

2.3 Control

Realization of a human haptic interaction with a remote environment requires controlling the motion-force relation between the operator and the haptic interfaces. This can be achieved by either controlling the interaction force of the device with the operator (impedance display mode) or the device motion (admittance display mode).

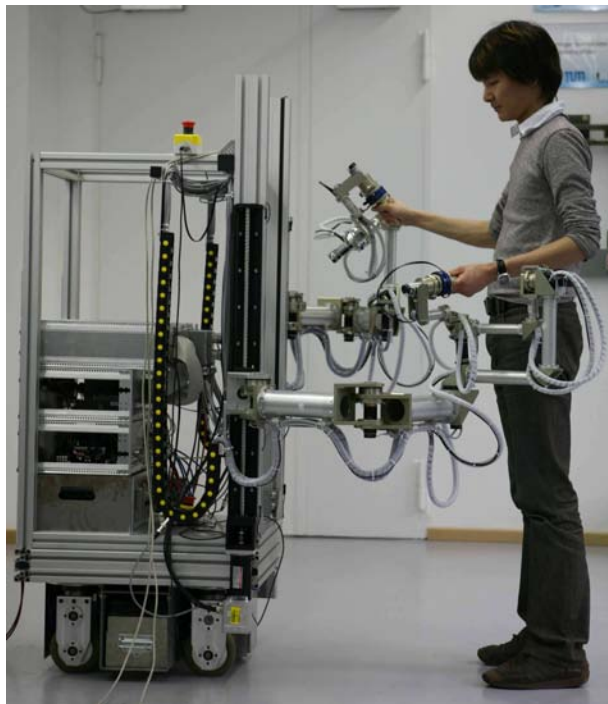


Figure 2.4: Bimanual mobile haptic interface consisting of two VISHARD7 mounted on a mobile platform

In order to provide effective compensation of the disturbances due to friction and the natural device dynamics, an admittance control strategy has been implemented for VISHARD7. In contrast to impedance control, which is frequently used for light and highly backdrivable devices, admittance control is particularly well suited for robots with high inertia and nonlinearities. The high-gain inner control loop closed on motion allows for an effective elimination of the nonlinear device dynamics, see [29]. A more detailed analysis of haptic control schemes can be found in [128].

The implemented admittance control is illustrated in Fig. 2.5. The interaction force \mathbf{h}_h of the human operator is measured by a force-torque sensor and subtracted from \mathbf{h}_d , which can be the measured interaction force of a telemanipulator with a remote environment or alternatively a force generated by a virtual environment.

The master dynamics relates the force $\Delta\mathbf{h}$ to the reference end-effector velocity $\dot{\mathbf{x}}_d$. An algorithm for inverse kinematics solution calculates the reference joint velocities $\dot{\mathbf{q}}_d$. Alternatively, the mapping of the end-effector to the joint motion can be realized at the position, velocity or acceleration level. The joint angles \mathbf{q}_d are the reference input to a conventional position control law, e.g., independent joint controllers (IJC) or a computed torque (CT) scheme.

In the following subsections, the main components of this admittance control scheme are discussed in detail.

2.3.1 Master Dynamics

Using an admittance control scheme, stability of the overall system can only be guaranteed if a minimum target inertia is implemented. When the human operator touches the device

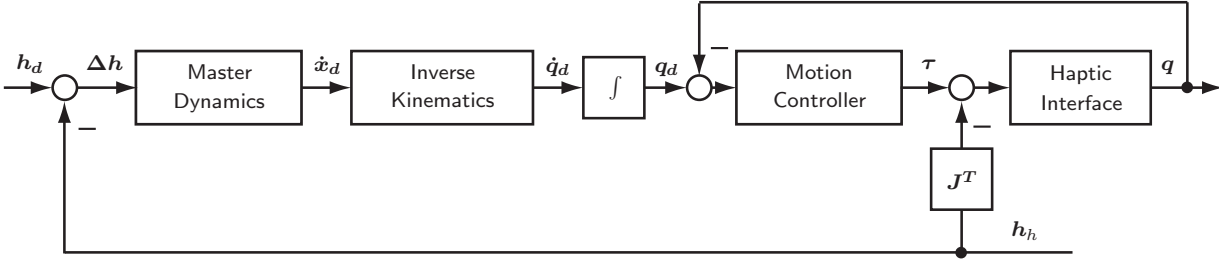


Figure 2.5: Admittance control scheme

and free space motion is rendered, the device needs to accelerate very quickly. This again implies very high control gains, which causes potential stability problems during free space motion. Thus, in free space motion, a minimum target inertia is necessary for stability. While the translational inertia \mathbf{M}_p is realized in form of a double integrator

$${}^N \mathbf{f} = \mathbf{M}_p {}^N \ddot{\mathbf{x}}, \quad (2.1)$$

the implementation of the minimum rotational inertia \mathbf{M}_o is based on the well known Euler's dynamical equation of rotation:

$${}^B \boldsymbol{\mu} = \mathbf{M}_o {}^B \dot{\boldsymbol{\omega}} + ({}^B \boldsymbol{\omega} \times \mathbf{M}_o {}^B \boldsymbol{\omega}) {}^B \boldsymbol{\omega}. \quad (2.2)$$

In this context the indices N and B refer to the Newtonian frame $\{N\}$ and the body coordinate frame $\{B\}$ defined in Fig. 2.2.

2.3.2 Motion Controller

From the huge variety of motion controllers that are known in literature, two different approaches were implemented: IJCs as well as a CT scheme [70], see Fig. 2.6. While the first approach neglects the nonlinear behavior of the plant and cross couplings between the linkages, the latter linearizes and decouples the system in a series of double integrators, which can be controlled independently. Thus, the IJCs are more conservative since the control gains depend hardly on the nonlinearities in the system which change according to the actual working position. In order to compensate for this effect the CT scheme has been used.

The corresponding control laws for both types of controllers are given by

$$\boldsymbol{\tau} = \mathbf{D}_j(\dot{\mathbf{q}}_d - \dot{\mathbf{q}}) + \mathbf{K}_j(\mathbf{q}_d - \mathbf{q}) \quad (2.3)$$

for the IJCs and

$$\boldsymbol{\tau} = \tilde{\mathbf{M}}(\mathbf{q}) \mathbf{u}_q + \tilde{\mathbf{h}}_N(\mathbf{q}, \dot{\mathbf{q}}), \quad (2.4)$$

$$\mathbf{u}_q = \ddot{\mathbf{q}}_d + \mathbf{D}_{ct}(\dot{\mathbf{q}}_d - \dot{\mathbf{q}}) + \mathbf{K}_{ct}(\mathbf{q}_d - \mathbf{q}) \quad (2.5)$$

for the CT scheme, where $\tilde{\mathbf{M}}(\mathbf{q})$ and $\tilde{\mathbf{h}}_N(\mathbf{q}, \dot{\mathbf{q}})$ denote estimates of the mass matrix, coriolis, friction and gravity forces and \mathbf{D}_j , \mathbf{K}_j , \mathbf{D}_{ct} , \mathbf{K}_{ct} are control parameters.

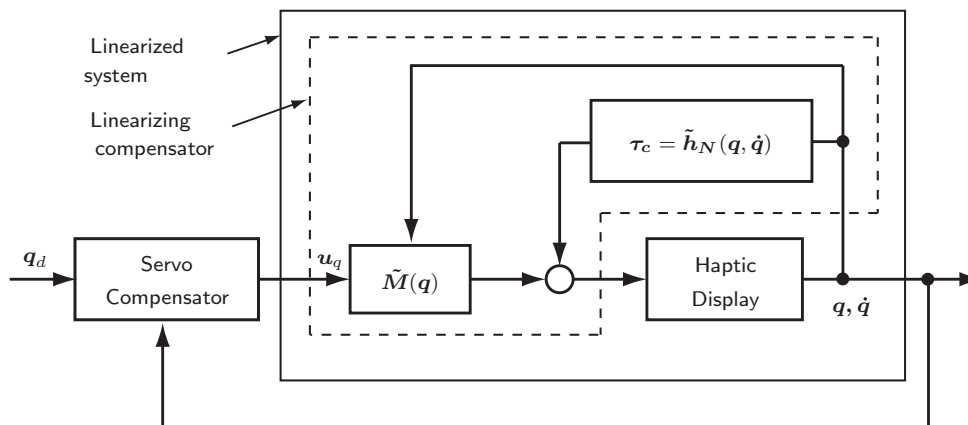


Figure 2.6: Computed torque scheme and servo compensator [141]

2.3.3 Inverse Kinematics

The inverse kinematics, the mapping of the end-effector to the joint motion, can be either realized on the position or on the velocity level

$$\mathbf{q} = \mathbf{f}(\mathbf{x}) \quad \text{or} \quad \dot{\mathbf{q}} = \mathbf{f}(\dot{\mathbf{x}}), \quad (2.6)$$

whereby $\mathbf{q}, \dot{\mathbf{q}} \in \mathbf{R}^n$ are the joint angle and velocity and $\mathbf{x}, \dot{\mathbf{x}} \in \mathbf{R}^m$ the end-effector position and velocity. Since for ViSHARD7 $n > m$ the manipulator is redundant with respect to the end-effector task. This redundancy allows changing of the internal configuration without changing the position and orientation of the end-effector. This implies that no unique solution for the inverse kinematics problem given by (2.6) can be derived.

To solve this problem for ViSHARD7, two different approaches are investigated:

- an inverse function for the whole haptic interface,
- a combination of inverse function and pseudoinverse control.

It should be noted that the decoupling of translational from rotational movements is common for both approaches. This simplifies the interaction with the mobile platform as shown in our original work [160].

Inverse Function

A possible approach to solve the redundancy is to define a single inverse function giving the joint angles for each point of the end-effector space. A simple inverse function is defined when using the following mapping from joint angles to Cartesian positions:

$$q_1 = \left(\frac{2\pi}{0.01} \right) z, \quad (2.7)$$

$$q_2 = \arctan 2(y, x) + \cos^{-1} \left(\frac{x^2 + y^2}{2l\sqrt{x^2 + y^2}} \right), \quad (2.8)$$

$$q_3 = \cos^{-1} \left(1 - \frac{x^2 + y^2}{2l^2} \right) + \pi, \quad (2.9)$$

where (x, y, z) is the end-effector position with respect to the haptic interface base coordinate system S_N , q_i are the joint angles of the i -th joint, and l is the link length of link 2 and 3. By setting joint angle 4 to $q_4 = q_{4,0} - \sum_{i=2}^3 q_i$, a decoupling of translational and rotational motions can be achieved. It should be noted that this special inverse function implies a singular configuration at the point $x = y = 0$, which has to be omitted.

For the rotational part, an inverse kinematics solution operating at the angular velocity level has been applied. In a first step, the time derivative of the end-effector orientation by means of yzx -Euler-angles $[\alpha, \beta, \gamma]$, can be calculated from the angular velocity of the endeffector ${}^B\boldsymbol{\omega}$

$$\begin{pmatrix} \dot{\alpha} \\ \dot{\beta} \\ \dot{\gamma} \end{pmatrix} = \begin{pmatrix} 0 & \frac{\cos \gamma}{\cos \beta} & -\frac{\sin \gamma}{\cos \beta} \\ 0 & \sin \gamma & \cos \gamma \\ 1 & -\frac{\sin \beta \cos \gamma}{\cos \beta} & \frac{\sin \beta \sin \gamma}{\cos \beta} \end{pmatrix} {}^B\boldsymbol{\omega}. \quad (2.10)$$

Choosing the Euler angles in such a way that they correspond to the joint angles q_5, q_6 and q_7 the inverse function for the rotational part is given by

$$q_5 = \alpha, \quad (2.11)$$

$$q_6 = -\beta + \pi/2, \quad (2.12)$$

$$q_7 = \gamma. \quad (2.13)$$

This inverse kinematics solution has a singular configuration for $\beta = k\pi/2$ with $k \in \mathbf{N}$, which, however, can be easily avoided by introducing a joint limitation for q_6 . The drawback of this measure is obvious: The available rotational workspace is restricted to $\beta \in]-\pi/2 \ \pi/2[$.

Partitioned Inverse Kinematic Solution

To overcome this drawback and to enlarge the rotational workspace of the device, a partitioned inverse kinematic solution has been implemented. This solution uses the already mentioned inverse function for translational movements, but applies a pseudoinverse control [84] for the rotational part.

Using pseudoinverse control, a solution to the inverse problem given by (2.6) can be formulated as follows:

$$\dot{\mathbf{q}} = \mathbf{J}^\# \dot{\mathbf{x}} + [\mathbf{I} - \mathbf{J}^\# \mathbf{J}] \dot{\mathbf{q}}_0, \quad (2.14)$$

where the Moore-Penrose generalized inverse $\mathbf{J}^\# = \mathbf{J}^T (\mathbf{J} \mathbf{J}^T)^{-1}$ of the Jacobian matrix is used. While the first term describes the minimum norm joint velocity solution, $[\mathbf{I} - \mathbf{J}^\# \mathbf{J}] \dot{\mathbf{q}}_0$ represents the homogeneous solution of (2.6), which projects an arbitrary joint velocity vector $\dot{\mathbf{q}}_0$ onto the nullspace of \mathbf{J} . The homogeneous solution can be used to improve the device performance when choosing $\dot{\mathbf{q}}_0$ to optimize a performance criterion $H(\mathbf{q})$, a scalar function of the joint angles. Redundancy can then be solved by substituting $\dot{\mathbf{q}}_0$ with $\mu \nabla H(\mathbf{q})$ resulting in

$$\dot{\mathbf{q}} = \mathbf{J}^\# \dot{\mathbf{x}} + [\mathbf{I} - \mathbf{J}^\# \mathbf{J}] \mu \nabla H(\mathbf{q}), \quad (2.15)$$

with μ the step length of the gradient.

Replacing the Moore-Penrose generalized inverse $\mathbf{J}^\#$ by a weighted pseudo inverse

$$\mathbf{J}^+ = \mathbf{W}^{-1} \mathbf{J}^T (\mathbf{J} \mathbf{W}^{-1} \mathbf{J}^T)^{-1} \quad (2.16)$$

with \mathbf{W} the weighting matrix, the influence of certain joints on the end-effector motion can further be increased or penalized (for further information see singularity-robust inverse in [90]). This can be of interest in the case of different joint velocity capabilities or mass distributions amongst the joints.

Under all these assumptions and considering that $\mathbf{q}_{\text{rot}}^T = [q_4^* \ q_5 \ q_6 \ q_7]$ with $q_4^* = q_4 + \sum_{i=2}^3 q_i$, (2.15) becomes

$$\dot{\mathbf{q}}_{\text{rot}} = \mathbf{J}_{\text{rot}}^+ \boldsymbol{\omega} + [\mathbf{I} - \mathbf{J}_{\text{rot}}^+ \mathbf{J}_{\text{rot}}] \mu_{\text{rot}} \nabla H_{\text{rot}}, \quad (2.17)$$

where $\boldsymbol{\omega}$ is the rotational Cartesian velocity command and $\mathbf{J}_{\text{rot}} \in \mathbf{R}^{3 \times 4}$ the Jacobian relating \mathbf{q}_{rot} to $\boldsymbol{\omega}$.

In order to avoid singularities, one of the manipulability indices $m = f(\mathbf{J})$ reported in [169] can be chosen as a performance criterion. However, the most convincing results in terms of predictability of motions, could be achieved using a rather simple performance criterion:

$$H = q_6^2 - \pi q_6. \quad (2.18)$$

It tries to keep the 6th joint fixed to $\pi/2$, which is the position farthest away from the singular configuration.

If other criteria as e.g. collision avoidance with the human operator as well as of the robot with itself are also of interest, additional performance criteria can be defined. The overall performance index to be considered in (2.17) then consists of a weighted sum of all single criteria. See [150] for further details.

2.4 Stability Analysis

As it was already mentioned in Sec. 2.3.1 and is well known from experiments, in admittance control the minimum target mass and inertia of the haptic interface is bound by stability. This effect is analyzed in detail in this section. On this account simple linear models are assumed for haptic interface, as well as human operator and stability is analyzed by testing asymptotic stability of the overall system.

Definition (asymptotic stability): A linear time invariant system described by the state-space model

$$\dot{\mathbf{x}} = \mathbf{A}\mathbf{x} + \mathbf{B}\mathbf{u}, \quad (2.19)$$

$$\mathbf{y} = \mathbf{C}\mathbf{x} + \mathbf{D}\mathbf{u}, \quad (2.20)$$

is asymptotic stable, if for all eigenvalues λ_i of the system matrix \mathbf{A} holds:

$$\text{Re} \{ \lambda_i(\mathbf{A}) \} = \sigma_i < 0 \quad \forall \quad i. \quad (2.21)$$

2.4.1 Models for Haptic Interface and Human Operator

Below, two different types of linear models for the haptic interface are presented: a rigid and a compliant model. While the first assumes the haptic interface to be rigid, the latter takes into account the structural compliance of the robotic arm, which is mainly due to the elasticity of the harmonic drive gears. Typical values for the stiffness of harmonic drive gears are namely in the range of 1 000 to 15 000 Nm/rad, which is far below the structural stiffness of the aluminum elements used to connect them.

Rigid model

A very simple way to model a haptic interface is to use a mass-damper system [139] as shown in Fig. 2.7. In this context m_m means the haptic interface mass and b_m the damping coefficient. The actuator force is modelled by f_m .

Since the human operator interacts with the haptic interface also a simple model of the human arm is needed. According to [78] a simple mass-spring-damper model can be used. In this context m_h means the human arm mass, c_h the human arm stiffness and b_h the human arm damping. The factor $\alpha \in [0, 1]$ is used to take into account variable human arm impedances. The exogeneous force applied by the human operator is modelled by f_h . Finally m_{em} means the end-effector mass and f_{sm} the force measured by the force-torque sensor located at the tip of the haptic interface.

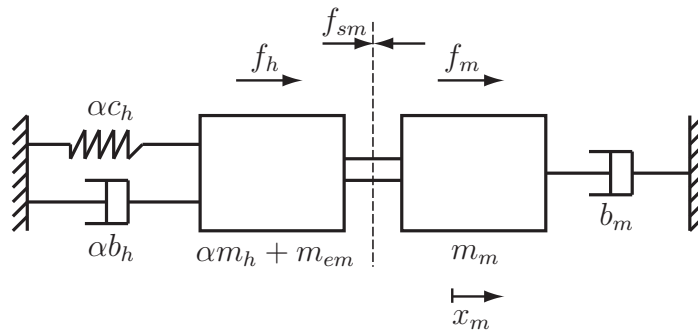


Figure 2.7: Rigid model of haptic interface and human operator

The overall system described in Fig. 2.7 is represented by the following differential equations:

$$\begin{aligned} 0 &= f_h + f_{sm} - (\alpha m_h + m_{em}) \ddot{x}_m - \alpha b_h \dot{x}_m - \alpha c_h x_m, \\ 0 &= f_{sm} - f_m + m_m \ddot{x}_m + b_m \dot{x}_m. \end{aligned} \quad (2.22)$$

Compliant model

If the haptic interface cannot be assumed to be rigid, an advanced model as proposed by [74, 94] can be used, which assumes that the compliance of the haptic interface is concentrated in a single spring-damper system c_m, b_{m2} . This advanced model is shown in Fig. 2.8.

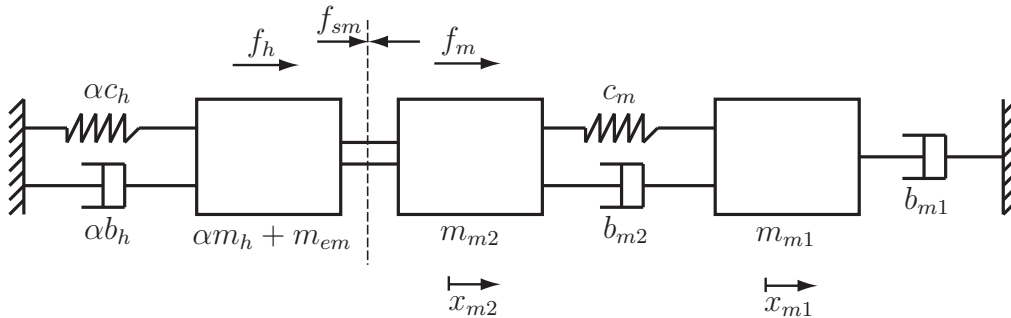


Figure 2.8: Compliant model of haptic interface and human

Again the system can be represented by a series of differential equations:

$$\begin{aligned} 0 &= f_h + f_{sm} - (\alpha m_h + m_{em}) \ddot{x}_{m2} - \alpha b_h \dot{x}_{m2} - \alpha c_h x_{m2}, \\ 0 &= f_{sm} - f_m + m_{m2} \ddot{x}_{m2} + b_{m2} (\dot{x}_{m2} - \dot{x}_{m1}) + c_m (x_{m2} - x_{m1}), \\ 0 &= m_{m1} \ddot{x}_{m1} + b_{m2} (\dot{x}_{m1} - \dot{x}_{m2}) + c_m (x_{m1} - x_{m2}) + b_{m1} \dot{x}_{m1}. \end{aligned} \quad (2.23)$$

2.4.2 Actuator and Sensor Dynamics

In order to reproduce effects visible in the real hardware experiment, the non-ideal actuator and sensor dynamics have to be considered. As actuators, dc or brushless dc motors are used in the experiment. The time constant introduced by these components is given by their electrical time constant T_a , which can be derived from the quotient of motor inductance and resistance. A simple low-pass filter is used to model this effect:

$$\hat{f}_m = f_m \frac{1}{1 + sT_a}. \quad (2.24)$$

Basically two types of sensors are used in the hardware experiment: incremental encoders as position sensors and a force-torque sensor. While the process of the encoder information is really fast ($T < 0.1$ ms) and thus this time constant is negligible, the measurements of the force-torque sensor are typically very noisy and have to be filtered appropriately. In the experiments, a low pass filter with time constant T_f has been used, which leads to the following model:

$$\hat{f}_{sm} = f_{sm} \frac{1}{1 + sT_f}. \quad (2.25)$$

2.4.3 Simulation Results

Using the models presented above, asymptotic stability is analyzed for an admittance controlled haptic interface. The analysis for VISHARD7 is simplified, when the cross-couplings between the linkages are assumed to be compensated by a CT control scheme, so that each DOF can be evaluated separately. Moreover, in order to reduce the number of control parameters, the low level position controllers are assumed to be already tuned. The resulting control law can be formulated as follows:

$$f_m = D_{xm} (\dot{x}_{dm} - \dot{x}_m) + K_{xm} (x_{dm} - x_m), \quad (2.26)$$

$$-f_{sm} = m_d \ddot{x}_{dm} + b_d \dot{x}_{dm}, \quad (2.27)$$

whereby K_{xm} and D_{xm} mean control parameters of the low level position controller and m_d , b_d denote the minimal mass and damping parameters necessary to guarantee stability. The stability boundary is determined by applying a bisection algorithm, which tries to find for a given mass m_d the corresponding damping b_d , which keeps the system on the stability boundary. All simulations are carried out by using the model parameters reported in appendix C.

Fig. 2.9 shows the simulation results obtained by using the rigid model, whereby the human arm impedance is varied. As expected, instability occurs for small mass and damping coefficients m_d and b_d . If no damping is assumed, a minimum target mass has to be implemented, which guarantees stability of the overall system. Moreover, a strong dependency

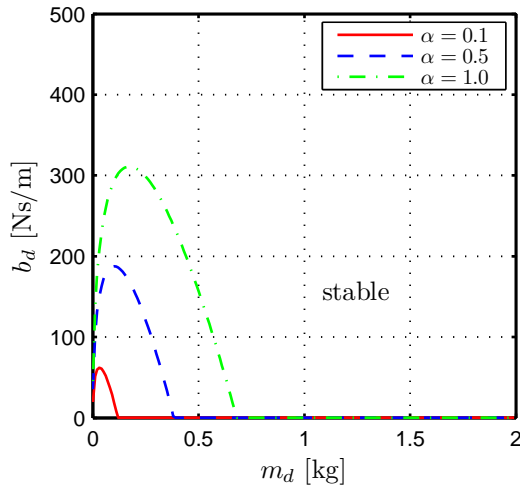


Figure 2.9: Rigid model: Stability boundaries in the (m_d, b_d) -plane for varying human arm impedance α ($T_f = 0.0015$ s, $T_a = 0.003$ s).

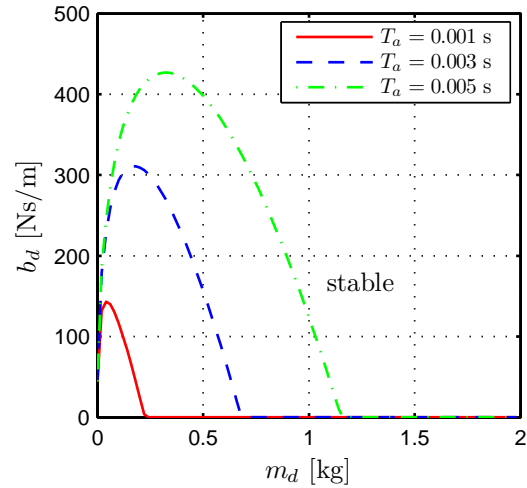


Figure 2.10: Rigid model: Stability boundaries in the (m_d, b_d) -plane for varying actuator time constant T_a ($T_f = 0.0015$ s, $\alpha = 1$).

on the human arm impedance can be observed. The higher the arm impedance, the higher is the required minimal mass. As a consequence instability occurs when the human operator grasps the device very strongly. Interestingly, increasing the stiffness c_h of the human arm does not affect the stability boundaries, so that the effect mentioned before can be clearly ascribed to the mass of the human arm which is coupled to the system. This again implies that stability can be influenced by mounting end-effectors with different weights.

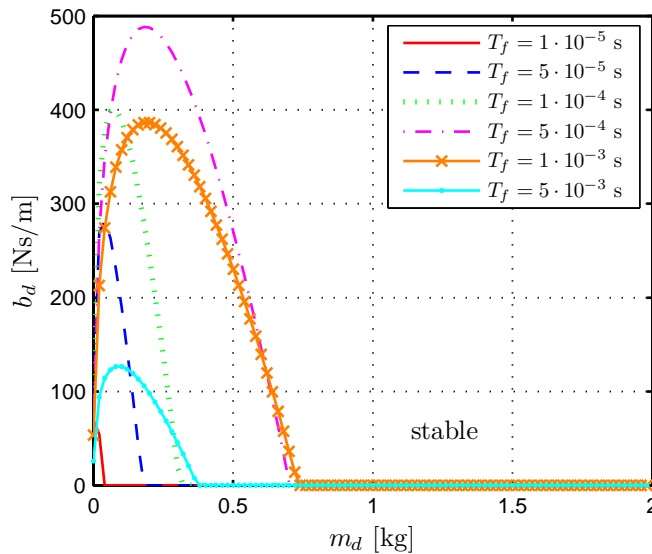


Figure 2.11: Rigid model: Stability boundaries in the (m_d, b_d) -plane for varying force filter constants T_f ($T_a = 0.003$ s, $\alpha = 1$).

Since it is expected that the dynamics of actuators and sensors also influences the stability region, stability is analyzed for different actuator and force filter time constants. The corresponding results are reported in Fig 2.10 and Fig. 2.11. It can be observed that the actuator time constant T_a significantly influences the stability region. The bigger the time constant, the bigger the instability region. Increasing the force filter constant T_f results initially in an enlargement of the instability region, but filtering even more surprisingly enhances stability of the overall system.

The same simulations were carried out with the compliant model of the haptic interface. As already observed when using the rigid model, stability increases with decreasing human arm impedance, see Fig. 2.12. But, in contrast to the rigid model, the actuator time constant T_a does not affect stability and a bigger force filter constant always has a negative effect on stability, see Fig. 2.13. Very interesting is the effect of the structural stiffness on stability. As can be seen in Fig. 2.14 an increasing stiffness increases the instability region.

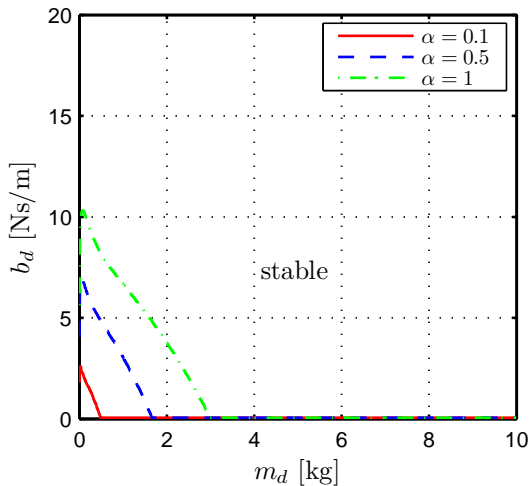


Figure 2.12: Compliant model: Stability boundaries in the (m_d, b_d) -plane for varying human arm impedance ($T_f = 0.0015$ s, $T_a = 0.003$ s, $c_m = 30\,000$ N/m).

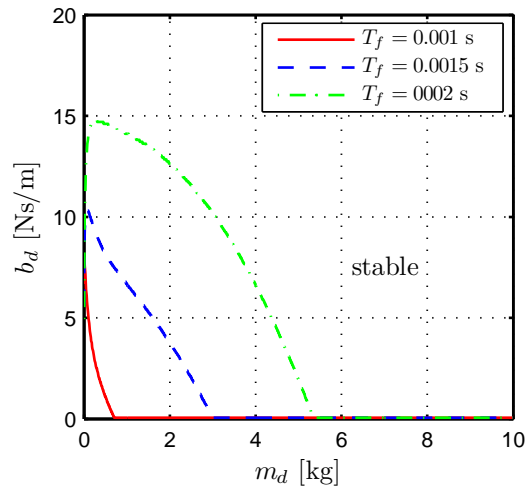


Figure 2.13: Compliant model: Stability boundaries in the (m_d, b_d) -plane for varying force filter constants T_f ($T_a = 0.003$ s, $c_m = 30\,000$ N/m, $\alpha = 1$).

To summarize, it can be stated that a small target mass and damping always results in instability of the overall system. Moreover, a bigger human arm impedance increases the instability region, independently of the model used for simulation. A force filter constant has mostly a negative effect on stability and the effect of the actuator dynamics is dependent on whether the haptic interface is rigid or compliant. If the haptic interface can be considered as rigid, an increasing actuator time constant requires a higher target mass to guarantee stability.

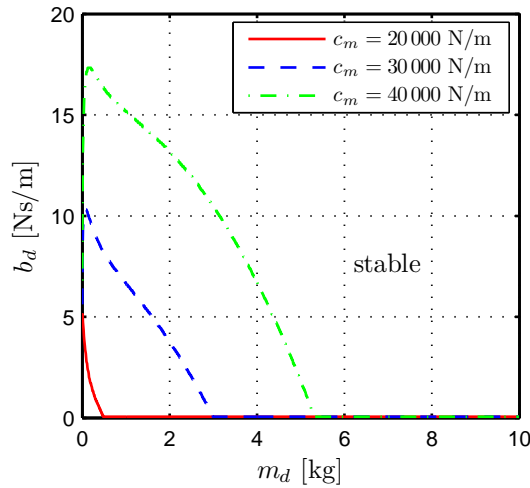


Figure 2.14: Compliant model: Stability boundaries in the (m_d, b_d) -plane for varying stiffness constant c_m ($\alpha = 1$, $T_f = 0.0015$ s, $T_a = 0.003$ s).

2.5 Performance Measures

While the prior sections mainly focused on the design and control of the new haptic interface, the following sections are devoted to the evaluation of it. Different performance measures and measurement procedures for the evaluation of haptic interfaces have been proposed in the past, see [22, 55, 127]. In the following, the most common performance measures will be reported. According to [127], basically two types of performance measures can be distinguished: hardware-related measures and, the so-called, closed-loop performance measures.

Hardware-Related Measures: These performance measures depend on the hardware design of the haptic interface. The most important ones are as follows:

- dextrous workspace: number and nature (translational or rotational) of DOF, translational and rotational workspace free of singularities;
- output capability: maximum peak and continuous force, maximum velocity, maximum acceleration, maximum payload;
- sensorial capability: measured quantities and resolution at the human body interface.

Closed-Loop Performance Measures: Closed-loop performance measures depend on the control of the device. The following criteria can be distinguished:

- force precision: maximum steady state force error at zero motion;
- dynamic force precision: force control frequency response;
- backdrivability: minimum apparent mass and inertia at the tip, maximum force error, impedance frequency response;
- stiffness: apparent stiffness at the human-body interface;
- smallest grating that can be rendered correctly.

Instead of specifying the presented measures only for one special operating point, as is common in the literature, [55] suggests specifying best and worst case figures over the entire workspace of the device. Since this would result in a huge number of measurements, [127] proposes obtaining some of the performance measures by a model-based performance evaluation. In this work, some of the performance measures will be obtained by model-based, others by measurement-based performance evaluation.

Different approaches have been proposed in the past to determine the above listed measures, but no general procedures have been established. The main reasons for that are the high dependency of evaluation results on the operating point and the behavior of the human operator, which is part of the system. In order to get reproducible measurement conditions, the human operator has to be replaced by a machine which simulates the human grasping behavior. Unfortunately, in the literature, still no clear design specification for such a system can be found.

2.6 Performance Evaluation

In the following sections, the evaluation results will be presented. Performance measures such as dextrous workspace and output capability (maximum peak and continuous force, maximum velocity, maximum acceleration, maximum payload) are obtained by model-based, the backdrivability and some mechatronic device measures by measurement-based performance evaluation. The results are based on the previously presented control algorithms, the kinematic model shown in Fig. 2.2, the link length design summarized in Table 2.1, as well as the hardware specifications of gears and motors reported in appendix A.

It should be noted that considering the performance measures presented in Sec. 2.5, difficulties arise when the system is redundant: Most of the known measurement and simulation procedures cannot be applied to such systems, because they act on the assumption that a certain Cartesian position in space can be achieved only by one joint space configuration. Thus, most of the following evaluation results have been carried out by using the inverse function, as presented in Sec. 2.3.3.

2.6.1 Model-based Performance Evaluation

Dextrous Workspace

In order to analyze the input-output transmission of the device, the velocity manipulability measure

$$m(\mathbf{q}) = \sqrt{\det(\mathbf{J}(\mathbf{q})\mathbf{J}^T(\mathbf{q}))} \quad (2.28)$$

has been computed. The result is shown in Fig. 2.15 and 2.16. It can be clearly seen that the manipulability measure decreases in the proximity of the singularities and the boundaries of the workspace. Thus, the dextrous workspace of the device has been chosen, as stated in Table 2.2, excluding the areas with low manipulability.

Furthermore, the form of the manipulability ellipsoids can be used as a measure for the isotropic behavior of a device. The closer the ellipsoids to the sphere, the more uniform the haptic interface can move in different directions. Fig. 2.16 shows the manipulability ellipsoids in different positions of the translational workspace. Considering only the dex-

trous workspace of the device, the ellipsoids do not differ very much in size and orientation. This again reveals that the translational motion is very uniform over the whole workspace.

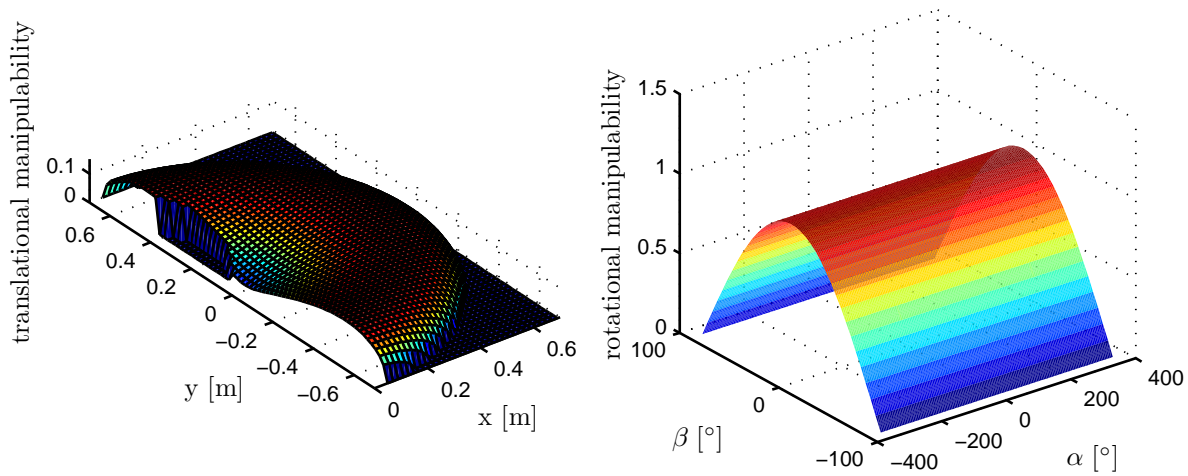


Figure 2.15: Translational and rotational velocity manipulability

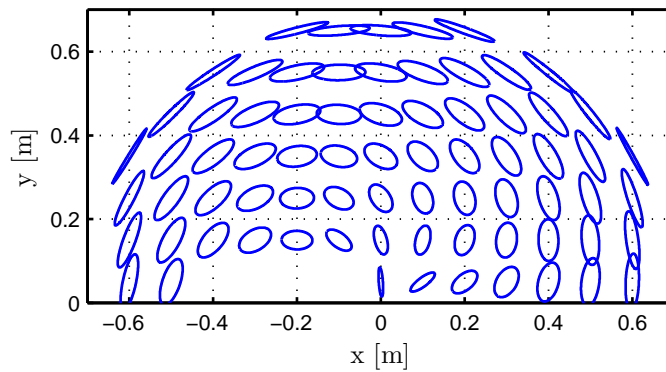


Figure 2.16: Translational velocity manipulability ellipsoids

Output Capability

Typical performance measures which can be derived from model-based performance evaluation are the output and sensorial capabilities of the device. These capabilities are directly dependent on the hardware design and can be estimated using adequate kinematic and dynamic models of the device, as well as considering the performance characteristics of single components.

In this work, the minimum output capability of the device has been computed according to an algorithm introduced in [127], which allows analysis of the force/torque, acceleration and velocity capability of the device. In contrast to other approaches based on the manipulability ellipsoid, see [60, 142], this approach follows a different strategy. The problem to determine the minimum output capability of the device is formulated as optimization problem. The basic idea is to find in a given working point, the direction of manipulation in which the performance of the device is worst. Extending this procedure over the whole workspace allows the determination of the minimum output capability of the device.

The computation of the minimum output capability is based on the following equations, which define the velocity, force, and acceleration of the device:

$$\begin{pmatrix} \dot{\mathbf{x}} \\ \boldsymbol{\omega} \end{pmatrix} = \mathbf{J}\dot{\mathbf{q}} \quad (2.29)$$

$$\mathbf{h} = (\mathbf{J}^{-1})^T \boldsymbol{\tau}; \quad \dot{\mathbf{q}} = 0 \quad (2.30)$$

$$\begin{pmatrix} \ddot{\mathbf{x}} \\ \dot{\boldsymbol{\omega}} \end{pmatrix} = \mathbf{J}\mathbf{M}^{-1}\boldsymbol{\tau}; \quad \dot{\mathbf{q}}, \mathbf{h} = 0 \quad (2.31)$$

where \mathbf{J} is the Jacobian, which relates the joint velocities $\dot{\mathbf{q}}$ to the Cartesian velocity $\dot{\mathbf{x}}$ and the angular velocity $\boldsymbol{\omega}$. Assuming the system is in a static case ($\dot{\mathbf{q}} = 0$) and gravity and friction forces can be neglected, (2.30) shows the relation between the joint torques $\boldsymbol{\tau}$ and the translational and rotational forces \mathbf{h} acting at the end-effector. Finally, (2.31) denotes the relation between the joint torques $\boldsymbol{\tau}$ and linear and angular acceleration $\ddot{\mathbf{x}}$ and $\dot{\boldsymbol{\omega}}$, whereby no external forces and torques are exerted on the system and \mathbf{M} means the mass matrix of the system.

Applying the aforementioned algorithm to VISHARD7, the following constraints have to be taken into account. Since VISHARD7 is redundant and the presented algorithm cannot be applied to such systems, only the non-redundant case can be considered. Thus, the redundancy of the haptic interface is solved by the inverse function presented in Sec. 2.3.3, which decouples the rotational and translational movements of the robot. This again means that the translational output capability will not be affected by the rotational one and vice versa. In the following paragraphs, the obtained evaluation results are presented.

The continuous and peak force capability of the haptic interface is depicted in Fig. 2.17. As the figure shows a constant value over the whole workspace, either joint 1 or 3 must be in saturation. While the linear axis can attain a maximum continuous/peak force of about 470/533 N, joint 3 can only provide about 27.9/154 N at the end-effector. It must be noted that the maximum forces of the second and third joint are nearly the same and thus, these joints represent the bottleneck of the force output capability.

Fig. 2.18 (left) shows the horizontal translational velocity capability of the device. As supposed, the velocity performance decreases in the vicinity of the singularity near to the base and at the boundaries of the reachable workspace, whereby the asymmetry around the base is a result of mechanical joint limitations. Fig. 2.19 (left) shows the corresponding contour plot. Considering a dextrous workspace, as stated in Table 2.2, the maximum translational velocity for a horizontal motion results in 1.1 m/s. The maximum vertical velocity depends on the maximum velocity of the linear axis, which is given by 0.895 m/s. This indicates that the performance of the overall system could be significantly improved by decreasing the dextrous workspace and using a motor with a higher maximum motor speed for the linear axis. Unfortunately, no motor which meets also all other requirements

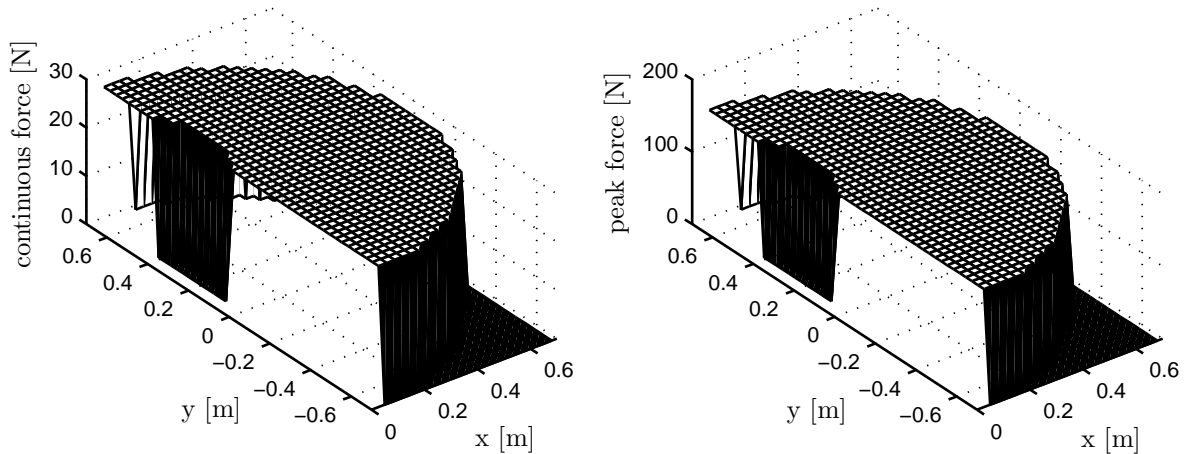


Figure 2.17: Horizontal translational continuous and peak force capability

as high acceleration capability, low inertia, and high output torque, is available on the market.

In order to determine the acceleration capability, a dynamical model of the device is necessary. Such a model is created by extracting the inertial properties from the CAD model of the device and computing the mass matrix with Autolev (see [63]). Fig. 2.18 (right) shows the horizontal translational acceleration capability of the system. It should be noted that the acceleration performance decreases significantly in the vicinity of singularities. Considering the dextrous workspace stated in Table 2.2 and Fig. 2.19 (right), the worst case horizontal acceleration capability is given by 13.5 m/s^2 . The maximum vertical acceleration can be calculated by dividing the peak force of the linear axis through the mass of all moving parts. Thereby, the inertia of the axis itself ($831 \cdot 10^{-7} \text{ kgm}^2$), the rotor of the motor ($291 \cdot 10^{-7} \text{ kgm}^2$), and the coupling mechanism between motor and linear axis ($18 \cdot 10^{-7} \text{ kgm}^2$) have to be considered. This can be realized by computing an equivalent mass (45 kg) and adding it to the mass of all moving parts (13 kg). Thus, the vertical maximum acceleration is given by 9.2 m/s^2 .

For the analysis of the rotational output capability of the device the geometrical Jacobian has been used. Fig. 2.20 shows the rotational output capability against the Euler angles α and β , which correspond to the joint angles q_5 and q_6 . Using the inverse function presented in Sec. 2.3.3, the haptic interface has a singularity when $\beta = \pm\pi/2$. Thus, the range of the angle β significantly influences the results on the rotational output capability. To this extent the analysis of angular velocity and acceleration has been carried out for different ranges of the Euler angle β . Finally the results for $\beta = 60^\circ$ have been chosen as specifications of VISHARD7.

The limits of the torque capability of the device can be easily determined: Since the device is controlled by the inverse function described in Sec. 2.3.3 and the Euler angles are chosen in such a way that they correspond to the joint angles q_5 , q_6 , and q_7 the torque capability is given by the maximum torque of the corresponding motor/gear combination (see Table 2.2).

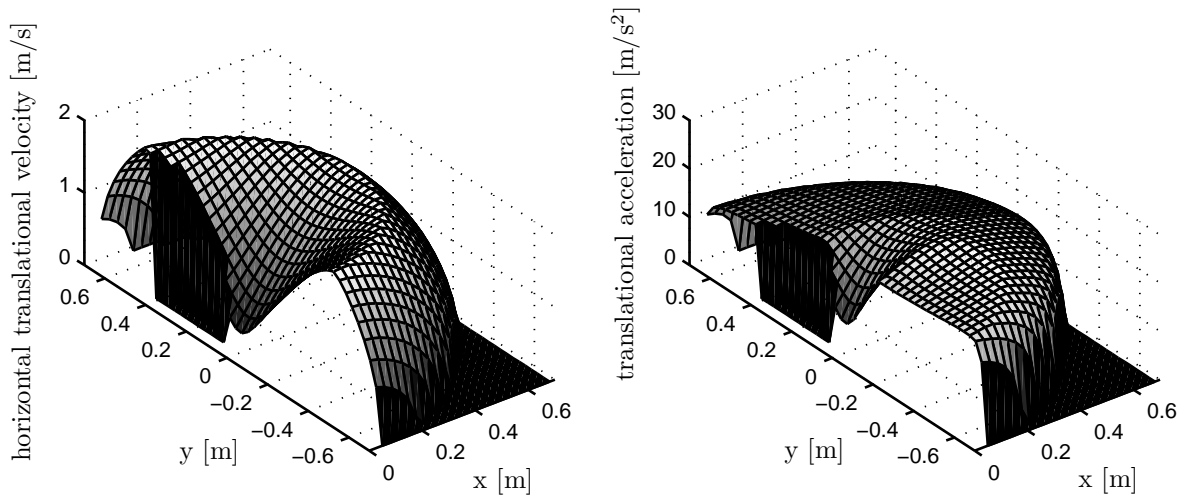


Figure 2.18: Maximum horizontal translational velocity and acceleration capability

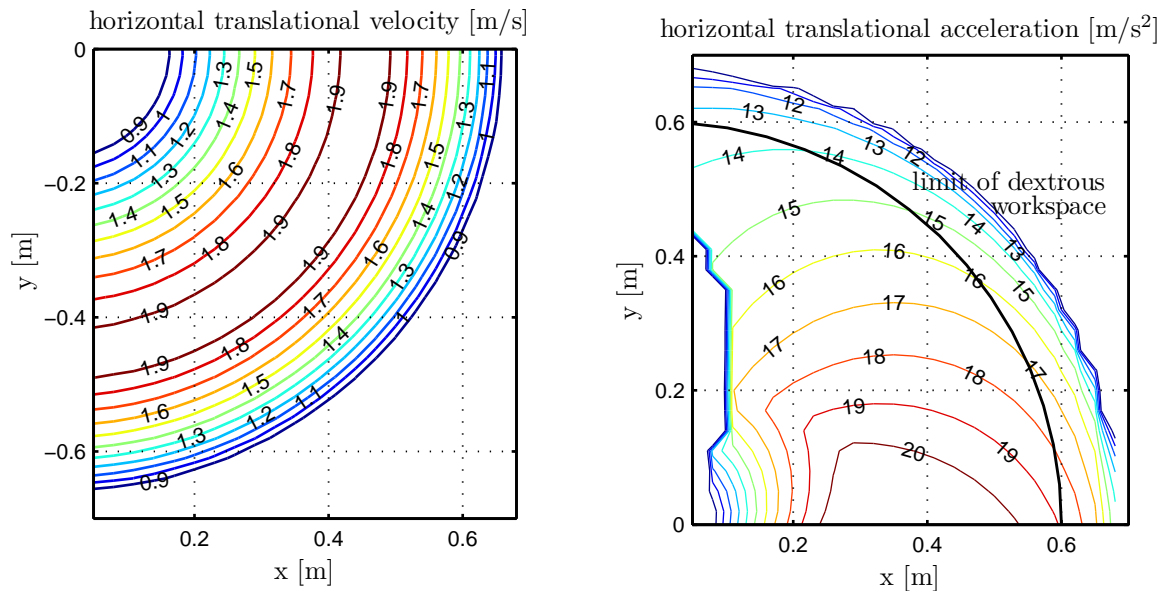


Figure 2.19: Contour plot of maximum horizontal translational velocity and acceleration capability

2.6.2 Measurement-Based Performance Evaluation

Backdrivability

Since in admittance control, the inner position control loop compensates for the natural device dynamics and friction effects, the evaluation of the backdrivability can be reduced to the determination of the minimum translational and rotational inertia M_p and M_o that can be commanded without producing instability, see Sec. 2.3.1 for more details. As shown above, the admissible lower bound for mass and inertia is strongly dependent on the firmness of the grasp of the human operator. In order to determine numbers for this lower

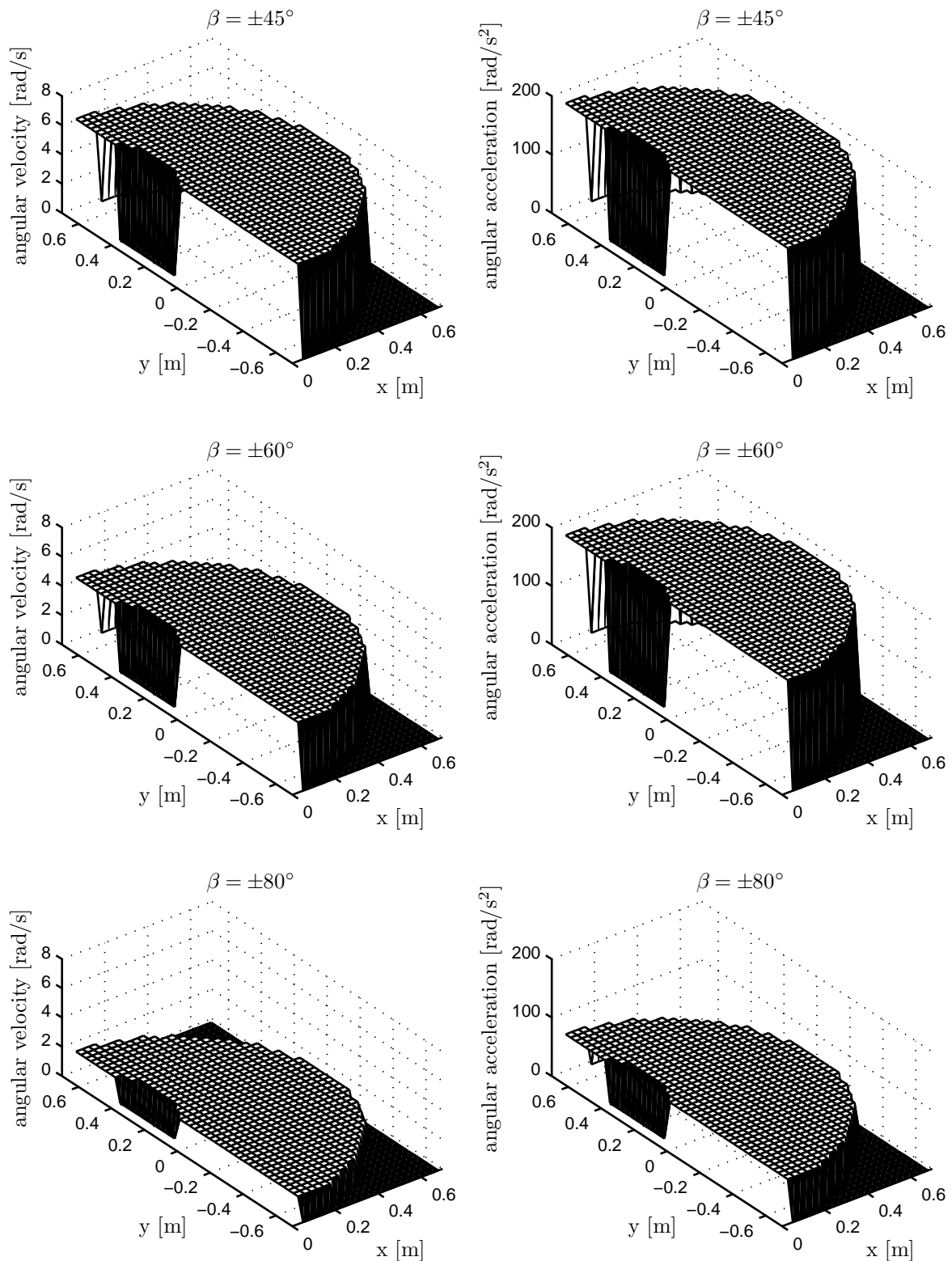


Figure 2.20: Maximum horizontal rotational velocity and acceleration capability for $\beta = \pm 45^\circ, \pm 60^\circ, \pm 80^\circ$

bound, the human operator tried to produce instability of the device by grasping it very strongly or pushing against it in different positions of the workspace. The target inertia was reduced as long as no point in the workspace could be found which causes instabilities.

Depending on the position control structure and the inverse kinematics, different lower bounds for the inertia can be obtained. In the experiments, simple IJCs of PD-type were compared with a more sophisticated position controller based on a CT scheme and acceleration feedforward. Concerning the inverse kinematics, two different solutions, the inverse function and the partitioned inverse kinematic solution, see Sec. 2.3.3, were compared. To make the results comparable the motion controllers (IJCs and CT scheme without acceleration feedforward) were tuned to have the same step responses. In order to do so, the following procedure was used: After selecting critical damped control parameters for the CT scheme, the device was positioned in its working position, steps of 5 cm respectively 5 degrees were performed for each joint, and the control parameters for the IJCs were adjusted in such a way, that the step responses of both controllers became the same. The obtained control parameters are listed in Table 2.3.

Table 2.3 finally shows also the measurement results of the backdrivability experiment. For each architecture, the control parameters as well as the minimum mass and inertia are given. Please note that independently of the type of inverse kinematics, the advanced position controller with CT scheme allows to significantly reduce the minimum mass and inertia. Among the two types of inverse kinematics small differences in the minimum inertia can be observed. Considering that the two types of inverse kinematics move the corresponding joints in a different way, these effects can be explained by the slightly different inertias of the moving parts.

Using pseudoinverse control, the motion behavior of the rotatory part of the display can be significantly influenced by choosing an appropriate weighting matrix. The weighting matrix, which has been used in the experiments, is given in Table 2.3. It has been empirically found and is chosen in such a way that motions around joint 5 and 7 are encouraged while motions around joint 4 are penalized. This prevents really fast motions around joint 4, which may result in collisions with the mobile platform or the human operator.

Mechatronic Device Performance

In order to define measures of the mechatronic device performance two experiments were performed: The first experiment evaluates the Cartesian position tracking performance and the second experiment aims to investigate the impedance display fidelity of the device.

To measure the tracking performance of the device, it was positioned in its working position and step responses for every task space coordinate were recorded. Since the velocity and acceleration capability of the device are limited (see Table 2.2), a smooth approximation of a rectangular pulse was used

$$u = \frac{A}{2} \left(1 + \frac{\text{atan}(B(t - t_1))}{\pi/2} \right) - \frac{A}{2} \left(1 + \frac{\text{atan}(B(t - t_2))}{\pi/2} \right) \quad (2.32)$$

where $u \in \{x, y, z, \alpha, \beta, \gamma\}$ denotes a Cartesian coordinate, A and B are constants, which define amplitude and rising time of the step, and t_1, t_2 mean the moment of rising and falling edge, respectively. The parameters A and B of this function are chosen to meet the target specifications of the device: For the translational part, $A = 0.1$ m and $B = 20$, and for the rotational part, $A = 0.087$ rad and $B = 100$ have been set. In doing so, a maximum

Table 2.3: Minimum mass and inertia for different inverse kinematics and motion controllers

Inverse kinematics	Control	Control parameters	Minimum mass and inertia
Inverse function	IJC	$\mathbf{K}_j = \text{diag}(80000, 16, 14, 2, 3, 1.8, 0.5)$ $\mathbf{D}_j = \text{diag}(8000, 1, 1, 0.2, 0.2, 0.1, 0.03)$	$\mathbf{M}_p = \text{diag}(3.5, 3.5, 6) \text{ kg}$ $\mathbf{M}_o = \text{diag}(0.008, 0.04, 0.03) \text{ kgm}^2$
	CT	$\mathbf{K}_{ct} = \text{diag}(400, 1000, 1000, 500, 1500, 1500, 1500)$ $\mathbf{D}_{ct} = \text{diag}(40, 63.3, 63.3, 44.7, 77.5, 77.5, 77.5)$	$\mathbf{M}_p = \text{diag}(2.5, 3, 3) \text{ kg}$ $\mathbf{M}_o = \text{diag}(0.0015, 0.02, 0.02) \text{ kgm}^2$
Partitioned inverse kinematics $\mathbf{W}^{\frac{1}{2}} = \text{diag}(3, 0.2, 1, 0.1)$ $\mu_{\text{rot}} = -1$	IJC	$\mathbf{K}_j = \text{diag}(80000, 16, 14, 2, 3, 1.8, 0.5)$ $\mathbf{D}_j = \text{diag}(8000, 1, 1, 0.2, 0.2, 0.1, 0.03)$	$\mathbf{M}_p = \text{diag}(4, 4, 6) \text{ kg}$ $\mathbf{M}_o = \text{diag}(0.01, 0.04, 0.03) \text{ kgm}^2$
	CT	$\mathbf{K}_{ct} = \text{diag}(400, 1000, 1000, 500, 1500, 1500, 1500)$ $\mathbf{D}_{ct} = \text{diag}(40, 63.3, 63.3, 44.7, 77.5, 77.5, 77.5)$	$\mathbf{M}_p = \text{diag}(2.5, 3, 3) \text{ kg}$ $\mathbf{M}_o = \text{diag}(0.0008, 0.01, 0.01) \text{ kgm}^2$

translational velocity of 0.64 m/s, a maximum translational acceleration of 8.27 m/s², a maximum rotational velocity of 2.77 rad/s, and a maximum rotational acceleration of 179 rad/s² can be achieved. Since pseudoinverse control doesn't allow a reference input on the position level, the derivative of the above presented step has been used.

The experiment was carried out for two different inverse kinematics (inverse function and partitioned inverse kinematics) and two different motion controllers (IJC and CT scheme). For the motion controllers the control parameters introduced in Table 2.3 were used.

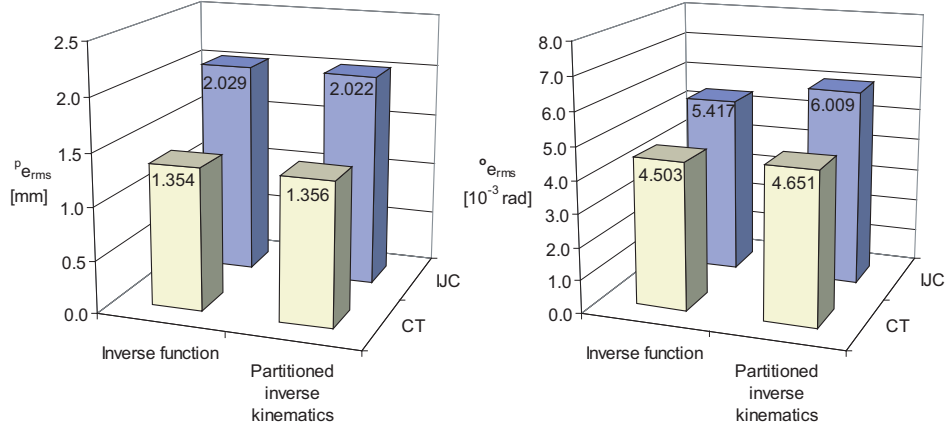


Figure 2.21: Position tracking performance: translational and rotational root mean square tracking error

For each controller, the translational root-mean-square (RMS) error ${}^p e_{rms}$ can be computed as follows:

$${}^p e_{rms} = \sqrt{\frac{\sum_{i=0}^N |{}^p \mathbf{e}_i|^2}{N}} = \sqrt{\frac{\sum_{i=0}^N |\mathbf{x}_{ti} - \mathbf{x}_{mi}|^2}{N}}, \quad (2.23)$$

where \mathbf{x}_{ti} , \mathbf{x}_{mi} are the target and measured Cartesian position at the time step i and N denotes the total number of time steps.

The rotational error for one time step is given by the vector part $\boldsymbol{\varepsilon}$ of the Quaternion $\mathbf{Q}_{tm} = [\eta_{tm}, \boldsymbol{\varepsilon}_{tm}]$ that describes the rotation between the target and measured frame

$$\mathbf{Q}_{tm} = \mathbf{Q}_m^{-1} * \mathbf{Q}_t. \quad (2.24)$$

Taking this into account the rotational RMS error is given by

$${}^o e_{rms} = \sqrt{\frac{\sum_{i=0}^N |{}^o \mathbf{e}_i|^2}{N}} = \sqrt{\frac{\sum_{i=0}^N |\boldsymbol{\varepsilon}_{tm}|^2}{N}}. \quad (2.25)$$

The translational error ${}^p \mathbf{e}_i = (e_{xi}, e_{yi}, e_{zi})$ consists of three components, which describe the error in x , y , and z direction. The decomposed RMS tracking error for each axis, see Fig. 2.22, is then defined as follows:

$${}^{px} e_{rms} = \sqrt{\frac{\sum_{i=1}^N e_{xi}^2}{N}}, \quad {}^{py} e_{rms} = \sqrt{\frac{\sum_{i=1}^N e_{yi}^2}{N}}, \quad {}^{pz} e_{rms} = \sqrt{\frac{\sum_{i=1}^N e_{zi}^2}{N}}. \quad (2.26)$$

The same holds for the decomposed tracking errors of the rotational part ${}^{ox}e_{rms}$, ${}^{oy}e_{rms}$, and ${}^{oz}e_{rms}$.

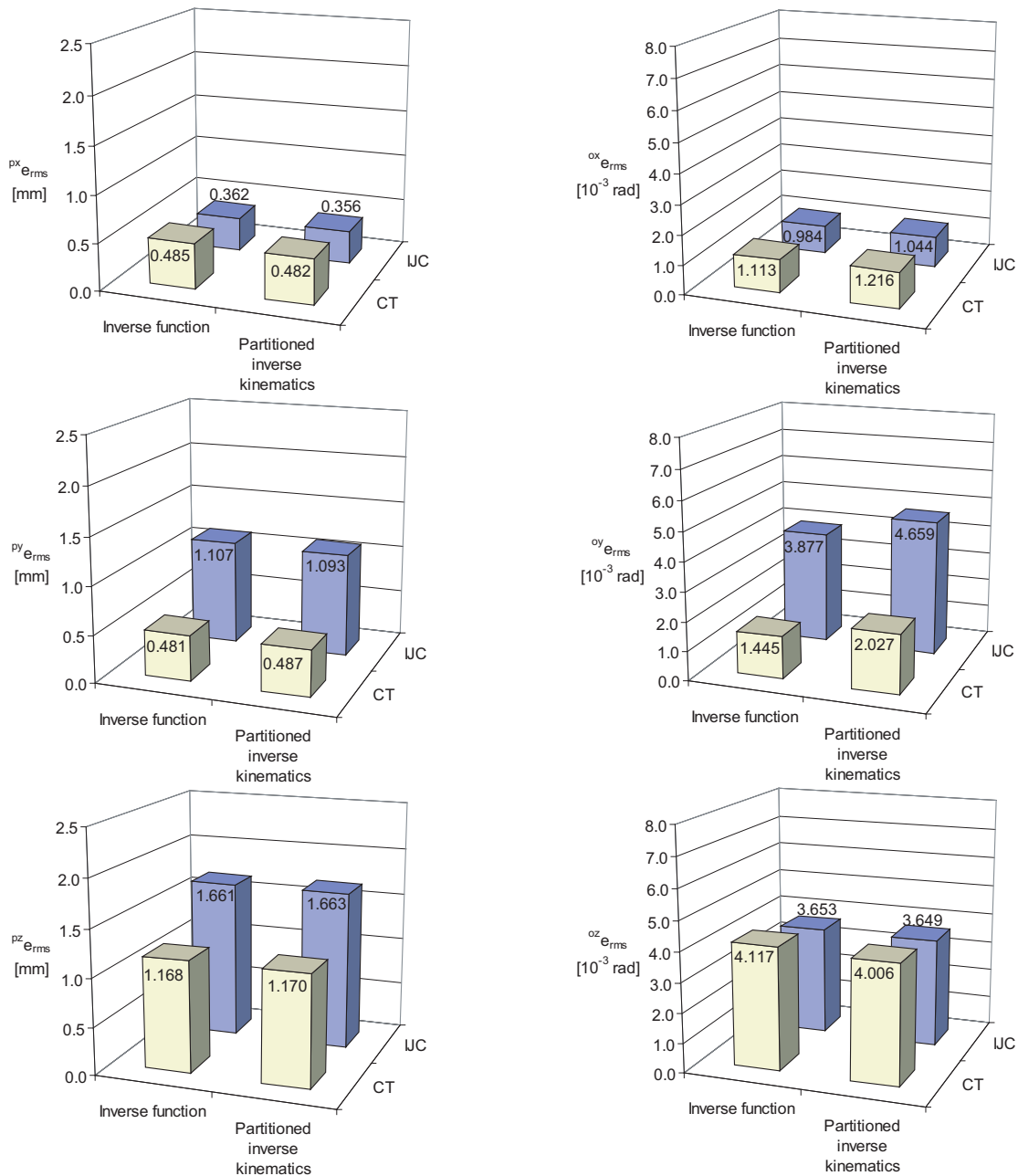


Figure 2.22: Position tracking performance: decomposed root mean square tracking error

As can be seen, the tracking error does not depend on the inverse kinematics, but varies with the motion controller used. For the translational part in general smaller deviations can be observed when using the pseudoinverse controller than when using an independent joint controller. This is due to the smaller transient and steady-state errors of the CT-controller, which are a result of the compensated cross couplings between the linkages and the gravity compensation. For the rotational part the differences between the motion controllers are not so big, as the masses of the rotational part of the robot are small compared to the translational part. It should be noted that the obtained results cannot be ascribed to

differences in the stiffness of both controllers since the experiment was carried out in the vicinity of the working position and the two joint space motion controllers were tuned to have the same joint angle step response.

The second experiment makes a comparison between the target impedance specified in the virtual environment and the rendered impedance, which can be felt by the human operator. In this experiment linear target impedances (mass-spring-damper systems), ranging from free space to hard contact, are implemented. In order to identify the displayed impedance force and position are measured and the rendered impedance is estimated by using the *System Identification Toolbox* of *Matlab/Simulink*. Two different identification conditions are distinguished: A free space experiment to identify the displayed mass and damping coefficients and a contact experiment, which is used to identify the rendered stiffness of the device. It should be noted that the identification of dynamical parameters requires persistent excitation and a good signal-to-noise ratio. This means that high velocities and accelerations with different frequencies have to be applied.

In the free space experiment, different values for mass and damping coefficient are set (no stiffness), and the human operator is asked to interact with this virtual impedance by moving the end-effector with different amplitudes and frequencies. In this experiment, the force and joint velocity (calculated by differentiating the measured position) are used for estimation. In order to reduce the measurements only results for impedances measured in x -direction are reported. The corresponding results are shown in Table 2.4. Since the inverse kinematics for the translational part is unique for the *inverse function* and *partitioned inverse kinematics* solution, measurements are only taken for different kind of motion controllers, namely the IJCs and CT scheme with and without acceleration feedforward. The same control parameters as mentioned in Table 2.3 were used.

The fidelity factor ζ describes the relationship between the apparent impedance and the impedance specified in the virtual environment, e.g., for the damping fidelity ζ_b the following equation holds:

$$\zeta_b = 1 - \frac{|b_t - b_i|}{b_t} \quad (2.37)$$

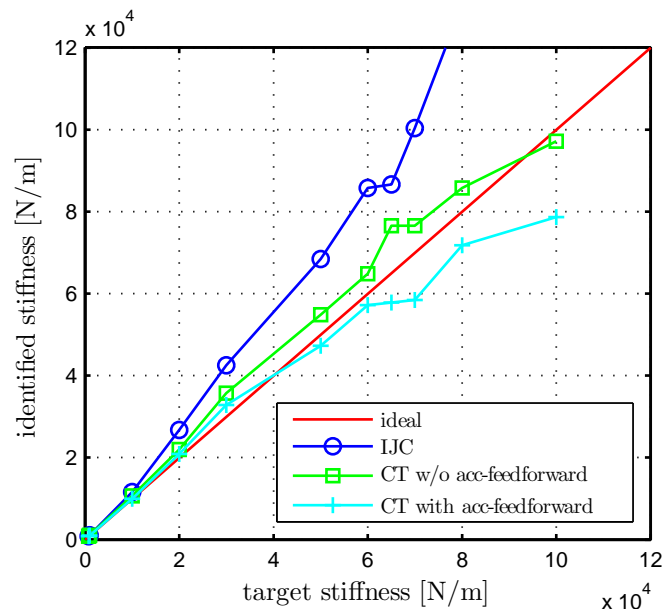
where b_t and b_i mean the target and identified damping coefficient.

The measurement results indicate good impedance fidelity of the device, values above 0.9 can be reached for all kind of motion controllers. In general, the IJCs show a better impedance fidelity than the controller based on CT scheme. Finally, it should be noted that due to the high noise in the velocity signal (velocity is derived by simply differentiating the position measurement) and the consequential bad signal-to-noise ratio, no identification results for free space motion (zero damping and small mass) could be obtained. Usage of low-pass filters could reduce this noise, but the introduced time constant would distort the result of the parameter identification. In order to be able to identify such impedances, a velocity and/or an acceleration sensor would be necessary.

The contact experiment aims at identifying the rendered stiffness of the device. This can be realized by implementing virtual walls with different stiffnesses and forcing the robot to push against this wall. In a steady-state condition the apparent stiffness can then be identified as a zero order impedance by measuring the applied force and the resulting displacement of the device. Since the human operator is not able to provide a constant input force, the necessary force is commanded by using \mathbf{h}_d (see Sec. 2.3) as desired value. All measurements were carried out with a force of 30 N in negative x_N -direction. Fig. 2.23 shows the corresponding measurement results.

Table 2.4: Mass and damping fidelity

Motion Control	target impedance		identified impedance		fidelity	
	b_t [Nm/s]	m_t [kg]	b_i [Nm/s]	m_i [kg]	ζ_b	ζ_m
IJC	10	5	9.057	5.135	0.094	0.973
	20	5	19.165	5.137	1.042	0.973
	50	5	49.346	5.201	1.013	0.960
	100	5	96.154	4.944	1.038	1.011
	20	10	18.978	10.448	1.051	0.955
	20	20	18.745	21.564	1.063	0.922
	20	50	21.617	58.645	0.919	0.827
CT	10	5	7.946	5.295	1.205	0.941
	20	5	18.634	5.414	1.068	0.917
	50	5	49.012	5.814	1.020	0.837
	100	5	100.910	6.778	0.991	0.644
	20	10	17.573	10.603	1.121	0.940
	20	20	14.794	21.353	1.260	0.932
	20	50	14.336	51.715	1.283	0.966


Figure 2.23: Stiffness fidelity

In this experiment, the controller with CT scheme shows a significantly better impedance fidelity than the IJCs with the same joint angle step response. Moreover, differences between the CT-controller with and without acceleration feedforward can be observed. In general, the best result could be achieved by using a CT-controller with acceleration feedforward. Allowing a maximum error of 5 % the maximum displayable stiffness for this controller is given by 65 000 N/m. Stiffnesses beyond these values cannot be displayed with an adequate precision and should be omitted.

Summarizing, the control based on CT scheme shows the best performance concerning the position tracking fidelity and the stiffness fidelity of the device. Furthermore, this controller allows to significantly reduce the minimal mass, which is necessary for stability, so that the rendering of free space motion is improved. Concerning the stiffness fidelity of the device, subjects who interacted with it, also reported a more realistic impression of stiff walls. This might be ascribed to a better performance during transient phases, which occur, e.g., in the moment of contact with a virtual wall [79]. This, again, can be explained by an increased bandwidth of the overall system due to the feed forward term in the controller.

2.7 Discussion

In this chapter a concept for a new mobile haptic interface has been developed, that allows bimanual 6 DOF manipulations in large remote environments. According to the formulated requirements, a modular system has been proposed which consists of independently designed and controlled components, namely two haptic interfaces and a mobile platform. Coupling of these two components by solving an optimization task allows extension of the workspace of the device to very large scale environments. Depending on the kinematic configuration of the manipulators, this can be done either offline or has to be performed in real time. In this work, an appropriate design and inverse kinematics of the haptic interfaces is described which assures a decoupling of translational from rotational movements and thus simplifies this optimization task significantly. Two types of inverse kinematics, an inverse function and a partitioned inverse kinematic solution have been presented, which realize this behavior.

One of the main requirements on the interaction with a haptic interface is stability of the overall system, independent of changing human operator behavior. In this work, an admittance control strategy has been applied and stability of the haptic interface has been analyzed by evaluating asymptotic stability. On this account, simple linear models for human operator as well as for haptic interface were assumed. The results indicate that a minimal target inertia has to be implemented to guarantee stability. Moreover, a strong dependency on the human arm impedance could be observed, whereby higher impedances potentially cause instability of the system. Finally, also a negative effect of the force/torque filter time constant on stability was found.

In contrast to other haptic interfaces presented in the literature, the new developed systems have been intensively evaluated and a huge number of performance indexes have been determined by either model-based or measurement-based performance evaluation. The following performance measures were analyzed in detail: dextrous workspace, output capability (maximum peak and continuous force, maximum velocity, maximum acceleration, maximum payload) and backdrivability.

Finally, the mechatronic device performance was analyzed by means of the Cartesian position tracking performance and the impedance display fidelity. The evaluation results show different position tracking performances and impedance display fidelities depending on the type of motion controller used. Two different motion controllers were analyzed in this work: an independent joint controller and a controller based on computed torque scheme. Using motion controllers with equal joint angle step response, in general better results could be achieved with the computed torque controller. It should be noted

that even though the computed torque controller showed a smaller position tracking error, smaller minimal inertias could be implemented, which results in a better free space performance. Concerning the impedance display fidelity and the position tracking performance, of course better results could be achieved with a stiffer independent joint controller, but this would result in higher values for the minimal inertia that can be implemented. As a consequence, rendering of free space motion becomes even more difficult. The computed torque controller, however, seems to be able to realize a good impedance display fidelity in the two extremes a) contact and b) free space motion, and thus, it is more appropriate for admittance-type haptic interfaces.

The new developed haptic interfaces represent only one part of the overall teleoperation system. In the next chapter other components and their integration into a high fidelity teleoperation system are described.

3 Development of Integrated Teleoperation Systems

In the prior section the focus was on the development of a novel haptic interface, which allows performance of manipulation tasks in large remote environments. Hereby, mainly interactions of the human operator with the device itself and some virtual introduced dynamics were studied. This chapter aims at extending the presented system to a highly integrated multi-modal teleoperation system, which allows the interaction with *real* remote environments.

In a typical teleoperation system, a human operator interacts with a human-system interface and controls a remotely located teleoperator. This teleoperator again interacts with the remote environment and executes the manipulation task. One of the main efforts of this thesis is the development of an intuitive teleoperation system, which does not restrict the human operator in performing manipulations and requires only minor adaptations of the user to the technical system. This can be achieved by building a teleoperation system, which mimicks the anthropomorphic manipulation capabilities of a human being. In this chapter, mechatronic design requirements on such a system are formulated.

In contrast to state-of-the-art teleoperation systems that cannot meet all the formulated requirements at the same time, a newly developed, highly integrated teleoperation system of superior performance is presented. This system allows to perform 6 DOF tele-assembling and tele-manipulation tasks. On this account, different components for visual, auditory, and haptic feedback are integrated into one single teleoperation system. Providing such multi-modal feedback increases the feeling of telepresence and thus simplifies the interaction with the remote environment. A detailed description of all necessary components is given and their integration into the teleoperation system is described. The overall system is assembled of components built in preceding works, commercially available components as well as new developed systems.

In Sec. 3.1.1 requirements on a high quality teleoperation system are formulated. Sec. 3.1.2 reviews state-of-the-art teleoperation systems and clearly shows their deficiencies. The new developed, highly integrated teleoperation system is presented in Sec. 3.1.3. Due to the high complexity, components for multi-fingered teleoperation are presented in a separate section. Beside device descriptions Sec. 3.2 focuses on implemented position and force mappings, which allow for mapping between human hand and used robotic grippers. Finally Sec. 3.4 is devoted to a linear one DOF teleoperation system, which has been developed to study principle effects in teleoperation systems.

3.1 Bimanual Teleoperation System with 6 DOF

Telepresence systems can be used to perform tasks in distant, dangerous or hardly accessible environments. Many application scenarios like disaster operations, rescue and maintenance tasks require highly dextrous manipulations. In order to avoid operator fatigue and

to ease the interaction with the technical system, this thesis aims at developing a teleoperation system which is able to mimic human manipulation capabilities when performing bimanual 6 DOF tele-assembling and tele-manipulation tasks. Hereby, the manipulation of stiff objects such as tubes, handwheels, and metal parts of several kind and the usage of tools like screwdrivers and pincers is envisaged.

3.1.1 Requirements on Teleoperation System

Typical mechatronic requirements on such a teleoperation system can be formulated as follows:

Workspace: The workspace of a teleoperation system is defined by the number of degrees of freedom and the operating domain of the haptic interface as well as the teleoperator. Typically the size of the workspace is restricted by construction or/and by kinematic or algebraic singularities. Hereby, kinematic singularities result from the selected kinematical design and algebraic singularities depend on the chosen orientation representation. If devices with different kinematical design are used in one teleoperation setup, the overall workspace is given by the intersection of the dextrous workspaces of the single devices. Hereby master and slave devices do not necessarily have to be of the same size: If devices with different workspace sizes are used, motions and feedback forces need to be scaled appropriately. In case the workspace of the slave exceeds the workspace of the master device, indexing and shifting techniques can be applied. But these techniques are mostly unintuitive, time consuming and fatiguing.

Depending on the actual application, different requirements on the workspace of a teleoperation system can be formulated. In view of the above presented application scenario haptic interfaces as well as telemanipulators are required, which enable manipulations in 6 DOF and have a workspace of the human arm reach so that fatiguing indexing and shifting techniques can be avoided. The workspace should be further free of singularities. Finally, also bimanual manipulation tasks should be possible. On this account devices for left and right hand must be provided, whereby the corresponding workspaces must intersect with each other.

Displayable stiffness: Since the application scenario foresees handling of stiff objects, one of the main requirements is the ability to display stiff remote environments. Boundaries for the maximum displayable stiffness are hereby given by the mechanical rigidity of the single devices as well as by the control architecture used for teleoperation (for the latter see chapter 4 for details).

Extensibility: If the teleoperation system should be used to perform dextrous manipulation tasks, a high payload of the robotic arms is required to mount task specific end-effectors. Such end-effectors include e.g. an exoskeleton or data glove system for the human hand at the master side and a robotic gripper or hand at the slave side.

Kinematical design: According to [56] self-identification with an avatar and thus the feeling of telepresence increases with the similarity of the visual appearance of avatar and human operator. Moreover, the mapping of human operator movements to teleoperator

movements plays an important role for the feeling of telepresence. The better the mapping, the better the feeling of telepresence, because the human operator does not have to think about how to create control actions [91]. Taking this into account, an anthropomorphic kinematic design and a human-scaled workspace of the telemanipulator are required.

Multimodality: The human operator perceives its own body and the surrounding environment via multiple sources of sensory information. This sensory information, derived from different modalities, converges into one multi-modal percept of body and environment [43]. The more sensory information is provided, the more reliable is the percept and thus the more realistic is the impression of the remote environment. On this account different kinds of sensory information should be provided to the human operator. This includes basically visual, auditory, and haptic information.

In the following subsection state-of-the-art teleoperation systems are analyzed with respect to these requirements.

3.1.2 State-of-the-Art Teleoperation Systems

Although many teleoperation systems exist nowadays, they exhibit severe limitations of different kinds: limited degrees of freedom, limited workspace (due to small constructions of haptic input device or telemanipulator, or due to kinematic or algebraic singularities which restrict the size of the workspace), the necessity of indexing/shifting techniques, the disability to display stiff environments, as well as lacking possibilities to mount task specific end-effectors.

The literature provides a considerable number of teleoperation systems, which are limited to a few degrees of freedoms and/or relatively small workspace, so that full spatial immersion is not achieved. Only a few more advanced telemanipulation systems operating in 6 DOF and using a telemanipulator with human scaled workspace are known. In [27, 54] a teleoperation system with 6 DOF haptic interfaces and telemanipulators is presented. The haptic interfaces provide only a small workspace so that indexing and shifting techniques are necessary, which are unnatural and fatiguing to the operator. Moreover, due to the missing redundancy in the system, singularities cannot be avoided by changing the internal configuration of the manipulators, so that the motion of the device must be constrained and the workspace is reduced. Finally, the structure of the telemanipulators is also not anthropomorphic, as classical industrial robots are used. In [140] a combination of a 6 DOF haptic interface and a 7 DOF telemanipulator is used. While the haptic input device is designed in such a way that kinematic singularities can be omitted, it is not clear how the telemanipulator redundancy is used to handle kinematic singularities at the remote site. Because of the small workspace of the haptic input device, even in this approach, indexing and shifting techniques are required. Finally, [24] as well as [53, 123] deal with a teleoperation system with 7 DOF exoskeletons used as haptic input devices and 7 DOF humanoid telemanipulators. But as reported in [109], working with exoskeletons is very fatiguing since the entire range of human arm movements is restricted, and/or long time operations are not possible because of the high weight of the system. In addition, mounting of application specific end-effectors is extremely difficult.

Thus at present, no teleoperation system which meets all the above presented requirements, namely a human-scaled workspace free of kinematic and algebraic singularities, the possibility to operate in full 6 DOF using the redundancy of the human arm, the possibility

to mount task specific end-effectors, as well as the capability to display stiff environments, is known. On this account a new teleoperation system of superior performance has been developed.

3.1.3 System Description

The developed integrated teleoperation system is depicted in Fig. 3.1. It consists of devices for visual and haptic feedback and allows telemanipulation with two arms in full 6 DOF. The single components are further on described in detail:

Teleoperation Master and Slave Devices

Accomplishing complex telemanipulation tasks requires master and slave devices, which allow manipulation in full 6 DOF. The corresponding hardware solutions are presented below:

Haptic Interface: In order to enable intuitive telemanipulation and to meet the requirements mentioned above, an adequate haptic interface is required. Two different hardware solutions as shown in Fig. 3.1 and 3.2 are used in this work: the redundant haptic interface VISHARD7 presented in chapter 2, as well as the hyper-redundant haptic interface VISHARD10 [127, 129]. Both devices are characterized by a very large workspace free of singularities, a high payload capability to accommodate various application specific end-effectors, foreseen redundancy to avoid kinematic singularities and user interferences and the possibility for dual-arm haptic interaction with full 6 DOF.

Telemanipulator: As reported above, an intuitive teleoperation requires an anthropomorphic telemanipulator design. Since it is well known that the superior manipulation-dexterity of humans is a result of the kinematic redundancy of their arms, an anthropomorphic bimanual redundant telemanipulator developed by [120, 121] is used in this work, see Fig. 3.1. It consists of two identical, human-scaled arms, whereby each arm further consists of two spherical joints with 3 DOF at shoulder and wrist, and one revolute joint at the elbow.

Stereo-Vision System

Visual feedback is provided by using a stereo-vision system. The stereo-vision system consists of two CCD firewire cameras placed on a 3 DOF pan-tilt-roll head, see [13] for more details. The video streams are recorded, transmitted to the master site and displayed either on a head mounted display (HMD; NVIS nVisor SX, resolution 1280 x 1024) carried by the human operator or on a stereo projection wall by using a stereo-projection system. In the latter case, the human operator has to wear 3D-glasses to get a 3D impression [126]. Efficient low-latency real-time video is made possible by the usage of a UDP-based, MPEG-4-compressed transmission approach using the XviD-codec. Requesting independently encoded frames in case of packet loss on the network ensures error resilience. The HMD is additionally equipped with a built-in tracker (MotionStar or IS900), which is used for controlling the camera head motion, so that the user can look around in the remote environment just by turning his/her own head.

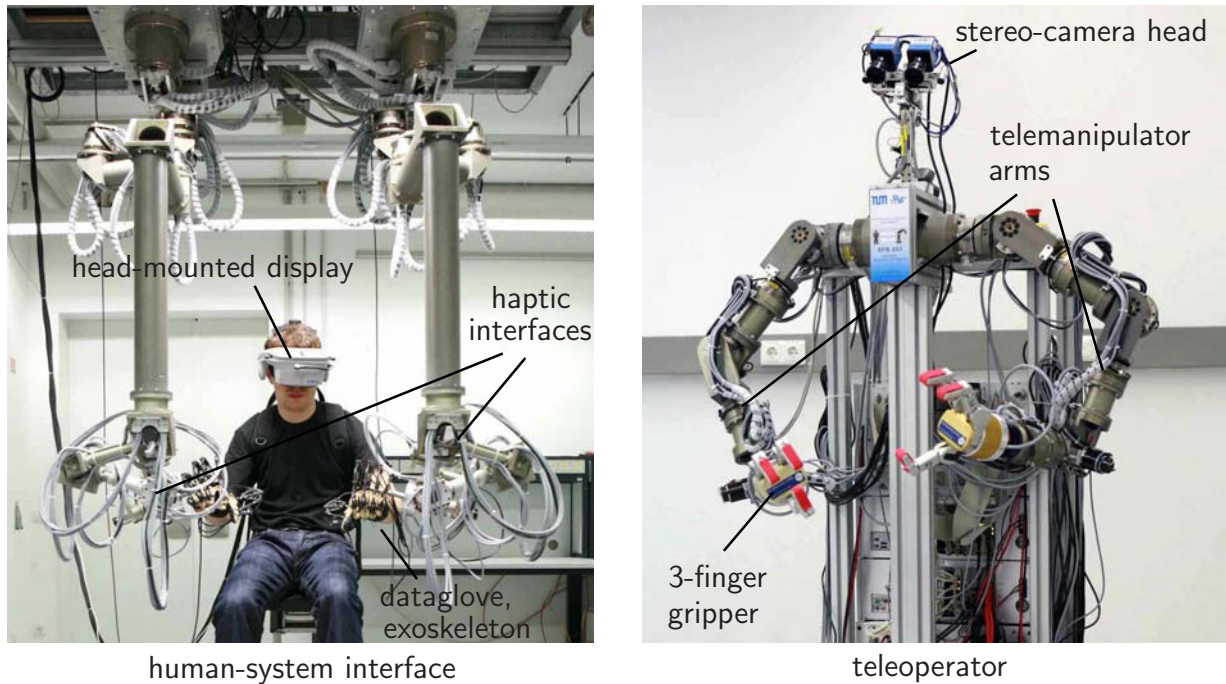


Figure 3.1: Bimanual teleoperation system using VISHARD10 as haptic interface and dual arm telemanipulator

Audio System

To capture audio data, two microphones are installed in the stereo-camera head of the teleoperator. As audio transmission systems are already rather advanced, a free available VoIP software is used to provide audio information to the human operator. Using a real-time 3D sound synthesis algorithm for spatial audio reproduction the degree of immersion can be further increased, see [66, 67] for more details.

The so far described teleoperation system allows exploration of the remote environment and execution of very simple manipulation tasks as e.g. pushing an object. To also perform fine and dextrous manipulations, multi-fingered interaction with the remote environment is necessary. On this account, a multi-fingered teleoperation system has been developed and also integrated in the overall teleoperation system.

3.2 Multi-Fingered Teleoperation System

If dextrous telemanipulation tasks are required, the telemanipulator is additionally equipped with robotic grippers or robot hands, which must be controlled by the human operator. In the following, the developed multi-fingered teleoperation system is described in detail.

3.2.1 System Description

In order to perform complex manipulation tasks a multi-fingered telemanipulation system consisting of three-finger robotic grippers (BarrettHand), datagloves (CyberGlove) and

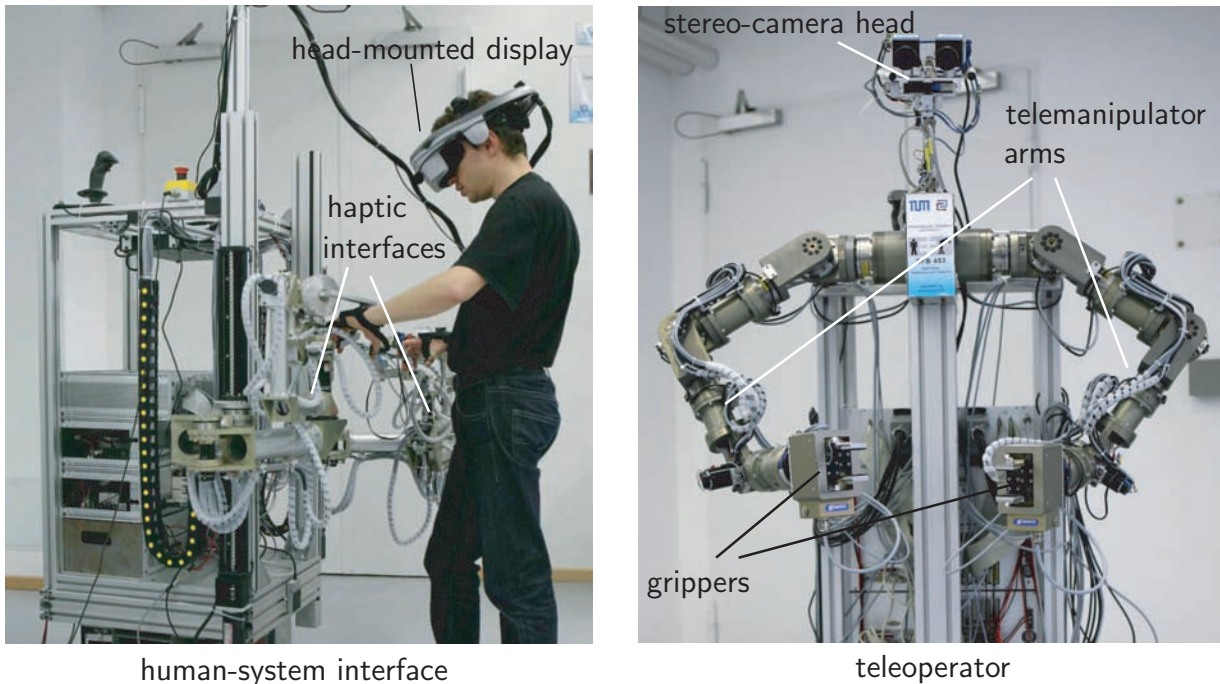


Figure 3.2: Bimanual teleoperation system using VISHARD7 as haptic interface and dual arm telemanipulator

exoskeletons (CyberGrasp) has been developed. The usage of universal grippers allows operation in highly variable, unstructured, unknown or dynamic working environments. As a part of a telemanipulation system, the grippers are controlled by a human operator. On this account human hand and finger motions are measured using a data glove system and then mapped to the grippers. Sensed interaction forces are fed back to the operator and displayed through a haptic display, an exoskeleton. Since human hand and grippers have different kinematic structures, appropriate mappings for forces and motion between the finger and the gripper are required. Fig. 3.3 shows the resulting system architecture. Below their components are presented in detail.

Grippers

A *BarrettHand* (BH) from Barrett Technology Inc. is used as gripper, see [1]. The BarrettHand has three fingers with four actuated degrees of freedom. Each finger consists of two coupled joints driven by a single dc brushless servo motor. In addition, two fingers can rotate synchronously and symmetrically around the base joint in a spreading action. Each finger is equipped with a strain gage joint torque sensor, for measuring the torque externally applied about the distal joint over a range of ± 1 Nm. Real time operation of the motors is assured by a low level velocity controller. The high level controllers, as e.g. position control, are realized on the PC using MATLAB/Simulink Real-Time Workshop and RTAI Linux.

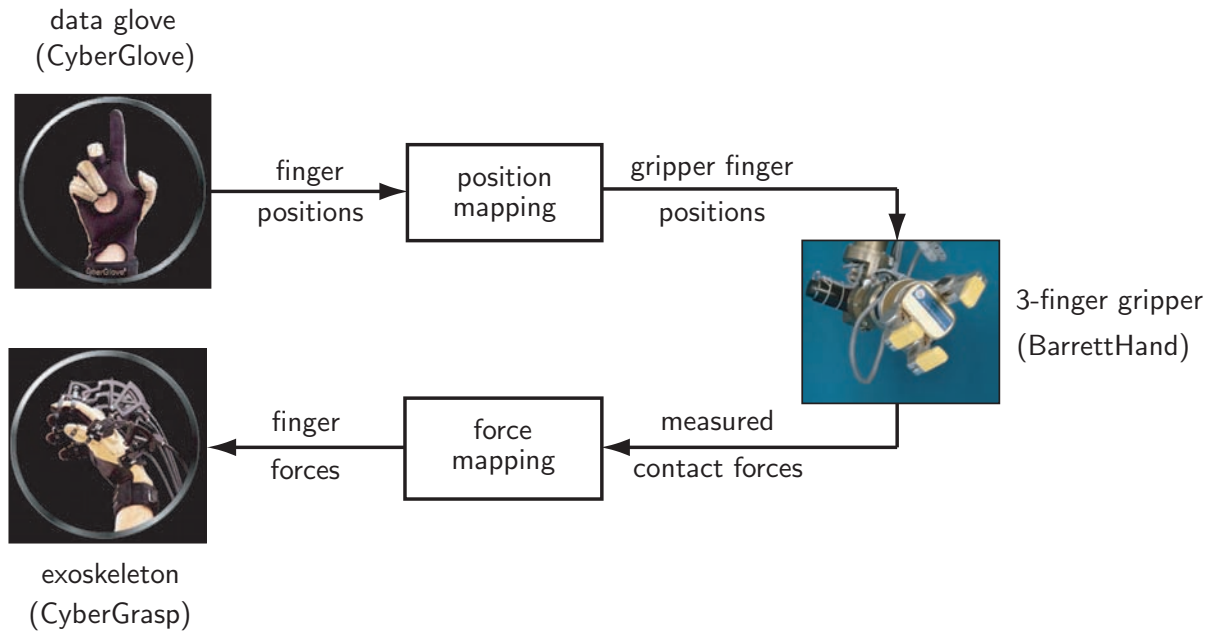


Figure 3.3: System architecture of multi-fingered telemanipulation system

Data Glove System

To capture finger and hand motions the data glove system *CyberGlove* from Immersion Corporation, see [3], is used. The data glove is equipped with 22 sensors located over or near the joints of the hand and the wrist. A resistive bend-sensing technology is used to transform hand and finger motions into real-time digital joint-angle data. In order to map human hand to robot hand motions, an appropriate position mapping has to be implemented.

Exoskeleton

In order to provide force feedback to the human operator the *CyberGrasp* system, an exoskeleton from Immersion Corporation, see [2], is used. The exoskeleton is attached to the back of the human hand and guides force-applying tendons to the user's fingertips. Desired force values are sent to the local force controller provided by the manufacturer. Since each finger is only equipped with one tendon only pull but no push-forces can be applied. Similar to the position mapping algorithm, a force mapping algorithm is also necessary. In the following, these algorithms are described in more detail.

3.2.2 Position Mapping

As already mentioned above, in a multi-fingered telemanipulation system a kinematic mapping between human and robot hand motions is necessary. Commonly, the following three mapping methods can be distinguished: joint-to-joint mapping, pose mapping, and point-to-point mapping.

The joint-to-joint mapping (or joint angle mapping) is typically applied to telemanipulation systems with an anthropomorphic robot hand [76]. The similarity between human and robot hand kinematics allows simple mapping of the finger joint angles without any

further transformation. In some works, the similarity of human and robot hand motion is further achieved by restricting the human finger motions with an exoskeleton [138]. The joint-to-joint mapping is especially suitable for enveloping and power grasps. Unfortunately, many of the existing robot hands are not of anthropomorphic type and thus this method is not applicable.

The pose mapping tries to find robot hand poses, which can be correlated to human hand poses. In [98] a corresponding transformation matrix with human finger angles as input and robot joint angles as output has been derived; an interpolation algorithm is used when switching between the single poses. Recently, grasp identification methods based on neural networks have also been developed [137]. Dependent on the identified grasp, different types of predefined joint-to-joint mappings (which represent a special pose) are applied. [39] uses hidden markov models to identify the grasp type and a neural network to choose between predefined joint angle mappings.

Some sorts of pose mapping can also be found in the field of “programming-by-demonstration”. In [7] a nearest neighbor grasp recognition algorithm based on the analysis of the measured finger joint angles is presented. A joint-to-joint mapping is applied to generate different grasp patterns which are stored in a library and carried out if the corresponding grasp type is identified. In [37] firstly the grasp type is identified, then a correct grasp pose is chosen and a force-controlled grasping by closing the fingers is applied. In [65] finally a mapping method based on a virtual finger is presented.

Another type of pose mapping is based on the idea of object-action abstraction (see [15]), whereby the object to be manipulated and the action to be performed on this object have to be identified first. Then a set of predefined grasp types is applied. A learning algorithm finally extends this approach to unknown or slightly modified objects.

When applying one of the presented pose mappings for a telemanipulation system, the reliability and stability of the grasp identification process plays an important role. This is the case since in a telemanipulation scenario continuous identification of the human grasp type is necessary. A well known problem of the pose mapping is namely the unpredictable switching of the robot hand between different kind of grasp types, when small changes of the human hand posture occur. On this account only simple grasp postures can be realized and hence the method is applied in a limited way in telemanipulation systems.

The most common approach used for mapping of human to robot hand postures is the point-to-point or fingertip mapping, whereby the fingertip positions of the human hand are mapped to the robot fingertip positions [44, 59, 104]. In order to apply such an approach the computation of the forward kinematics of the human hand, the mapping of the fingertip positions, and finally the determination of the robot joint angles by applying the corresponding inverse kinematics are required. Such a mapping algorithm is appropriate to represent fingertip positions and is therefore commonly applied for precision grasps.

In the following two subsections a point-to-point mapping algorithm for the above presented multi-fingered telemanipulation system which allows to map fingertip motions of the human hand to a three-finger robotic gripper, the BarrettHand, is presented. Existing mapping algorithms for this gripper, see [15], allow only semi-autonomous teleoperation, whereby prior knowledge about the user’s intention and the object to be manipulated is used to select an appropriate grasp type, which is then executed autonomously. The reliability of this mapping algorithm depends strongly on the identification process of objects and the estimation of human’s intention. By contrast, the here presented mapping algorithm does not require any knowledge about size and form of objects or human’s intention.

This makes it more reliable as well as easier to understand and to predict. Moreover, no library with predefined grasp types is necessary.

Principle of Applied Position Mapping Algorithm

For the mapping of the human to robot hand motions, a point-to-point position mapping has been applied. The principle of the implemented algorithm is shown in Fig. 3.4. The already presented data glove system is used to measure the human finger joint angles. These angles, in combination with some prior knowledge about the human hand kinematics, are used to compute the fingertip positions of the human hand (FK). These fingertip positions again are mapped to fingertip positions of the robotic gripper. Finally, the motor joint angles of the BarrettHand are determined by using the corresponding inverse kinematics (IK). A detailed description of each component is given in the following.

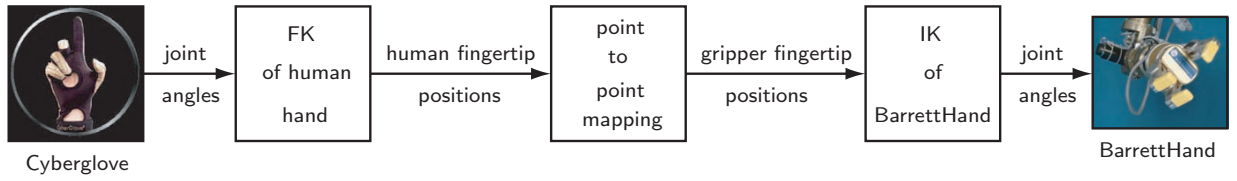


Figure 3.4: Scheme of position mapping

Kinematics of Human Hand

Fig. 3.5 shows the human hand kinematics. A finger is composed of a distal $l_{k,d}$, proximal $l_{k,p}$ and metacarpal $l_{k,m}$ link connected by the corresponding joint angles $q_{k,d}$, $q_{k,p}$, $q_{k,m}$ with $k = 1, \dots, 5$. The abduction is described by the joint angle $q_{k,a}$. According to this kinematic model the fingertip positions with respect to the hand coordinate system can be calculated as follows:

$${}^H \mathbf{x}_k(\mathbf{q}_k) = \mathbf{a}_k(\mathbf{q}_k) + \mathbf{r}_k \quad \text{with } k = 1, \dots, 5, \quad (3.1)$$

whereby $\mathbf{q}_k = [q_{k,d}, q_{k,p}, q_{k,m}, q_{k,a}]^T$ denotes the joint angles of the k-th finger and \mathbf{r}_k is a translation vector. The vectors $\mathbf{a}_k(\mathbf{q}_k)$ are defined as follows:

$$\mathbf{a}_k(\mathbf{q}_k) = \begin{bmatrix} \sin q_{k,a} (l_{k,m} \cos q_{k,m} + l_{k,p} \cos(q_{k,m} + q_{k,p}) + l_{k,d} \cos(q_{k,m} + q_{k,p} + q_{k,d})) \\ \cos q_{k,a} (l_{k,m} \cos q_{k,m} + l_{k,p} \cos(q_{k,m} + q_{k,p}) + l_{k,d} \cos(q_{k,m} + q_{k,p} + q_{k,d})) \\ l_{k,m} \sin q_{k,m} + l_{k,p} \sin(q_{k,m} + q_{k,p}) + l_{k,d} \sin(q_{k,m} + q_{k,p} + q_{k,d}) \end{bmatrix} \quad (3.2)$$

for the index, middle, ring finger and pinkie ($k = 2, \dots, 5$) and

$$\mathbf{a}_1(\mathbf{q}_k) = \begin{bmatrix} l_{1,d} (-\sin q_{1,m} \sin(q_{1,p} + q_{1,d}) + \cos q_{1,m} \cos \hat{q}_{1,a} \cos(q_{1,p} + q_{1,d})) \\ -\sin \hat{q}_{1,a} (l_{1,m} + l_{1,p} \cos q_{1,p} + l_{1,d} \cos(q_{1,p} + q_{1,d})) \\ -l_{1,d} (\sin q_{1,m} \cos \hat{q}_{1,a} \cos(q_{1,p} + q_{1,d}) + \cos q_{1,m} \sin(q_{1,p} + q_{1,d})) \end{bmatrix} + \begin{bmatrix} l_{1,p} (\cos q_{1,m} \cos \hat{q}_{1,a} \cos q_{1,p} - \sin q_{1,m} \sin q_{1,p}) + l_{1,m} \cos q_{1,m} \cos \hat{q}_{1,a} \\ 0 \\ -l_{1,p} (\sin q_{1,m} \cos \hat{q}_{1,a} \cos q_{1,p} + \cos q_{1,m} \sin q_{1,p}) - l_{1,m} \sin q_{1,m} \cos \hat{q}_{1,a} \end{bmatrix} \quad (3.3)$$

for the thumb ($k = 1$), whereby $\hat{q}_{1,a} = q_{1,a} + q_{1,a}^o$ with $q_{1,a}^o$ a joint angle offset.

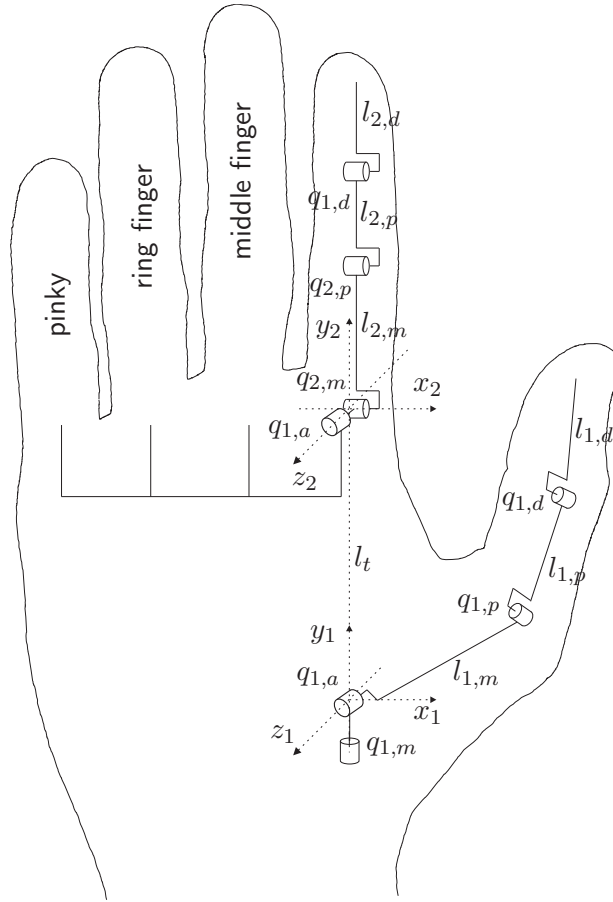


Figure 3.5: Kinematic model of the right human hand

Kinematics of BarrettHand

In this subsection some details about the BarrettHand kinematics are given, whereby all technical figures are taken from [14].

The BarrettHand is a gripper with three identical fingers. While the finger F3 is fixed to the carpus, the fingers F1 and F2 are able to rotate 180° around the base. Each finger consists of three links with the lengths l_1, l_2, l_3 and two joints with the joint angles $q_{Fk,2}$ and $q_{Fk,3}$, whereby the index Fk stands for the k -th finger. Fig. 3.6 shows a side view of the BarrettHand with all mentioned parameters. The fingers F1 and F3 are completely opened and finger F2 is flexed. The spread angle $q_{Fk,1}$ is shown in Fig. 3.7.

Since the BarrettHand fingers cannot be stretched completely, the joint angle $q_{Fk,2}$ is composed of a variable $\Theta_{Fk,2}$ and a constant part $\Phi_2 = 2.46^\circ$

$$q_{Fk,2} = \Theta_{Fk,2} + \Phi_2 \quad \text{with} \quad 0^\circ \leq \Theta_{Fk,2} \leq 140^\circ. \quad (3.4)$$

Similarly the joint angle $q_{Fk,3}$ is given by

$$q_{Fk,3} = \Theta_{Fk,3} + \Phi_3 \quad \text{with} \quad 0^\circ \leq \Theta_{Fk,3} \leq 48^\circ \quad \text{and} \quad \Phi_3 = 50^\circ. \quad (3.5)$$

The BarrettHand disposes of four actuators, one per finger plus one for the abduction. The relation between the four motor joints Θ_{M1} to Θ_{M4} and the variable part $\Theta_{Fk,i}$ of the

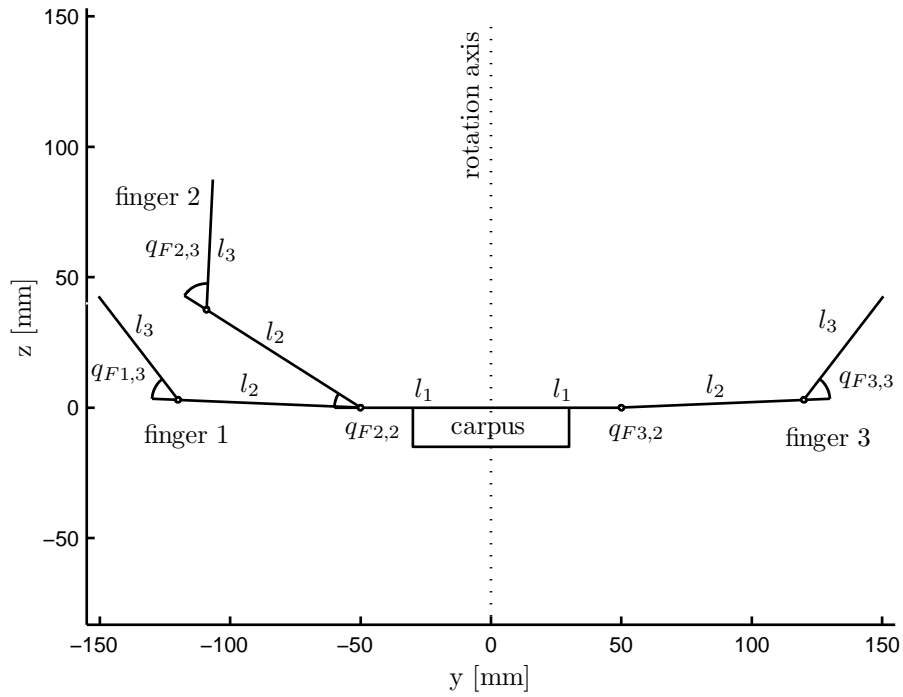


Figure 3.6: Side view of BarrettHand

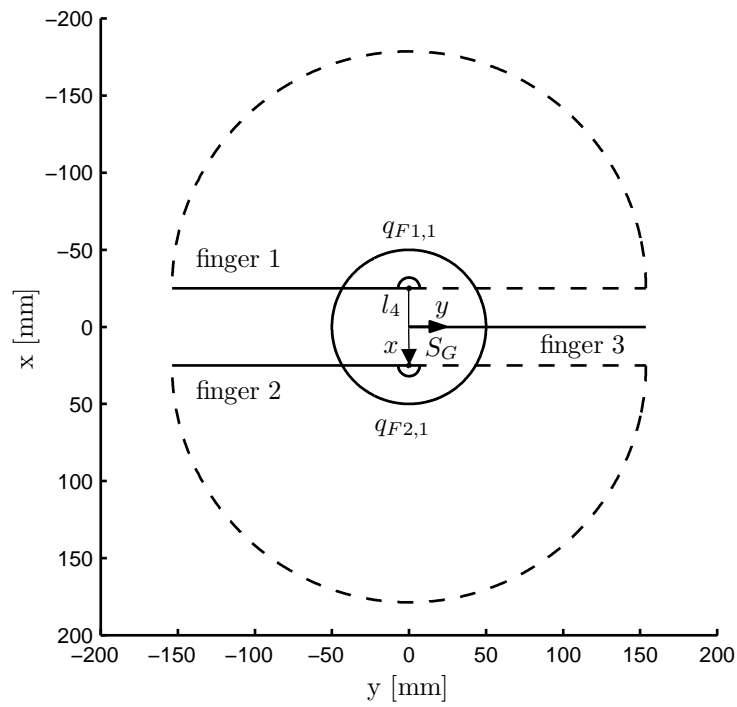


Figure 3.7: Top view of BarrettHand

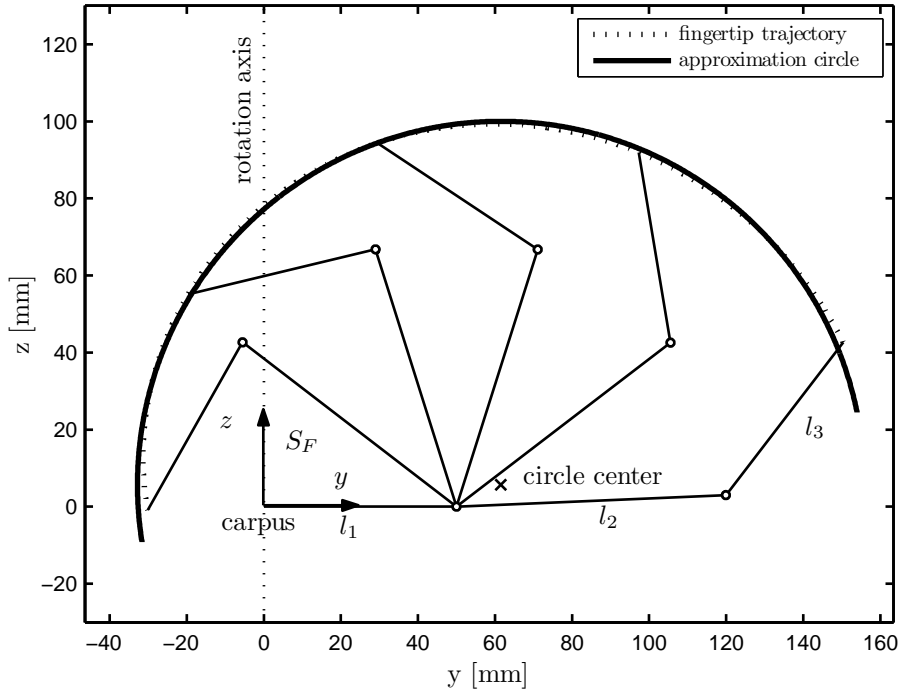


Figure 3.8: Trajectory of the gripper fingertips in the finger coordinate system

joint angles $q_{Fk,i}$ is described by the following equation:

$$\begin{bmatrix} \Theta_{F1,1} \\ \Theta_{F1,2} \\ \Theta_{F1,3} \\ \Theta_{F2,1} \\ \Theta_{F2,2} \\ \Theta_{F2,3} \\ \Theta_{F3,2} \\ \Theta_{F3,3} \end{bmatrix} = \begin{bmatrix} 0 & 0 & 0 & -2/35 \\ 1/125 & 0 & 0 & 0 \\ 1/375 & 0 & 0 & 0 \\ 0 & 0 & 0 & 2/35 \\ 0 & 1/125 & 0 & 0 \\ 0 & 1/375 & 0 & 0 \\ 0 & 0 & 1/125 & 0 \\ 0 & 0 & 1/375 & 0 \end{bmatrix} \cdot \begin{bmatrix} \Theta_{M1} \\ \Theta_{M2} \\ \Theta_{M3} \\ \Theta_{M4} \end{bmatrix} . \quad (3.6)$$

As can be seen from these equations, the two spread angles $q_{F1,1}$ and $q_{F2,1}$ are coupled and thus the following relationship holds:

$$q_{F1,1} = \Theta_{F1,1} = -\Theta_{F2,1} = -q_{F2,1} . \quad (3.7)$$

Also the joint angles $q_{Fk,2}$ and $q_{Fk,3}$ are coupled:

$$\Theta_{Fk,2} = 3\Theta_{Fk,3} , \quad (3.8)$$

$$q_{Fk,2} - \Phi_2 = 3(q_{Fk,3} - \Phi_3) . \quad (3.9)$$

These couplings have severe consequences, since the fingertips cannot be positioned in an arbitrary manner, but can only be moved along a certain trajectory. This trajectory is shown in Fig. 3.8.

Forward kinematics: The forward kinematics of the BarrettHand describes the Cartesian fingertip position ${}^G \mathbf{x}_k$ in the gripper coordinate system S_G as a function of the motor angles Θ_{M1} to Θ_{M4} . The fingertip position in the corresponding finger coordinate system S_F (see Fig. 3.8) is given by:

$${}^F \mathbf{x}_{Fk} = \begin{bmatrix} 0 \\ l_1 + l_2 \cos q_{Fk,2} + l_3 \cos(q_{Fk,2} + q_{Fk,3}) \\ l_2 \sin q_{Fk,2} + l_3 \sin(q_{Fk,2} + q_{Fk,3}) \end{bmatrix}. \quad (3.10)$$

To compute the Cartesian position in the gripper coordinate system, ${}^F \mathbf{x}_{Fk}$ must be multiplied by a rotation matrix \mathbf{R} and displaced by a translation vector \mathbf{t} :

$${}^G \mathbf{x}_{Fk} = \mathbf{R}(\gamma) {}^F \mathbf{x}_{Fk} + \mathbf{t}, \quad (3.11)$$

whereby

$$\mathbf{R}(\gamma) = \begin{bmatrix} \cos(\gamma) & \sin(\gamma) & 0 \\ -\sin(\gamma) & \cos(\gamma) & 0 \\ 0 & 0 & 1 \end{bmatrix}, \quad \gamma \in \{q_{F1,1}, -q_{F2,1}, \pi\}$$

and

$$\mathbf{t} = [jl_4, 0, 0]^T, \quad j \in \{-1, 1, 0\}$$

for the corresponding finger $\{F1, F2, F3\}$.

Inverse kinematics: For the BarrettHand an analytical inverse kinematics can be computed: In a first step the spread angle $q_{Fk,1}$ has to be determined. In order to do so the fingertip positions given in the gripper coordinate system S_G are transformed into an equal oriented coordinate system $S_{G'}$ with origin in the finger base point:

$${}^{G'} \mathbf{x}_{Fk} = {}^G \mathbf{x}_{Fk} - \mathbf{t}. \quad (3.12)$$

Given the fingertip position of F1 in this transformed coordinate system ${}^{G'} \mathbf{x}_{F1} = [x'_1, y'_1, z'_1]$, the joint angle $q_{F1,1}$ can be easily worked out:

$$q_{F1,1} = -\arctan \frac{x'_1}{y'_1}. \quad (3.13)$$

The motor angle Θ_{M4} can then be calculated by using (3.6) and (3.7).

Using the spread angle $q_{Fk,1}$, the Cartesian position in the finger coordinate system S_F can be computed by solving (3.11) for ${}^F \mathbf{x}_{Fk}$. Inserting these fingertip positions into

$$q_{Fk,3} = \arccos \left(\frac{(y_{Fk} - l_1)^2 + z_{Fk}^2 - l_2^2 - l_3^2}{2l_2l_3} \right), \quad (3.14)$$

$$q_{Fk,2} = \arccos \left(\frac{z_{Fk} (l_3 \sin q_{Fk,3}) + (y_{Fk} - l_1) (l_2 + l_3 \cos q_{Fk,3})}{(l_2 + l_3 \cos q_{Fk,3})^2 + l_3^2 \sin^2 q_{Fk,3}} \right) \quad (3.15)$$

the corresponding joint angles result. (3.14) and (3.15) are hereby determined when solving (3.10) for $q_{Fk,2}$ and $q_{Fk,3}$. Finally considering (3.4), (3.5) and (3.6) the motor joint angle Θ_{Mk} is given by

$$\Theta_{Mk} = 125 (q_{Fk,2} - \Phi_2) \frac{180}{\pi}, \quad \text{or} \quad (3.16)$$

$$\Theta_{Mk} = 375 (q_{Fk,3} - \Phi_3) \frac{180}{\pi}. \quad (3.17)$$

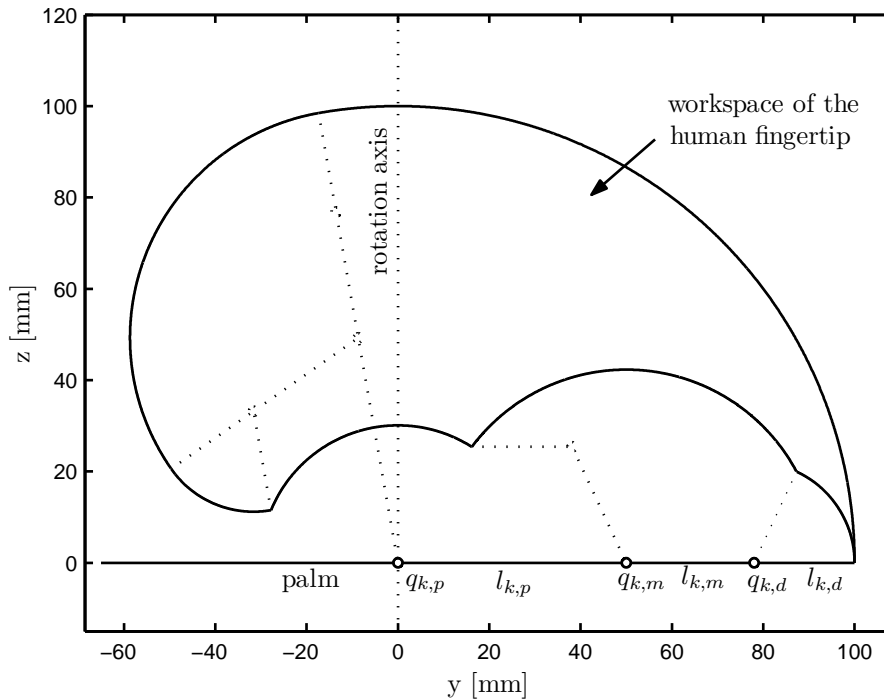


Figure 3.9: Workspace of a typical human finger in y-z-plane with the link lengths $l_m = 50\text{mm}$, $l_p = 28\text{mm}$, $l_d = 22\text{mm}$

If two different solutions are obtained, the desired position is not reachable with the BarrettHand.

Point-to-Point Mapping by Vertical Projection

Fig. 3.9 shows the workspace of a typical human finger. Since hyperextension is not important when grasping an object, for this drawing the minimal joint angles have been set to zero. The maximal considered joint angles have been taken from [36] and are reported in Table 3.1.

Table 3.1: Minimal and maximal joint angles of a human finger [36]

joint angles	q_m	q_p	q_d
minimal	0	0	0
maximal	100	115	65

Comparing the workspace of a human finger with that of a BarrettHand finger (as shown in Fig. 3.8) one can see that the human fingertip position has to be projected onto a trajectory feasible with the BarrettHand. The drawback of this method is obvious: different positions of the human fingertip are mapped onto the same fingertip position of the robotic gripper. This is the case because of the prior presented couplings of the BarrettHand joint angles. A possible projection method is presented in the following paragraphs:

In the first step, each BarrettHand finger must be assigned to a human finger. Since F3 of the BarrettHand is opposed to F1 and F2, this finger is mapped to the thumb. Considering the right hand, F1 is used to map the index finger. For F2 either middle finger, ring finger or pinky can be selected. Since the pinky does not play an important role in manipulations, typically the middle or ring finger is mapped. As the range of abduction of the BarrettHand is quite huge, the ring finger is selected.

The proposed position mapping algorithm adapts the workspace of the human fingers to the workspace of the BarrettHand by using a scaling factor. For simplicity, a simple scalar scaling factor g_p is used. Then, the workspace of the human fingers is vertically projected onto the trajectory of the BarrettHand. Fig. 3.10 shows the workspace of the human finger, the workspace of the BarrettHand, as well as the projection principle. For the sake of clarity, the workspace of the human finger is drawn above the BarrettHand trajectory.

Aligning the rotation axis of the human index finger and one of the BarrettHand fingers, the abduction angle to be set for the gripper can be easily determined from the abduction angles of the human hand. Given the abduction between index and middle finger $q_{2,a}$ and between middle and ring finger $q_{3,a}$, the abduction angle for the BarrettHand is defined as follows

$$q_{F1,1} = -q_{F2,1} = \frac{1}{2}(q_{2,a} + q_{3,a}) \quad . \quad (3.18)$$

The factor 1/2 results from the fact that the angle between F1 and F2 of the BarrettHand is given by $2q_{Fk,1}$.

The adaptation of the human hand workspace to the BarrettHand workspace is realized by a scaling factor g_p . Hereby, the ratio of maximally opened human and BarrettHand finger is used. For the index and ring finger the scaling factor is given by

$$g_{p_k} = \frac{l_1 + l_2 \cos \Phi_2 + l_3 \cos (\Phi_2 + \Phi_3)}{(l_{k,m} + l_{k,p} + l_{k,d})} \quad \text{for } k = 1, 2 \quad (3.19)$$

and for the thumb by

$$g_{p_3} = \frac{l_1 + l_2 \cos \Phi_2 + l_3 \cos (\Phi_2 + \Phi_3)}{l_t} \quad . \quad (3.20)$$

To finally project the finger position on the BarrettHand trajectory the motor angles for a given y -coordinate of the scaled human hand position have to be computed. Since the inverse kinematics given by (3.14) and (3.15) requires the knowledge of the y and z -coordinate of the BarrettHand finger, the corresponding z -coordinate has to be determined first. As without knowledge of the single joint angles it is not possible to compute the z -coordinate of the BarrettHand finger if the y -coordinate is given, the trajectory of the BarrettHand is approximated by a circle as shown in Fig. 3.8. Except for the two extreme positions, the error introduced by this approximation is less than one millimeter. Other approximation methods as splines might be able to better fit the fingertip trajectory, but do not provide any benefit taking into account the human ability for fingertip position perception. In the first step, the finger position is projected on the approximation circle and then the motor joint angle is computed by using the exact inverse kinematics given by (3.15) and (3.16) or (3.14) and (3.17).

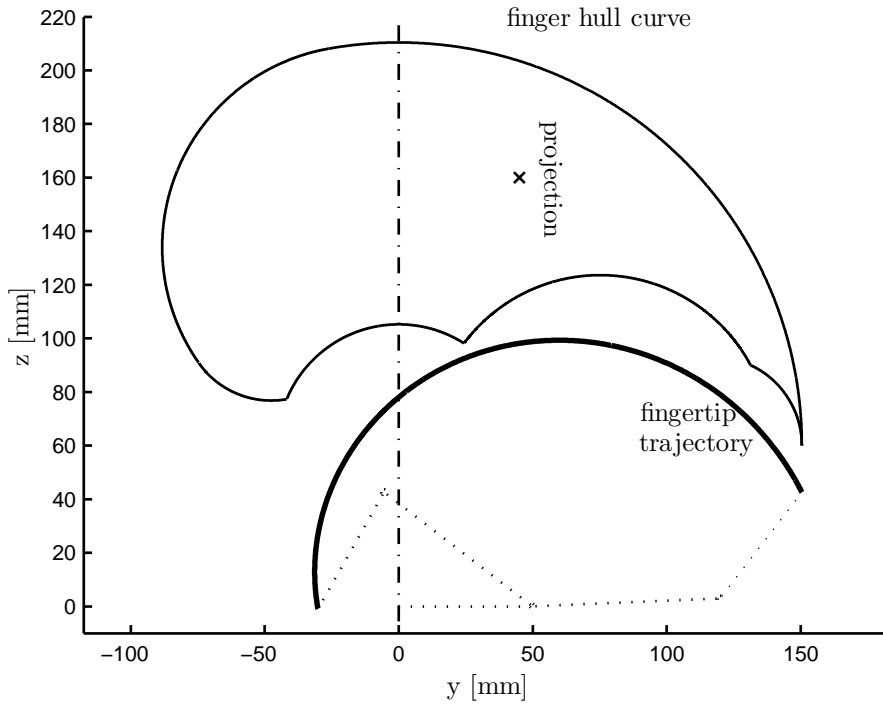


Figure 3.10: Vertical projection of fingertip position on BarrettHand trajectory

3.2.3 Force Mapping

Each finger of the BarrettHand is equipped with a strain gage joint torque sensor, which allows measuring the torque applied on the distal joint. On this account, normal forces F_k applied to the fingertip can be determined as follows:

$$f_k = \frac{\tau_k}{l_3} \quad \text{for } k = 1, \dots, 3, \quad (3.21)$$

whereby τ_k is the measured torque and l_3 the corresponding moment arm. These forces are fed back to the master site and displayed by the exoskeleton. To guarantee stability of the overall teleoperation system the forces are multiplied by a scaling factor g_f , which has to be selected appropriately.

3.2.4 Experimental Evaluation

The above presented mapping algorithms for position and force have been implemented in the real hardware setup, whereby the single components are connected as already depicted in Fig. 3.3 and communicate over a UDP network. Some of the obtained results are further discussed in succeeding paragraphs.

Using the position mapping algorithm described in Sec. 3.2.2, distances between the fingertips and the corresponding finger coordinate system are mapped with a scaling factor g_p onto the BarrettHand. One of the advantages of this position mapping is that the principle form of the grasp type is hereby maintained, which makes it easy to predict the gripper motion and thus simplifies the execution of the telemanipulation task. Fig. 3.11

shows some examples of different poses of the human hand and the corresponding pose of the BarrettHand. For the sake of clarity the pictures have been made without wearing the CyberGrasp. As can be seen, different grasp types, as defined by [32], namely precision and power grasps, can be performed. Thus, the mapping is suitable for a variety of different manipulation tasks.

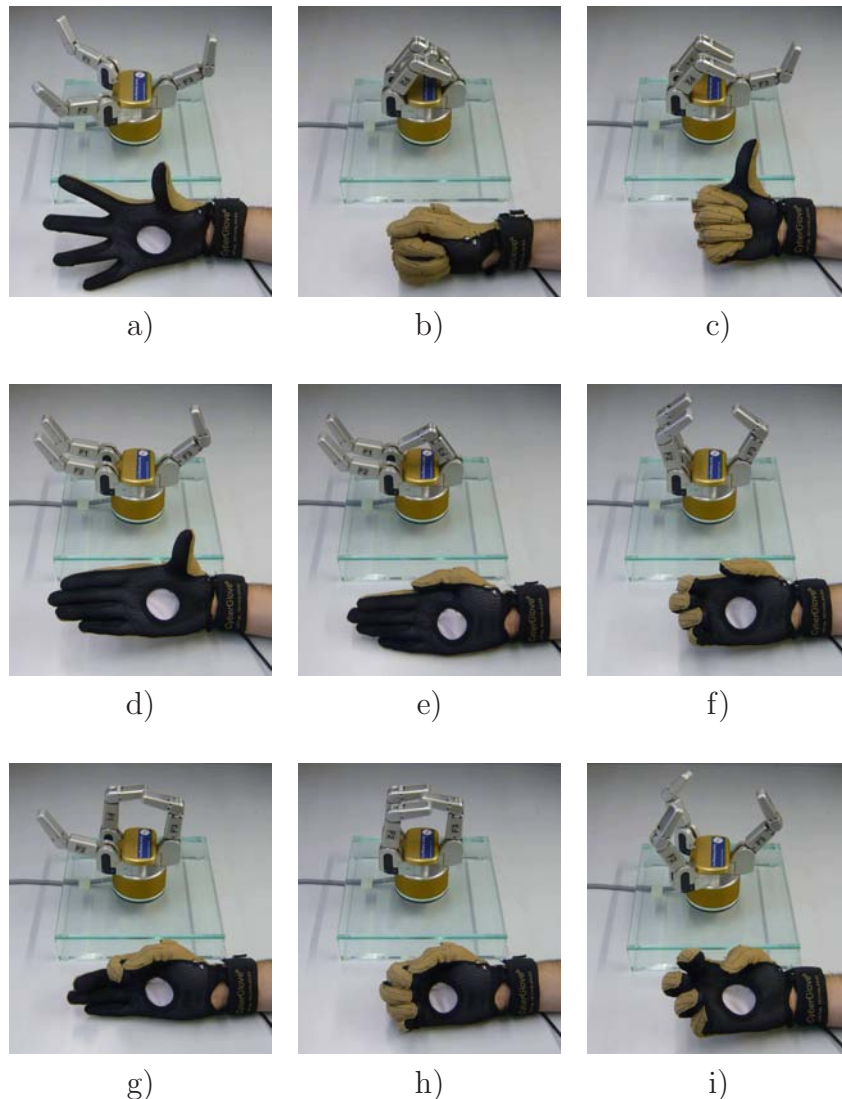


Figure 3.11: Human hand and corresponding BarrettHand poses

One drawback of this position mapping method is that the workspace of the human hand is not completely covered by the BarrettHand. As can be seen from Fig. 3.10, finger positions with small y -values cannot be mapped. As such finger configurations are only rarely used in manipulation tasks this effect is of minor importance. Nonetheless, it should be mentioned that there exist also other possibilities to project the human finger position onto the BarrettHand trajectory. A further possibility, not reported here, is presented in [38], which tries to better fit the workspace of human and BarrettHand fingers.

Evaluations of the proposed force mapping algorithm indicate that people can clearly distinguish between a soft and a strong grasp. The limited range of the BarrettHand torque sensor however, restricts the range of applicable forces significantly. A further difficulty

observed here is that the BarrettHand uses torque and not force sensors. If humans touch objects vertically with one of the fingertips no interaction forces can be detected as the moment arm is zero. This has to be taken into account if interacting with objects. Finally, it should be mentioned that the quite huge friction in the tendons of the CyberGrasp makes it difficult to apply really small forces. This can be explained by stick-slip effects that occur in the tendons.

Nonetheless it can be stated that the implemented position and force mapping algorithms allow interaction in a very intuitive way with the remote environment, despite a non-anthropomorphic kinematics of the grippers and a relative poor force feedback performance.

3.3 Integration of Single Components

All the components described in the prior sections are integrated into one teleoperation system as shown in Fig. 3.12. Master and slave devices as haptic interfaces, exoskeletons, telemanipulators, and grippers are controlled locally, whereby forces and positions are exchanged over a communication channel. More details about the used local controllers for haptic interfaces and telemanipulators, the corresponding redundancy resolution schemes, and the applied bilateral control architectures are discussed in the next chapter.

Beside haptic information, visual and auditory information is also exchanged. While video streams are captured by stereo cameras and displayed on a HMD or stereo-projection wall, audio information is captured by installed microphones and displayed to the human operator through headphones. When using a HMD, the head position is additionally tracked, and used to control the remotely located stereo-camera head.

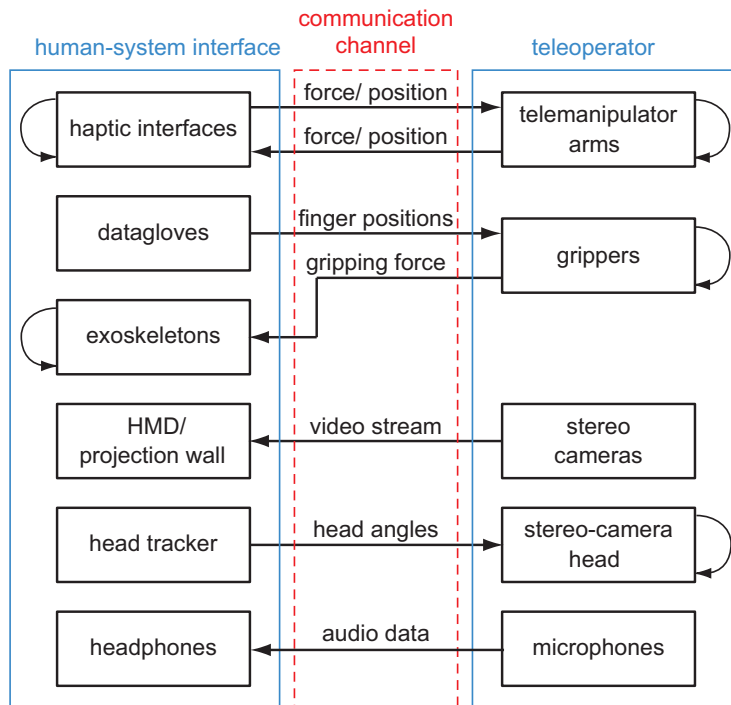


Figure 3.12: Integration of single components into overall teleoperation system

3.4 Linear one DOF Teleoperation System

In the prior sections a highly integrated teleoperation system with multiple DOF has been presented. Studying principle effects in such a complex system is extremely difficult. On this account a one DOF teleoperation system, as shown in Fig. 3.13, has been developed. The teleoperation system consists of two identical linear axes (Thrusttube module) of Copley Controls Corp., which can be used as master as well as slave devices. To measure the interaction force, each device is equipped with a one DOF force sensor (Burster, Model 2524). Position is measured by an optical encoder with a resolution of $1 \mu\text{m}$. The system is characterized by its linearity. No trigonometric functions are necessary to compute the position of the end-effector as e.g. necessary when using rotary joints. Moreover, due to its simplicity, exact mathematical models can be found which describe the overall system. These features are extremely helpful when testing new control algorithms.

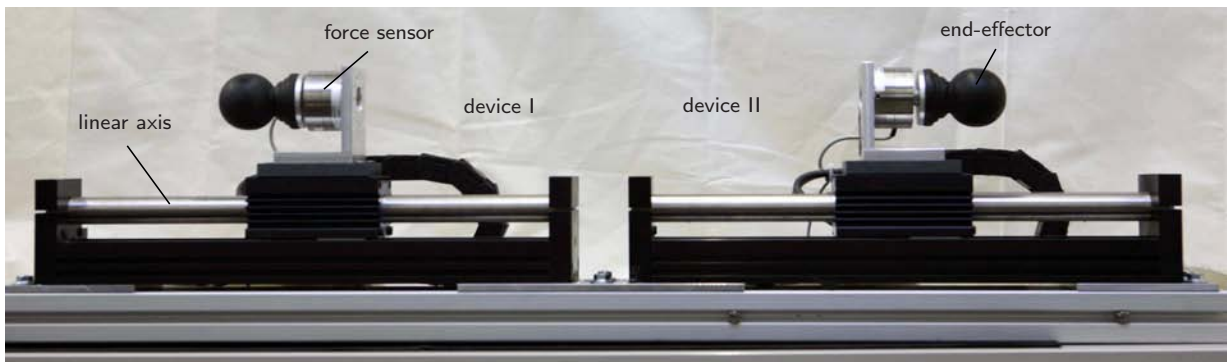


Figure 3.13: Linear one DOF teleoperation system

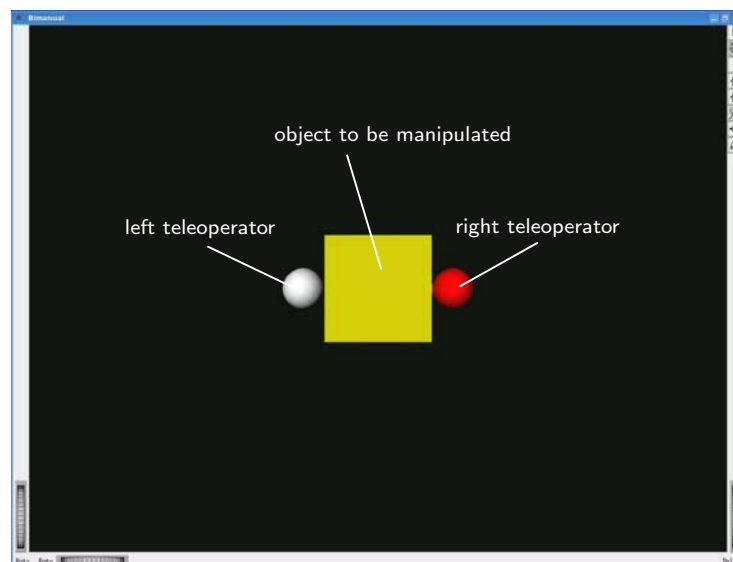


Figure 3.14: Bimanual virtual teleoperator

To study bimanual interactions a simple bimanual virtual teleoperator is used, as shown in Fig. 3.14. Hereby, the dynamics of the telemanipulator is modelled by a mass-damper

system and implemented in Matlab/Simulink. The corresponding parameters have been identified in the real hardware setup (see appendix C) resulting in a teleoperation system with four equal devices.

Using this very simple hardware setup, principle effects in teleoperation systems can be studied and new developed algorithms can be easily tested before implementing them on more complex systems.

3.5 Discussion

Multi-modal interaction with a remote environment by means of a teleoperation system requires the integration of components for visual and auditory feedback, as well as haptic interaction. The less adaptations of the human operator to the technical system are necessary, the more intuitive is the interaction and the better is the feeling of telepresence. In this chapter typical requirements on such an intuitive teleoperation system have been formulated: a human scaled workspace free of kinematic and algebraic singularities, the possibility to operate in full 6 DOF, the possibility to mount task specific end-effectors, the capability to display stiff environments, an anthropomorphic design of the teleoperator, as well as multi-modal feedback.

Since none of the state-of-the-art teleoperation systems fulfill all these requirements at the same time, a new enhanced teleoperation system has been developed. On this account, a variety of single components have been integrated into one teleoperation system. This includes redundant haptic interfaces and telemanipulators, as well as a stereo-vision-system.

As many manipulation tasks require also dextrous and sensitive operations, the teleoperation system has to be additionally equipped with components for multi-fingered manipulation. The human hand is able to realize a huge variety of different grasp types ranging from precision to power grasps. A high quality multi-fingered teleoperation system must cover at least a certain number of them. Thus, quality of a multi-fingered teleoperation system depends considerably on the kinematics of the robotic gripper or hand used at teleoperator site, and the mapping algorithm which transfers human hand motions to the robotic gripper. In this work a three-finger robotic gripper, the BarrettHand, is used. To map the human hand motion onto this gripper, a simple, but very efficient point-to-point position mapping is proposed. Since the robotic gripper is not anthropomorphic and each finger is only allowed to move on a certain trajectory, the position mapping is based on a vertical projection of human finger positions. The proposed mapping method maintains the overall form of the grasp and allows realization of a variety of different grasp types. Due to its simplicity it is furthermore easy to understand and people are able to immediately predict the gripper finger positions.

The resulting overall teleoperation system composed of all mentioned components is of superior performance and allows execution of a variety of different dextrous manipulation tasks, that cannot be carried out using state-of-the-art teleoperation systems.

Beside this very complex teleoperation system, also a one DOF teleoperation system consisting of two haptic interfaces and two virtual teleoperators is presented. Due to the simple design, precise linear mathematical models of it can be derived, which allow the analysis of principle effects in teleoperation systems. Thus, testing of control algorithms is significantly simplified, as will be shown in the next chapter.

4 Bilateral Control of Teleoperation Systems using Admittance-Type Devices

The realization of an intuitive teleoperation system requires not only an adequate mechatronic design, as already discussed in the prior chapters, but also the implementation of appropriate control algorithms. While in chapter 2 controllers for the developed haptic interface were analyzed, this chapter aims at extending this analysis to different control architectures for bilateral teleoperation systems. In contrast to other works that mainly deal with impedance-type devices, the focus of this chapter is on the analysis of different types of bilateral control algorithms for teleoperation systems using admittance-type devices.

In a typical teleoperation scenario the human operator interacts with a variety of objects which are characterized by different mechanical properties. This may include very stiff objects as e.g. metal parts and tools, as well as very soft objects like tissues. Depending on the actual task, the human operator also changes her/his behavior by e.g. adapting the stiffness of her/his arm. While dextrous and fine manipulations are typically performed with low stiffness, carrying or pushing of heavy objects requires higher stiffnesses. Thus, one of the main challenges in telerobotics is the selection of control architectures and control parameters, which are able to robustly stabilize the overall teleoperation system despite changing environment and human operator impedances.

In this chapter different bilateral control architectures using admittance-type devices are proposed and robust stability of these is investigated by using the parameter space approach, which allows the analysis of uncertain systems with varying plant parameters. While Sec. 4.1 starts with a description of basic components of a bilateral teleoperation system and formulates demands on it, Sec. 4.2 introduces the proposed bilateral control architectures. Sec. 4.3 explains the parameter space approach method and the usage of it for controller design, as well as for robustness analysis. In Sec. 4.4 simple linear models for human operator, human-system interface, teleoperator, as well as remote environment are described, which are required for the stability analysis. The second part of this chapter is devoted to the stability analysis of two different kinds of mechatronic teleoperation systems. While corresponding simulation results are reported in Sec. 4.5, Sec. 4.6 validates the used approach by investigating stability in real hardware experiments.

4.1 Bilateral Teleoperation Systems

Before going into detail, the typical structure of a bilateral teleoperation system and its components are presented. Fig. 4.1 shows a bilateral teleoperation system formed by the main components: human operator, human-system interface, communication channel, teleoperator, and environment. As shown in this diagram, the single components interact with each other and exchange information in form of energy. Hereby, human-system interface and human operator are mechanically coupled. The same is true for teleoperator and remote environment. Master and slave devices, however, which are commonly separated in

their location, interact with each other over a communication channel. Depending on the type and quality of this channel, algorithms have to deal with non-ideal network conditions. In the context of this chapter only *ideal* communication channels with negligible time-delay and packet loss are considered.

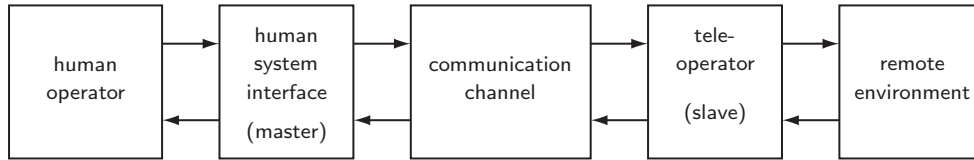


Figure 4.1: Bilateral teleoperation system

Basically two demands can be formulated on such a bilateral teleoperation system:

- **Stability:** Stability of a teleoperation system is a very crucial demand. Due to the coupling of the single components and the corresponding energy exchange instability can occur in a teleoperation system. These instabilities can e.g. cause oscillations when interacting with remote environments so that no stable contact is possible. Hence, one of the main goals when designing a teleoperation system is to realize stable contact with different kinds of remote environments ranging from free space to hard contact.
- **Transparency:** A telepresence system is transparent if the remote environment is exactly displayed to the human operator without being affected by the dynamics of human-system interface, teleoperator, as well as communication channel. This can only be achieved if the two devices become “invisible” to the human operator and an ideal communication channel is assumed. Several transparency measures have been already defined in the literature: The most common ones are either based on the comparison of positions and forces at operator and teleoperator side [139] or the comparison of displayed and environmental impedance the human operator is interacting with [77].

Typically these two demands are contradictory and cannot be met at the same time. Thus, a compromise must be accepted, which either attaches more importance on stability or transparency of the overall system.

In the following sections bilateral control architectures for admittance-type devices are analyzed. Hereby, special attention is paid to find control parameters, which are able to stabilize the overall system over a wide range of human operator and remote environment impedances. The influence of the obtained control parameters on transparency is also discussed.

4.2 Bilateral Control Architectures for Admittance-Type Devices

Control architectures for bilateral teleoperation systems are commonly classified according to the number and kind of variables transmitted between master and slave device, see [57] for an overview. So called two-channel control architectures, whereby master and

slave are connected with each other via two communication channels, represent possibly the most popular bilateral controllers, see [71] for details. Hereby, forces/positions are exchanged between master and slave device and local position or force controllers are used. While for impedance-type devices, which are characterized by very light-weight constructions with low inertia and friction, high performance force controllers can be implemented, for admittance-type devices, force control can only be realized with a very poor performance [42, 128]. This is mainly due to the high dynamic properties and friction effects of admittance-type devices, which can only be compensated by using some kind of low level position controller. On this account, classical bilateral control architectures with local force control are usually not very appropriate for teleoperation systems using admittance-type master and slave devices.

Commonly admittance-type devices are controlled by using a so called position-based admittance control architecture, as already presented in chapter 2. The hereby implemented low-level position controller compensates for the before mentioned non-linear effects. Depending on the application, such an architecture can be used either to render a target dynamics as e.g. the mass of a tool or to achieve a certain compliant behavior when being in contact with the environment. In both cases the desired behavior is achieved by implementing admittances in the form of simple mass-spring-damper systems

$$\mathbf{f} = \mathbf{M}\ddot{\mathbf{x}} + \mathbf{B}\dot{\mathbf{x}} + \mathbf{C}\mathbf{x}, \quad (4.1)$$

whereby \mathbf{x} are positions, \mathbf{f} are forces and \mathbf{M} means the mass, \mathbf{B} the damping and \mathbf{C} the stiffness matrix.

When rendering desired impedances, as shown in Fig. 4.2, the impedance is used to implement a desired target dynamics, e.g. the dynamics of a tool, which is attached to the end-effector. When trying to achieve a compliant behavior, however, as shown in Fig. 4.3, the impedance is used to modulate the desired position x_d , whereby the stiffness parameter defines an upper bound of displayable stiffnesses. As reported later, in both cases the impedance is lower bounded due to actuator limitations. For the sake of clarity the Fig. 4.2 and Fig. 4.3 show block diagrams for one DOF only. The extension to multi DOF is discussed later in this chapter.

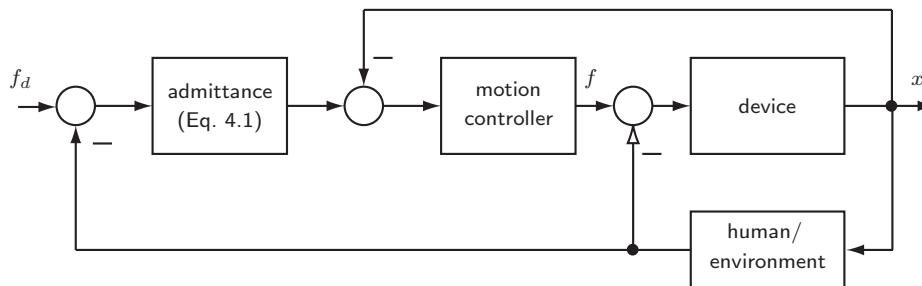


Figure 4.2: Position-based admittance control used to render a target dynamics (Fa)

In view of the classical two-channel control architectures, position-based admittance controllers can be implemented for master as well as slave devices and combined into a teleoperation control architecture when positions and forces are exchanged. Observe that

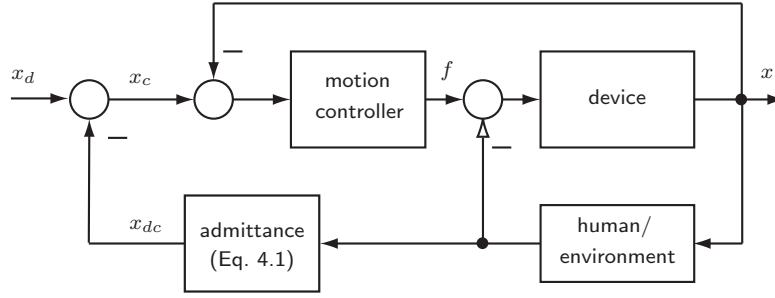


Figure 4.3: Position-based admittance control used to achieve compliant behavior when being in contact (Pa)

then ideal transparency can no longer be achieved as e.g. possible for a classical two-channel force-position and position-force architecture. This is due to the implemented desired master and slave impedances which affect transparency.

Taking this into account in principle four different basic bilateral control architectures can be realized.

Position-position control (PP): Position-position control, see Fig. 4.4, is one of the oldest bilateral teleoperation schemes. It is well known that this architecture is characterized by a poor force and position tracking performance [9]. Performance of this architecture is namely directly correlated to the implemented control parameters, which have to be selected to guarantee stability for a wide range of remote environmental conditions. The control law of a position-position controller is given as follows:

$$f_m = D_{xm}(\dot{x}_{dm} - \dot{x}_m) + K_{xm}(x_{dm} - x_m), \quad (4.2)$$

$$f_s = D_{xs}(\dot{x}_{ds} - \dot{x}_s) + K_{xs}(x_{ds} - x_s), \quad (4.3)$$

whereby high control parameters K_x and D_x result in a better performance, but cause instability of the system. Further problems arise, when no task space controller is used and only joint space controllers are available. Lowering the joint space control parameters inevitably causes a low tracking performance in task space and a somewhat sluggish behavior of the teleoperation system. In order to overcome these limitations, the following three alternative bilateral control schemes are analyzed:

Position-based admittance control with position-force exchange (FaPa): In the position-based admittance control with position-force exchange, which is slightly adapted from the control architecture introduced in [25], positions are sent from master to slave and forces from slave to master, see Fig. 4.5. Admittance-type controllers are used to control master as well as slave device. The corresponding control laws are given by

$$f_m = D_{xm}(\dot{x}_{dm} - \dot{x}_m) + K_{xm}(x_{dm} - x_m), \quad (4.4)$$

$$f_s = D_{xs}(\dot{x}_m - \dot{x}_{ds} - \dot{x}_s) + K_{xs}(x_m - x_{ds} - x_s), \quad (4.5)$$

$$f_{ss} - f_{sm} = m_{dm}\ddot{x}_{dm} + b_{dm}\dot{x}_{dm}, \quad (4.6)$$

$$f_{ss} = m_{ds}\ddot{x}_{ds} + b_{ds}\dot{x}_{ds} + c_{ds}x_{ds} \quad (4.7)$$

for master and slave. While at master side a sort of force control is implemented, at slave side a compliant controller is realized. During free space motion only the master impedance given by m_{dm} and b_{dm} is active, the slave side is controlled by a pure position controller. In contact the slave impedance is also active and both controllers influence the impression of the remote environment. It should particularly be noted that the stiffness parameter c_{ds} defines an upper bound of displayable stiffnesses.

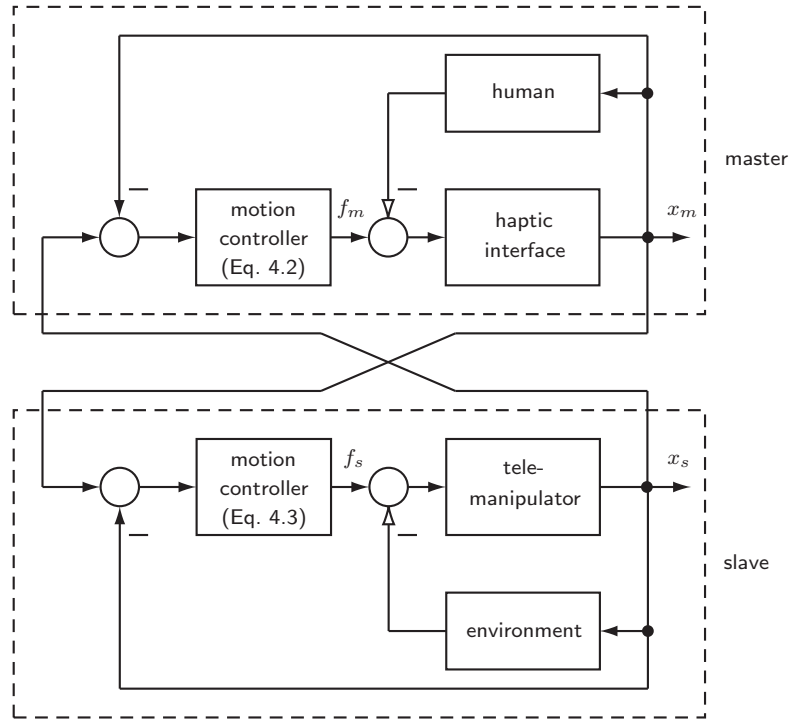


Figure 4.4: Position-position control (PP)

Position-based admittance control with force-position exchange (PaFa): The position-based admittance control with force-position exchange represents the mirrored version of the last presented control architecture: forces are sent from master to slave and positions from slave to master. The corresponding control laws are given by

$$f_m = D_{xm}(\dot{x}_s - \dot{x}_{dm} - \dot{x}_m) + K_{xm}(x_s - x_{dm} - x_m), \quad (4.8)$$

$$f_s = D_{xs}(\dot{x}_{ds} - \dot{x}_s) + K_{xs}(x_{ds} - x_s), \quad (4.9)$$

$$-f_{sm} = m_{dm}\ddot{x}_{dm} + b_{dm}\dot{x}_{dm} + c_{dm}x_{dm}, \quad (4.10)$$

$$f_{ss} - f_{sm} = m_{ds}\ddot{x}_{ds} + b_{ds}\dot{x}_{ds}. \quad (4.11)$$

Position-based admittance control with force-force exchange (FaFa): Finally, the position-based admittance control with force-force exchange, see Fig. 4.7, is characterized by a bilateral force-force exchange between master and slave. At both sides an admittance

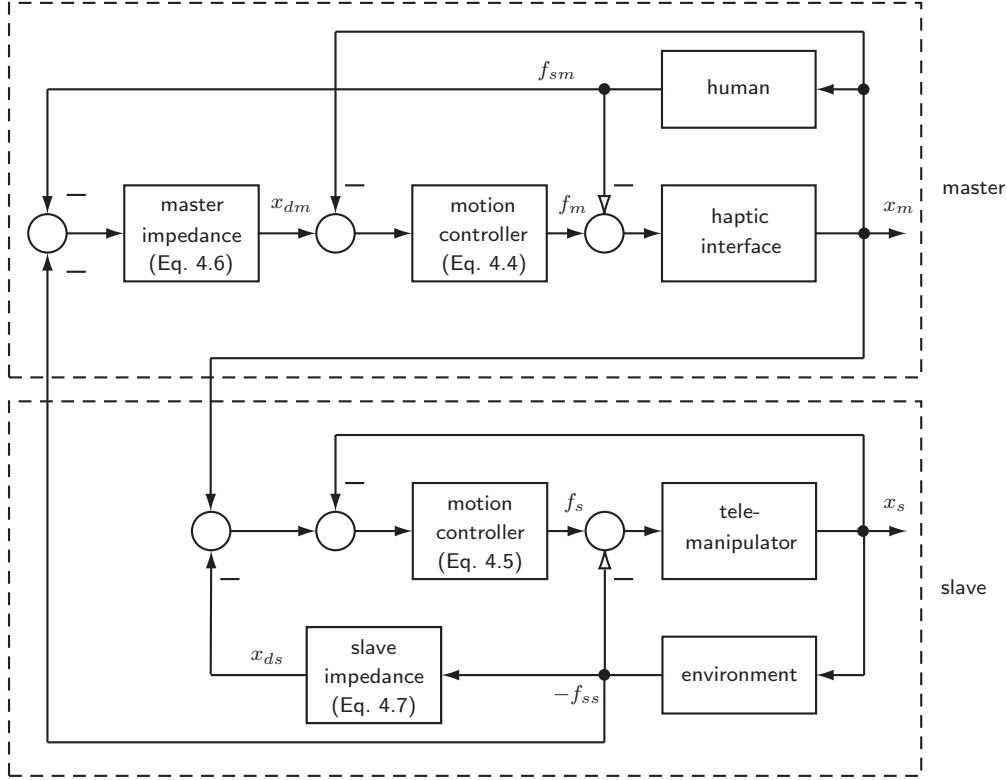


Figure 4.5: Position-based admittance control with position-force exchange (FaPa)

control strategy is implemented:

$$f_m = D_{xm} (\dot{x}_{dm} - \dot{x}_m) + K_{xm} (x_{dm} - x_m), \quad (4.12)$$

$$f_s = D_{xs} (\dot{x}_{ds} - \dot{x}_s) + K_{xs} (x_{ds} - x_s), \quad (4.13)$$

$$f_{ss} - f_{sm} = m_d \ddot{x}_{dm} + b_d \dot{x}_{dm}, \quad (4.14)$$

$$f_{ss} - f_{sm} = m_d \ddot{x}_{ds} + b_d \dot{x}_{ds}. \quad (4.15)$$

In order to guarantee position tracking, the same impedances given by the mass m_d and the damping b_d have to be implemented for master and slave. On this account, only two control parameters have to be selected, which simplifies tuning of the controller significantly.

In the next section the parameter space approach, which is used to analyze stability of the presented bilateral control architectures is introduced.

4.3 Parameter Space Approach

As already mentioned above, in a teleoperation system human and environment impedances vary significantly over time. Thus, when analyzing stability of such a system we have to deal with a plant with uncertain plant parameters \mathbf{p} . As the parameters are typically upper and lower bounded, the corresponding operating domain P can be described as follows:

$$P = \{\mathbf{p} \mid p_i \in [p_i^-, p_i^+], i = 1, 2, \dots, l\}. \quad (4.16)$$

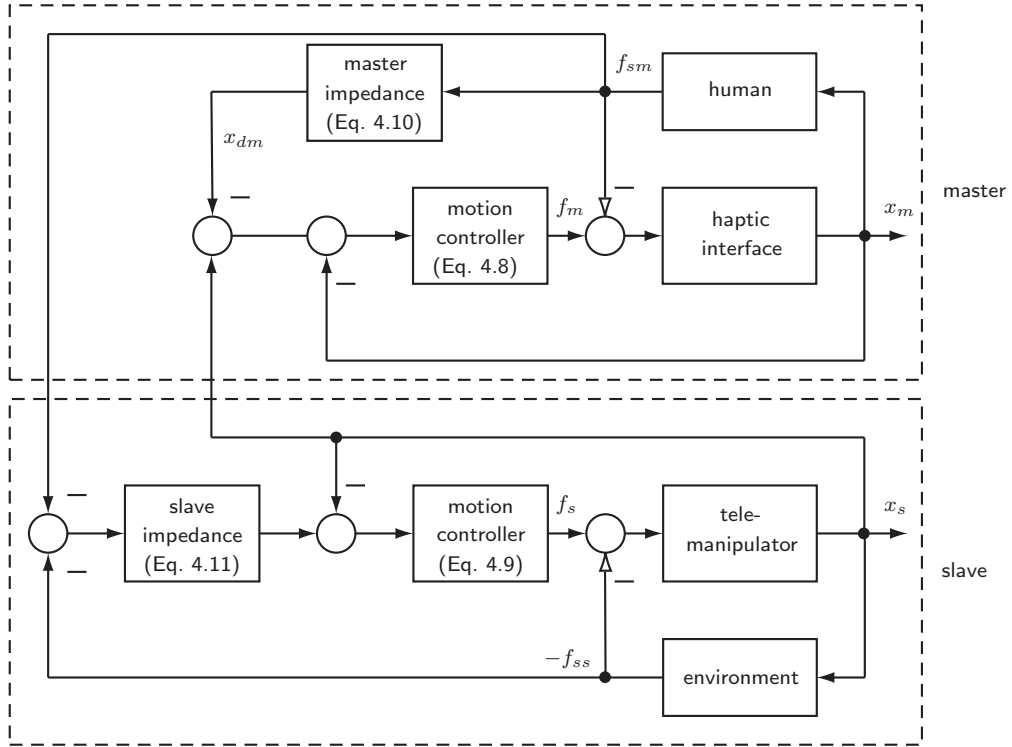


Figure 4.6: Position-based admittance control with force-position exchange (PaFa)

Typical approaches for the stability analysis of such uncertain systems are either based on the passivity theorem [100], see e.g. [77, 82, 139], or the analysis of absolute stability by using Llewellyns stability criteria [85], see [6, 52] for examples. But the drawback of these approaches is that a passive human operator and remote environment have to be assumed and no desired dynamics of the teleoperation system can be commanded. This work aims to analyze stability by using the so called parameter space approach [5], which allows the analysis of uncertain systems with varying plant parameters without assuming passive behavior. It is used in the first step for controller design and in the second step for robustness analysis. The parameter space approach has been already used in [74, 75] to analyze stability of classical bilateral teleoperation controllers, but the investigations were limited only to robustness analysis.

The parameter space method is based on the boundary crossing theorem of polynomials stated by Frazer and Duncan [46]. Given the linear state space model

$$\begin{aligned}\dot{\mathbf{x}} &= \mathbf{A}\mathbf{x} + \mathbf{B}\mathbf{u}, \\ \mathbf{y} &= \mathbf{C}\mathbf{x} + \mathbf{D}\mathbf{u},\end{aligned}\quad (4.17)$$

and the corresponding characteristic polynomial

$$p(s, \mathbf{p}) = \det(s\mathbf{E} - \mathbf{A}) = 0, \quad (4.18)$$

robust stability can be analyzed by mapping stability regions (further on referred as Γ -regions) defined in the s -plane into the parameter space formed by l uncertain plant or control parameters collected in the parameter vector \mathbf{p} .

For Hurwitz stability e.g. the boundary of the Γ -region is given by

$$\delta\Gamma := \{s \mid s = j\omega, 0 \leq \omega < \infty\}. \quad (4.19)$$

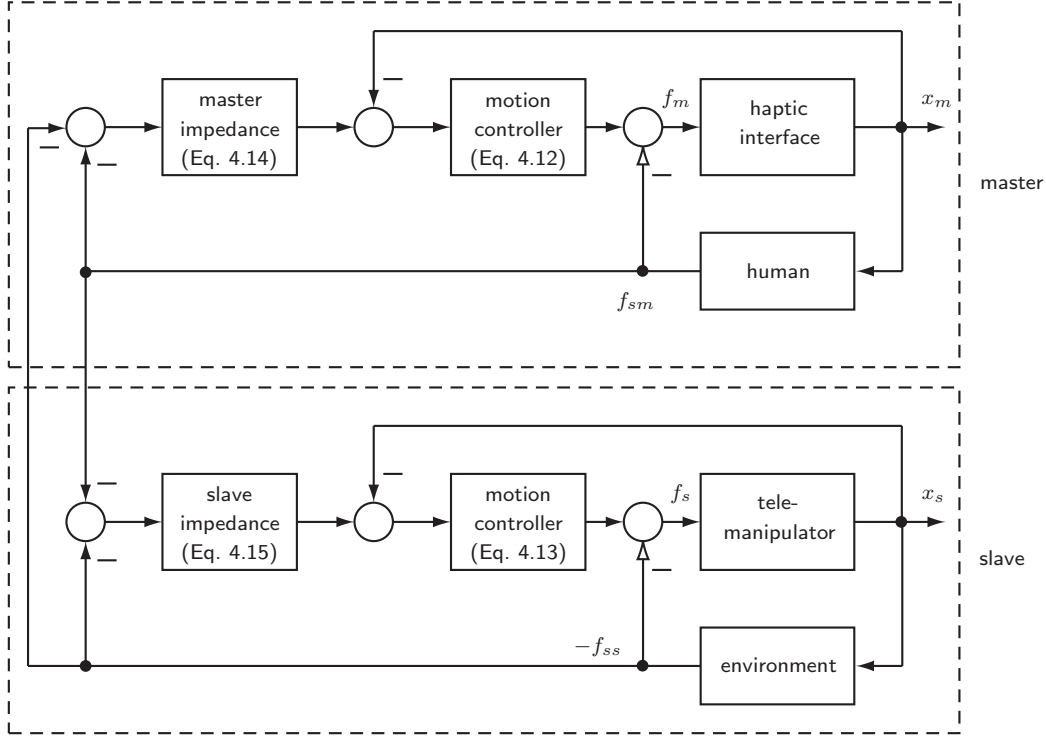


Figure 4.7: Position-based admittance control with force-force exchange (FaFa)

According to the boundary crossing theorem, starting from a stable characteristic polynomial $p(s, \mathbf{p})$, a polynomial

$$p(s, \mathbf{p}) = a_0(\mathbf{p}) + a_1(\mathbf{p})s + \dots + a_n(\mathbf{p})s^n = p_{\text{even}}(s^2, \mathbf{p}) + sp_{\text{odd}}(s^2, \mathbf{p}) \quad (4.20)$$

with *real* coefficients $a_i(\mathbf{p})$ can only become unstable if the system crosses the stability boundary. Depending on whether the stability boundary is crossed on the real axis, imaginary axis or at infinity, real root boundaries (RRB), complex root boundaries (CRB) and infinite root boundaries (IRB) are distinguished, which can be computed as follows:

$$CRB : \operatorname{Re} p(j\omega) = 0, \quad \operatorname{Im} p(j\omega) = 0, \quad (4.21)$$

$$RRB : a_0(\mathbf{p}) = 0, \quad (4.22)$$

$$IRB : a_n(\mathbf{p}) = 0. \quad (4.23)$$

Mapping these boundaries into the parameter space requires solving (4.21) to (4.23) for the parameter vector $\mathbf{p} = f(\omega)$ and sweeping ω over real frequencies. This finally yields the complete set of critical points which form the stability boundary in the parameter space.

Also other pole regions Γ defined by

$$\delta\Gamma := \{s \mid s = \sigma(\lambda) + j\omega(\lambda), \lambda \in [\lambda^-, \lambda^+]\} \quad (4.24)$$

can be considered, whereby λ means a generalized frequency. Also in this case a RRB, CRB and IRB can be computed and mapped into the parameter space:

$$RRB : p(\sigma_0, \mathbf{p}) = 0 \quad \text{with } \sigma_0 \text{ the intersection point of the real axis with } \delta\Gamma, \quad (4.25)$$

$$IRB : \lim_{\alpha \rightarrow \infty} p(\sigma(\lambda) + j\omega(\lambda), \mathbf{p}) = 0, \quad (4.26)$$

$$CRB : \Gamma_{CRB} := \{\mathbf{p} \mid p(\sigma(\lambda) + j\omega(\lambda), \mathbf{p}) = 0, p(\sigma + j\omega) \in \delta\Gamma, \lambda \in [\lambda^-, \lambda^+]\} \quad (4.27)$$

The parameter space method can be either used for controller design or for robustness analysis, depending on whether the stability region is mapped into the parameter space of control parameters or varying plant parameters.

Controller design: The stability boundaries are mapped into a plane formed by two control parameters k_1, k_2 . This allows determination of the set of control parameters for which the system is Γ -stable. If a system with n control parameters is considered, $n - 2$ control parameters must be fixed to a certain value, while the rest can be gridded. For each grid point the Γ -stability boundaries are computed and projected into the selected parameter plane.

Designing a controller for an uncertain plant requires basically two steps: In the first step, sets of stabilizing controllers for some representative operating points (typically the vertices of the operating domain) have to be computed. The intersection of all these sets guarantees Γ -stability for all representative operating points, but not necessarily for the whole operating domain. After selection of appropriate control parameters, this has to be verified in the second step by a robustness analysis.

Robustness analysis: The stability boundaries are mapped into a plane formed by two varying plant parameters p_1, p_2 . The system is robustly Γ -stable if the entire operating domain is contained in the Γ -stable parameter set.

4.4 Modelling of Teleoperation System

To analyze stability of the teleoperation system by using the parameter space approach, a state space model of the overall system including haptic interface, telemanipulator, human and environment is needed. As the communication channel is assumed to be ideal, it is neglected in this chapter. For the haptic interface as well as the human operator, the already introduced models presented in Sec. 2.4.1 are used. Also the models for actuator and sensor dynamics are the same as reported in Sec. 2.4.2. Finally, the models for telemanipulator and remote environment are presented below.

4.4.1 Models for Telemanipulator and Remote Environment

The telemanipulator is modelled in a similar way as the haptic interface, whereby m_s means the telemanipulator mass, b_s the telemanipulator damping, and f_s the force applied by the actuators. The environment the telemanipulator interacts with is modelled by a mass-spring-damper model. The end-effector mass and load is modelled by m_{es} , c_e and b_e denote the environmental stiffness and damping coefficient. The overall system is shown in Fig. 4.8 and can be described by using the following differential equations:

$$\begin{aligned} 0 &= f_s + f_{ss} - m_s \ddot{x}_s - b_s \dot{x}_s, \\ 0 &= f_{ss} + m_{es} \ddot{x}_s + b_e \dot{x}_s + c_e x_s. \end{aligned} \quad (4.28)$$

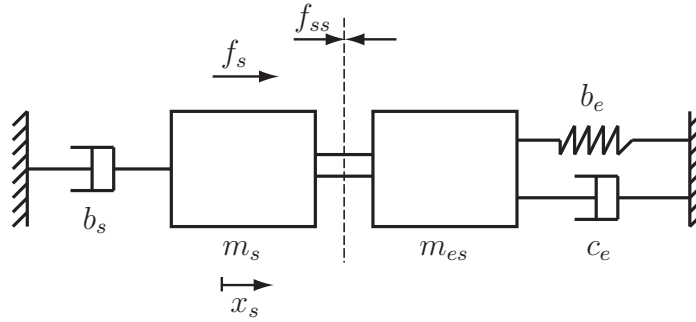


Figure 4.8: Model of telemanipulator and remote environment

4.5 Stability Analysis of Bilateral Teleoperation Systems

In this section, stability of the above presented control algorithms for bilateral teleoperation is analyzed by using the parameter space approach. Hereby, firstly sets of control parameters which stabilize the overall teleoperation system in characteristic points of the operating domain are determined, and then a robustness analysis is carried out for one selected set of control parameters.

The numerical stability analysis is carried out for two different types of teleoperation systems: the linear one DOF teleoperation system already presented in Sec. 3.4, and the multi DOF telemanipulation system described in Sec. 3.1. In order to simplify the analysis of the multi DOF system, dynamic compensation of the cross couplings between the linkages is assumed, so that each DOF can be evaluated separately. This can be achieved by using a CT controller as already introduced in Sec. 2.3. Moreover, in order to reduce the number of control parameters, the low level position controllers are assumed to be already tuned. They are selected in such a way that aperiodic transient responses are achieved. For both systems simulations using the before presented models have been carried out. The corresponding model parameters used for simulation are reported in appendix C.

All simulations were performed for a three-dimensional operating domain P formed by the varying parameters: environment stiffness $c_e \in [0 \quad 10\,000]$ N/m, environment damping $b_e \in [0 \quad 200]$ Ns/m, and load mass $m_{es} \in [m_{es}^{min} \quad m_{es}^{min} + 1]$ kg, see Fig. 4.9. This assumption is made because in a teleoperation system the operator can interact with different kinds of environments, ranging from free space to hard contact. In addition, the operator can grasp objects, which has to be considered in the model. On this account a varying load mass m_{es} is introduced, whereby the lower bound is given by the end-effector mass m_{es}^{min} only.

In the following sections, results of the numerical stability analysis for the above presented bilateral teleoperation control schemes are reported.

4.5.1 Linear one DOF Device

In the first step, stability of the linear one DOF device is analyzed. Due to its simple mechanical design, device parameters, which are necessary for simulation, can be determined relatively exactly, see Table C.3. While the mass of each carriage and end-effector is measured, the damping coefficient is estimated by system identification and the motor

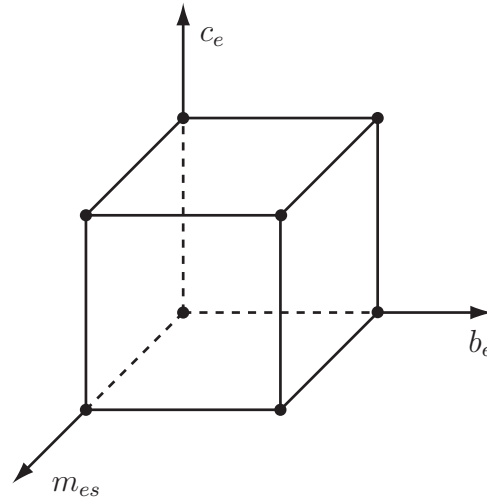


Figure 4.9: Operating domain formed by the varying plant parameters environment stiffness, environment damping, and end-effector mass (including load mass)

time-constant is taken from the technical data sheet. Finally, the force filter constant is selected to provide a good signal to noise ratio. In the coming paragraphs, basic simulation results for this device are collected and discussed in detail.

Position-based Admittance Control with Position-Force Exchange (FaPa)

Using the position-based admittance control with position-force exchange five control parameters m_{dm} , b_{dm} , m_{ds} , b_{ds} , and c_{ds} have to be selected to guarantee stability of the overall teleoperation system. Hereby, m_{dm} , b_{dm} mostly affect the free space behavior and m_{ds} , b_{ds} , c_{ds} the impression of contact. Further, it is known that due to the admittance-type control the minimum target inertia of the master device is bounded by stability, see Sec. 2.4. On this account m_{dm} has been set to a value which stabilizes the haptic interface, when used in standalone mode. In order to further reduce the number of control parameters $c_{ds}=1000$ N/m has been fixed. It should be noted that the stiffness parameter c_{ds} mainly influences the perception of stiff environments since it introduces an upper bound for displayable stiffnesses. Thus, it should be selected carefully.

In the first step, Hurwitz stability is analyzed. Fig. 4.10 shows the resulting stability boundaries which are mapped into the m_{ds} , b_{ds} plane, whereby b_{dm} is gridded. Each of the lines represent a set of stability margins determined for one of the eight vertices of the operating domain, see Fig. 4.9. The intersection of all these sets describes control parameters which stabilize all representative operating points. In order to distinguish stable and non-stable regions it is enough to check stability of an arbitrary point per region. If the point is stable, then, according to the boundary crossing theorem of polynomials, all control parameters in this region stabilize all representative operating points. As can be seen an increasing damping factor at master side increases the set of stabilizing controllers.

Fig. 4.11 further shows the influence of different values of the force-torque filter constants. With increasing filter constant the stability region decreases. This again implies that high quality force-torque sensors with low noise level should be used.

Finally, Fig. 4.12 (left) shows the dependency on the human arm impedance, whereby lowering the impedance significantly reduces the set of stabilizing controllers. Again, selecting one controller out of the set of stabilizing controllers (*) allows robust Γ -stabilization of the teleoperation system in representative operating points, despite varying human arm impedance. When selecting this controller the smallest possible damping at operator site should be chosen since this parameter directly affects the impression of the remote environment and reduces transparency of the overall teleoperation system. To finally check if the selected controller not only stabilizes the representative operating points, but also the whole operating domain, a robustness analysis must be performed, see Fig. 4.12 (right). As can be seen, the selected controller allows to robustly Γ -stabilize the teleoperation system since the entire operating domain is enclosed by the Γ -stability margins. Hereby each line stays for lower and upper bound of the end-effector mass m_{es} .

After implementing this controller in the real hardware setup, a relatively low damped behavior could be observed when touching stiff environments. On this account, the analysis presented before has been carried out again for a new Γ -region as shown in Fig. 4.17. This new Γ -region guarantees a certain damping $d = -\sigma_i/\omega_0$ of the overall system. Fig. 4.13 (left) shows the results in the control parameter plane, Fig. 4.13 (right) the results of the robustness analysis. Although a relatively small damping has been selected, the set of stabilizing controllers is significantly reduced. Increasing the damping even further would cause a dramatical reduction of stabilizing controller sets. Summarizing it can be stated that a certain amount of slave damping and a low slave mass have to be implemented in order to guarantee a good damped behavior, otherwise the interaction with stiff environments would inevitably cause oscillations. A further very interesting result is that the damping parameter b_{ds} is not only lower, but also upper bounded, which indicates that introducing more damping into the teleoperation system does not always help to robustly stabilize it.

Position-based Admittance Control with Force-Position Exchange (PaFa)

Again five control parameters m_{dm} , b_{dm} , c_{dm} , m_{ds} , b_{ds} have to be selected in order to guarantee Γ -stabilizing behavior. The same principle as presented above is used to reduce the number of variable control parameters: m_{ds} is selected to stabilize the telemanipulator alone and c_{dm} is fixed.

The results gained from the parameter space approach are shown in Fig. 4.14. The bigger the slave damping b_{ds} , the larger is the set of stabilizing control parameters. Fig. 4.15 shows the stability margins dependent on the human arm impedance. In contrast to the before presented architecture, smaller human operator impedances have a stabilizing effect on the overall teleoperation system.

In order to be able to manipulate objects and to interact with different kind of impedances, a well damped behavior of the overall system is necessary. Thus, the influence of the required damping on the control parameters is analyzed in Fig. 4.16. Again a Γ -region with damping $d = -0.1$ is selected and the stability margins are plotted. The analysis shows that the region of stabilizing controllers is significantly reduced. Especially for high human arm impedances the overall system can only be robustly Γ -stabilized if small values for the master mass m_{dm} and a certain amount of damping b_{dm} are selected, whereby also an upper bound on this damping parameter must be taken into account.

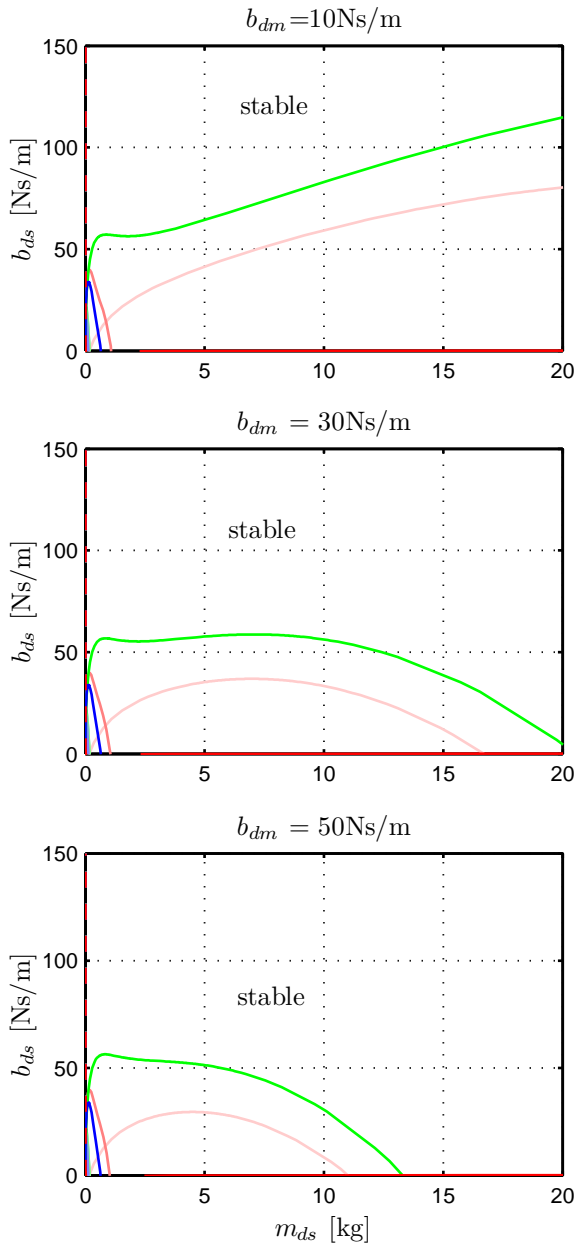


Figure 4.10: FaPa architecture (linear one DOF device): Stability boundaries of the vertices of the operating domain in the (m_{ds}, b_{ds}) -plane depending on the damping parameter b_{dm} ($\alpha = 1$, $m_{dm} = 3$ kg, $c_{ds} = 1000$ N/m).

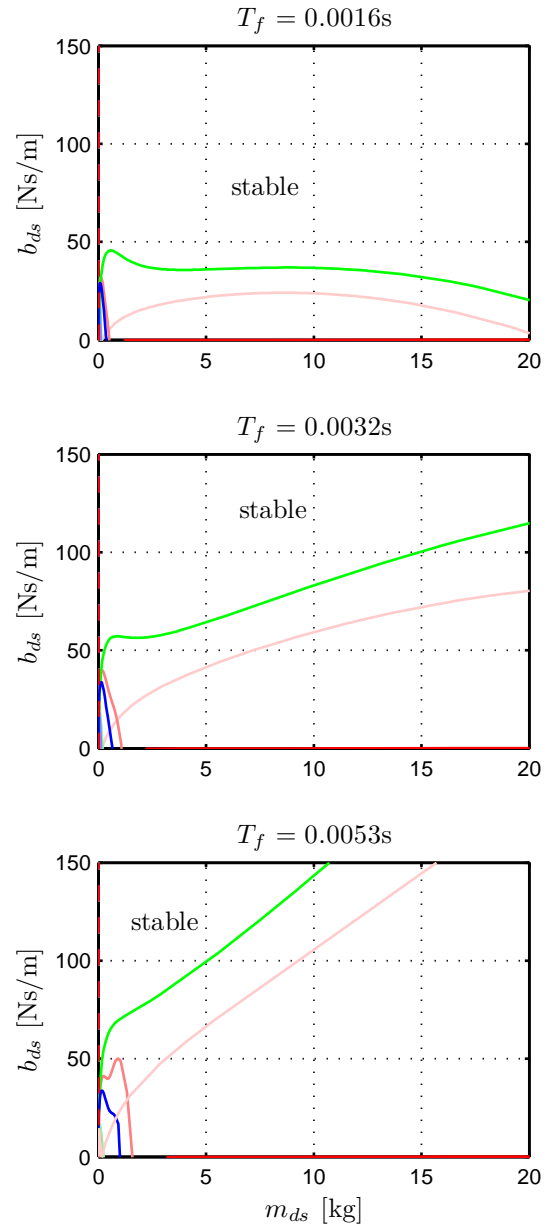


Figure 4.11: FaPa architecture (linear one DOF device): Stability boundaries of the vertices of the operating domain in the (m_{ds}, b_{ds}) -plane depending on the force-torque filter constant T_f ($\alpha = 1$, $m_{dm} = 3$ kg, $b_{dm} = 10$ Ns/m, $c_{ds} = 1000$ N/m).

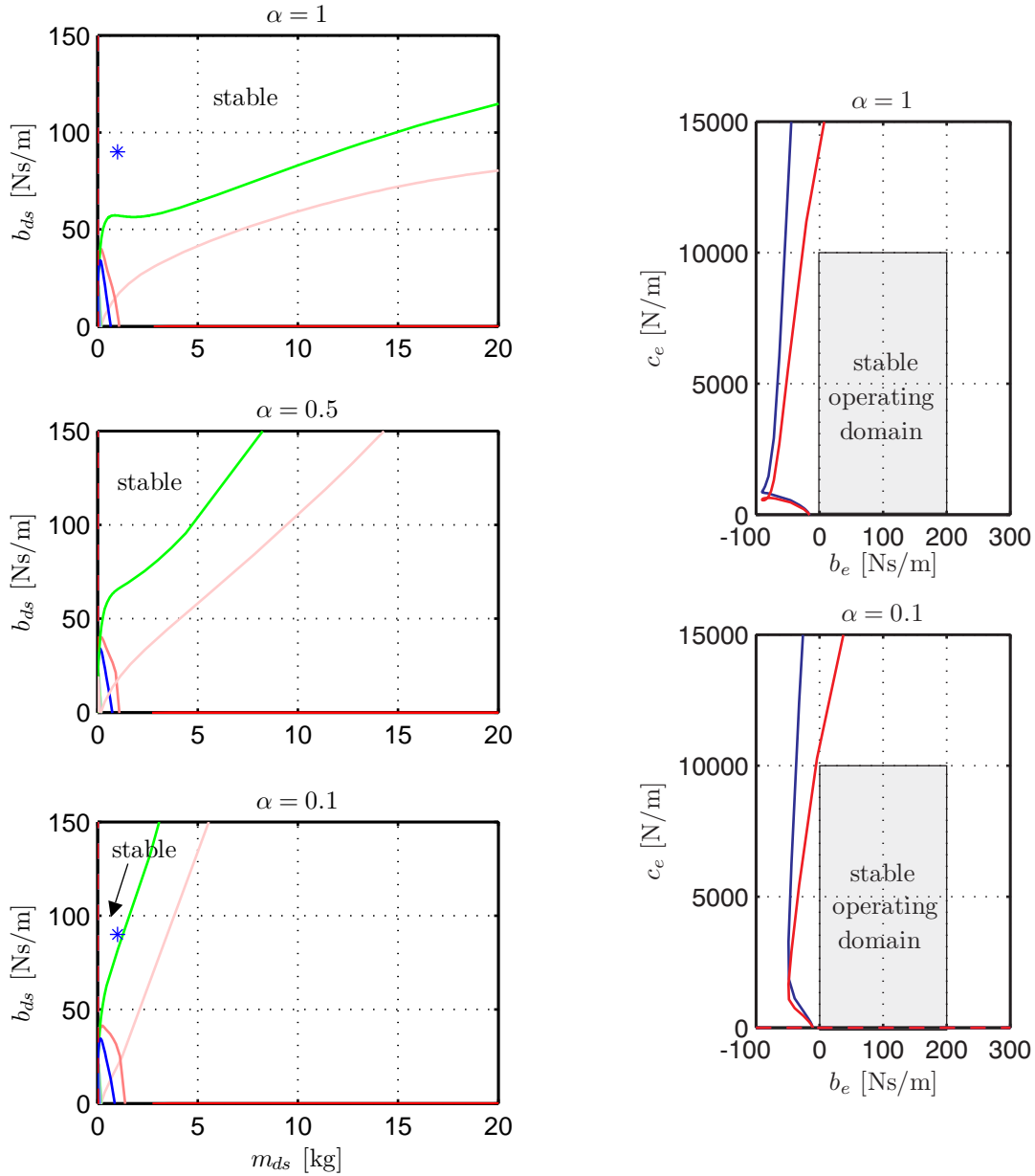


Figure 4.12: FaPa architecture (linear one DOF device): Stability boundaries of the vertices of the operating domain in the (m_{ds}, b_{ds}) -plane and robustness analysis in the (b_e, c_e) -plane for a varying human arm impedance α ($m_{dm} = 3$ kg, $b_{dm} = 10$ Ns/m, $m_{ds} = 1$ kg, $b_{ds} = 90$ Ns/m, $c_{ds} = 1000$ N/m).

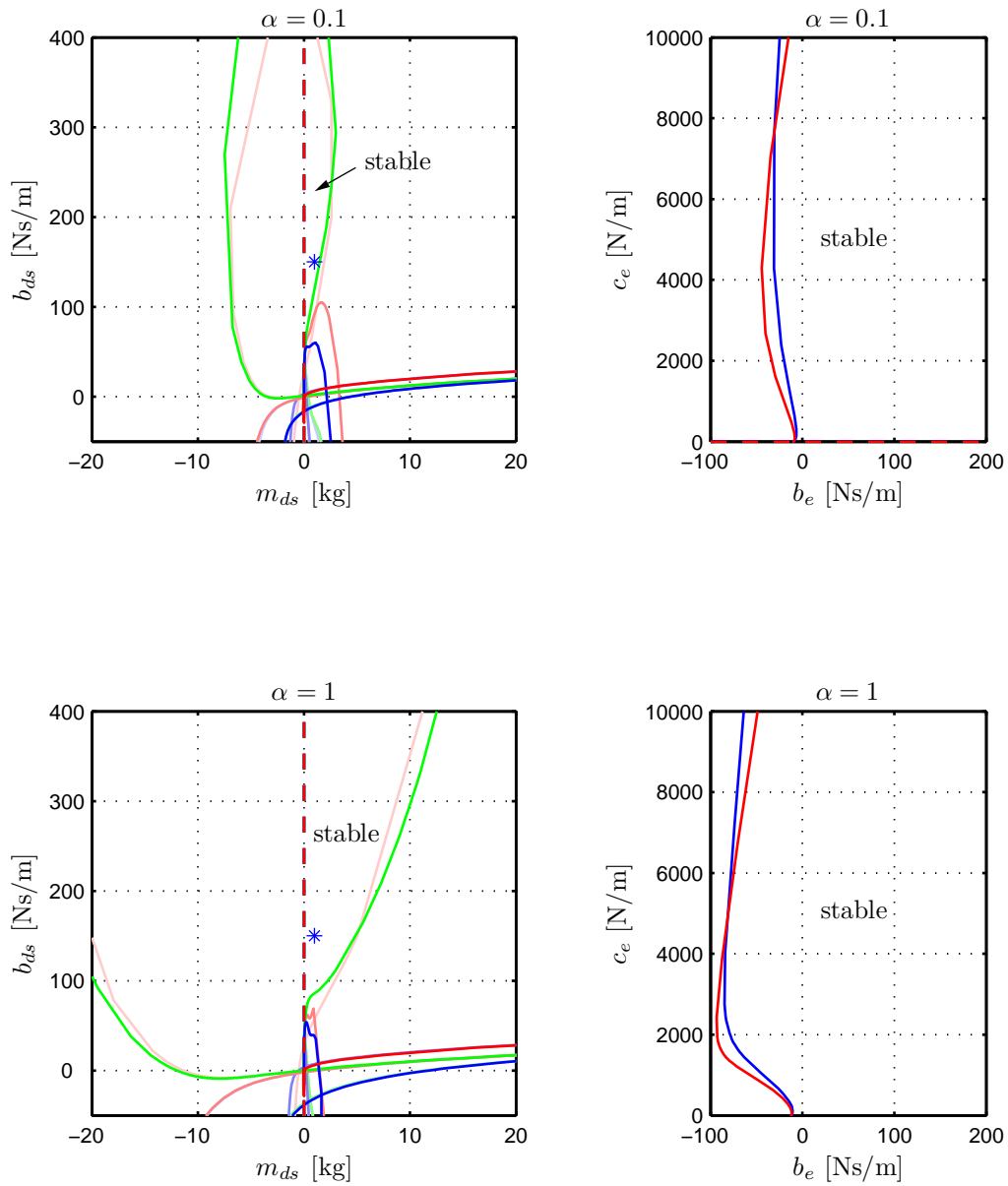


Figure 4.13: FaPa architecture (linear one DOF device): Stability boundaries of the vertices of the operating domain in the (m_{ds}, b_{ds}) -plane and robustness analysis in the (b_e, c_e) -plane for a damping of $d = -0.1$ and varying human arm impedance α ($m_{dm} = 3$ kg, $b_{dm} = 10$ Ns/m, $m_{ds} = 1$ kg, $b_{ds} = 150$ Ns/m, $c_{ds} = 1000$ N/m).

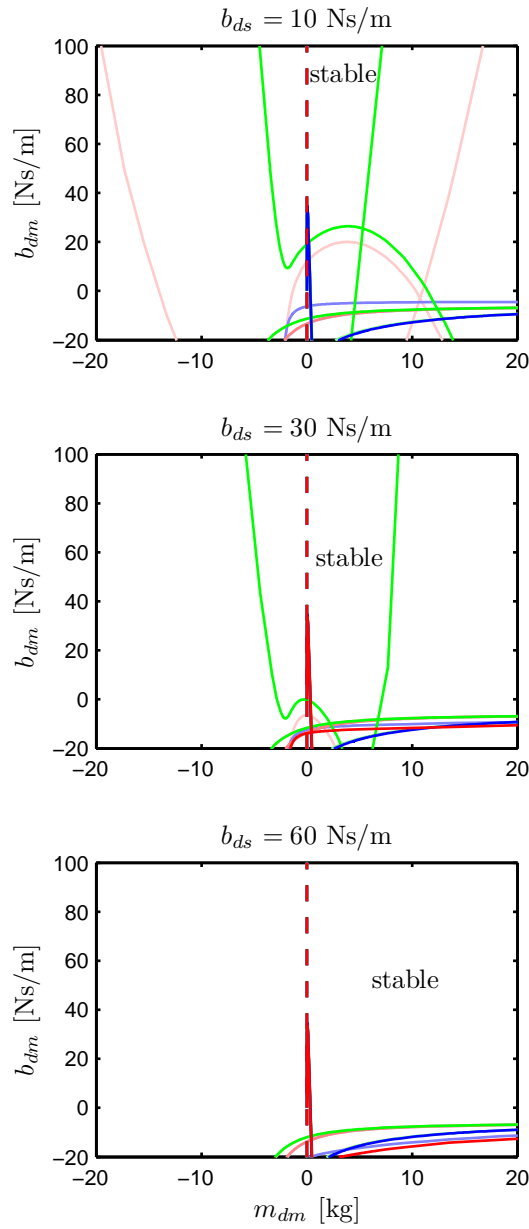


Figure 4.14: PaFa architecture (linear one DOF device): Stability boundaries of the vertices of the operating domain in the (m_{dm}, b_{dm}) -plane depending on the damping parameter b_{ds} ($\alpha = 1$, $m_{ds} = 3$ kg, $c_{dm} = 1000$ N/m).

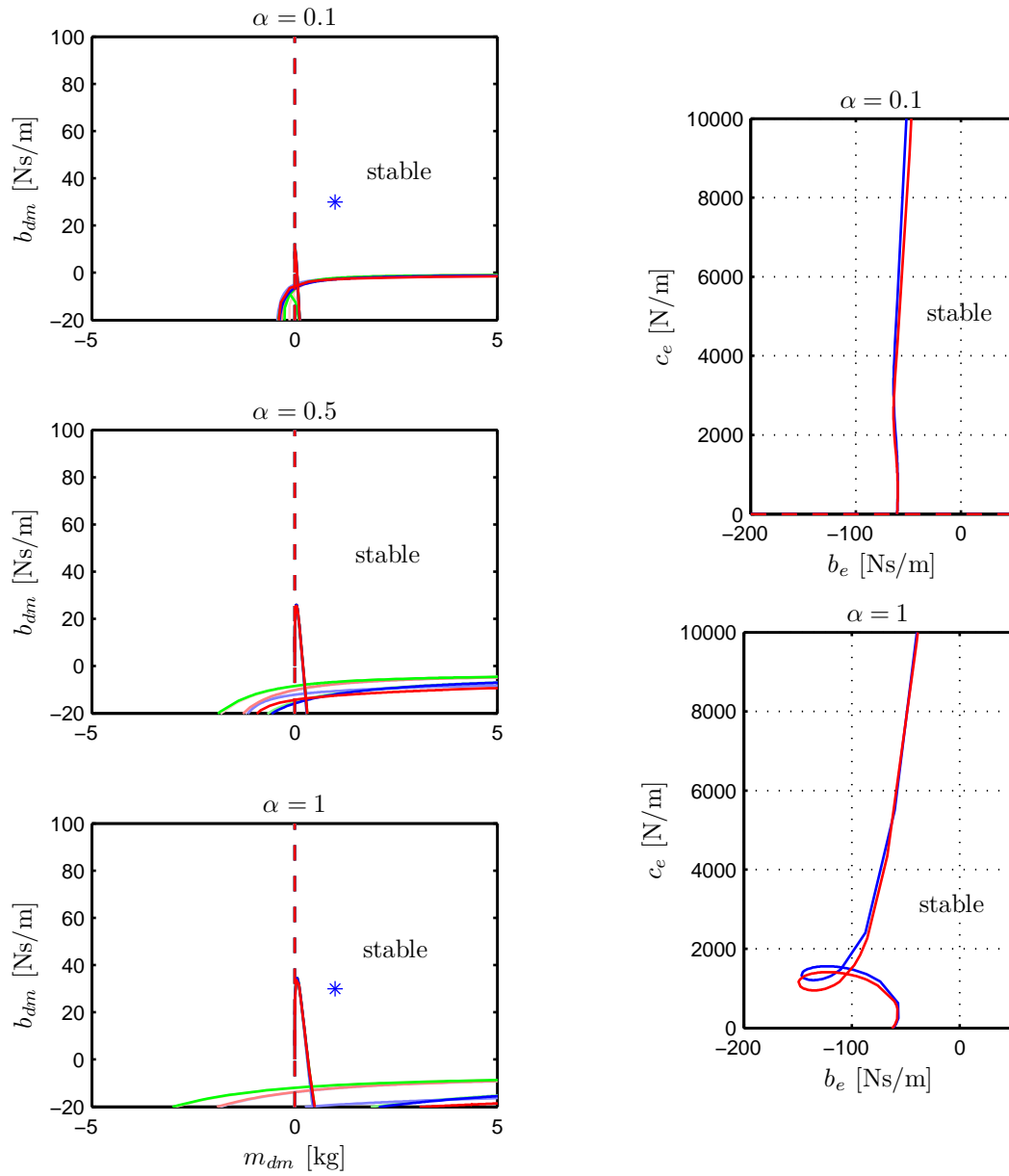


Figure 4.15: PaFa architecture (linear one DOF device): Stability boundaries of the vertices of the operating domain in the (m_{dm}, b_{dm}) -plane and robustness analysis in the (b_e, c_e) -plane for a varying human arm impedance α ($m_{ds} = 3$ kg, $b_{ds} = 60$ Ns/m, $m_{dm} = 1$ kg, $b_{dm} = 30$ Ns/m, $c_{dm} = 1000$ N/m).

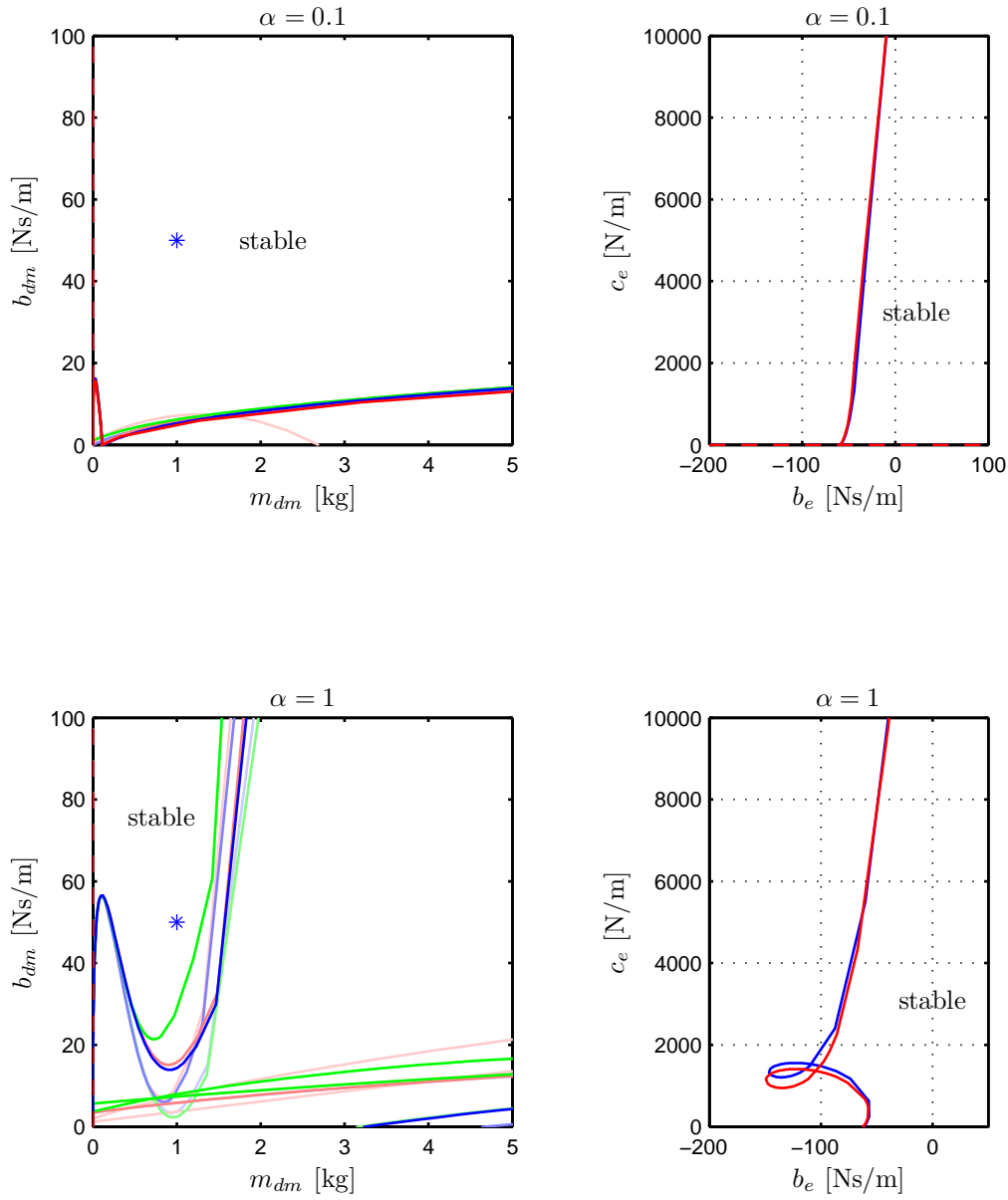


Figure 4.16: PaFa architecture (linear one DOF device): Stability boundaries of the vertices of the operating domain in the (m_{dm}, b_{dm}) -plane and robustness analysis in the (b_e, c_e) -plane for a damping of $d = -0.1$ and varying human arm impedance α ($m_{ds} = 3$ kg, $b_{ds} = 60$ Ns/m, $c_{dm} = 1000$ N/m).

Please note that all obtained results for this architecture are somehow dual to the position-based admittance control architecture with position-force exchange.

Position-based Admittance Control with Force-Force Exchange (FaFa)

Using a position-based admittance control with force-force exchange, position tracking can only be guaranteed if equal desired impedances are selected at master, as well as slave side. Thus, the number of control parameters can be reduced to a minimum of two variable parameters m_d, b_d .

The result is shown in Fig. 4.18 (left). Selecting a desired mass m_d , in general a certain amount of damping b_d is necessary to Γ -stabilize the system. There is only a very small area where a desired mass m_d stabilizes the system without implementing additional damping. The parameter m_d should be selected at least so large that haptic interface and telemanipulator are stable when they are operated alone. Fig. 4.18 (right) shows the stability boundaries in the b_e, c_e -plane. It can be seen that the selected control parameters stabilize the overall operating domain. Finally, selecting a Γ -region with damping $d = -0.1$ a certain amount of damping is necessary to Γ -stabilize the system when being in contact with stiff remote environments, see Fig. 4.19.

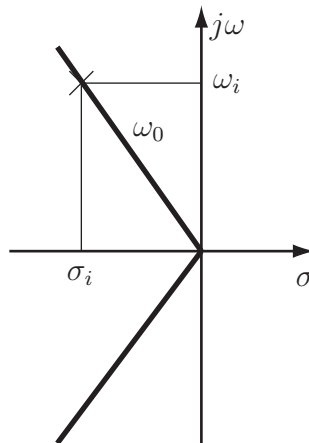


Figure 4.17: Γ -region with damping $d = -\sigma_i/\omega_0$

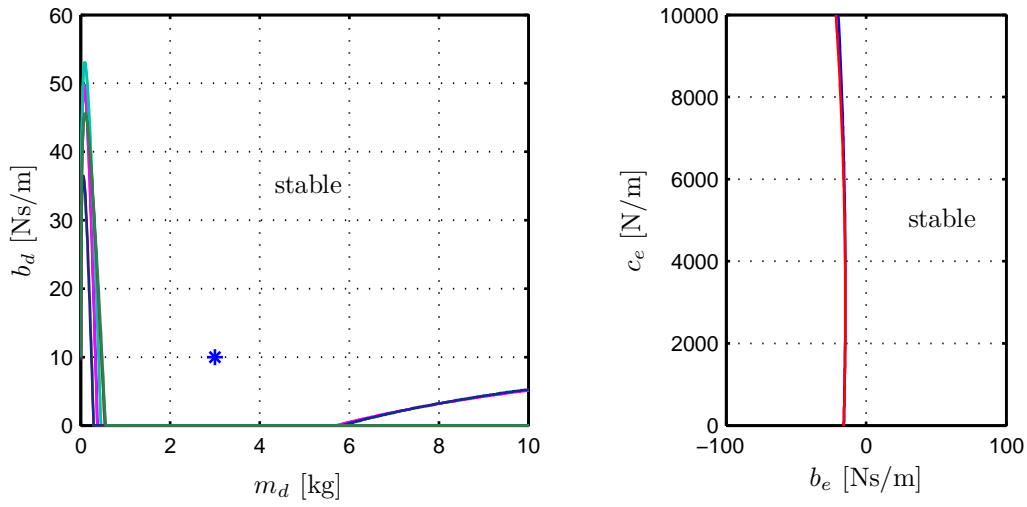


Figure 4.18: FaFa architecture (linear one DOF device): Stability boundaries of the vertices of the operating domain in the (m_d, b_d) -plane and robustness analysis in the (b_e, c_e) -plane ($\alpha = 1$, $m_d = 3$ kg, $b_d = 10$ Ns/m).

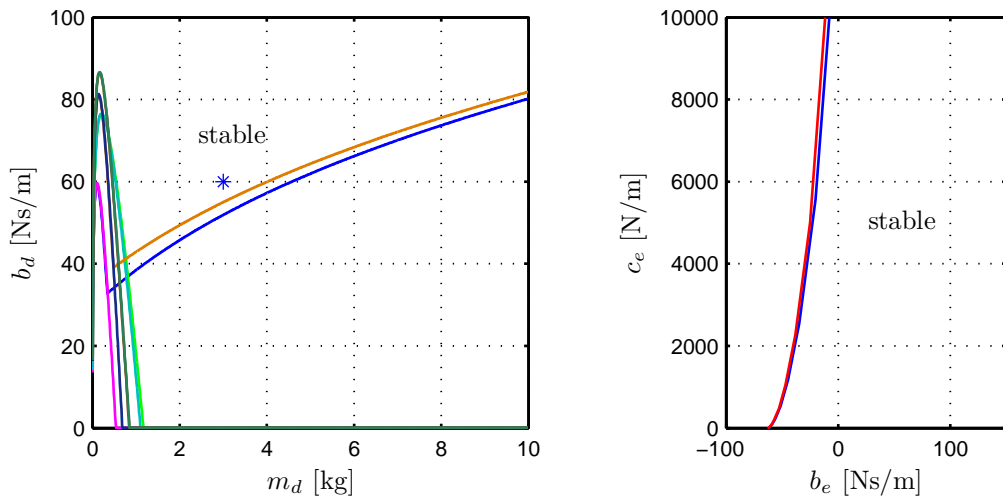


Figure 4.19: FaFa architecture (linear one DOF device): Stability boundaries of the vertices of the operating domain in the (m_d, b_d) -plane and robustness analysis in the (b_e, c_e) -plane for a damping of $d = -0.1$ ($\alpha = 1$, $m_d = 3$ kg, $b_d = 60$ Ns/m).

4.5.2 ViSHaRD10 - Dual Arm Telemanipulator

The same analysis as for the one degree of freedom system has been carried out for the teleoperation system presented in Sec. 3.1. The system consists of a redundant haptic interface as well as a redundant telemanipulator. Again, different control algorithms are analyzed.

Position-based Admittance Control with Position-Force Exchange (FaPa)

The results of the Hurwitz-stability analysis are shown in Fig. 4.20. Comparing the result with the prior achieved results for the one DOF teleoperation system, the set of stabilizing controllers is a bit bigger, but the stability margins look similar. Considering a Γ -region with damping $d = -0.1$, again the same behavior as already found for the one DOF teleoperation system can be observed: To stabilize the overall system a small value for the slave mass m_{ds} and a certain amount of slave damping b_{ds} have to be implemented, see Fig. 4.22. Hereby again an upper bound on the slave damping b_{ds} has to be taken into account. Further, in contrary to the one DOF system, not only an upper bound, but also a lower bound on the slave mass m_{ds} was found, which is mainly due to actuator limitations.

Position-based Admittance Control with Force-Position Exchange (PaFa)

The results gained from the parameter space approach are shown in Fig. 4.21. Again the same form of stability margins as already observed in the one DOF teleoperation system were found, whereby smaller human operator impedances enlarge the set of stabilizing controllers. If considering further a Γ -region with damping $d = -0.1$, also for this setup a relatively high master damping b_{dm} and low master mass m_{dm} have to be implemented to guarantee robust stability. In contrast to the architecture presented before the unstable region close to zero, which is mainly due to the actuator limitations, is more developed. Summarizing, dual to the position-based admittance control with position-force exchange, upper and lower bounds on the master mass and damping coefficients exist.

Position-based Admittance Control with Force-Force Exchange (FaFa)

For the position-based admittance control with force-force exchange the result is shown in Fig. 4.24. It can be observed that a single mass is enough to stabilize the overall teleoperation system, a small damping, however, enhances stability. Hereby, m_d should be selected at least so large that haptic interface and telemanipulator are stable when they are operated alone. Fig. 4.24 (right) shows the stability boundaries in the b_e, c_e -plane. It can be seen that the selected control parameters stabilize the overall operating domain. Finally, selecting a Γ -region with damping $d = -0.1$, similar to the one DOF teleoperation system, a certain amount of damping is necessary to Γ -stabilize the system when in contact with stiff remote environments, see Fig. 4.25.

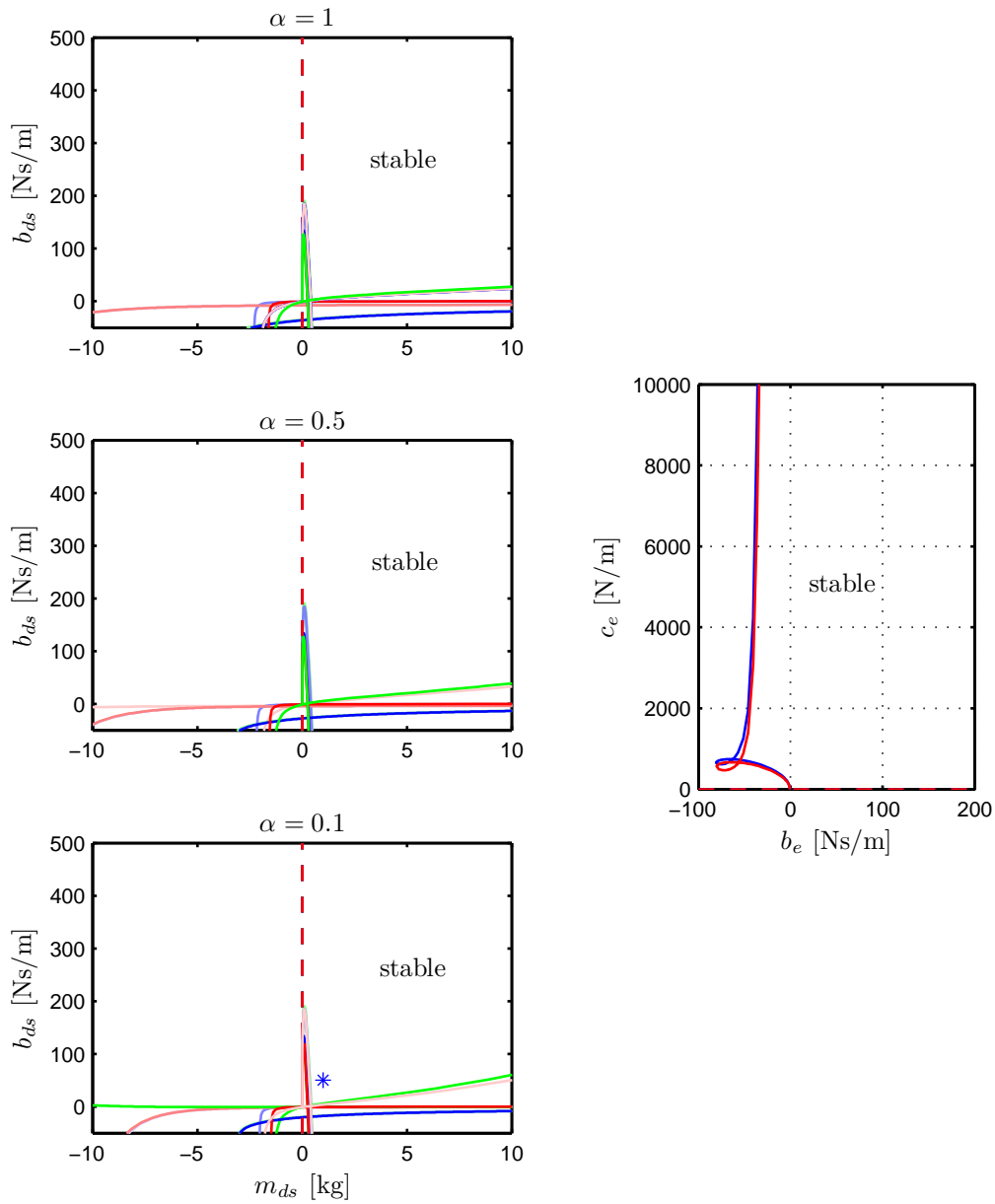


Figure 4.20: FaPa architecture (ViSHARD10- dual arm telemanipulator): Stability boundaries of the vertices of the operating domain in the (m_{ds}, b_{ds}) -plane and robustness analysis in the (b_e, c_e) -plane for $\alpha = 0.1$ ($m_{dm} = 6$ kg, $b_{dm} = 0$ Ns/m, $m_{ds} = 1$ kg, $b_{ds} = 50$ Ns/m, $c_{ds} = 600$ N/m).

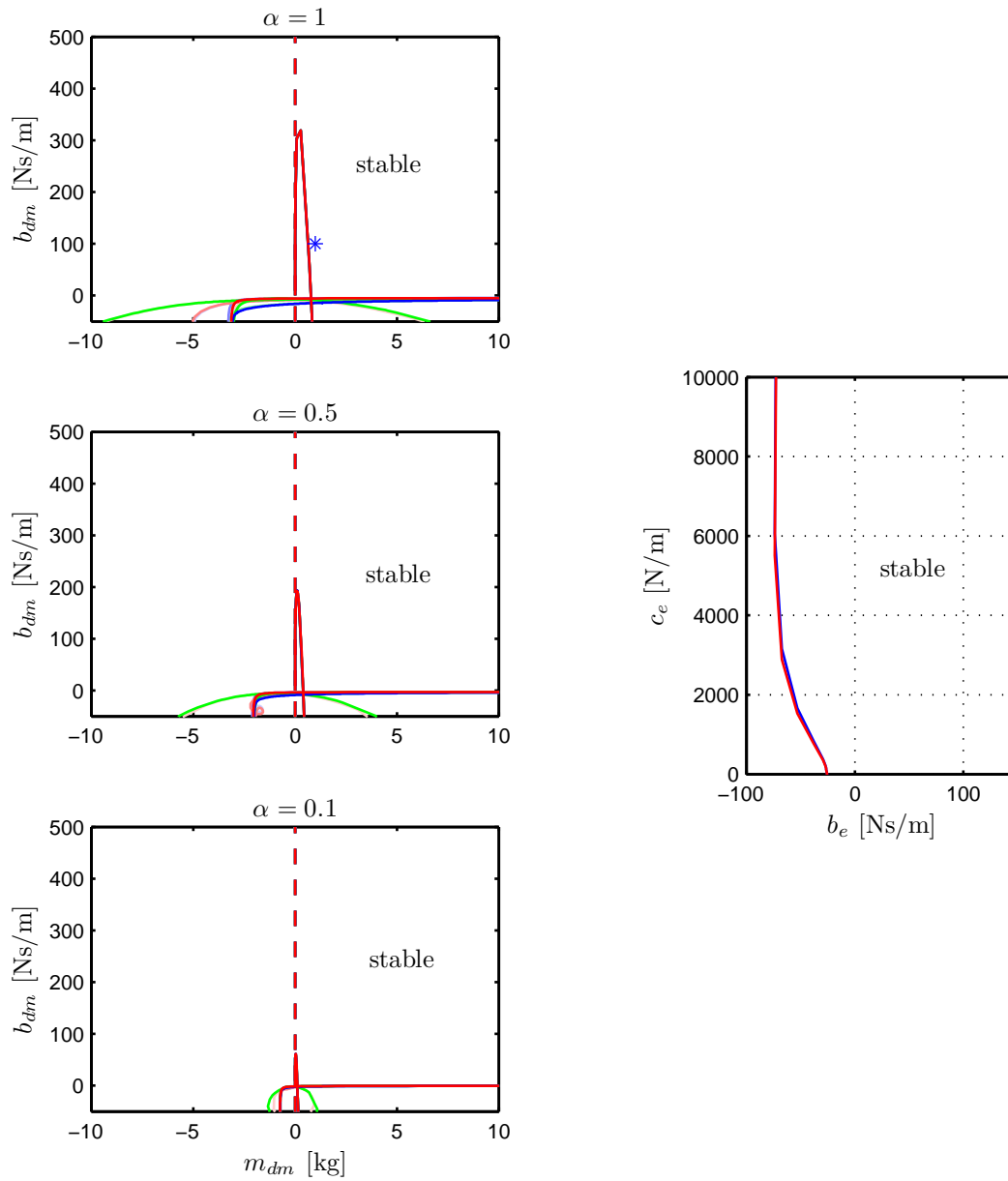


Figure 4.21: PaFa architecture (ViSHARD10- dual arm telemanipulator): Stability boundaries of the vertices of the operating domain in the (m_{dm}, b_{dm}) -plane and robustness analysis in the (b_e, c_e) -plane for $\alpha = 1$ ($m_{dm} = 1$ kg, $b_{dm} = 100$ Ns/m, $m_{ds} = 6$ kg, $b_{ds} = 20$ Ns/m, $c_{dm} = 600$ N/m).

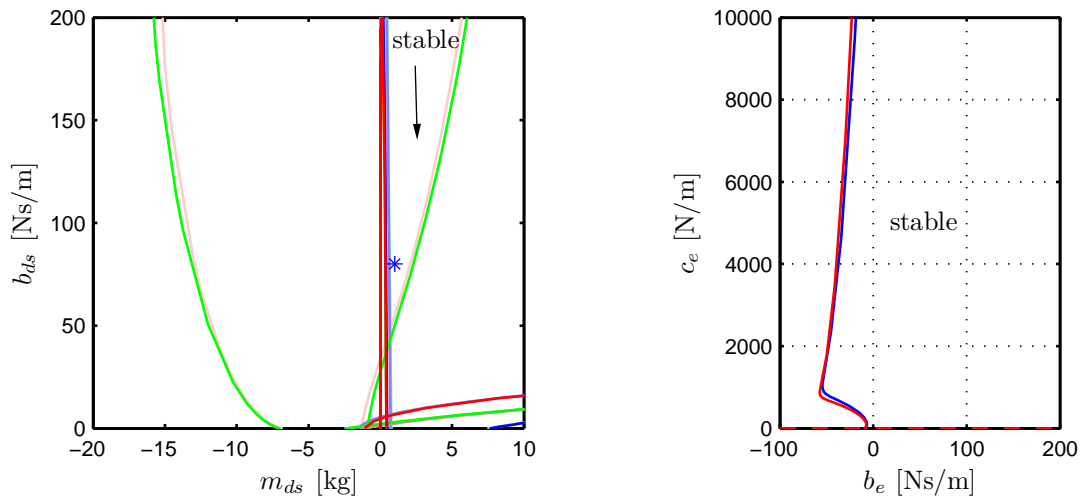


Figure 4.22: FaPa architecture (ViSHARD10- dual arm telemanipulator): Stability boundaries of the vertices of the operating domain in the (m_{ds}, b_{ds}) -plane and robustness analysis in the (b_e, c_e) -plane for a damping of $d = -0.1$ ($\alpha = 0.1$, $m_{dm} = 6$ kg, $b_{dm} = 20$ Nm/s, $m_{ds} = 1$ kg, $b_{ds} = 80$ Ns/m, $c_{ds} = 600$ N/m).

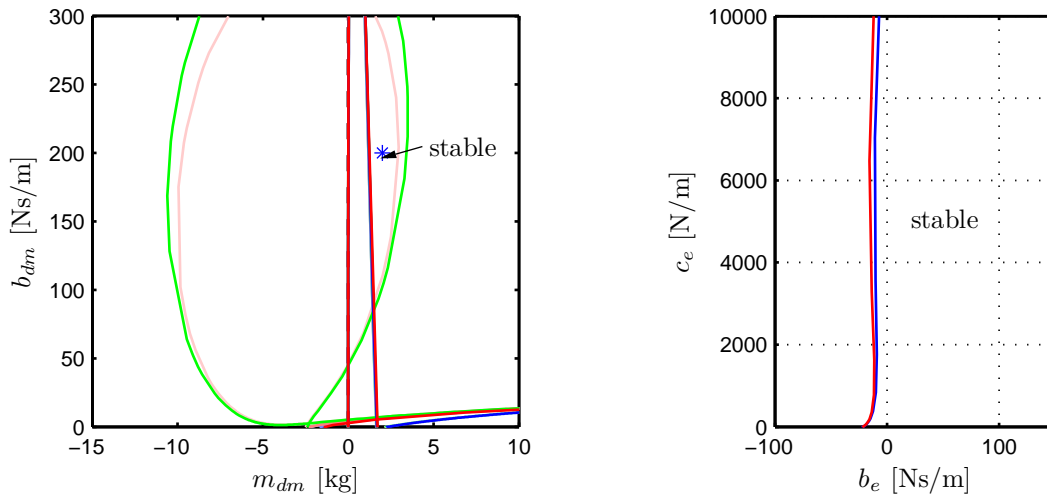


Figure 4.23: PaFa architecture (ViSHARD10- dual arm telemanipulator): Stability boundaries of the vertices of the operating domain in the (m_{dm}, b_{dm}) -plane and robustness analysis in the (b_e, c_e) -plane for a damping of $d = -0.1$ ($\alpha = 1$, $m_{dm} = 2$ kg, $b_{dm} = 200$ Nm/s, $c_{dm} = 600$ N/m, $m_{ds} = 6$ kg, $b_{ds} = 20$ Nm/s).

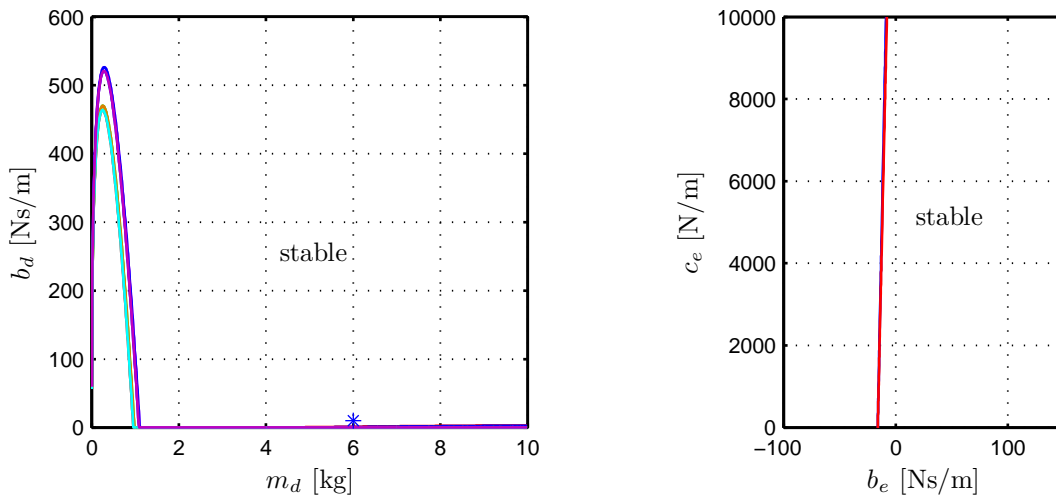


Figure 4.24: FaFa architecture (ViSHARD10- dual arm telemanipulator): Stability boundaries of the vertices of the operating domain in the (m_d, b_d) -plane and robustness analysis in the (b_e, c_e) -plane ($\alpha = 1, m_d = 6$ kg, $b_d = 10$ Ns/m).

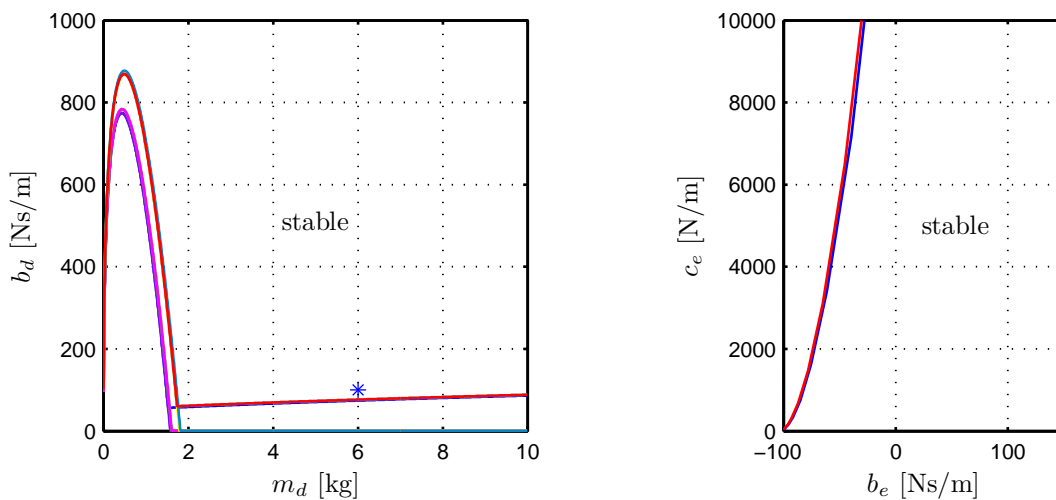


Figure 4.25: FaFa architecture (ViSHARD10- dual arm telemanipulator): Stability boundaries of the vertices of the operating domain in the (m_d, b_d) -plane and robustness analysis in the (b_e, c_e) -plane a damping of $d = -0.1$ ($\alpha = 1, m_d = 6$ kg, $b_d = 100$ Ns/m).

4.5.3 Summary

In the prior sections, robust stability of different bilateral control architectures has been analyzed by using the parameter space approach and guidelines for the control parameter selection were derived. Table 4.1 summarizes again the main obtained results.

Table 4.1: Boundaries imposed by robust stability on admittance parameters of local controllers

para- meters	control architecture		
	FaPa	PaFa	FaFa
m_{dm}	lower limit	{lower and} upper limit	lower limit
b_{dm}	$b_{dm} \uparrow \Rightarrow$ set of stabilizing controllers \uparrow	lower and upper limit	lower limit
m_{ds}	{lower and} upper limit	lower limit	lower limit
b_{ds}	lower and upper limit	$b_{ds} \uparrow \Rightarrow$ set of stabilizing controllers \uparrow	lower limit
α	$\alpha \uparrow \Rightarrow$ set of stabilizing controllers \uparrow	$\alpha \uparrow \Rightarrow$ set of stabilizing controllers \downarrow	$\alpha \uparrow \Rightarrow$ set of stabilizing controllers \downarrow

It can be seen that for all analyzed control architectures robust stabilizing control parameter sets could be found. Hereby the form of the found stability boundaries do not differ significantly among different analyzed teleoperation systems. Thus, it can be concluded that the obtained results are generalizable, even though the exact numerical values are valid only for the special analyzed systems.

Comparing the results of the position-based admittance control with position-force exchange (FaPa) with the results of the position-based admittance control with force-position exchange (PaFa) a dual behavior can be observed. Boundaries found for the master parameters of one architecture can be found also for the slave parameters of the other architecture. Very interesting is further that at the side of the compliant controllers the mass and damping parameters have to be selected out of a certain interval as lower and upper bounds are imposed on these parameters as shows the stability analysis. This indicates for example that increasing the damping in the local compliant controllers does not necessarily improve robust stability of the overall teleoperation system. Concerning the mass parameter, only very small values guarantee a well damped behavior of the overall teleoperation system, whereby also a lower bound on this parameter, due to actuator limitations, has to be taken into account. Finally, an increasing human operator impedance was found to increase the set of stabilizing controllers for the FaPa architecture, while the same behavior resulted in a decrease of the set of stabilizing controllers for the PaFa architecture.

The position-based admittance control architecture with force-force exchange resulted to be very easy to tune as only two control parameters have to be selected and only lower bounds on the single control parameters have to be taken into account. This simplifies the selection of appropriate control parameters significantly. In detail the following guidelines for control parameter selection were found: Depending on the mass distribution in the teleoperation system, the overall system can be stabilized by implementing either a desired mass only or a certain combination of mass and damping coefficient, whereby increasing the damping coefficient allows to achieve a well damped behavior. Finally, an increasing human operator impedance led to a reduction of stabilizing control parameter sets.

Comparing the architectures from a performance point of view, the position-based admittance control with position-force exchange achieves the best transparency as only low

admittance parameters are necessary at operator side. The position-based admittance control with force-force exchange, however, is much easier to tune, because of the limited number of control parameters. For a multi-d.o.f. system this is of special importance, as the number of parameters increases with each motion possibility and already selected parameters for one degree of motion can influence the others.

4.6 Experimental Evaluation

To verify the obtained simulation results, the presented control architectures are implemented in the real hardware setup and interactions with different kind of remote environments are tested. As the results are similar for both kind of analyzed teleoperation systems, only results obtained with the multi-DOF system are reported in this section. But before going into detail, the above presented control architectures have to be extended to multiple DOF, which requires taking into account some specialties reported in the following sections.

4.6.1 Quaternion-based Admittance Control

In the first step, the before analyzed control architectures have to be implemented for a 6 DOF teleoperation system using the already presented redundant haptic interfaces as well as telemanipulator arms. This involves the implementation of desired impedances for translational, as well as rotational motions.

For the translational part desired impedances can be implemented in form of simple mass-spring-damper systems

$$\mathbf{f} = \mathbf{M}_p \ddot{\mathbf{x}}_{dc} + \mathbf{B}_p \dot{\mathbf{x}}_{dc} + \mathbf{C}_p \mathbf{x}_{dc}, \quad (4.29)$$

where \mathbf{f} denotes the Cartesian force, \mathbf{M}_p , \mathbf{B}_p and \mathbf{C}_p are inertia, damping and stiffness matrices and $\ddot{\mathbf{x}}_{dc}$, $\dot{\mathbf{x}}_{dc}$ and \mathbf{x}_{dc} acceleration, velocity and displacement.

While forward integration of (4.29) is straightforward and does not pose any difficulty, the implementation of a corresponding rotational impedance is problematic and requires special attention.

Rotational motion is naturally described by the torque $\boldsymbol{\mu}$ and rotational velocity $\boldsymbol{\omega}$. The problem is that the simple integral $\int \boldsymbol{\omega} dt$ does not have a physical meaning and is unsuitable for the description of the rotational displacement and rotational stiffness. The commonly used three parameter orientation representations (Euler angles, RPY angles, etc.) are also unsuitable due to the algebraic singularities at certain workspace points (see [121] and chapter 2), and geometric inconsistency with the rotational velocity. On this account the unit quaternion $\mathbf{Q} = \{\eta, \boldsymbol{\varepsilon}\}$, as a singularity-free representation, is chosen, see [20]. The rotational impedance is then given by

$$\boldsymbol{\mu} = \mathbf{M}_o \dot{\boldsymbol{\omega}}_{dc} + \mathbf{B}_o \boldsymbol{\omega}_{dc} + \mathbf{C}_o \boldsymbol{\varepsilon}_{dc}, \quad (4.30)$$

where \mathbf{M}_o , \mathbf{B}_o , and \mathbf{C}_o are virtual Cartesian inertia, damping and stiffness matrices for the orientation with

$$\mathbf{C}_o = 2\mathbf{E}^T(\eta, \boldsymbol{\varepsilon}) \mathbf{C}'_o, \quad (4.31)$$

$$\mathbf{E} = \eta \mathbf{I} - \mathbf{S}(\boldsymbol{\varepsilon}). \quad (4.32)$$

The operator $\mathbf{S}(\cdot)$ hereby performs the cross product between two (3 x 1) vectors, and the rotational velocity and the unit quaternion are related by the following quaternion propagation rule

$$\dot{\eta} = -\frac{1}{2}\boldsymbol{\varepsilon}^T\boldsymbol{\omega}, \quad (4.33)$$

$$\dot{\boldsymbol{\varepsilon}} = \frac{1}{2}\mathbf{E}(\eta, \boldsymbol{\varepsilon})\boldsymbol{\omega}. \quad (4.34)$$

All control architectures presented below, use this type of impedance implementation.

4.6.2 Redundancy Resolution

As redundant manipulators are used as haptic interface and telemanipulator, adequate redundancy resolution schemes must be adopted. At master side, redundancy is solved by using an inverse kinematic algorithm based on Pseudoinverse control, as presented in Sec. 2.3.3. The redundancy of the telemanipulator arms is solved by using an augmented task space formulation. One of the serious problems in Pseudoinverse-based control is namely the non-repeatability of the joint motion and the inability to specify the self motion in an open way. While at the operator site the self-motion does not affect the manipulation performance, at the teleoperator site a predictable manipulator motion is very important. On this account, a position-based inverse kinematics using an extended task space formulation is used [121, 167]. Hereby, the task space vector \mathbf{x} is extended with a vector lying in the null space of the Jacobian, so that the Jacobian becomes square and can be inverted. To extend the task space formulation, an additional equation must be formulated which constrains the variety of possible motion possibilities. In this work, an additional equation for the elbow angle θ of the telemanipulator is used as such a constraint $\mathbf{x}_E = [\mathbf{x}, \theta]^T$. In case the elbow angle of the human operator can be measured, it can be used as an input for the inverse kinematics, otherwise the elbow angle can be set to a constant value.

4.6.3 Overall Control Structure

The block diagram of a position-based admittance control with position-force exchange shown in Fig. 4.26 is exemplary for all bilateral control architectures, and combines the control of haptic input device and telemanipulator to a two-channel architecture. While for the haptic interface admittance control is used to render a target dynamics, for the telemanipulator admittance control is used to achieve a compliant behavior when being in contact with the environment. Desired positions are sent to the telemanipulator and the measured interaction forces are fed back to the operator site. For the purpose of solving redundancy at teleoperator site, an additional parameter for the elbow angle has to be provided, as mentioned above. On this account, the elbow motion of the human operator has to be tracked and used as an input to the inverse kinematics. To keep the measurements simple and to avoid additional tracking equipment, a constant elbow angle $\theta_d = 0$ is used in the following experiments.

All other bilateral control architectures are implemented analogously.

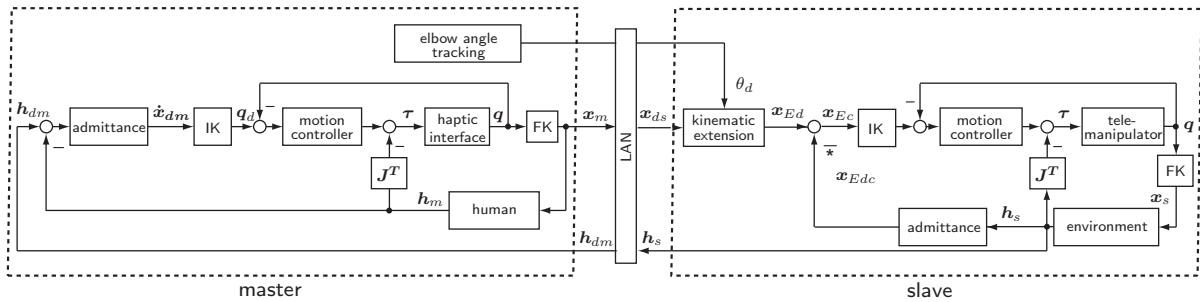


Figure 4.26: Overall teleoperation control architecture of a position-based admittance control with position-force exchange

4.6.4 Experimental Setup

The experimental setup, see Fig. 4.27, consists of the haptic input device ViSHARD10, the 7 DOF slave manipulator and the stereo vision system already introduced in Sec. 3.1. According to the bilateral control structure, position and force information is exchanged. The devices communicate over a UDP network with a sampling rate of 1kHz, which is the same as for the local loop control. To make the experiments simple the elbow angle θ is kept constant.

The experiment consists of the following two tasks:

- tracking of free space motion
- haptic exploration of different materials (soft and stiff)

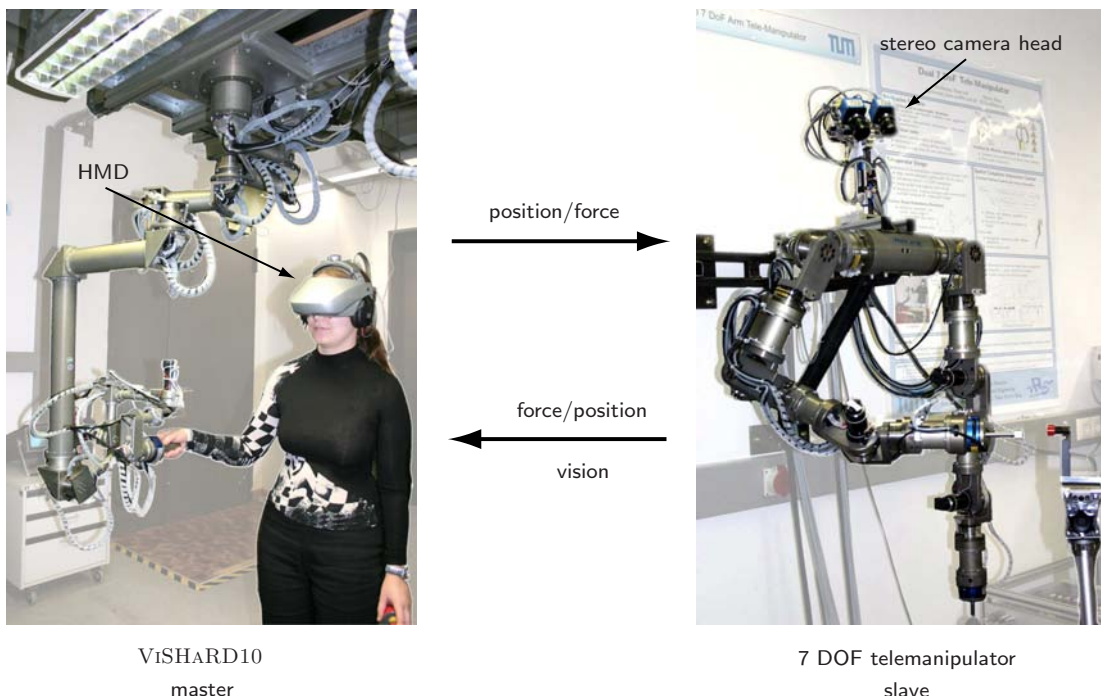


Figure 4.27: Experimental setup consisting of haptic interface ViSHARD10, dual arm telemanipulator and stereo-vision system

4.6.5 Experimental Results

The following paragraphs report the obtained experimental results for the above introduced control architectures. To realize a uniform behavior for all directions, diagonal mass, stiffness and damping matrices $\mathbf{M}_{p/o} = M_{p/o}\mathbf{E}$, $\mathbf{D}_{p/o} = D_{p/o}\mathbf{E}$, $\mathbf{C}_{p/o} = C_{p/o}\mathbf{E}$ have been selected.

Position-based Admittance Control with Force-Position Exchange (FaPa)

Using a position-based admittance control with force-position exchange architecture, the reference position of the teleoperator is modified according to (4.29) and (4.30). Consequently, transparency is influenced by the parameter settings of the slave impedance control. The stiffer the impedance control of the slave, the smaller the position deviation and the better the real environment impedance is reproduced. But this stays in contrast to the stability behavior of the overall system.

Transparency is also affected by the master control, since perfect transparency requires the master mass to be set to zero. However, this is not possible because the minimum target inertia of the haptic interface is bounded by stability, see Sec. 2.4. Thus, in free space motion a minimal mass and inertia necessary for stability of the master control can be felt.

Fig. 4.28 shows the position and force tracking performance during haptic exploration of different materials. Hereby, the control parameters were selected according to Fig. 4.22 to guarantee a damped behavior of the overall system. Thus, a slave damping of $B_p = 200$ Nm/s, $B_o = 10$ Nms/rad and a slave inertia of $M_p = 2$ kg, $M_o = 0.1$ kgm² have been implemented. Due to the lower bound of the master inertia, a relatively high rotational master inertia of $M_o = 0.5$ kgm² was necessary.

The shaded areas indicate the contact phases. One can see that during free space motion the position tracking of the slave arm works very well, while in contact, as a consequence of the implemented impedance controller, the slave position differs from the master position. It should be noted that as the force tracking is very good, this position displacement influences the displayed and felt environmental impedance in such a way that hard objects are perceived softer than they are. As the master controller is of admittance type which reacts on the human force input, small forces during free space motion are necessary to change the actual end-effector position. Ideal transparency would require zero measured forces.

Finally, Fig. 4.29 shows the force tracking performance when selecting a high slave inertia. According to Fig. 4.22 this would cause a low damped behavior of the overall system. As can be observed in the measurements, low damped oscillations occur when coming in contact with the remote environment. In particular, contact with hard objects results in high frequency oscillations.

Position-based Admittance Control with Position-Force Exchange (PaFa)

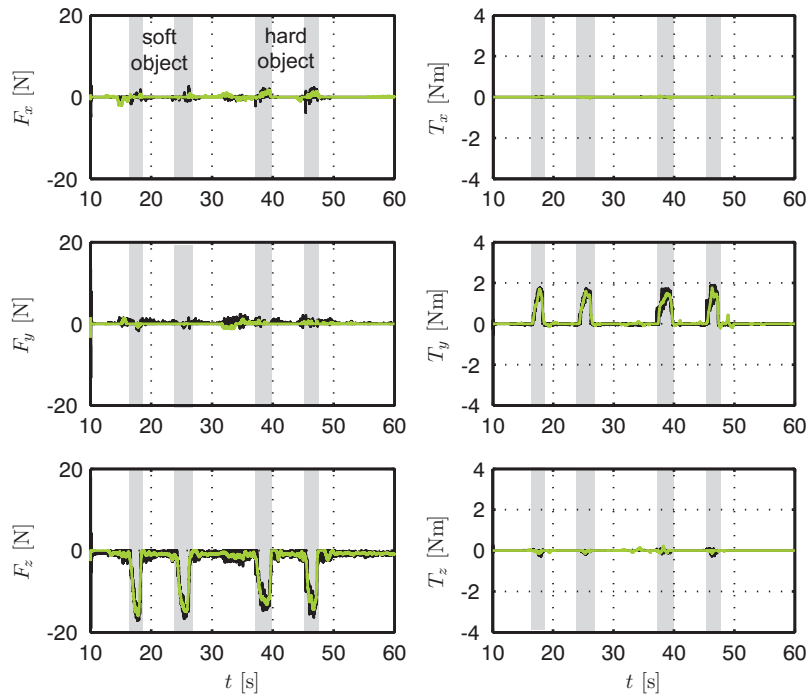
Using a position-based admittance control with position-force exchange, similar measurement results as already obtained with the mirrored version emerge. Since master and slave impedance are active in free space motion *and* contact, both impedances deteriorate the impression of the remote environment simultaneously. Fig. 4.30 shows the position and force tracking performance, whereby the admittance parameters were selected according

to Fig. 4.23. Thus, a certain amount of master damping and a small master inertia have been implemented. The selection of a high master inertia causes low damped behavior, as can be observed in Fig. 4.31. While contact with stiff remote environments caused no problems when selecting appropriate admittance parameters, during free space motion subjects reported a somewhat joggling behavior when interacting with the haptic interface. This effect might be ascribed to the small deadband introduced in the force measurement of master and slave device to compensate for modelling errors in the gravity compensation of the end-effectors.

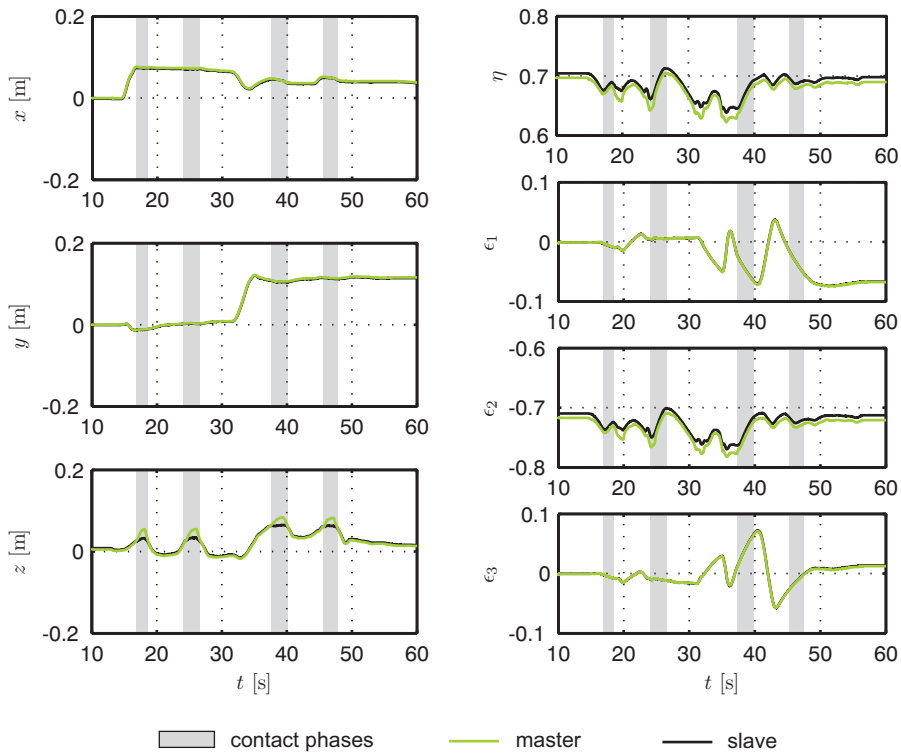
Position-based Admittance Control with Force-Force Exchange (FaFa)

Finally, the results for the position-based admittance control with force-force exchange are reported. As Fig. 4.25 shows, robust stability is guaranteed if a certain amount of inertia and damping are implemented for master as well as slave device. For the experiments an inertia of $M_p = 6$ kg and $M_o = 0.2$ kgm² have been selected. Fig. 4.32 and Fig. 4.33 show measurement results for a high and low value of implemented damping. If contact with stiff remote environments is considered, the low damping case shows a larger settling time than the high damping case. On the other hand, the force tracking error during free space motion is larger in the high damping case. This indicates that the selection of an appropriate damping coefficient means to accept a compromise between stability and transparency of the overall teleoperation system.

Force tracking



Position tracking

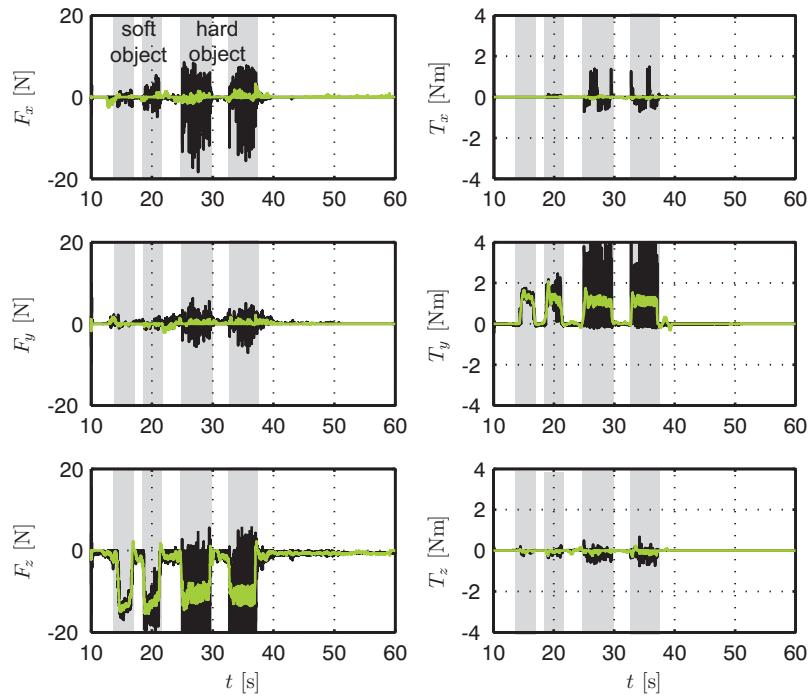


Legend: contact phases master slave

Figure 4.28: FaPa architecture: force and position tracking

(master: $M_p = 10$ kg, $B_p = 20$ Nm/s, $C_p = 0$ N/m, $M_o = 0.5$ kgm², $B_o = 0.1$ Nms/rad, $C_o = 0$ Nm/rad, slave: $M_p = 2$ kg, $B_p = 200$ Nm/s, $C_p = 600$ N/m, $M_o = 0.1$ kgm², $B_o = 10$ Nms/rad, $C_o = 100$ Nm/rad)

Force tracking



Position tracking

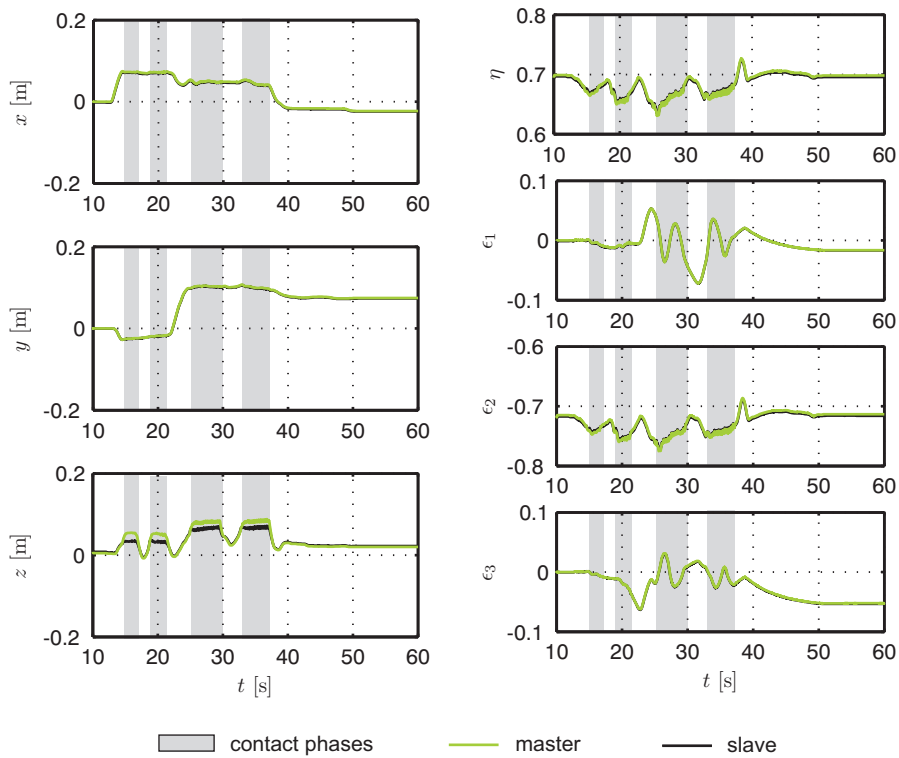
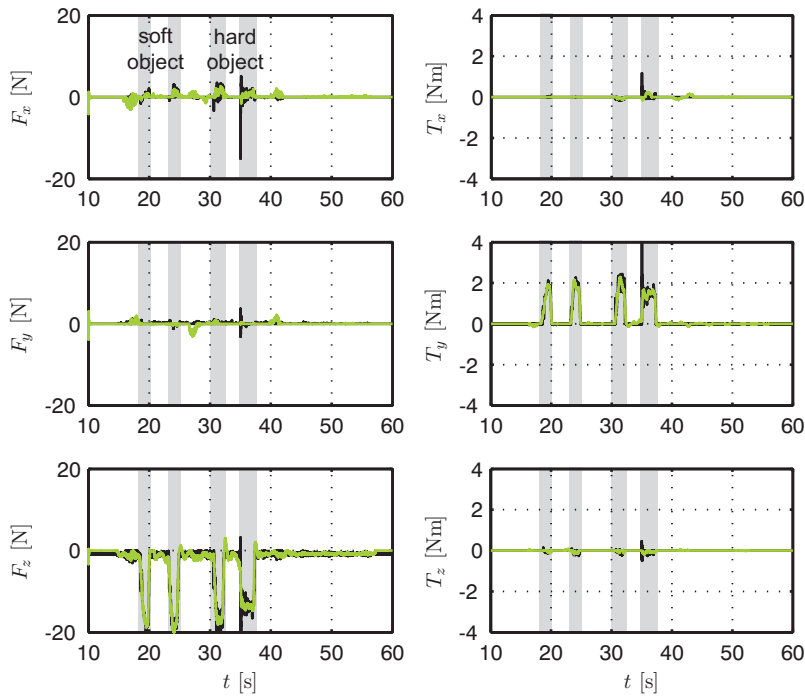


Figure 4.29: FaPa architecture: force and position tracking for low damped behavior
(master: $M_p = 10$ kg, $B_p = 20$ Nm/s, $C_p = 0$ N/m, $M_o = 0.5$ kgm², $B_o = 0.1$ Nms/rad, $C_o = 0$ Nm/rad, slave: $M_p = 20$ kg, $B_p = 200$ Nm/s, $C_p = 600$ N/m, $M_o = 1$ kgm², $B_o = 10$ Nms/rad, $C_o = 100$ Nm/rad)

Force tracking



Position tracking

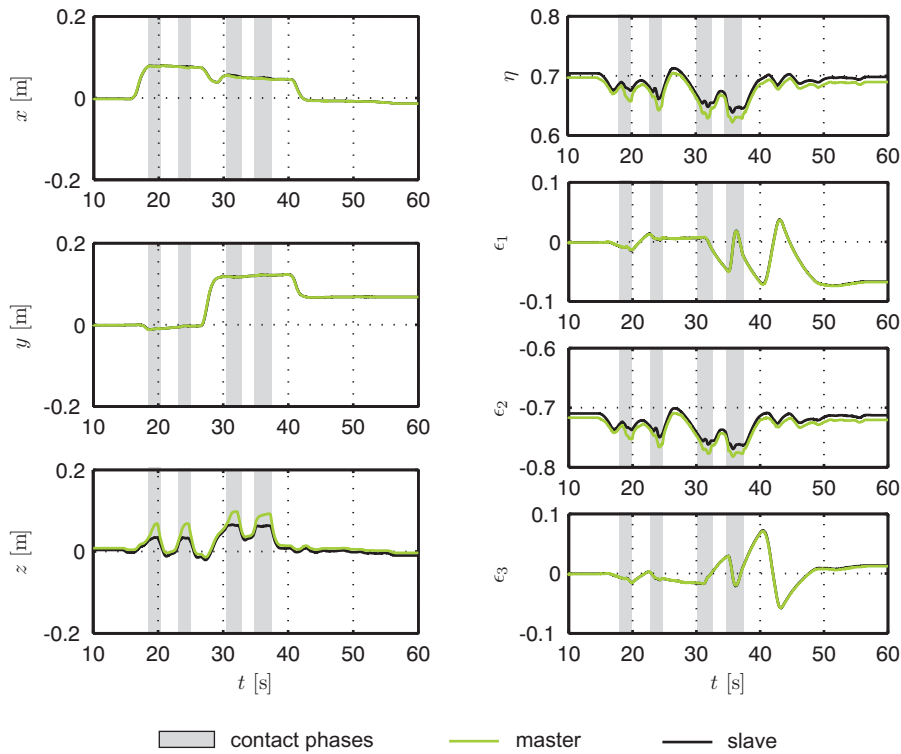
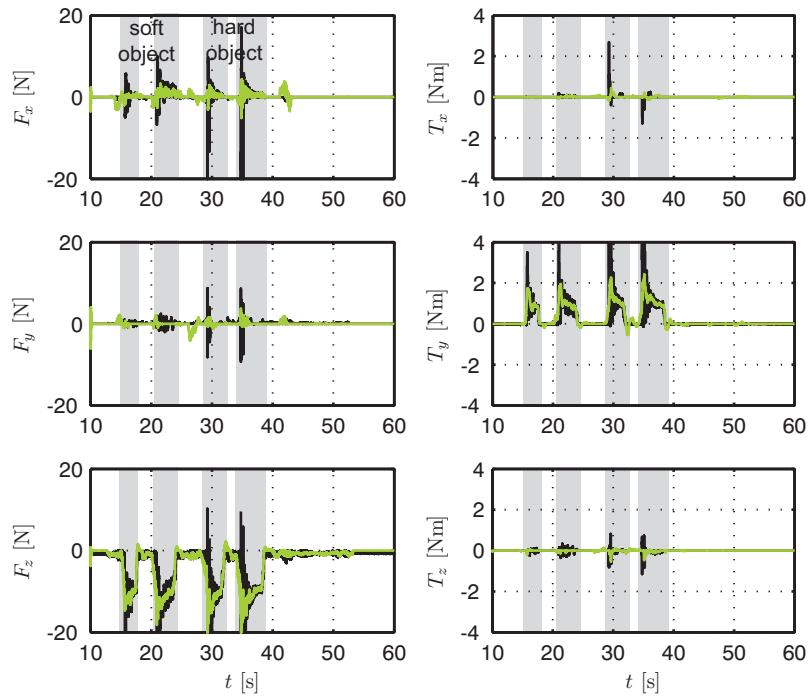


Figure 4.30: PaFa architecture: force and position tracking

(master: $M_p = 2$ kg, $B_p = 200$ Nm/s, $C_p = 600$ N/m, $M_o = 0.1$ kgm², $B_o = 10$ Nms/rad, $C_o = 100$ Nm/rad, slave: $M_p = 10$ kg, $B_p = 20$ Nm/s, $C_p = 0$ N/m, $M_o = 0.5$ kgm², $B_o = 0.1$ Nms/rad, $C_o = 0$ Nm/rad)

Force tracking



Position tracking

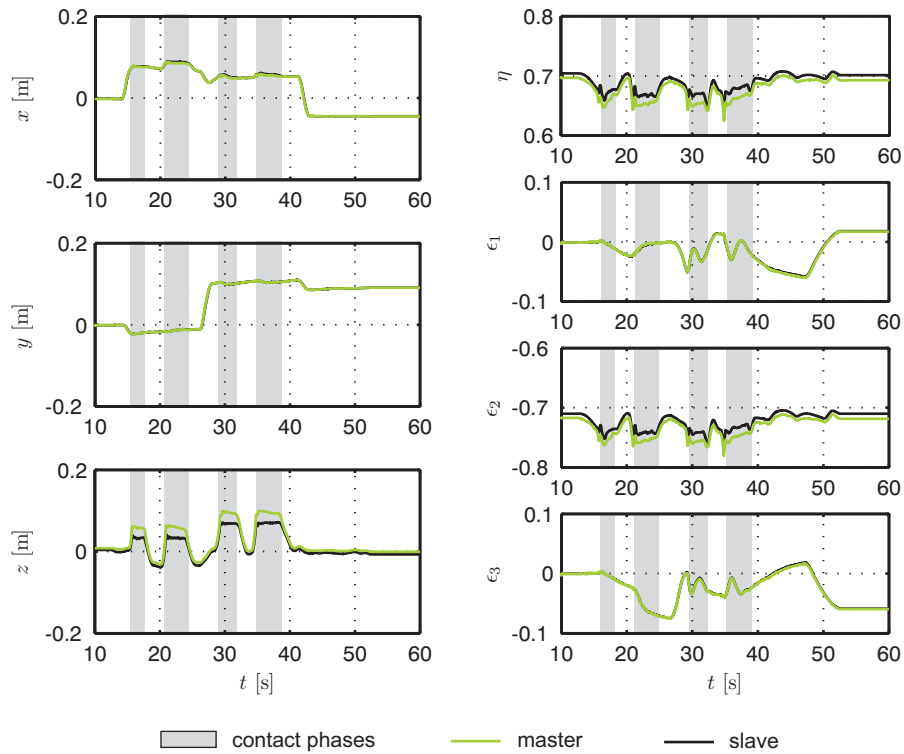
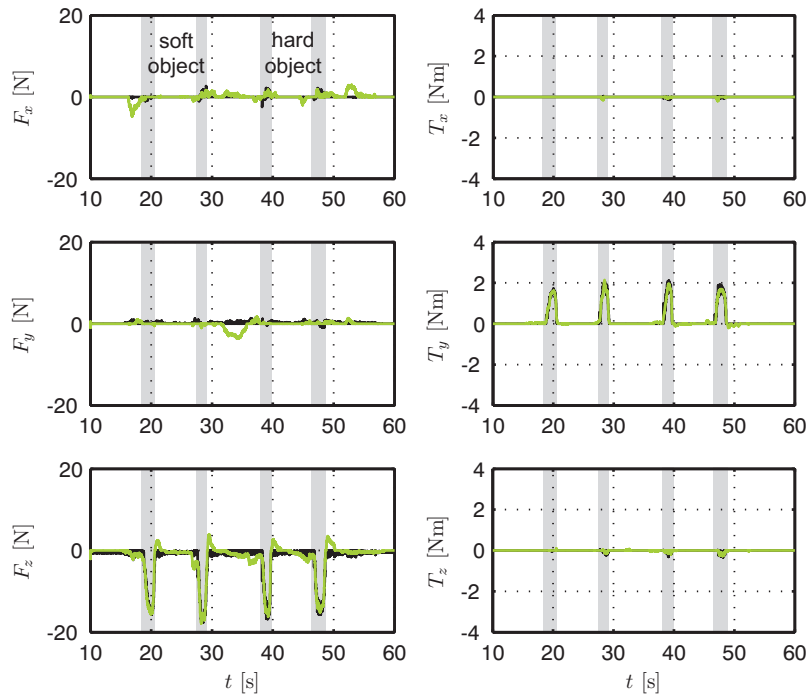


Figure 4.31: PaFa architecture: force and position tracking for low damped behavior
(master: $M_p = 20$ kg, $B_p = 200$ Nm/s, $C_p = 600$ N/m, $M_o = 1$ kgm²,
 $B_o = 10$ Nms/rad, $C_o = 100$ Nm/rad, slave: $M_p = 10$ kg, $B_p = 20$ Nm/s, $C_p = 0$ N/m,
 $M_o = 0.5$ kgm², $B_o = 0.1$ Nms/rad, $C_o = 0$ Nm/rad)

Force tracking



Position tracking

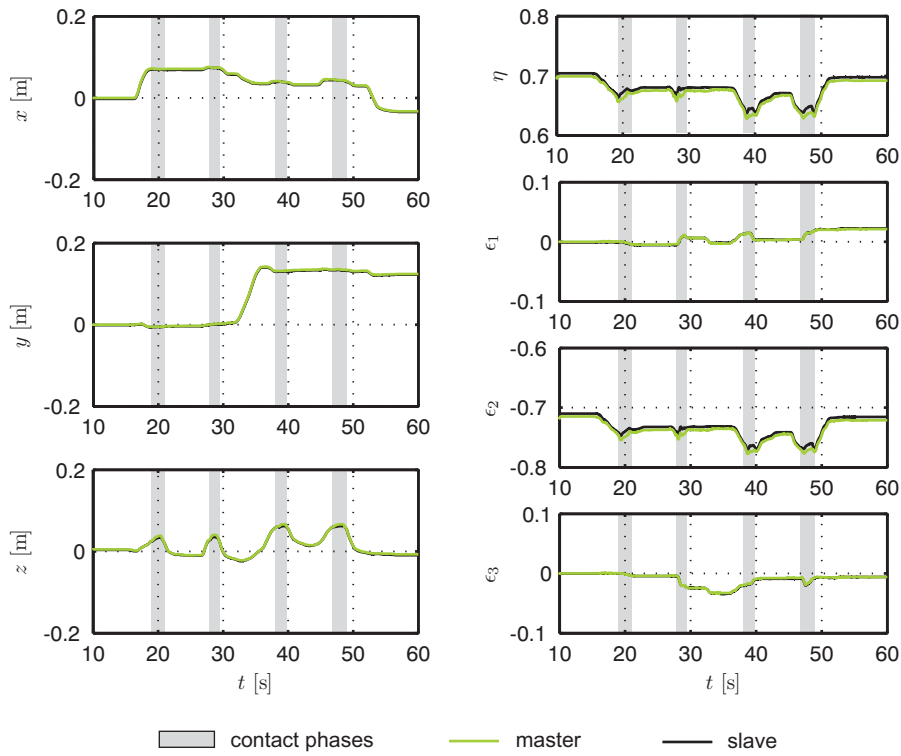
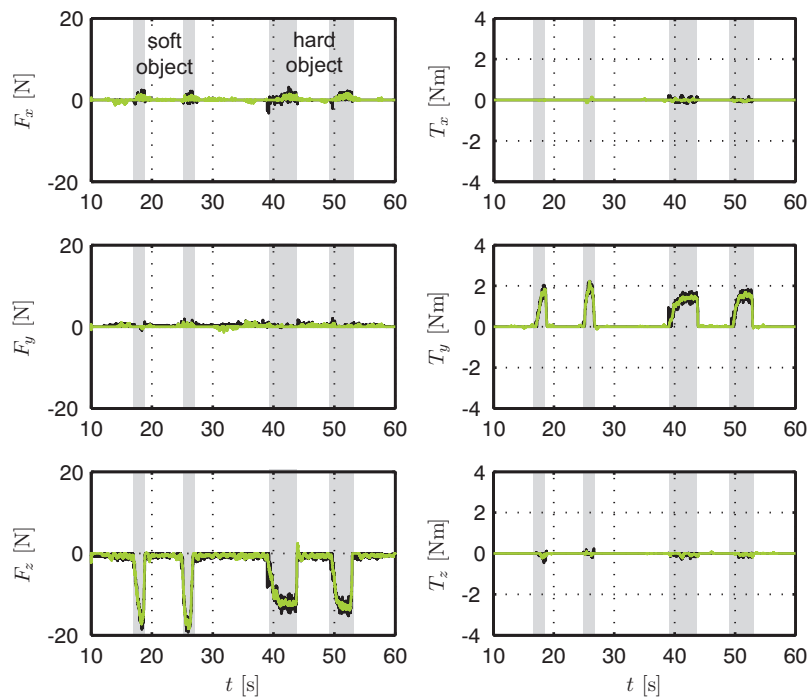


Figure 4.32: FaFa architecture: force and position tracking
 $(M_p = 6 \text{ kg}, B_p = 70 \text{ Nm/s}, M_o = 0.2 \text{ kgm}^2, B_o = 1 \text{ Nms/rad})$

Force tracking



Position tracking

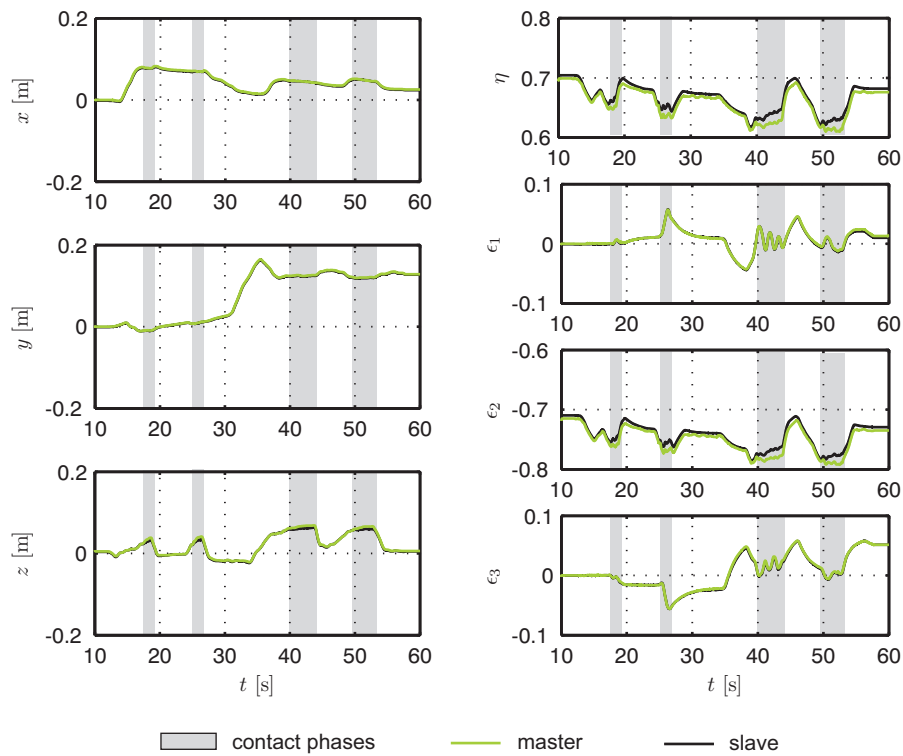


Figure 4.33: FaFa architecture: force and position tracking for low damped behavior ($M_p = 6$ kg, $B_p = 10$ Nm/s, $M_o = 0.2$ kgm², $B_o = 0.1$ Nms/rad)

4.7 Discussion

Beside mechatronic design criteria, the selection of an appropriate control architecture also significantly contributes to the quality of a telerobotic system. The control of a teleoperation system differs from many other control applications as many parameters are not constant and thus cannot be determined by extraction from CAD data, technical data sheets or by the application of classical methods of system identification. The control of a telerobotic system requires dealing with a highly variable operating domain as human operator and remote environment impedance change significantly over time. On this account, one of the main challenges in telerobotics is the selection of robustly stable control architectures and control parameters. In the selection of these typically a compromise between the two basic demands, namely stability and transparency, must be accepted.

In this chapter, a stability analysis for different types of bilateral teleoperation control architectures was carried out. While most existing publications in this field focus on control algorithms for impedance-type devices, this work analyzed different bilateral control algorithms for teleoperation systems using admittance-type devices. Their robust stability was investigated by using the parameter space approach, which allows the analysis of uncertain systems with varying plant parameters. The main advantage of this method is that in contrast to other approaches known in the literature, no passive human operator or remote environment have to be assumed and a desired dynamics of the overall teleoperation system can be guaranteed. Simple varying impedance models with varying parameters were used instead. In addition, effects as actuator and sensor dynamics were considered by simply incorporating them in the dynamical equations.

The performed stability analysis and the corresponding experimental results showed that for all considered control architectures robustly stabilizing control parameters could be found. Hereby, the best performance could be achieved by using a position-based admittance control with position-force exchange, as transparency was affected the least. Much easier to tune because of only two variable control parameters however, was a position-based admittance controller with force-force exchange. This feature is of special importance if control parameters for systems with multiple DOF have to be selected.

Although the obtained specific numerical results are only valid for the analyzed teleoperation system, the form of the stability regions is generalizable and holds also for other admittance-type teleoperation systems controlled by the same proposed control architectures.

So far, always all available DOF of a teleoperation system have been freed. In order to further improve the interaction with the developed systems, it should be analyzed how humans utilize these DOF and whether the number of freed DOF should be varied dependent on the actual task to be performed. This questions will be addressed in the next chapter.

5 Experimental Evaluation: Effects of Varied Human Movement Control on Task Performance and Feeling of Telepresence

In the prior chapters a highly integrated teleoperation system has been presented, which allows execution of a huge variety of different manipulation tasks. Tasks requiring only a few DOF, as well as tasks requiring all six DOF can be easily performed. The redundancy in the manipulators allows hereby realization of telemanipulator movements similar to that of the human arm movements and takes care of singularity avoidance.

To improve the feeling of telepresence when interacting with this teleoperation system, a variety of mechatronic design guidelines have been proposed and appropriate control architectures have been implemented. This chapter aims at further improving this feeling by considering also human factors in the development process. Our special interest concentrates on how varied human movement control can contribute to increase task performance and feeling of telepresence.

Previous research showed that humans perform translational movements more efficiently than rotational movements and that humans group available DOF to coordinated motoric units. Hence known design guidelines for teleoperation systems suggest providing only those movement dimensions which are required to complete a task, because this would lead to a better task performance. But it is still unclear how this would affect the feeling of telepresence and whether human movement control is really driven by task performance. As shown below, two different consequences can be drawn from findings in the literature. If human movement control is driven by task performance, telepresence can be increased by restricting the number of available DOF to the absolutely necessary ones, but if it is driven by intuition, this would decrease telepresence. In order to test these two views against each other and to derive appropriate design guidelines, a telemanipulation experiment with varying freed DOF is conducted. One of the questions is hereby how humans utilize DOF provided by the human-system interface and whether human movement control is driven by intuition or task performance. To answer these questions the effects of varied human movement control on task performance and feeling of telepresence are analyzed.

In the first step the state-of-the-art in the field of human movement control is reviewed. Depending on the reported findings, adequate hypotheses are derived and collected in Sec. 5.3. Sec. 5.4 explains the method used for the analysis and finally Sec. 5.5 reports on the obtained results.

5.1 Definitions

Before going into detail, some explanations for the terms varied human movement control, task performance and feeling of telepresence are given.

Varied human movement control: In three-dimensional space, human movement control can be described by six DOF, consisting of three translational and three rotational DOF as shown in Fig. 5.1. In a teleoperation system the human operator controls a remote

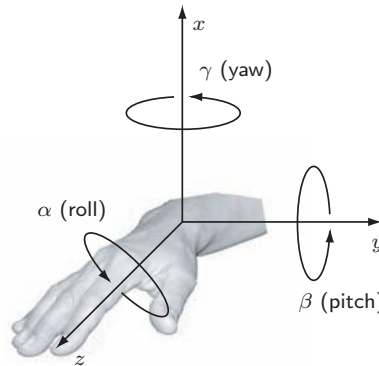


Figure 5.1: Translational and rotational degrees of freedom $x, y, z, \alpha, \beta, \gamma$

teleoperator via a haptic interface. Depending on the type of haptic interface and telemanipulator, different numbers of DOF are provided for human movement control. Using an advanced telemanipulation system, as described in Sec. 3.1, that enables manipulations in all six DOF, the number of freed DOF (from one to six) can be modified by control. This allows analysis of the effects of varied human movement control on task performance and feeling of telepresence.

Task performance: Task performance is a measure for efficiency and quality of a performed task. In [35] task performance is defined as learning success and the execution of a learned behavior. Despite the measurement of task performance being strongly related to the specific task, most measures concentrate on the accuracy or task completion time. Some typical task performance measures for different modalities are discussed in [91].

Telepresence: Telepresence describes the “sense of being there” in the remote environment even when one is physically situated at operator site [91, 136]. Subjective and objective presence measures are distinguished in the literature [61, 105]: Subjective measures include rating scales, subjective reports, paired comparisons and crossmodality matchings. Objective measures are more concentrated on the measurement of physiological (e.g. heart rate, skin temperature, electrodermal activity, eye motion) or behavioral responses (e.g. reflexive motor acts) of the human operator.

5.2 State-of-the-Art

Early studies about human movement control often showed poor human performance, which has been attributed to the lack of humans’ ability to coordinate movements in multiple DOF. Especially for tracking tasks with multiple DOF control devices, it has been reported that high human coordination performance in one dimension leads to more tracking errors in at least one other dimension [41, 47, 114]. From these results it was

concluded that for human operators the ability of goal-oriented coordination of multiple DOF is limited.

Conversely, later multi-degree of freedom tracking studies showed that this limited ability of coordination found in earlier studies was likely due to the restrictions of human-system interfaces at that time. With well designed interfaces, human operators were able to integrate and control both translational and rotational movements simultaneously [34, 88, 144, 145].

Aside from this ability of simultaneous coordination, some researchers found that it was much easier for subjects to control translational than rotational movements. Thus, translational movements could be performed more efficiently than rotational movements, whereas the degree of efficiency depended not only on humans' coordination abilities, but also on the task and the respective human-system interface [34, 134, 143].

In addition, it is known that humans control their motoric subgroups in such a way that as few DOF as possible are involved in performing a task. The composition of these so called coordinated motoric units has been referred to as the degrees-of-freedom problem [16, 125].

Design guidelines arising from these results suggest that in telepresence and teleaction systems, the human-system interface should only provide those movement dimensions which are required to complete a task successfully. Furthermore, it has been advised to give as much visual depth information as possible to the human operator, since with an increasing number of visual depth cues, a better movement coordination has been found [34].

However, from the research regarding human movement control it stays unclear how especially rotational DOF which are provided by a human-system interface are utilized by a human operator. Because coordination and integration of both translational and rotational movements are possible, rotary motions can be regarded as general motion units of humans. According to this view, rotational movements are performed intuitively by the human operator without considering the efficiency of task performance (cf. [86]). Optimization of task performance by restricting the number of DOF of the human-system interface would consequently lead to a worse feeling of telepresence. With regard to the finding that rotary motions are less efficient performed than translational movements, it can be suggested that rotational movements are generally avoided by a human operator to achieve a better task performance. Thus, restricting the number of DOF would result in a better feeling of telepresence and in a more intuitive usage of the teleoperation system.

In order to test these two views against each other and to investigate the human operator's usage of rotational movements, in this work a telemanipulative task was realized which could be more efficiently performed using only translational movements, but evoked the intuitive usage of rotary motions. Providing different numbers of DOF, the effects of this varied human movement control on task performance and feeling of telepresence are investigated.

5.3 Hypotheses

Regarding the human task performance, the following hypotheses were gained from previous research reported above:

H_{DOF1} : *The task should be more efficiently performed by the human operator with a fewer number of provided DOF.*

H_{DOF2} : *When human movement control is driven primarily by intuition, provided rotational movements should be exploited by the human operator. Accordingly, the feeling of telepresence should be higher with the possibility of rotatory motions. Contrary, when human movement control is driven by efficiency of task performance, rotational movements should be avoided by the human operator, the feeling of telepresence should be equal or less when providing rotary motions.*

H_{DOF3} : *With an increasing amount of visual depth cues, the human task performance should become better.*

Since not all tasks require the same number of DOF, the following hypothesis is formulated:

H_{DOF4} : *The usage of rotary motions is task-dependent.*

A very interesting question is whether the usage of rotary motions can be influenced by letting the subjects train with different numbers of freed DOF. If human movement control is driven by intuition, this would have no effect on the usage of rotary motions during the experimental session; if it is driven by task performance, subjects trained with a fewer number of freed DOF will not use the rotary motions as much as people trained with all DOF. On this account, the following hypothesis is formulated:

H_{DOF5} : *The usage of rotary motions depends on the prior experience of the subject.*

5.4 Method

In order to test the hypotheses proposed in the former section, a tele-experiment was conducted whereby the human task performance and the feeling of telepresence with movement control in three, four and six DOF were compared. Additionally, the amount of visual depth cues was varied by two different modes of visual feedback.

5.4.1 Measures for Performance, Rotation, and Feeling of Telepresence

The dependent variables in this experiment resulted to be task performance, usage of rotary motions and feeling of telepresence. They can be operationalized as follows:

Performance Measures

A typical performance measure is the *task completion time* T , which describes the period from starting a task at time t_s and finishing it at time t_e :

$$T = t_e - t_s. \quad (5.1)$$

Another measure for task performance is the *covered distance* s when performing a manipulation task. The smaller the covered distance, the more efficiently the task has been carried out. This measure is determined by calculating the Euclidean norm of the vector difference $\Delta \mathbf{x} = [\Delta x, \Delta y, \Delta z]$ of two consecutive measured positions and summing up these distances over a certain time period given by n time-steps.

$$s = \sum_{i=1}^n \|\Delta \mathbf{x}\|. \quad (5.2)$$

Since the telemanipulation system provides force-feedback information, the *average and maximum of the exerted force* f_{mean} and f_{max} , measured by the force-torque sensor located at the tip of the robotic arms, can also be used as performance indexes. They result when computing the Euclidean norm of the force vector for each time step i with n to be considered time steps and taking its average and maximum value:

$$f_{mean} = \frac{1}{n} \sum_{i=1}^n \|\mathbf{f}_i\|, \quad (5.3)$$

$$f_{max} = \max(\|\mathbf{f}_1\|, \dots, \|\mathbf{f}_n\|). \quad (5.4)$$

Beside the already presented performance measures, which are based on real measurements, performance can be also measured subjectively by rating scales. In this experiment two instructors rated independently the *quality of the performed task* on a scale from 1 to 10, where 1 meant “very bad” and 10 “very good”.

Rotation Measures

Since this experiment also aims to analyze the usage of rotary motions, appropriate rotation measures have to be derived. In the context of this experiment, orientations were given in form of Quaternions $Q = [\eta \ \varepsilon_x \ \varepsilon_y \ \varepsilon_z]$. Thus, the corresponding *rotation angle* θ and the *axis of rotation* \mathbf{r} are defined as follows:

$$\theta = 2 \arccos \eta \quad (5.5)$$

$$\mathbf{r} = \frac{1}{\sin(\theta/2)} \boldsymbol{\varepsilon} \quad \text{with} \quad \boldsymbol{\varepsilon} = [\varepsilon_x \ \varepsilon_y \ \varepsilon_z]. \quad (5.6)$$

The difference of the maximum and minimum rotation angle, as well as the difference of the maximum and minimum of the Euclidean norm of the rotation axis, form the used rotation measures.

Finally, *average and maximum torque* also serve as rotation measures, whereby $\boldsymbol{\mu}_i$ describes the torque-vector measured at time step i :

$$\mu_{mean} = \frac{1}{n} \sum_{i=1}^n \|\boldsymbol{\mu}_i\|, \quad (5.7)$$

$$\mu_{max} = \max(\|\boldsymbol{\mu}_1\|, \dots, \|\boldsymbol{\mu}_n\|). \quad (5.8)$$

Feeling of Telepresence

The feeling of telepresence is evaluated by using a subjective presence measure. After each experimental trial the participants were requested to rank the following three questions, which were adapted from the *presence questionnaire* formulated by [108], on a scale from 1 to 7, where 1 meant “very weakly” and 7 “very strongly”, in order to determine their feeling of telepresence:

1. How natural did your interaction with the environment seem?
2. How well could you move or manipulate objects in the remote environment?
3. How strongly did you feel immersed in the remote environment?

5.4.2 Experimental Setup

The experiment was conducted with the teleoperation system presented in chapter 3. The complete experimental setup, consisting of components for bimanual and multi-fingered haptic telemanipulation and different types of stereo vision systems, is shown in Fig. 5.2.

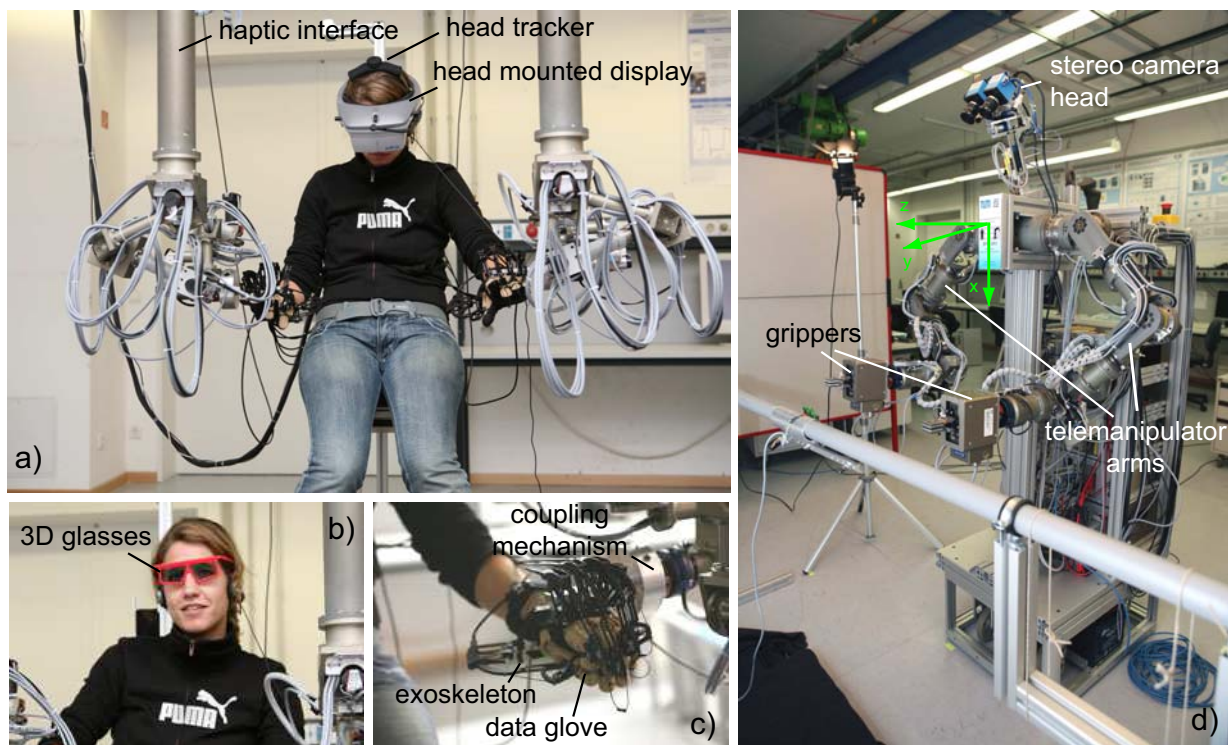


Figure 5.2: Experimental setup: operator site (a-c), teleoperator site (d)

The two hyper-redundant haptic interfaces ViSHaRD10 [127, 129] are used to control the dual arm redundant 7 DOF telemanipulator arms [120, 121] located at the remote site. Using different control algorithms, the number of DOF is changed to meet the actual task requirements. In order to allow fine-manipulations, the telemanipulator is additionally equipped with two-finger grippers (Schunk, PG70), which can be controlled by the human operator. On this account human finger motions are also measured using a data glove

system (CyberGlove) and mapped to the grippers. Finally, finger-interaction forces are measured by using strain gauges and displayed through a haptic interface, an exoskeleton (CyberGrasp). In order to provide an effective compensation of disturbances, position-based admittance control as presented in chapter 3.1 has been implemented for both devices. To close the teleoperation loop a position-based admittance control architecture with force-force exchange (see chapter 4 for details) has been used. For the experiment the following matrices have been selected for haptic interface as well as telemanipulator: $\mathbf{M}_p = \text{diag}\{6, 6, 6\}$ kg, $\mathbf{B}_p = \text{diag}\{70, 70, 70\}$ Ns/m, $\mathbf{M}_o = \text{diag}\{0.2, 0.2, 0.2\}$ kgm², and $\mathbf{B}_o = \text{diag}\{1, 1, 1\}$ Nms/rad. Hereby \mathbf{M}_p , \mathbf{B}_p represent translational and \mathbf{M}_o , and \mathbf{B}_o rotational 3x3 mass and damping matrices.

The stereo-vision system used is described in detail in Sec. 3.1. Two different types of methods to display visual information are used: a head mounted display (HMD; NVIS nVisor SX, resolution 1280 x 1024) worn by the human operator or a stereo-projection system. In the latter case, subjects had to wear 3D-glasses to get a 3D impression, see Fig. 5.2. The HMD is additionally equipped with a magnetic built-in tracker, which allows control of the position of the camera head motion, so that the user can look around in the remote environment just by turning her/his own head. In case of using the stereo-projection-wall a fixed view has been used.

5.4.3 Procedure

In the first step the participants were assisted in putting on the datagloves and the exoskeletons for the finger force-feedback. After coupling the hands to the haptic interfaces they got a short briefing in the usage of the haptic input devices. In the condition “projection wall” the participants had to wear 3D-glasses, in the condition “HMD” a head mounted display was used for visual feedback. In the latter case, the eye base was adjusted in order to gain a good 3D view for each participant. After the adjustment to the system, the participants had to perform four training sequences where they learned to execute the task appropriately. In this training phase, the provision of either three, four or six DOF served as between-subjects factor. In the case of 3 DOF, only translational movements were provided, in the case of 4 DOF a rotation around the x-axis (“roll”) was additionally freed. Finally, in the case of 6 DOF motions in all translational and rotational dimensions were possible. This was done in order to determine whether the participants retain the established strategy of task execution during the subsequent experimental trials, when different numbers of DOF are provided.

After these four training sequences, the participants performed six experimental trials, in which they executed the same task as already done in the training phase. During the experimental session pink noise was presented over closed headphones in order to mask any sounds made by the system. Each condition of DOF (3, 4 vs. 6) was presented two times to each participant. The order was balanced sequentially across participants. The participants were instructed to try out the available movement dimensions, i.e. the number of provided DOF, before executing the experimental task.

The experimental task consisted of the repair of a pipe burst by using a clamp as shown in Fig. 5.3. First, the participants had to grasp the clamp with their right hand. Then, the participants had to move the clamp over the two tube ends (phase 1). At the beginning of each trial both tube ends were aligned to each other and could be moved afterwards by the subject. After accomplishing the positioning of the clamp over the tube ends, the

participants should grasp the red knob at the left end of the clamp and turn the green wheel by the right hand in clockwise direction (phase 2). The LED on top of the clamp was switched off automatically when one round was accomplished. After each trial the two tube ends, as well as the wheel, were returned to the initial position by the instructor. The task induced different degrees of motions. While the positioning of the clamp required

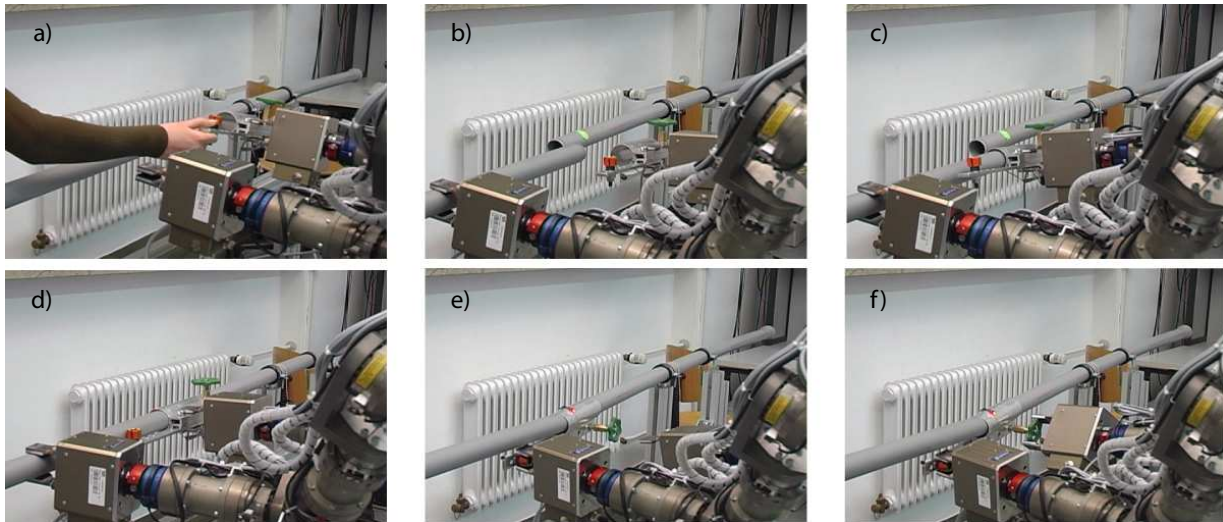


Figure 5.3: Experimental task: repair of a pipe burst, phase1: a-d, phase2: e,f

only translational movements, the turning of the wheel was constructed in such a way that it was more intuitive to use the fourth rotational DOF to turn the wheel. However, the wheel could also be turned using only translational motions when simply pressing against the circumferential grooves. This translational movement strategy was more efficient than the rotational movement strategy, since the task could be performed in a shorter time with less movements. The participants were not informed at any time how to perform the task, therefore they had to create their own strategy of how to accomplish the positioning of the clamp and the turning of the wheel.

After each experimental trial the participants were requested to rank the three presence questions and the two instructors rated the quality of the performed task.

At the end, the participants filled out a questionnaire that included a query of biographical data on items such as age, gender, handedness, amount of experience with virtual environments and telepresence systems, and the amount of hours spent playing 3D computer games per month (see appendix E).

5.4.4 Experimental Design

For each experimental phase within each trial and each participant, the task completion time, the covered distance (derived from the actual positions of the human operator), the average and maximum exerted force, the average and maximum exerted torque, the angle and the axis of rotation, the ratings of the telemanipulation quality, the ratings for the feeling of telepresence, and the applied task execution strategy served as dependent variables.

The independent variables were the number of freed DOF during the training session (3, 4 vs. 6), and the mode of the visual feedback (projection wall vs. HMD) as between-subjects factors, the number of freed DOF during the experimental session (3, 4 vs. 6), the experimental phase (phase 1 or phase 2), the repetition (2 levels), and the hand (left and right) as within-subjects factors.

5.4.5 Participants

Sixteen subjects participated in this experiment. They were between 20 and 34 years old (mean 26.25 years, standard deviation 3.96 years). Eight subjects were female, eight male. All were right-handed. Fifteen participants had none to middle experience with virtual environments or telepresence systems, one participant high degree of experience with such systems. The average time spent playing 3D computer games was stated to be 2.64 hours per month (standard deviation 5.54 hours, range from 0 to 20 hours). Half of the participants had visual feedback by using the projection wall, the other half by using the HMD. Six subjects had training sequences with 3 DOF, six with 4 DOF and four with 6 DOF

5.5 Results

The task completion time, the covered distance and the average and maximum exerted force as well as the quality ratings of the instructors served as efficiency measures, whereas the average and maximum exerted torque and the angle and axis of rotation were the measures for the usage of rotary motions. The feeling of telepresence was assessed by the three rating questions.

None of the biographical data collected showed a relationship to any of the dependent variables. Thus, the results are independent from age, gender, experience with virtual environments or telepresence systems and average time spent playing 3D computer games.

The descriptive data for the dependent variables for each independent variable are depicted in appendix D. In the next section the experimental results are reported in detail.

5.5.1 Task Execution Strategy

Regarding the task execution strategy of the participants, two general patterns could be observed for each experimental phase. Concerning the positioning of the clamp over the tube ends in phase one, either one or two hands were used to accomplish the task. In the second phase the clamp was either positioned horizontally or vertically (see Fig. 5.4). Regarding the turning of the wheel, in the condition with three DOF provided, only translational movements could be used to turn the wheel by pressing against the circumferential grooves. With both, 4 and 6 DOF, the usage of the rotational movements was only possible when the clamp has been oriented horizontally. Table 5.1 shows the frequency of the used strategies over all experimental trials and subjects.

The two strategies were coded for each experimental phase and used as additional dependent variable in the following analysis.

Table 5.1: Frequency of the used strategies for first and second experimental phase over all experimental trials and subjects

		freed DOF during experimental session		
		3 DOF	4 DOF	6 DOF
phase 1	one-handed	15	12	14
	two-handed	17	20	18
phase 2	rotary motions	0	17	17
	translational motions	32*	15	15

* here only this strategy was possible due to the experimental conditions



Figure 5.4: Used strategies of the participants. Left: horizontal orientation of clamp. Middle: vertical orientation of clamp, fixing of wheel by pushing against grooves. Right: vertical orientation of clamp, fixing of wheel by rotation

5.5.2 Analysis of Variance

In order to test the hypotheses established in Sec. 5.2, a multi-variate analysis of variance with mixed design using the between-subjects factors mode of visual feedback (projection wall vs. HMD) and number of freed DOF during the training session and the within-subjects factors number of freed DOF during the experimental session (3, 4 vs. 6), experimental phase (phase 1 vs. phase 2), repetition (2 levels), and hand (left vs. right) was computed. As dependent variables the efficiency measures, the measures for the usage of rotary motions, the quality ratings of the instructors, and the ratings of the feeling of telepresence had been taken.

According to Hypothesis 1, there should be a main effect of the number of freed DOF during the experimental session on the efficiency measures. Considering Hypothesis 2, when human movement control is primarily driven by intuition, main effects of the factor number of freed DOF on the feeling of telepresence and the rotary motions are expected. If the movement control is primarily driven by efficiency of task execution, there should be no effect of the factor freed DOF on the before mentioned dependent measures. Since the visual feedback using the HMD yields more visual depth cues (especially head tracking) the factor mode of visual feedback should show a main effect on the efficiency measures (Hypothesis 3). If the usage of rotary motions is task dependent a main effect of the factors task phase and hand on the efficiency measure and the rotation measure is expected (Hypothesis 4). Finally, if the usage of rotary motions depends on the prior experience of

a subject, a main effect of the factors training and repetition on the rotation and efficiency measures must be observed (Hypothesis 5).

The main effects as result of the computed analysis of variance are explained here, whereby detailed numbers are reported in appendix D:

H_{DOF1}: As can be seen from Tab. D.4, the number of freed DOF only shows an effect on the mean of the exerted force, but not on the other efficiency measures task completion time, maximum exerted force, covered distance and quality rating. According to Table D.2, the exerted force becomes smaller with additional freed rotational DOF and contrary to the prediction, the task is not performed more efficiently with decreasing numbers of DOF, as stated in Hypothesis 1. When also taking into account the rotation measures additional effects on the applied torque and the angle and axis of rotation can be observed, see Table D.4. While for the torque similar results as for the applied forces are obtained, the angle and axis of rotation increase with additional freed DOF, so people tend to really use the additional provided DOF.

H_{DOF2}: The factor freed number of DOF has significant effects on all measures for the usage of rotary motions and on the feeling of telepresence. According to Table D.1, the applied torques do not differ very much comparing the 3 and 4 DOF condition, but are significantly reduced in the 6 DOF condition. Also the amount of rotations increases with the number of freed DOF, see Table D.2. Further, an adaptation of the selected strategy can be observed: With increasing number of freed DOF the strategy is adapted in such a way that mostly rotary motions are used to turn the wheel. Finally, also the feeling of telepresence increases with an increasing number of freed DOF, see Table D.3. Therefore, rotational movements are primarily exerted intuitively. The participants tended to exert the familiar rotational motions, and thus, applied reduced forces and torques to the system. Hereby, the efficiency of task performance, given by the path length, is of minor importance.

H_{DOF3}: The factor mode of visual feedback shows main effects on exerted force, covered distance, and quality rating, see Table D.5. As depicted in Table D.1 the human task performance for these two dependent variables is better when wearing a HMD than in the condition with the projection wall. It can be concluded that the additional visual depth cues provided by the HMD lead to the better task performance.

H_{DOF4}: While testing hypothesis four, main effects of the factor task phase on the maximum of the exerted force and the covered distance can be observed, see Table D.6. During the first phase of the experiment, higher forces are exerted and longer paths are recorded, which seems to be plausible considering the experimental conditions. An additional effect of the task phase on the maximum exerted torque can be seen. Contrary to the expectations, higher torques are exerted in the first phase of the experiment. This can be explained by the fact that in the first phase of the experiment the clamp and the tube ends can tilt. The effect on the rotation axis is also significant and as expected, turned out to be bigger in the second phase.

In addition, significant effects of the factor hand can be observed on the covered distance and on the rotation measures, see Table D.7. This can be explained by the fact that all subjects were right-handed and main parts of the task had to be carried out by using this hand. Summarizing it can be stated that the usage of rotary motions is task-dependent.

H_{DOF5}: As Table D.8 shows the factor training has effect on neither of the dependent variables. On this account, the training does not influence the task execution during the experimental session. The factor repetition, see Table D.9, only shows effects on the task completion time and the quality rating. Since these effects can be directly explained by training effects due to the increased number of trials, they are not further considered. Summarizing, it can be stated that the directly induced prior experience has no effect on the usage of rotary motions and thus Hypothesis 5 is refused.

5.6 Discussion

To improve the interaction with a teleoperation system, an optimization of the mechatronic design, as well as of the implemented control architectures is necessary. Thus, from a technical point of view controllers have been selected which optimize the main criteria stability and transparency of a developed system. But as the human operator is part of the teleoperation loop and significantly influences it, further improvements can be achieved when also considering human factors in the development process. One of the main questions answered in this chapter is how humans utilize DOF provided by the human-system interface, and how varied human movement control influences task performance and feeling of telepresence.

In contrast to earlier studies, not only the path length and the task completion time were used as a measure for task performance, but also the forces and torques applied during a telemanipulation task were considered. While the results obtained for the path length are in accordance with earlier studies that mainly focused on pointing tasks and used the task completion time as well as the path length for measuring task performance, the results on the applied forces and torques indicate that providing all 6 DOF for movement control in three-dimensional space led to a better task performance compared to providing a fewer number of DOF. In addition it has been found that the participants were able to integrate translational and rotational movements very well and used the rotational motions intuitively in a coordinated manner. Furthermore, providing the full range of three-dimensional movements had a beneficial effect on the feeling of telepresence, the participants felt more immersed when having the possibility to control all 6 DOF.

Thus, for high-quality human-system interfaces and teleoperation systems as used in this study, it is beneficial to allow movement control for all DOF to the human operator.

Also selection or usage of technical systems related to other modalities can be improved when considering human factors. So it could be shown that an increasing amount of visual depth cues comprised by a HMD, as opposed to a projection wall, improved human task performance and thus the interaction with the teleoperation system. It can be assumed that this effect is in large part due to the head tracking, which was present in the HMD condition, but not in the condition with the projection wall. These results indicate that a HMD with head tracking should be preferred to a projection wall, when developing a high-quality teleoperation system.

Prior parts of this thesis have been devoted to the development of a highly integrated and intuitive teleoperation system, whereby design and control aspects as well as human factors have been considered. Hereby, all investigations were limited to single-user teleoperation systems. Systems, considering also multiple users, are subject of the next chapter.

6 Collaborative Teleoperation Systems

Telerobotic systems combine skills like human adaptability and decision-making ability with the advantages of robotic manipulation. While the former enables operation in highly variable, unstructured, unknown or dynamic working environments, the latter allows performance of complex tasks in remote and inaccessible environments. In the past years several application areas for such telerobotic systems have been presented: space and underwater exploration, surgery, plant maintenance, telemanufacturing, training as well as entertainment.

Most telerobotic systems known in this context focus on single operator, single robot systems, whereby only one human operator is responsible for carrying out the task. If the execution of a task, however, exceeds the capabilities of a single person, further assistance is needed. As long as the task is known beforehand, special auxiliary tools can be used to extend the human capabilities. If this is not the case people typically collaborate and assist each other in performing a task. Hereby, different facilities and capabilities are shared among a group.

Extending a teleoperation system by the ability to collaborate with other people a so called collaborative teleoperation system results. As many problems for single operator, single robot teleoperation systems are still not solved and because collaborative teleoperation systems are characterized by an increased complexity, to date such systems are only little studied in the literature. This chapter aims at classifying collaborative teleoperation systems, formulating new research challenges, and making first attempts at analyzing stability of systems where multiple operators and/or multiple robots collaborate in order to perform a common task.

In the first step, Sec. 6.1 gives a definition and classification of collaborative teleoperation systems. Starting from this classification, five different collaborative teleoperation architectures are derived and discussed in detail. Sec. 6.2 reports on the state-of-the-art in the control of such collaborative teleoperation systems. The few known approaches are hereby divided into approaches dealing with unconstrained and constrained interaction between the single components. Deficiencies of the presented approaches are discussed and research challenges are formulated. The second part of this chapter is devoted to implementation of some of the presented collaborative teleoperation architectures. In particular a bimanual, a multi-user, and an intercontinental cooperative teleoperation system are investigated in detail.

6.1 Collaborative Teleoperation Architectures

In collaborative environments, humans multiply their output by sharing facilities and capabilities necessary to perform a common task or achieve a common goal. Collaboration is hereby characterized by a shared goal and a joint intention [124]. Combining this ability with classical teleoperation, a collaborative teleoperation system results. It should be

noted that the terms collaborative and cooperative are used interchangeably throughout this thesis.

In principle, the following collaborative teleoperation systems can be distinguished:

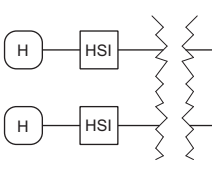
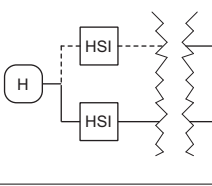
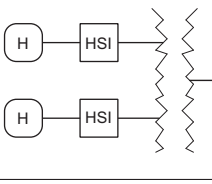
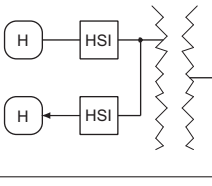
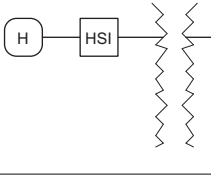
- multiple operator, multiple robot systems (MOMR),
- single operator, multiple robot systems (SOMR), and
- multiple operator, single robot systems (MOSR).

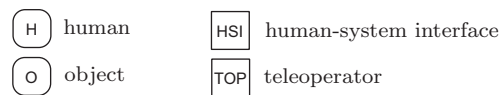
Referring to this classification, five different collaborative teleoperation architectures can be constructed, see Tab. 6.1. The first architecture represents a MOMR system. In order to control a robot located in a remote environment, each operator interacts with a human-system interface. Depending on the given task visual, auditory and haptic feedback are provided. To accomplish a common task the robots can share the same workspace. In such a case a collision free coordinated motion can be considered as the simplest form of collaboration. More complicated situations result when robots interact directly or via an object. Applications for such an architecture are situations when more than one person is required to perform a given task, as e.g. while transportation or assembling of heavy, bulky or fragile objects. Direct contact between the robots can be necessary to guide the motion of the collaborating operator or to call his attention. Also social conventions like hand-shaking are possible.

The second architecture describes a similar situation with similar interaction and collaboration possibilities, but in this case only one operator is responsible for multiple robots. E.g., bimanual telemanipulation can be treated as such an architecture, whereby each human-system interface is controlled by one human hand. Even possible is an architecture whereby the human operator controls multiple robots by using only one human-system interface. In this case the telerobots possess local intelligence which can be used to avoid collisions between other participants and the environment, to commonly grasp and/or hold an object or to achieve a superior mission which cannot be obtained by a single telerobot because of limited time or missing tools. Thus, such an architecture is suitable for inspection or transshipment tasks, whereby the transportation of heavy, bulky or fragile objects can also be considered. In the latter case, multiple robots can grasp an object and form a closed chain with it. While local force controllers guarantee the contact with the object, the human operator is responsible for the positioning of the object.

The third architecture shows a MOSR situation. In this case, multiple operators are simultaneously responsible for one robot that is controlled according to an average or sum of all operator inputs. Applications for such an architecture can be found in the entertainment sector, as well as in student/teacher scenarios, whereby the teacher interacts with the student, corrects him or gives instructions. Modifying this architecture in such a way that only one operator controls the robot which is located remotely, but the information provided by the human-system interface is available for more than one operator this architecture can be used to teach motion sequences and procedures. Such an architecture, described by the fourth scheme, can also be used to increase the situation awareness of an operator before the control of a robot is switched from one operator to the other.

Table 6.1: Architectures for collaborative teleoperation

N°	Type	Architecture
1	MOMR	
2	SOMR	
3	MOSR	
4	MOSR	
5	MOSR	



Finally, the fifth architecture shows a MOSR system, whereby a human collaborates with a robot controlled by a remote human operator. As for the first architecture, the simple case of coordinated motion, as well as the more complicated case of direct contact and interaction over an object can be considered. Such an architecture can be of interest when the task requires an expert who is not located at the remote site. In this case the expert can operate remotely assisted by a local human operator.

In all these systems, basically two different types of collaboration between the participants can be distinguished. Constrained collaboration refers to situations where multiple participants are in contact with the same object or with each other so that the motion of each participant is tightly associated with the other's motion. In the unconstrained case, each participant is controlled independently, but in order to perform a common task they share the same workspace and need to avoid collisions.

6.2 Control Approaches for Collaborative Teleoperation Systems

The specific type of collaboration plays an important role by the selection of an appropriate control algorithm since challenges on the control of collaborative teleoperation systems differ depending on the level of interaction. While unconstrained collaboration requires algorithms for collision avoidance and coordinated motion behavior, constrained collaboration requires higher precision, stricter synchronization and a higher level of coordination. In the past, many control algorithms were proposed for the SOSR system which were able to deal with linear and nonlinear telemanipulation systems [51, 77, 83, 139, 146] as well as time delay [8, 28, 93]. In the succeeding sections some state-of-the-art control concepts for unconstrained and constrained collaborative teleoperation systems are described.

6.2.1 Unconstrained Teleoperation Systems

The demands on control algorithms for unconstrained collaborative teleoperation systems can be summarized as follows:

- enable a coordinated motion behavior, and
- avoid collisions between the participants.

Several control concepts referring to one or both of these topics can be found in the literature:

In [122] concepts for the coordinated motion control of a distributed autonomous robotic system were developed. They presented a web-based framework for a human-system interface with visual and auditory feedback, which allows coordination of tasks and organization of mobile robots of a SOMR teleoperation system. For the purpose of carrying out inspection tasks cooperative formations among multiple mobile telerobots were proposed.

To improve collaboration and avoid collisions several approaches based on predictive graphical displays can also be listed. [72] presented a SOMR system which allows selection of one of multiple mobile telerobots and control of it in order to perform a certain task. To avoid collisions with the other participants, a distributed sensor-based path-planning algorithm at the remote site and a predictive graphical display at the human operator site is used.

6.2.2 Constrained Teleoperation Systems

While in unconstrained teleoperation systems the telerobots are in contact with different objects, and thus tasks can be described by decoupled parallel linkages, in constrained teleoperation systems the following two configurations must also be considered:

- direct coupled linkage between the robots: telerobots are in direct contact with their end-effectors and
- indirect coupled linkage via an object: the end-effectors of the telerobots are coupled via a common object.

These additional configurations enable an increased dexterity, loading and handling capability, as well as enhanced efficiency and feasibility. Beside these advantages, also increased safety (due to the distributed energy), and improved robustness (which results from the manipulation redundancy) can be achieved.

But in order to reap the benefits of such a system, stable control algorithms for all these possible configurations must be implemented. This means that depending on the actual configuration, control algorithms have to deal with uncertainties in the environment, the specific task trajectory and the object manipulation, as well as constraints on the motion of the robots and the manipulated object. Since the manipulation is accomplished remotely and all signals are typically send over LAN or internet, algorithms have also to be robust against non-ideal network conditions. Finally, properties as transparency and quality of tele-coordination should also be addressed. In order to implement an appropriate control algorithm which guarantees a synchronous operation, efficient coordination and safe manipulation, all these mentioned effects and requirements have to be considered.

While many investigations exist in the field of coordinated control of robots [17, 69, 111, 132, 135], only few works on constrained teleoperation systems have been conducted. Below, the few known approaches which address this problem, are discussed. Hereby, approaches using only one and approaches using multiple human-system interfaces are distinguished.

Approaches using One Human-System Interface

Approaches using only one human-system interface to control multiple teleoperators (see Fig. 6.1) are often based on a semi-autonomous teleoperation structure. This means e.g. that the cooperative grasping of an object is achieved by a local grasping controller, while the overall motion of the multiple teleoperators and the grasped object are commanded via teleoperation. This assures a permanent contact with the object and thus a secure grasping regardless of network time delay. Basically, the following two approaches which realize such a behavior can be found in the literature.

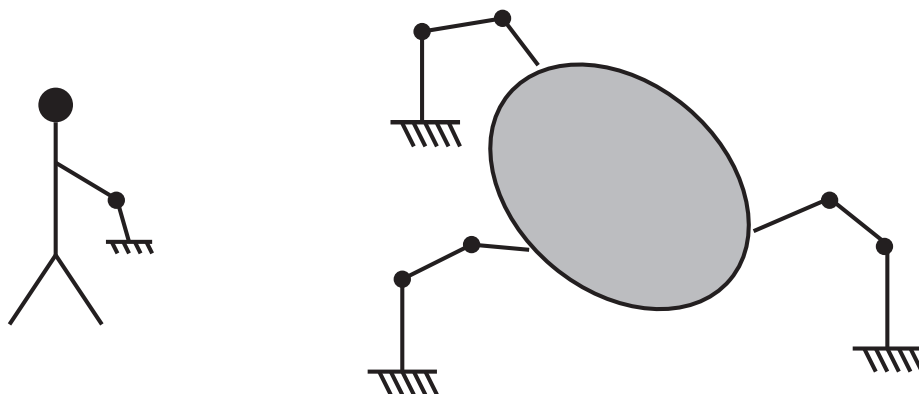


Figure 6.1: Telemanipulation system using only one human-system interface

Control of internal and external forces: The forces acting on the object can be split into forces which cause motion of the object and forces which cause internal forces to build up within the object and which produce no motion. The former are called move (external) forces \mathbf{f}_m , the latter squeeze (internal) forces \mathbf{f}_s . The sum of both forces represents the total force exerted on the object:

$$\mathbf{f} = \mathbf{f}_m + \mathbf{f}_s . \quad (6.1)$$

Consider an object held by two manipulators at different contact points which exert the forces \mathbf{f}_1 and \mathbf{f}_2 on the object. If C is a potential contact point with the environment, the forces acting at this point can be computed as follows:

$$\mathbf{f}_c = \mathbf{A}^T \mathbf{f} , \quad (6.2)$$

whereby

$$\mathbf{f} = \begin{bmatrix} \mathbf{f}_1 \\ \mathbf{f}_2 \end{bmatrix} . \quad (6.3)$$

Given that the components of the force vector \mathbf{f} which are in the nullspace of \mathbf{A}^T comprise the squeeze forces and the components in the vector space of \mathbf{A}^T comprise the move forces, \mathbf{f}_m can be computed using the Moore-Penrose inverse of \mathbf{A}^T

$$\mathbf{f}_m = \mathbf{A}^+ \mathbf{f}_c = \mathbf{A} (\mathbf{A}^T \mathbf{A})^{-1} \mathbf{A}^T \mathbf{f} . \quad (6.4)$$

Since the force \mathbf{f} is known by measurement and the internal and external forces can be computed from (6.1) and (6.4) they can be controlled independently. In order to do that [11] proposes a squeeze controller for the internal force control and a so called general compliant motion controller [10, 12] for the motion control of the object. The latter enables the control of the move forces, as well as the control of the motion inputs due to teleoperation.

Control based on passive decomposition: While in [11] no evidence of stability of the chosen approach is given, [81] follows an approach based on the passivity theorem, which guarantees stability of the overall teleoperation system. Using passive decomposition, the dynamics of multiple telerobots is decomposed into two decoupled dynamics while preserving energetic passivity: the shape system describing dynamics of the cooperative grasping, and the locked system representing the overall behavior of the multiple telerobots. Based on this, a local grasping controller can be developed which controls the shaped system consisting of multiple telerobots and the grasped object. In addition, a bilateral teleoperation loop can be constructed which allows the human operator to control the overall behavior of the shaped system and to perceive combined environmental forces acting on it. Combining this approach with a scattering based communication, which passifies the communication channel, an overall energetic passivity of the closed-loop system can be achieved.

Approaches using Multiple Human-System Interfaces

In contrast to the presented approaches using only one human-system interface to control multiple telerobots, approaches using multiple human-system interfaces (see Fig. 6.2) allow the extension to a bimanual, as well as to a MOMR teleoperation system (see the first and second presented architectures for collaborative teleoperation). Since the telerobots are no longer controlled autonomously but are teleoperated by different human operators, appropriate control algorithms must be defined. Some state-of-the-art approaches are discussed subsequently.

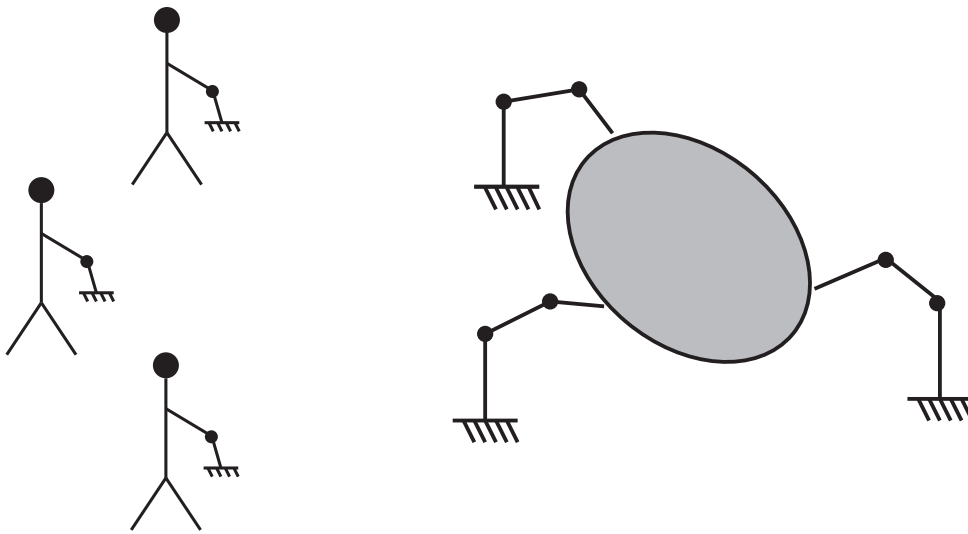


Figure 6.2: Telemanipulation system using multiple human-system interfaces

Replay of Preimplemented Primitives: In [133] a web-based framework for a human-system interface with visual and auditory feedback has been developed, which enables performance of cooperative tasks such as 'group-object-handling'. This is achieved by preimplementing primitives for recurrent actions and replaying them on demand. In this way, multiple human operators can accomplish collaborative telemanipulation tasks by selecting primitives, which will then be carried out autonomously by multiple teleoperators. Since only one operator is authorized to identify one step at a time, coordination between the operators can be guaranteed.

Event based control: While the last presented system provides only visual and auditory feedback, in the following, systems with additional force feedback are depicted. In [40] an approach for an event synchronous MOMR teleoperation system based on Petri Net models and the rigid grip condition has been presented. They defined a so called coordination index ε , which is a measure for the quality of coordination and devised that n robots coordinate with tolerance ε if $\max(|\mathbf{f}_{ei}(s)|) \leq \varepsilon$, whereby \mathbf{f}_{ei} denotes the external force sensed by the robot i , and s describes the action reference, a non-time based variable. Based on this definition the following control algorithm has been implemented:

If the measured force is equal or greater than the maximum allowed, that is the coordination index, the direction of desired motion is compared to the direction of force. If the direction of desired motion is in the reducing force direction the command is executed else it is discarded. Meanwhile, the measured force is fed back to the operator and displayed by the haptic display.

This algorithm guarantees a certain predefined coordination index in the non time-delay situation, but can only be used if the grasp is assumed to be rigid. Furthermore, since motion commands could be discarded, operator and teleoperator position can differ significantly. In [40] this approach has been also extended to teleoperation systems with delayed communication considering event-transparent and event-synchronous controlled robots. They show that n event-transparent and event-synchronous robots can be tele-coordinated via the Internet to any coordination index, which is possible under no delay conditions, with no assumptions regarding the delay encountered, the object manipulated or the external forces.

Bilateral teleoperation architectures / hybrid control: To enable bimanual constrained telemanipulation tasks [74] built a system consisting of two independent and bilateral SOSR controllers using common two or four channel telemanipulation architectures. It should be noted that designs based on single master/single slave teleoperation systems, which do not address the performance and stability requirements of collaborative teleoperation, often fail since they neglect the additional interaction possibilities. However, direct interaction or interaction through an object can lead to a violation of the passivity of the environment which can result in instability of the system. To analyze stability of this system under consideration of all possible interaction possibilities, the so called parameter space approach has been chosen, which needs a mathematical description of the system investigated. The analysis of the considered system showed that:

- hard contact with the environment can only be achieved using a position-force architecture (position control for the human-system interface and force control for the telerobot),
- a coupled linkage via an object with low stiffness can also be realized with a force-position architecture, and
- a high quality representation of free space motion requires generally force-position architectures.

Consequently, a dual-hybrid control architecture with position-force control during contact and force-position control to represent free space motion behavior is proposed. An online estimation of the environmental impedance is used as indicator to decide on switching from one architecture to the other. As a consequence of the overall system complexity, no evidence of stability of the resulting switching controller has been supplied and no transparency measure has been proposed.

μ -synthesis control: While the last presented system can be described by a collection of single master/single slave teleoperation units working in a shared environment, [117, 118] proposes a framework which allows for transmission of position and force information between all master and slave robots rather than merely between corresponding units. A linear

μ -synthesis-based controller design guarantees robust stability of the cooperative teleoperation in the presence of dynamic interaction between slave robots and the object, as well as unknown passive operators and environment dynamics. In addition, task coordination is enhanced by the optimization of relevant cooperative performance objectives, such as transparency measures, as well as internal force control. Combining all these objectives in the vector of performance indices \mathbf{E} , the overall objective of the controller design can be formulated as follows: *achieve robust stability in the presence of uncertain operators' and environment dynamics while optimizing the performance measure by minimizing $\|\mathbf{E}_\infty\|$.* This approach has been validated using a one DOF two master/two slave experiment.

Adaptive control: While this μ -synthesis controller assumes linearized models for the operators, masters, slaves and environment, the same group also proposes an adaptive nonlinear controller to accommodate nonlinearity and parametric uncertainty in the system dynamics, see [119]. Similarly to the linear approach, a multi-lateral controller is used instead of several bilateral control architectures. This allows establishment of a position-position kinematic correspondence between the masters and slaves and facilitates the coordination among the operators. The latter is achieved by imposing virtual constraints on the position of the slaves and masters and by introducing internal force components which help to maintain contact between the slaves and the object. As a controller, an adaptive motion/force controller inspired by [146] is used. This controller guarantees good force and position tracking, which enables good transparency conditions. Stability in the presence of parametric uncertainties in the dynamics is proven via Lyapunov analysis, whereby free space motion, and contact with flexible and rigid environments are considered.

Multi-model LQG control: Another approach proposed by [115] foresees the usage of a multi-model control strategy that enables multiple operators to cooperatively manipulate a rigid tool. In this approach a centralized controller is also used and information is exchanged between all entities. Distinct to the before presented approaches constant a priori known time delay can be handled. The LQG controller is used to optimize performance indices as position and force tracking and virtual tool impedance shaping. Since this approach is model based, adequate models for human operator, master, slave and remote environment are required and robust stability against parameter variations has to be analyzed.

6.2.3 Summary

Summarizing, it can be stated that approaches using only one human-system interface can not be extended to a bimanual or MOMR system. The shown event-based approach can only be applied for rigid grasp conditions and produces an error between master and slave positions. Designs based on single master/single slave teleoperation systems often fail, because they do not address the performance and stability requirements resulting from different interaction possibilities. Considering these interactions and using independent bilateral controllers, stable behavior has been experimentally shown by using a dual-hybrid control architecture. But neither a proof of stability, nor a transparency measure exists for this control scheme. In order to be able to facilitate the coordination and establish a kinematic correspondence between master and slave, multi-lateral controllers have been

proposed in the literature. But these controllers mostly require an exact knowledge of the dynamic model of the manipulators, which is difficult to obtain. Moreover, these approaches have only been tested in one DOF experiments using typical impedance-type devices.

In the context of this thesis, control algorithms for collaborative teleoperation systems using admittance-type devices are developed and tested in the real hardware setup. Three of the before presented collaborative teleoperation architectures are hereby analyzed in detail. In contrast to one DOF experiments described in the literature, experiments using all 6 DOF are conducted.

6.3 Bimanual Teleoperation

A bimanual configuration, as represented by architecture two (see Fig. 6.1), is the simplest form of collaborative teleoperation system. Hereby, only one human operator is responsible for the control of two teleoperator arms by using two human-system interfaces, one for the left and one for the right arm, see Fig. 6.3.

Depending on the actual task to be performed, different types of interactions with the remote environment can occur. Basically, constrained and unconstrained interactions can be distinguished. While unconstrained interactions refer to free space motion, constrained interaction is related to different contact situations with the remote environment. Performing a maintenance task as described in Sec. 5.4.3, the following contact situations can occur:

- interaction of one teleoperator arm (+ object) with the remote environment
- interaction of both teleoperator arms via an object

The first type of interaction occurs when one telemanipulator arm is in contact with one of the tube ends, which is the case when disaligning and aligning them, as well as when moving the clamp over them. The second type of interaction occurs in the screw tightening phase. In this phase a closed kinematic chain between left and right teleoperator arm is formed, whereby the chain is closed over an additional object, the clamp.

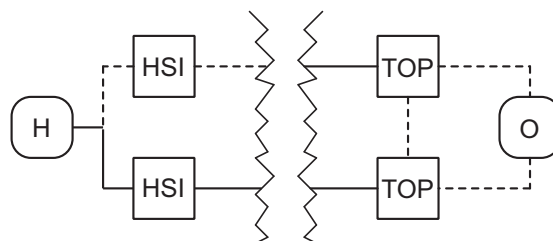


Figure 6.3: Bimanual teleoperation system: one human operator (H) interacts with a left and right handed haptic interface (HSI) and controls corresponding teleoperator arms (TOP)

One of the main goals in designing controllers for such a teleoperation system is to guarantee robust stability for all possible types of interaction. If only one teleoperator arm

is in contact with the environment, the stability results already obtained in chapter 4 can be used. But for the interaction of both teleoperator arms via an object, an appropriate control algorithm has to be selected and a stability analysis considering the closed kinematic chain between the two arms has to be performed.

As a variety of control algorithms have already been successfully implemented and tested for the SOSR teleoperation system, it stands to reason the same controllers can also be used in the bimanual setup. This would imply the control of left and right hand teleoperation system by two independently working bilateral controllers as already presented in chapter 4. Adopting such a configuration, stability for the bimanual case, including closed kinematic chains, has to be investigated.

In the coming sections stability of these closed chain configurations is evaluated by analyzing asymptotic stability. Since this analysis requires a dynamic model, a model of the closed kinematic chain formed by the two telemanipulators and the object is used.

6.3.1 Modelling of Bimanual Teleoperation System

When analyzing stability of a bimanual teleoperation system, the already derived models for human-system interface and teleoperator can be used, see Sec. 2.4.1 and Sec. 4.4 for details. The dynamic models for the human-system interface are shown in Fig. 6.4. The corresponding differential equations are given by

$$\begin{aligned} 0 &= f_h^l + f_{sm}^l - (\alpha m_h^l + m_{em}^l) \ddot{x}_m^l - \alpha b_h^l \dot{x}_m^l - \alpha c_h^l x_m^l, \\ 0 &= f_{sm}^l - f_m^l + m_m^l \ddot{x}_m^l + b_m^l \dot{x}_m^l, \end{aligned} \tag{6.5}$$

for the left and

$$\begin{aligned} 0 &= f_h^r + f_{sm}^r - (\alpha m_h^r + m_{em}^r) \ddot{x}_m^r - \alpha b_h^r \dot{x}_m^r - \alpha c_h^r x_m^r, \\ 0 &= f_{sm}^r - f_m^r + m_m^r \ddot{x}_m^r + b_m^r \dot{x}_m^r. \end{aligned} \tag{6.6}$$

for the right haptic interface.

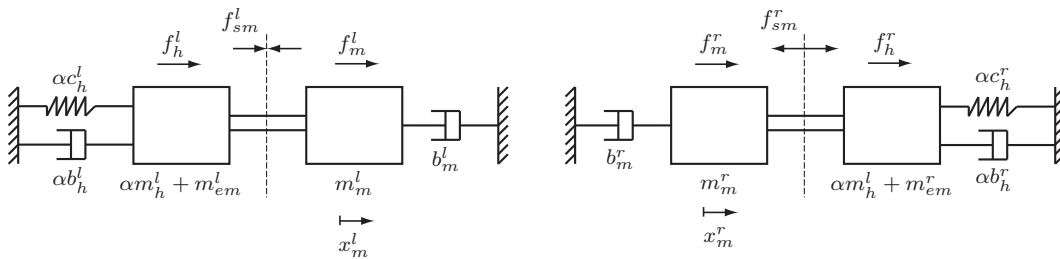


Figure 6.4: Model of bimanual human-system interface and human

As proposed by [74] the interaction of both teleoperator arms via an object is modelled by a closed kinematic chain shown in Fig. 6.5. Hereby, the object is represented by the mass m_e , and the strength of the grasp is modelled by two spring-damper systems c_e^l , b_e^l

and c_e^r, b_e^r . The differential equations of the overall system are given by:

$$\begin{aligned}
 0 &= f_s^l + f_{ss}^l - m_s^l \ddot{x}_s^l - b_s^l \dot{x}_s^l, \\
 0 &= f_{ss}^l + m_{es}^l \dot{x}_s^l + b_e^l (\dot{x}_s^l - \dot{x}_e^l) + c_e^l (x_s^l - x_e^l), \\
 0 &= m_e \ddot{x}_e + b_e (\dot{x}_e - \dot{x}_s^l) + c_e (x_e - x_s^l) + b_e (\dot{x}_e - \dot{x}_s^r) + c_e (x_e - x_s^r), \\
 0 &= f_{ss}^r + m_{es}^r \dot{x}_s^r + b_e^r (\dot{x}_s^r - \dot{x}_e^r) + c_e^r (x_s^r - x_e^r), \\
 0 &= f_s^r + f_{ss}^r - m_s^r \ddot{x}_s^r - b_s^r \dot{x}_s^r.
 \end{aligned} \tag{6.7}$$

Having a model of haptic interface, human, telemanipulator and environment, stability of the overall system can be analyzed.

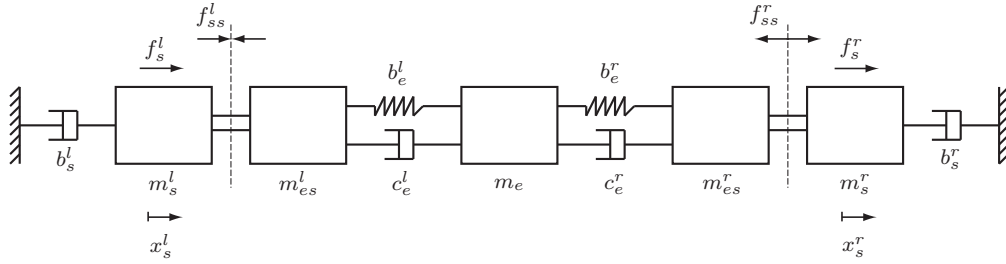


Figure 6.5: Model of bimanual telemanipulator and environment

6.3.2 Stability Analysis

As shown in chapter 4, the position-based admittance control with force-force exchange resulted to be the easiest to be tuned bilateral control architecture. Thus, it has also been selected for the bimanual manipulation case, whereby two independent bilateral controllers are used for left and right-handed teleoperation system. The corresponding controllers for one bilateral teleoperation pair are hereby given as follows:

$$\begin{aligned}
 f_m &= D_{xm} (\dot{x}_{dm} - \dot{x}_m) + K_{xm} (x_{dm} - x_m), \\
 f_s &= D_{xs} (\dot{x}_{ds} - \dot{x}_s) + K_{xs} (x_{ds} - x_s), \\
 f_{ss} - f_{sm} &= m_d \ddot{x}_{dm} + b_d \dot{x}_{dm}, \\
 f_{ss} - f_{sm} &= m_d \ddot{x}_{ds} + b_d \dot{x}_{ds}.
 \end{aligned} \tag{6.8}$$

As already mentioned in Sec. 4.5.1, for position tracking, equal parameters of the desired mass m_d and damping b_d have to be selected at operator as well as teleoperator site. Assuming additionally that the low level position controllers are already tuned, only two parameters have to be selected for stabilization of the overall teleoperation system. Hence, adequate parameter sets are determined by analyzing asymptotic stability.

For stability analysis the parameters m_d, b_d are gridded and the poles of the corresponding characteristic polynomial are computed. The stability margin is then determined by finding for a fixed m_d the corresponding parameter b_d which lies on the stability boundary. As instability typically occurs for hard contacts, the worst case scenario to be analyzed is characterized by $b_e^l = b_e^r = b_e$ and $c_e^l = c_e^r = c_e$, which means that left and right hand grasp the object with equal strength. If only this worst case scenario is taken into account, the analysis can be further simplified. Finally, a stability analysis for a two-dimensional operating domain formed by the varying parameters environment stiffness $c_e \in [0 \quad 10,000]$ N/m and environment damping $b_e \in [0 \quad 200]$ Ns/m is performed.

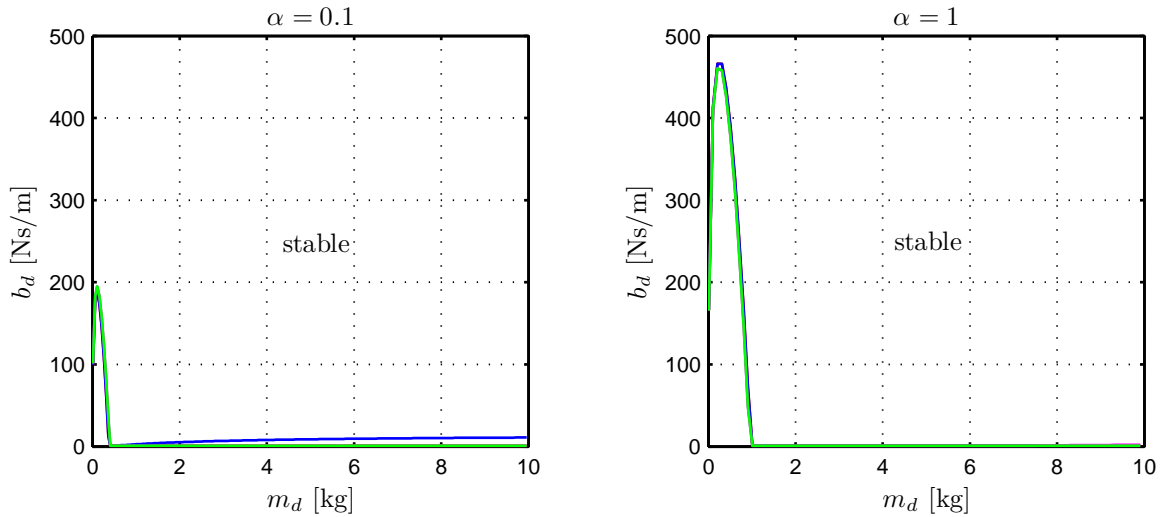


Figure 6.6: Stability region for the bimanual telemanipulation system in the m_d, b_d -plane for $m_e = 1$ kg and the usage of two bilateral position-based admittance controllers with force-force exchange

The results of the stability analysis are shown in Fig. 6.6, whereby different human operator impedances $\alpha^l = \alpha^r = \alpha$ are assumed. As can be clearly seen for small values of the desired mass m_d and damping b_d instability of the overall teleoperation system occurs. Moreover, an increasing human operator impedance reduces the set of stabilizing controllers. The strength of the grasp, however, did not influence stability. Comparing these results with the stability maps obtained for a single bilateral teleoperation system presented in Fig. 4.24, similarities can be observed. On this account, it can be stated that using a position-based admittance control with force-force exchange parameter sets can be found which stabilize the overall system independently of the type of interaction.

6.3.3 Experimental Results

To verify these results a bimanual telemanipulation task, as already presented in Sec. 5.4.3 and illustrated in Fig. 5.3, has been carried out, whereby only the case with all freed DOF has been considered. The task is divided into two phases:

1. grasping of the clamp with the right hand and positioning of it over the two tube ends
2. holding the clamp with the left hand and fixing the clamp by turning the green wheel with the right hand

While the first phase mainly contains sequences where only one hand is in contact with the environment or both hands are only loosely coupled, in the second phase both hands clearly form a closed kinematic chain over the clamp.

The setup presented in Sec. 4.6.4 and shown in Fig. 5.2 has been used again. The complete system consists of components for bimanual and multi-fingered haptic telemanipulation and a stereo-vision system (head mounted display). The telemanipulation devices ViSHARD10 and the dual arm redundant 7 DOF telemanipulator are controlled

by the before presented force-force bilateral teleoperation architecture. For the experiment the following matrices have been selected for haptic interface as well as telemanipulator: $\mathbf{M}_p = \text{diag}\{6, 6, 6\}$ kg, $\mathbf{B}_p = \text{diag}\{70, 70, 70\}$ Ns/m, $\mathbf{M}_o = \text{diag}\{0.2, 0.2, 0.2\}$ kgm², and $\mathbf{B}_o = \text{diag}\{1, 1, 1\}$ Nms/rad. Hereby, \mathbf{M}_p , \mathbf{B}_p represent translational and \mathbf{M}_o , and \mathbf{B}_o rotational 3x3 mass and damping matrices.

The experimental results are reported in Fig. 6.7 to 6.10, which show the force and position tracking performance of left and right hand for each phase of the experiment. For a better understanding, five sub-phases are distinguished: in sub-phase one the human operator grasps one of the tube ends with the left hand and disaligns both endings, in sub-phase two the right hand grasps the clamp and puts it over the left tube end, in sub-phase three the two tube ends are aligned and the left hand is used to move the clamp over the two tube ends, in sub-phase four the left hand grasps the red knob, and finally in sub-phase five the right hand turns the green wheel four times in clockwise direction. Shaded areas indicate experimental phases where both arms are tightly coupled and form a closed kinematic chain over the clamp.

In general, a good position tracking performance in free space and a good force tracking performance in contact can be observed. Due to the implemented impedances, some forces are necessary to move the device in free space motion, and in contact, positions slightly differ from each other. But stable behavior during all experimental phases can be achieved by selection of only one parameter set.

6.4 Multi-user Teleoperation

While for the before presented telemanipulation task the two tube endings were fixed in such a way that they always remained at the same height, and thus execution of the task by a single person was possible, below a more general case with looser tube endings or even flexible tubes is considered. If still only one person has to perform the task, the clamp has to be passed from left to right hand several times, which increases the risk to lose it. In the case of flexible tubes, carrying out the task by a single person is definitively not possible. This problem can be solved if a second person assists in performing the task, which results in a multi-user teleoperation system represented by architecture one. In this configuration multiple operator-teleoperator pairs exist and at least two people collaborate in achieving a common goal, see Fig. 6.11.

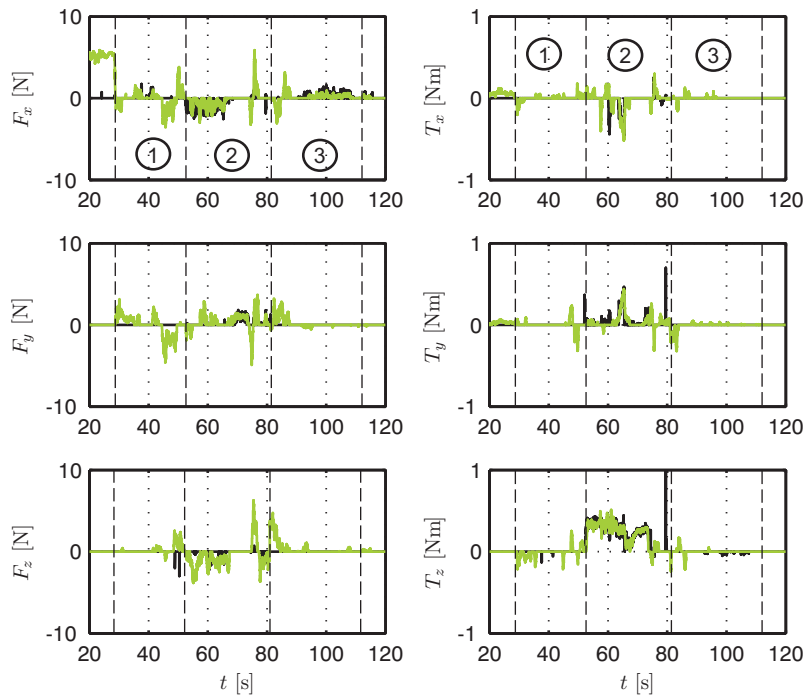
When repairing a broken pipe with flexible tube endings, sub-tasks have to be distributed among different human operators. While one person takes care e.g. of positioning the clamp, the other aligns both tube endings. In the second step one person holds the clamp in a certain position and the other tightens the screws. Analyzing this scenario, the following types of interactions can be distinguished:

- interaction of one teleoperator arm (+object) with the remote environment,
- interaction of two or more teleoperator arms via an object.

Especially in the second case, multiple kinematic chains are closed over different teleoperator arms, which may cause instability of the system.

The described collaborative task has been executed by using the teleoperation system depicted in Fig. 6.12, which consists of two human-system interfaces and two teleoperators. Sec. 3.1 describes the single components in detail. Each operator is responsible for

Force tracking of right arm



Position tracking of right arm

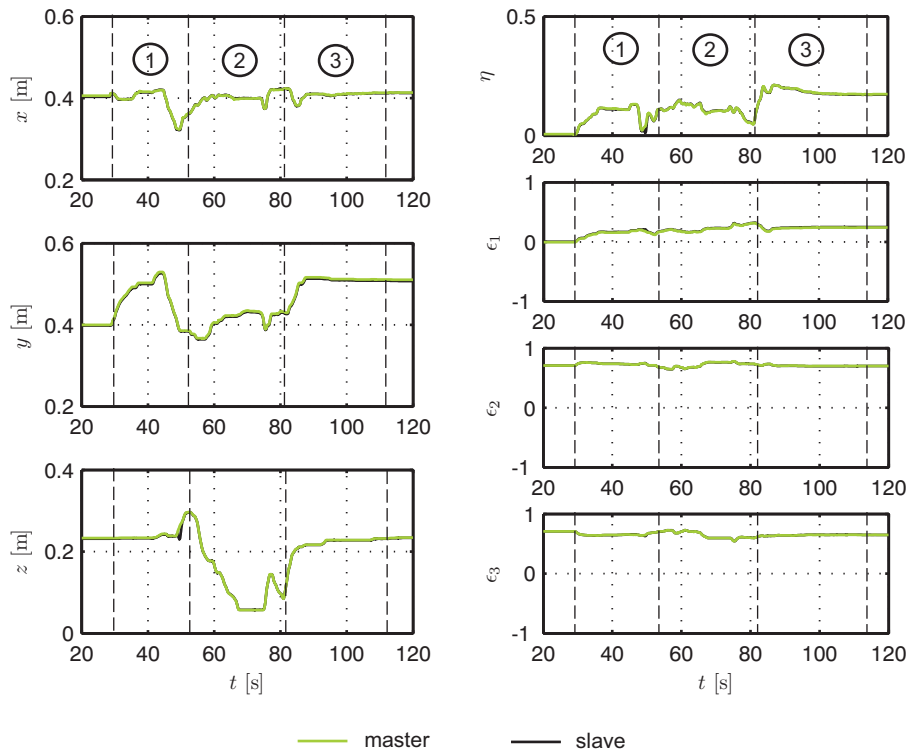
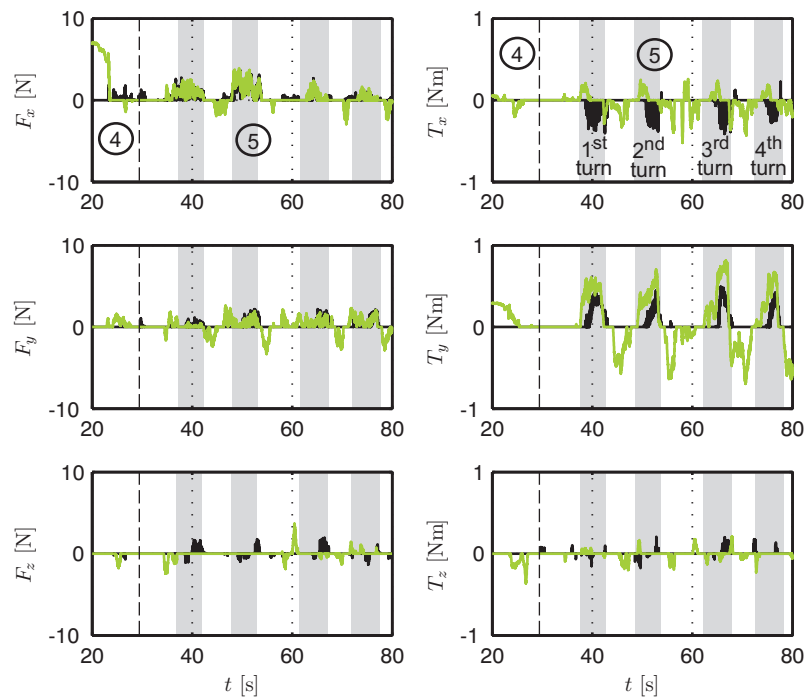


Figure 6.7: Force and position tracking of right arm during mounting phase.

Force tracking of right arm



Position tracking of right arm

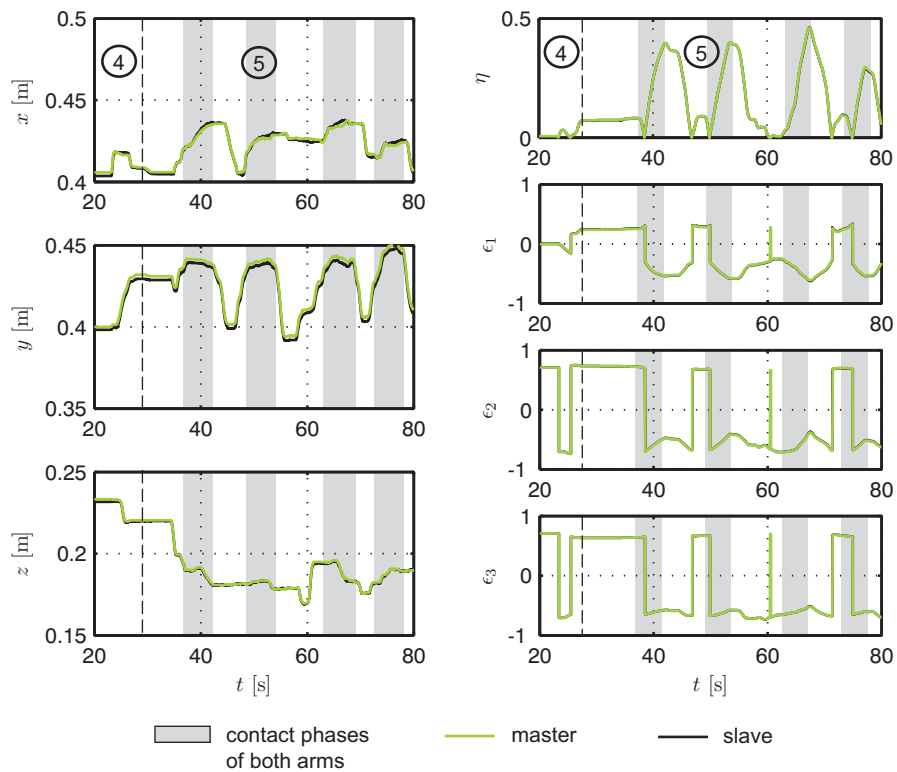
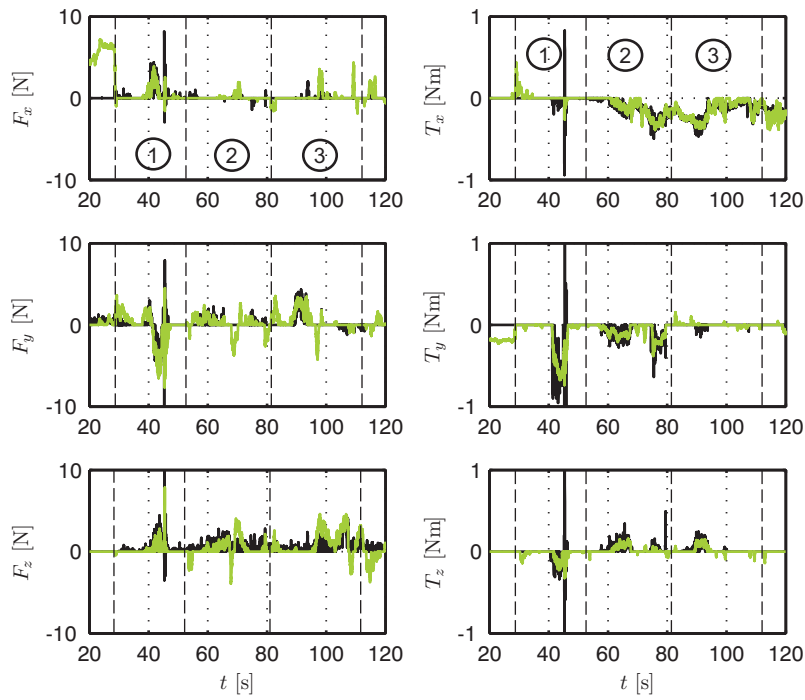


Figure 6.8: Force and position tracking of right arm during screw tightening phase.

Force tracking of left arm



Position tracking of left arm

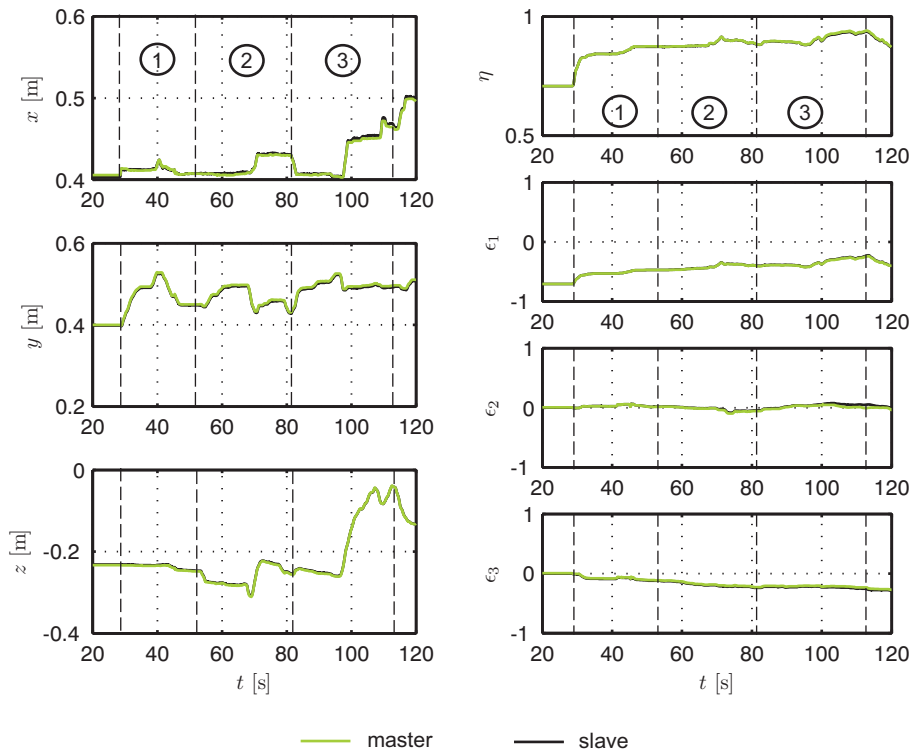
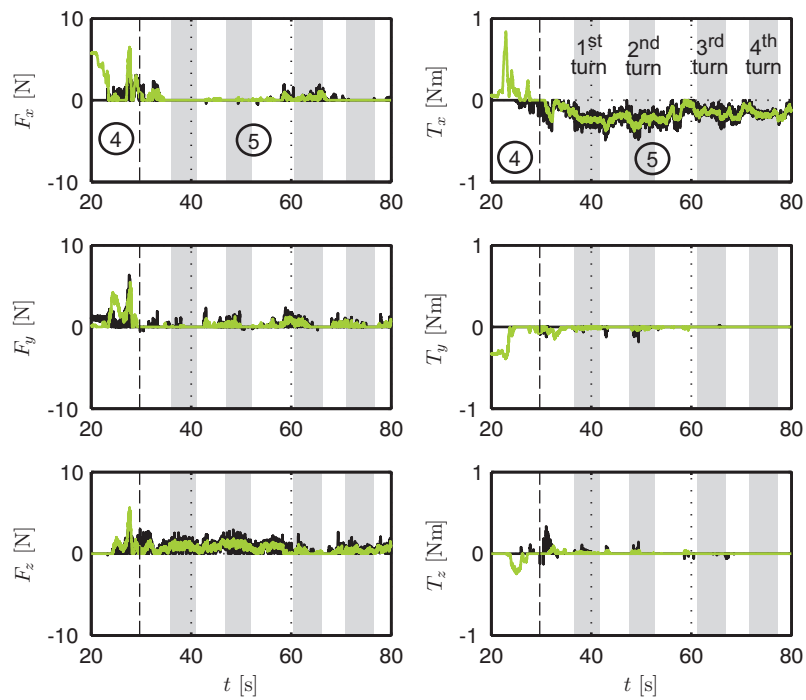


Figure 6.9: Force and position tracking of left arm during mounting phase.

Force tracking of left arm



Position tracking of left arm

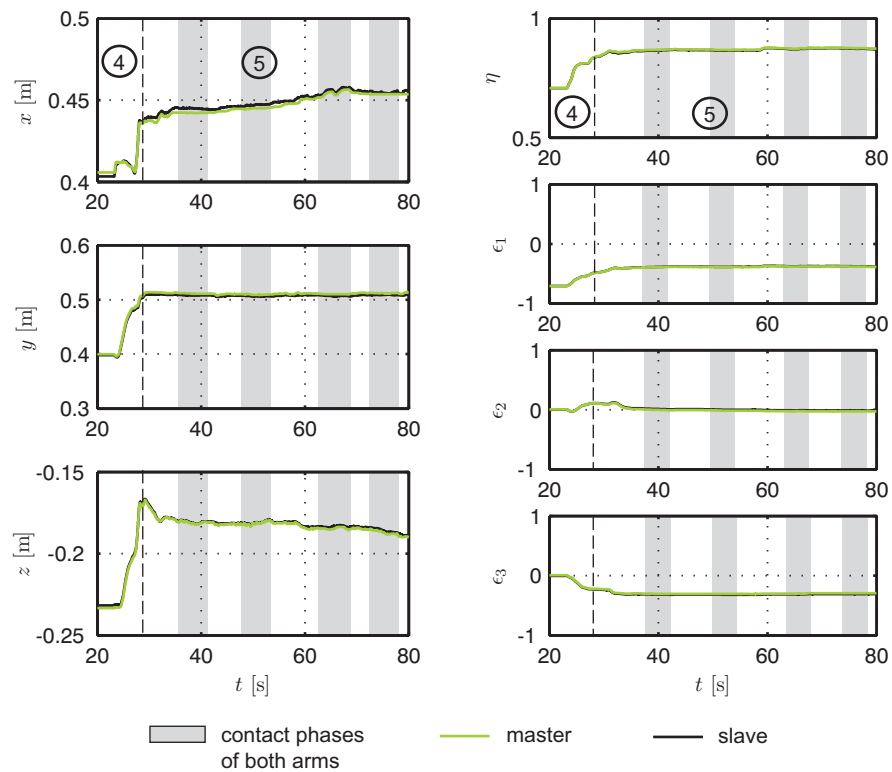


Figure 6.10: Force and position tracking of left arm during screw tightening phase.

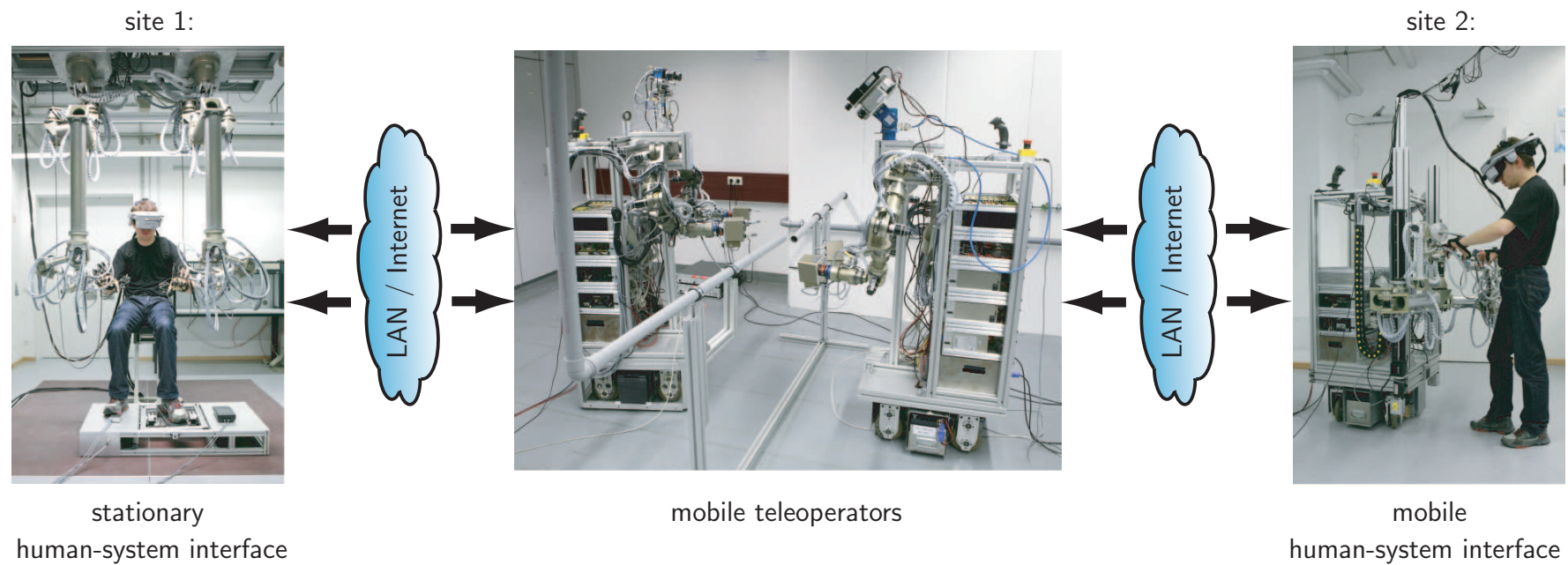


Figure 6.12: Multi-user teleoperation system consisting of a stationary and a mobile human-system interface (located at different sites) and two mobile teleoperators

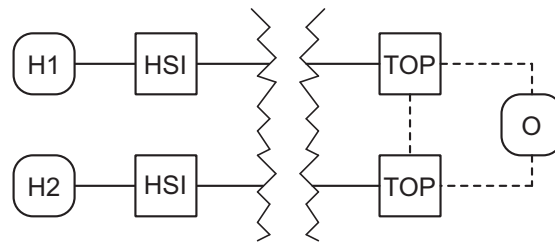


Figure 6.11: Multi-user teleoperation architecture: two human operators (H1, H2) interact with different human-system interfaces (HSI) and control corresponding teleoperators (TOP)

controlling of one of the teleoperators by using visual, auditory, and haptic information. Therefore, each teleoperation arm pair is independently controlled by a force-force bilateral teleoperation architecture, as presented in the former section. Fig. 6.13 shows some snapshots taken during the execution of the collaborative telemanipulation task. As the experimental results look quite similar to that of the bimanual setup, they are not reported any more. Also in this experiment, stable behavior for all possible configurations using only a single parameter set (the same as in the bimanual setup) could be achieved.

6.5 Intercontinental Cooperative Teleoperation

In this section another collaborative teleoperation architecture, which considers tele-cooperation of two humans located at distant sites, is analyzed in detail. While in the former section each human operator controlled a corresponding teleoperator, in the here presented scenario only one human operator teleoperates a remotely placed humanoid robot, but is assisted by another human, who is collocated with the telerobot. As shown in Fig. 6.14, a human operator (H1) controls a remotely located telerobot (TOP) via a human-system interface (HSI). When carrying out the task, she/he is assisted by another human (H2) located at the remote site. Such a configuration is useful, when a task requires an expert, who is not located at the building site or if a task is too difficult to be carried out by one teleoperated robot.

As the scenario clearly foresees human operators in distant locations, this architecture has been tested in an intercontinental, haptic tele-cooperation experiment between Germany and Japan. A human operator controlled a free-flying humanoid robot which collaborated with another human located at the remote site. The task to be carried out consisted in jointly grasping an object, moving it to a new position and finally releasing it. No similar experiment has been reported in the literature before. The closest related work is described in [48], where a collaborative telemanipulation task has been performed between the NASA's Robonaut and a human in order to evaluate the impact of force feedback on the telemanipulation performance.

As in our experiment operator and teleoperator site are located at different continents, signals have to be send over internet. Thus, one of the research challenges associated with such a tele-cooperation setup, is the time-delay in the communication channel, which can

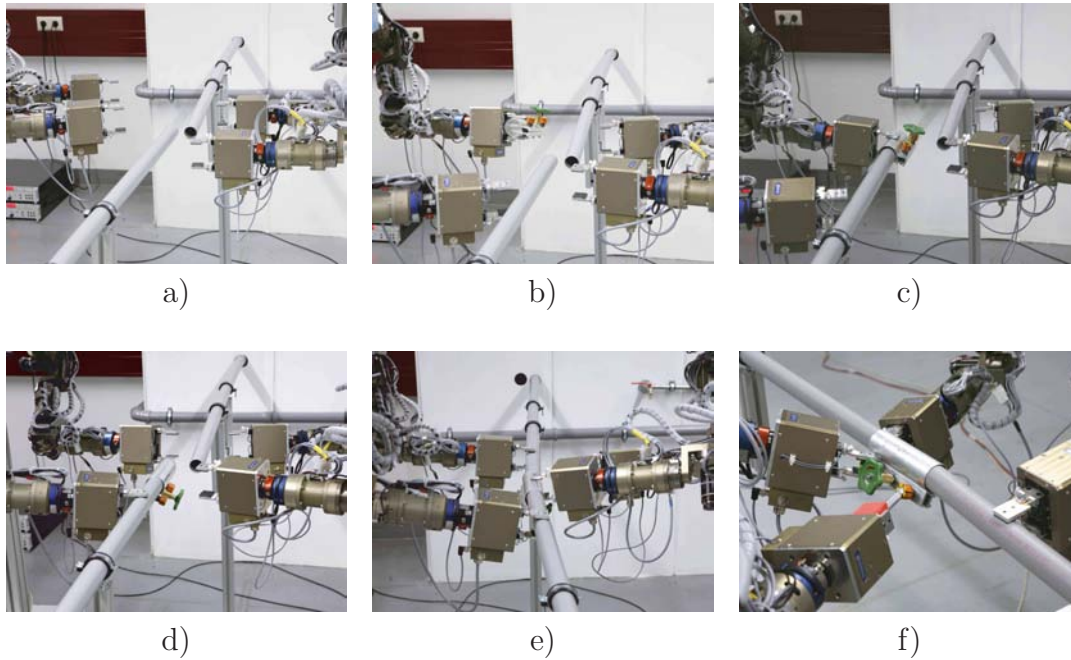


Figure 6.13: Collaborative fixing of a broken tube by telemanipulation. a) teleoperators approach maintenance site, b) operator I grasps clamp, c) operator I moves clamp over one tube ending, d) aligning of both tube endings, e) operator II moves clamp over both tube endings while operator I holds them, f) fixing of clamp by operator II

destabilize the overall system. In the context of tele-cooperation this issue is not addressed in prior works and thus it is subject of the following sections.

6.5.1 Stability Analysis

In the standard teleoperation stability analysis, passivity-based approaches commonly use the passivity argument for environment and human operator, see e.g. [57, 77, 82, 139]. As far as known, no results in known literature exist on how to model human operators in cooperative tasks. Because of the lack of concise results in this direction, it is assumed that both the human operator and the remotely located human collaborator behave like a passive system and have bounded impedances. In consequence, the stability of the overall teleoperation system can be analyzed using the concept of absolute stability. Further analyses concerning passivity in a cooperative telemanipulation task are subject of future research.

Definition: A linear two-port is said to be absolutely stable if no set of passive terminating one-port impedances exist for which the system is unstable. Otherwise, the system is potentially unstable.

A necessary and sufficient condition for absolute stability is given by Llewellyn's absolute stability criteria [85]:

- h_{11} and h_{22} have no poles in the right half plane

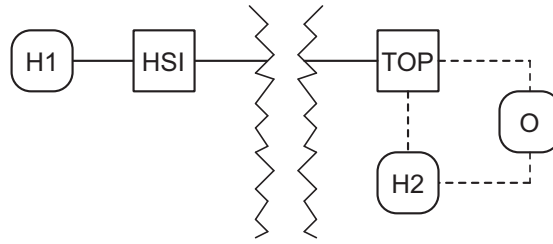


Figure 6.14: Multiple operator, single robot teleoperation system: an expert (H1) controls a remote teleoperator (TOP) and collaborates with another human (H2) located at the remote site

- any poles of h_{11} and h_{22} on the imaginary axis are simple with real and positive residues
- for all real values of the frequency ω , the following conditions hold:

$$\operatorname{Re}[h_{11}] \geq 0, \quad \operatorname{Re}[h_{22}] \geq 0, \quad (6.9)$$

$$2\operatorname{Re}[h_{11}]\operatorname{Re}[h_{22}] - \operatorname{Re}[h_{12}h_{21}] - |h_{12}h_{21}| \geq 0, \quad (6.10)$$

whereby h_{ij} with $i, j = 1, 2$ are parameters of the hybrid matrix [6], which describes the linear two-port.

If this criteria is satisfied by the two-port network, then the teleoperation system is stable if the two terminating impedances, namely the human operator interacting with the haptic interface, as well as the remotely located collaborating human, act in a passive way. Note that absolute stability allows passive terminating impedances, which results in a robust, but rather conservative control design.

As in this experiment a haptic interface and teleoperator of admittance-type are also used, the already presented bilateral teleoperation architectures, see Sec. 4 are analyzed for stability considering time-delay in the communication channel. Hereby, absolute stability of two of these bilateral teleoperation architectures, namely the position-based admittance control with force-position exchange and position-force exchange, is tested and design guidelines for the selection of control parameters are derived. The goal is to choose impedance parameters \mathbf{M} , \mathbf{B} , and \mathbf{C} , see (4.1), that stabilize the overall system despite changing human operator and environment impedances.

Assuming diagonal mass, damping and stiffness matrices, as well as CT control of the manipulators, the stability analysis of the overall system can be carried out for each degree-of-freedom separately. The hybrid matrices of the remaining one degree-of-freedom teleoperation system are given by

$$\begin{bmatrix} F_h(s) \\ -V_s(s) \end{bmatrix} = \begin{bmatrix} h_{11} & h_{12} \\ h_{21} & h_{22} \end{bmatrix} \begin{bmatrix} V_m(s) \\ F_e(s) \end{bmatrix} \quad (6.11)$$

for the position-based admittance control with position-force exchange and

$$\begin{bmatrix} V_m(s) \\ F_e(s) \end{bmatrix} = \begin{bmatrix} g_{11} & g_{12} \\ g_{21} & g_{22} \end{bmatrix} \begin{bmatrix} F_h(s) \\ -V_s(s) \end{bmatrix} \quad (6.12)$$

for the position-based admittance control with force-position exchange, where V_m , V_s , F_h , F_e are the Laplace transforms of \dot{x}_m , \dot{x}_s , f_h , and f_e , respectively.

If further high-gain position controllers and the compensation of external forces are assumed, Fig. 4.6 can be simplified significantly and the hybrid matrix of the resulting two-port network is given as follows, see [26] for more details:

$$h_{11}^c = \left. \frac{F_h(s)}{V_m(s)} \right|_{F_e=0} = \frac{m_{dm}s^2 + b_{dm}s + c_{dm}}{s}, \quad (6.13)$$

$$h_{12}^c = \left. \frac{F_h(s)}{F_e(s)} \right|_{V_m=0} = e^{-T_{sm}s}, \quad (6.14)$$

$$h_{21}^c = \left. \frac{-V_s(s)}{V_m(s)} \right|_{F_e=0} = -e^{-T_{ms}s}, \quad (6.15)$$

$$h_{22}^c = \left. \frac{-V_s(s)}{F_e(s)} \right|_{V_m=0} = \frac{s}{m_{ds}s^2 + b_{ds}s + c_{ds}}, \quad (6.16)$$

where T_{ms} and T_{sm} represent the time-delay from master to slave and slave to master, respectively. The time-delay is assumed to be constant, an assumption which is justified by measurements, see Sec. 4.6.

Testing absolute stability for this two-port network would give really conservative results, because infinite terminating impedances are considered. Taking into account that the human impedance is typically bounded, and adapting the two-port model to incorporate this knowledge, a much less conservative result can be obtained, see [52]. Hereby, $Z_{h,max}$ and $Z_{e,max}$ mean the maximum impedances of human operator and remote environment. The modified two-port network with limited human and remote impedances is shown in Fig. 6.15. The corresponding parameters h_{ij} are:

$$h_{11}^m = \frac{Z_{h,max}h_{11}^c}{Z_{h,max} + h_{11}^c}, \quad (6.17)$$

$$h_{12}^m = \frac{Z_{h,max}h_{12}^c}{Z_{h,max} + h_{11}^c}, \quad (6.18)$$

$$h_{21}^m = \frac{Z_{h,max}h_{21}^c}{Z_{h,max} + h_{11}^c}, \quad (6.19)$$

$$h_{22}^m = h_{22}^c - \frac{h_{12}^c h_{21}^c}{Z_{h,max} + h_{11}^c} + \frac{1}{Z_{e,max}}. \quad (6.20)$$

Analogously, the coefficients g_{ij}^c for the position-based admittance control with force-position exchange are given by

$$g_{11}^c = \left. \frac{V_m(s)}{F_h(s)} \right|_{V_s=0} = \frac{s}{m_{dm}s^2 + b_{dm}s + c_{dm}}, \quad (6.21)$$

$$g_{12}^c = \left. \frac{V_m(s)}{-V_s(s)} \right|_{F_h=0} = -e^{-T_{sm}s}, \quad (6.22)$$

$$g_{21}^c = \left. \frac{F_e(s)}{F_h(s)} \right|_{V_s=0} = e^{-T_{ms}s}, \quad (6.23)$$

$$g_{22}^c = \left. \frac{F_e(s)}{-V_s(s)} \right|_{F_h=0} = \frac{m_{ds}s^2 + b_{ds}s + c_{ds}}{s}, \quad (6.24)$$

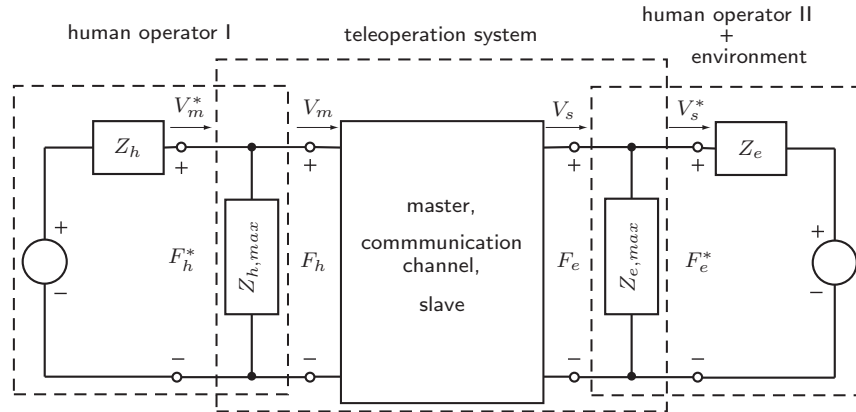


Figure 6.15: Two-port network with limited human impedances

and the coefficients g_{ij}^m describing the modified two-port network can be obtained from (6.17) to (6.20) by simply exchanging h with g , $Z_{e,max}$ with $Z_{h,max}$, h_{11} with h_{22} , as well as h_{12} with h_{21} .

Given these coefficients for the two before mentioned control architectures, stability can be analyzed by evaluating Llewellyn's stability criteria.

6.5.2 Numerical Stability Test

Considering a cooperative telemanipulation task, stability for two basic experimental conditions is required:

- stability when interacting with the remote collaborator
- stability when interacting with the remote environment

These two experimental conditions are represented by different upper bounds of the remote impedance $Z_{e,max}$. If the interaction with a human operator is considered, $Z_{e,max}$ reflects an upper bound for the human arm impedance, which can be modelled as follows

$$Z_{e,max} = b_{h,max} + \frac{c_{h,max}}{s}. \quad (6.25)$$

$c_{h,max} = 40\text{N/m}$ and $b_{h,max} = 6\text{Ns/m}$ denote the maximum stiffness and damping the human operator can apply to the system. The corresponding parameters are taken from [78]. If stability for the interaction with stiff remote environments should be tested, $Z_{e,max} = 10^4\text{N/m}$ is assumed.

For the analysis of the position-based admittance control with position-force exchange, c_{ds} is set to zero and $c_{dm} = 600\text{N/m}$. It should be noted that c_{dm} represents an upper bound for displayable stiffnesses on the master side and thus it should be selected carefully. To reduce further parameters, a constant mass m_{dm} for the desired master impedance is selected. Perfect transparency would require the master mass to be set to zero. However, in admittance control, this is not possible because the minimum target inertia is bounded by stability, see Sec. 2.4 and [30]. So a minimum mass m_{dm} has been selected, which is able to stabilize the master system when operated alone.

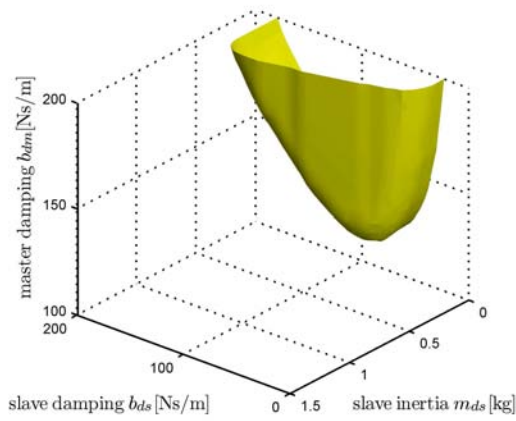


Figure 6.16: Position-based admittance control with position-force exchange: absolute stability for a fixed master mass $m_{dm} = 1$ kg

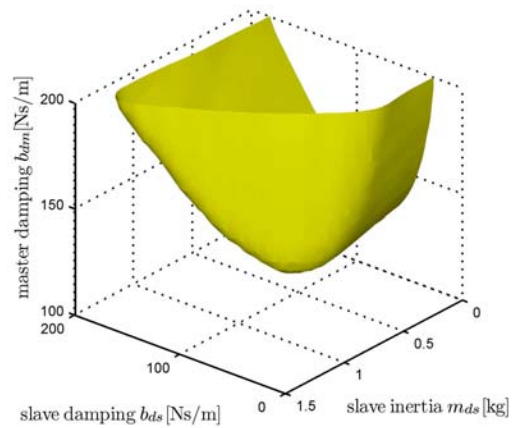


Figure 6.17: Position-based admittance control with position-force exchange: absolute stability for a fixed master mass $m_{dm} = 5$ kg

Finally, the remaining parameters m_{ds} , b_{ds} , and b_{dm} are gridded and absolute stability is tested for each grid point. For the analysis, a constant time-delay of $T_{sm} = T_{ms} = 150$ ms is assumed. Fig. 6.16 and 6.17 show the corresponding simulation results, whereby the area enclosed by the envelopes means control parameters, which stabilize the overall teleoperation system. As can be seen, stability can only be guaranteed if a certain amount of master and slave damping is implemented. Moreover, the number of stabilizing control parameters increases with increasing master mass m_{dm} . It should be noted that due to actuator limitations a certain amount of m_{ds} has to be implemented, which implies an appropriate selection of m_{dm} . Summarizing, it can be stated that for a position-based admittance control with position-force exchange stable behavior for the two conditions a) interaction with a remote collaborator and b) interaction with a stiff remote environment can be achieved if enough damping at master and slave side is provided.

For the position-based admittance control with force-position exchange, correspondingly $c_{dm} = 0$ N/m and $c_{ds} = 600$ N/m have been selected and the remaining parameters m_{dm} , b_{ds} , and b_{dm} are gridded. A stability analysis with $c_{h,max} = 40$ N/m and $b_{h,max} = 6$ Ns/m and $Z_{e,max} = 10^4$ N/m showed that absolute stability is always guaranteed when a minimal slave damping b_{ds} is implemented, see Fig. 6.18. Observe from the larger enclosed area that the force-position exchange architecture with local position-based admittance control allows a larger class of stabilizing controllers than the position-force exchange architecture.

6.5.3 Experimental Evaluation

One of the above presented control architectures has been tested in an intercontinental cooperative telemanipulation task, whereby the operator site is located in Munich, Germany and the teleoperator site in Tsukuba, Japan. As slave the humanoid robot HRP-2 and as master the haptic interface ViSHARD7 is used. The experimental task is shown in Fig. 6.19. The execution consists of jointly grasping an object, moving it to a new position

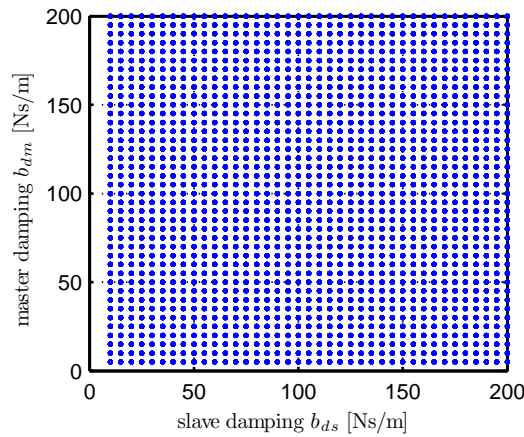


Figure 6.18: Position-based admittance control with force-position exchange: absolute stability for a fixed slave mass $m_{ds} = 5$ kg

and finally releasing it. Hereby the task of the human collaborator was to follow the motion commanded by the human controlling the telerobot. In order to give the human operator a realistic impression of the remote environment visual, auditory, and haptic information has been exchanged over Internet, see Fig. 6.22. The experimental setup is explained in detail in succeeding paragraphs.

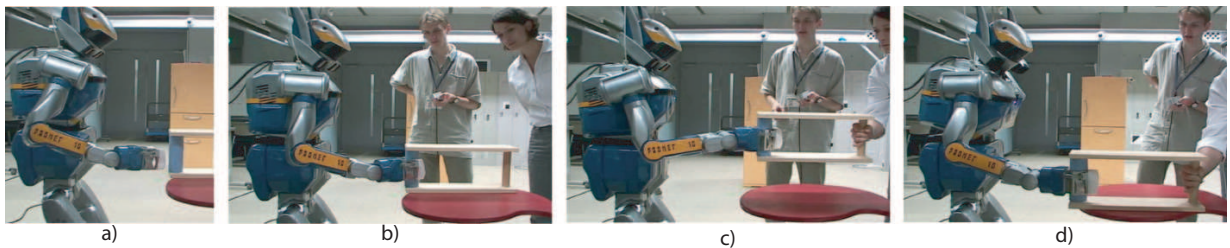


Figure 6.19: Cooperative telemanipulation task: a) approach, b) grasp, c) lift, d) put down

Experimental Setup

Teleoperator: Fig. 6.20 shows the HRP-2 humanoid robot when interacting with a human. HRP-2 has 30 DOF: six for each leg and arm, one for each gripper, two for the chest, and two for the head. In the experiment only the right arm and the head have been used, whereby the chest was allowed to rotate around the vertical axis to increase the manipulation area. HRP-2 has four cameras: one wide-angle and three narrow-angle cameras. For the teleoperation experiment the images of two narrow-angle cameras were used and send to the remotely located human operator. To provide force information HRP-2 is equipped with 6 DOF force/torque sensors located at the wrist of each hand. HRP-2 is controlled by using low-level high-gain joint PD controllers running at 1 kHz. The position reference signal is hereby provided by an outer control loop running at 200 Hz. More details about HRP-2 and the used full-body controller can be found in [64, 92].

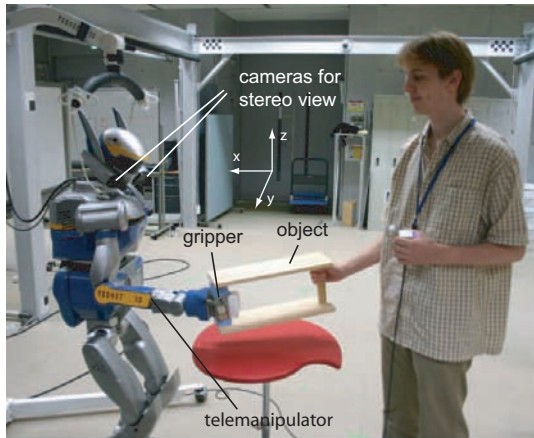


Figure 6.20: Remote site: HRP-2 collaborating with a local human

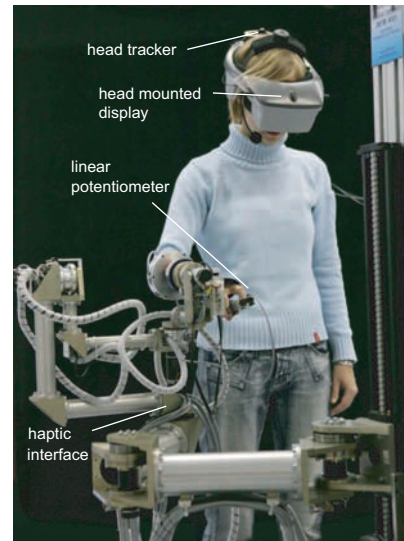


Figure 6.21: Operator site: human operator and human-system interface

Human-system interface: Fig. 6.21 shows a human operator interacting with the human-system interface, which consists of devices for visual, auditory and haptic feedback. The redundant haptic interface ViSHARD7, see chapter 2, is used to provide force-feedback information to the human operator and allows to control the remotely located telerobot. It is characterized by its relatively large workspace, high payload, as well as its redundancy to avoid kinematic singularities. In order to allow fine-manipulation, the telemanipulator is additionally equipped with a two-finger gripper. To open and close this gripper the distance of thumb and index finger is measured by a linear potentiometer. No finger-force feedback is provided.

The recorded video streams are transmitted to the operator site and then displayed on a head-mounted display (HMD; NVIS nVisor SX, resolution 1280 x 1024) carried by the human operator. The HMD is additionally equipped with an ultrasonic tracker (IS900), which is used for controlling of the camera head motion, so that the user can look around in the remote environment just by turning his/her own head.

Network: The packet rate, i.e. the network sampling rate, has been chosen to 50Hz. At this packet rate, the packet loss probability was negligible ($< 1\%$) while undesired effects of sampling on performance still remained hidden as observed in preliminary experiments as well as during the experiment itself. Similarly, the round trip time-delay between Germany and Japan was measured to $T_{ms} + T_{sm} = 278 \text{ ms} \pm 5 \text{ ms}$. Observe that the time-delay variance over time of 5ms is below the sampling time interval of 20ms justifying the assumption of approximately constant delay.

Overall control architecture: Since position-based admittance control with force-position exchange seems to have a greater variety of stabilizing controllers, this architecture has been implemented for the presented teleoperation system. As shown in Fig. 6.23, admittance-type controllers with low level joint-controllers are used for master, as well as slave devices and connected by using a two-channel force-position ar-

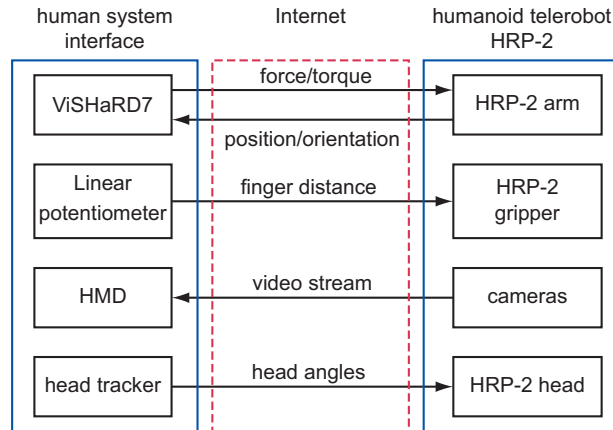


Figure 6.22: Data exchange in the teleoperation experiment

chitecture. Hereby, forces are sent from master to slave and positions from slave to master. The stability analysis presented above distinguishes between stable and non-stable regions, but gives no information about the transient behavior of the overall system. In order to guarantee a well damped behavior, the following parameters for the desired master and slave impedances have been found in the experiment: $m_{dm} = 1$ kg, $b_{dm} = 200$ Ns/m, $c_{dm} = 600$ N/m, $b_{ds} = 200$ Ns/m, $m_{ds} = 10$ kg for the translational part and $m_{dm} = 0.02$ kgm², $b_{dm} = 2$ Nms/rad, $c_{dm} = 20$ Nm/rad, $b_{ds} = 1$ Nms/rad, $m_{ds} = 0.2$ kgm² for the rotational part.

The relatively high mass and damping factor at slave side limits hereby the bandwidth of the system significantly and thus ensures stability of the overall teleoperation system despite of significant time delay in the communication channel.

In order to measure zero forces during free-space motion, the end-effector masses have been compensated. Since the center of gravity of the end-effectors is only approximately known, small deadzones are used. The small position errors introduced by these deadzones can be compensated by the human operator as she/he is provided with visual feedback of the remote scene.

Experimental Results

Fig. 6.24 shows a typical example for position and force tracking during the experiment. Basically, an approaching and grasping (1), moving (2), and releasing phase (3) can be distinguished. In the approaching phase the human operator approaches and grasps the object, in the moving phase the humans move the object from the starting to the target position and finally in the releasing phase the object is released after being in contact with the remote environment. During *free space motion* (phase 1) the position tracking is very good. While in this phase at slave site no forces can be measured, some forces at master site are necessary to change the position of the device. This is mainly due to the implemented impedances in the master and slave controllers. In the *contact phase* (phase 3), the force tracking is good and the positions slightly deviate from each other. This can be explained by the compliant behavior introduced by the admittance controller implemented at master site. As a consequence, the perception of the remote impedance is also altered. In y-direction, the remote collaborator behaves as a task follower, because the

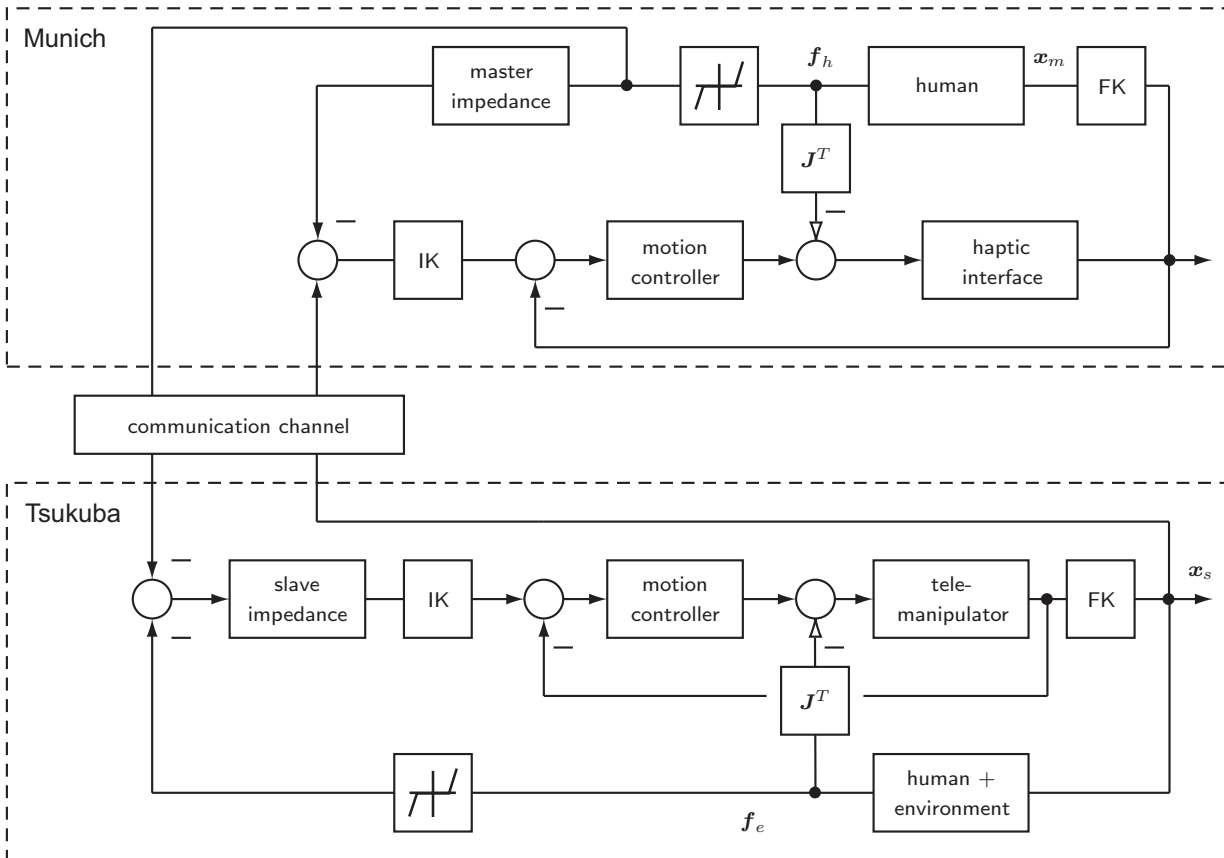


Figure 6.23: Overall control architecture: position based admittance control with force-position exchange

shape of the manipulated object makes it difficult to apply forces in these directions. On the contrary, the shaded area in phase 2 indicates a region, where the human collaborator located at the remote site applies forces in positive x-direction onto the carried object. This results in small deviations of master and slave position.

Summarizing, it can be stated that stable behavior during all experimental phases can be observed when implementing the proposed position-based admittance controller with force-position exchange.

6.6 Discussion

Many tasks in our daily life cannot be performed alone because the abilities of a single person are limited. This is e.g. the case when transporting heavy, bulky objects or when performing complicated manipulation tasks which require more than two hands. In such a case we strongly depend on the assistance of an auxiliary tool or the cooperation of other people. Auxiliary tools are typically used if the task is known before and/or it is carried out multiple times. A teleoperation scenario, however, is mostly characterized by unknown, varying environment conditions and thus the collaboration with other people, who can adapt to the actual situation, becomes necessary. Hence, so called collaborative teleoperation systems result.

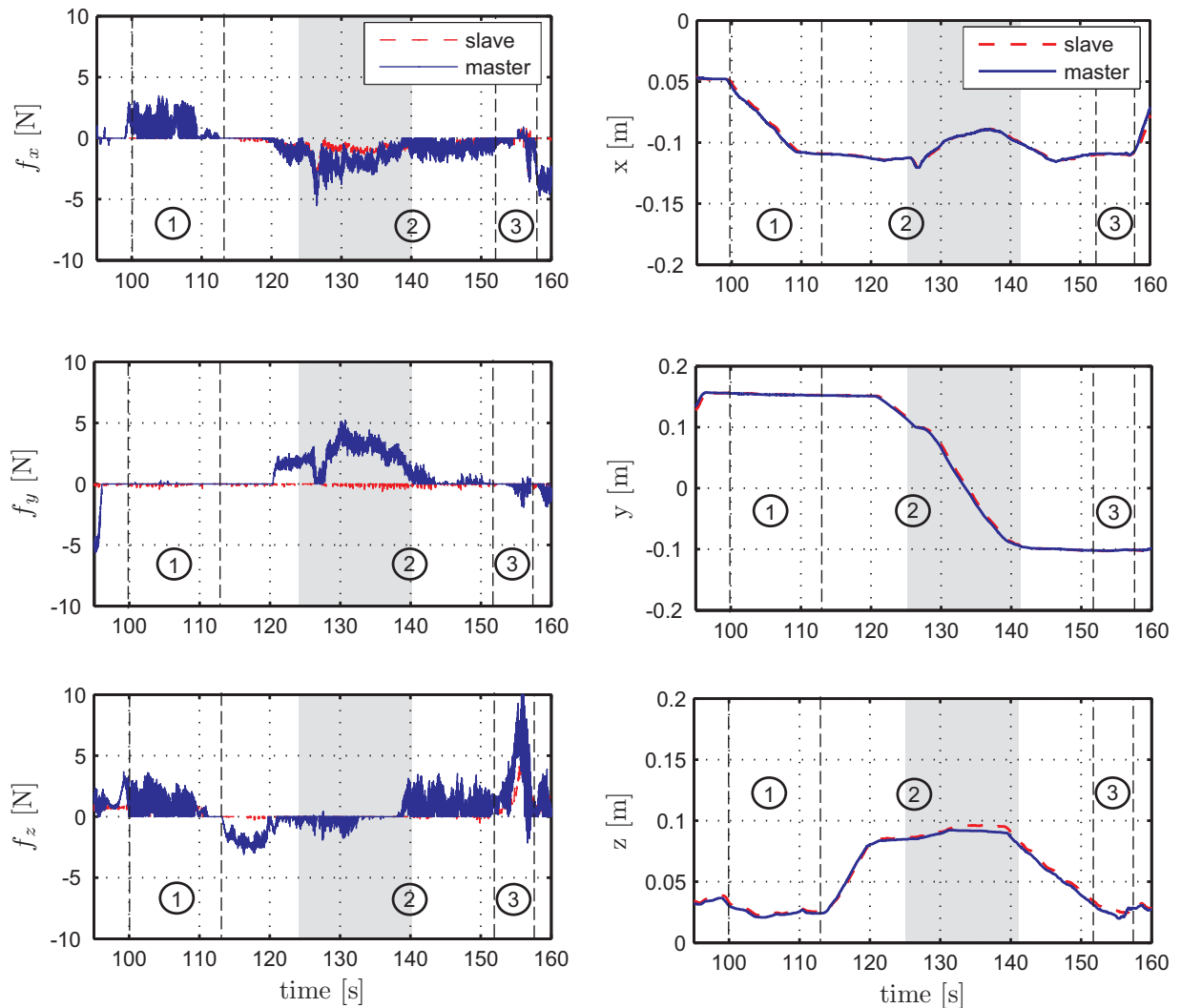


Figure 6.24: Force and position tracking during experiment. 1: approaching phase, 2: moving phase, 3: releasing phase, shaded area: human located at the remote site applies forces to the object

In this chapter, a definition and classification of collaborative teleoperation systems has been given. Starting from a classification into MOMR, SOMR and MOSR systems, five possible architectures for collaborative teleoperation have been derived. Thereby, different collaboration strategies have been formulated and typical application areas for each architecture have been described. Dependent on the type of interaction between the participants different challenges on the control of such systems, have been formulated. Typical challenges found in this context are: coordinated motion behavior, collision avoidance, synchronization, robust stability despite of uncertainties, changing kinematic configurations, closed kinematic chains, non-ideal network conditions, and safety issues.

Some of the few state-of-the-art approaches which deal with collaborative teleoperation systems, have been described. Hereby, approaches for unconstrained and constrained interaction as well as approaches using only one or multiple human-system interfaces are distinguished. The analysis of these algorithms showed that: Approaches using only one human-system interface cannot be extended to a bimanual or MOMR system. The event

based approach can only be applied for rigid grasp conditions and produces an error between master and slave positions. Designs based on single master/single slave teleoperation systems fail if they do not address the performance and stability requirements of collaborative teleoperation and the resulting additional interaction possibilities. The proposed multi-lateral controllers require a dynamic model of the manipulators and have only been tested for one DOF experiments using impedance-type devices.

As a first attempt to address some of the above formulated research challenges on collaborative teleoperation systems, three out of the five presented collaborative teleoperation architectures have been implemented by using prior presented hardware and software developments: a bimanual, a multi-user, and an intercontinental cooperative teleoperation architecture. No similar experiments of the described complexity have been presented before in the literature. The main focus in these investigations was on the finding of robustly stable controller parameters, which guarantee stability despite changing kinematic configurations and varying human operator and environment impedances. It could be shown that a position-based admittance control with force-force exchange can be used in the bimanual as well as multi-user setup, whereby a single parameter set allows stabilization of the system for all interaction possibilities. For the intercontinental cooperative teleoperation task, stabilizing controllers under the assumption of passive human operator behavior and environment could be also found. Hereby, the strong assumption on the passive human behavior during a cooperative manipulation task has to be verified in the future. A further open research question is whether advanced multi-lateral controllers as proposed in the literature can also be implemented for admittance-type devices and whether they are able to increase transparency of the overall system with respect to the here proposed bilateral controllers.

7 Conclusions and Future Directions

7.1 Concluding Remarks

This thesis describes the design and control of a world leading, highly integrated, multi-modal, and intuitive teleoperation system that can be used to perform a variety of manipulation tasks of different complexity. Hereby, tasks requiring bimanual and multi-fingered manipulations as well as tasks requiring more than one person are considered. Distinct to other developments, exclusively teleoperation systems using admittance-type devices are investigated.

The development of such a teleoperation system starts with the design of an appropriate human-system interface, which allows bimanual 6 DOF manipulations with high interaction forces in large remote environments. In chapter 2, typical requirements of such a system are formulated and a modular system, consisting of independently designed and controlled components, namely two haptic interfaces and a mobile platform, is proposed. When coupling the haptic interfaces with the mobile platform the workspace of the device can be extended to nearly arbitrarily large environments, but this requires solving an optimization task. In order to simplify this optimization, an appropriate design and inverse kinematics of the haptic interfaces which assure a decoupling of translational from rotational movements is described. When interacting with the haptic interface a stable behavior is required. The performed stability analysis showed a strong dependency on the human arm impedance, whereby higher impedances potentially cause instability of the system. In this context, the human arm mass had the biggest influence on stability. Additionally, a negative effect of the force/torque filter time constant on stability was found. The newly developed system has been intensively evaluated and a huge number of performance indexes, typically not available for other haptic interfaces known from literature, has been determined. Finally, the effect of different motion controllers on the performance of the device has been analyzed. The results indicate that a computed torque controller is able to realize a good impedance display fidelity in the two extremes contact and free space motion and that it is more appropriate for admittance-type haptic interfaces than an independent joint controller.

As the haptic interface represents only one component of the overall teleoperation system, the integration of other components for visual and auditory feedback, as well as haptic interaction is covered in chapter 3. To realize a very intuitive interaction with the teleoperation system, the main focus in the development is on a human-friendly design, so that the human operator needs to only slightly adapt to the technical system. Typical mechatronic design requirements for the realization of such a system were found to be a human scaled workspace free of kinematic and algebraic singularities, the possibility to operate in full 6 DOF, the possibility to mount task specific end-effectors, the capability to display stiff environments, an anthropomorphic design of the teleoperator, as well as multi-modal feedback. Taking into account all these requirements a novel, enhanced, and highly integrated teleoperation system consisting of redundant haptic interfaces and telemanipulators, as well as a stereo-vision system has been presented, which allows performance of bimanual

manipulation tasks. To be also able to realize dextrous, fine operations, this system has been extended by components for multi-fingered telemanipulation. On this account, the telemanipulator arms are equipped with three-finger robotic grippers that allow the realization of different grasp types ranging from precision to power grasps. A simple, but efficient position mapping algorithm, which maps human hand motions to robotic gripper motions is proposed and successfully evaluated in experiments. Although this mapping method is based on a vertical projection, the overall form of the grasp is basically maintained. Closing the loop by providing finger force feedback to the human operator finally allows a realistic impression of grasping remotely located objects.

Beside mechatronic design criteria, also the implemented control algorithm significantly influences the quality of a telerobotic system. On this account, chapter 4 analyzed different types of bilateral control architectures with special focus on teleoperation systems using admittance-type devices. In contrast to impedance-type devices, which are characterized by very light-weight constructions with low inertia and friction, admittance-type devices have higher dynamic properties and friction is typically not negligible. Hence, using admittance-type devices force controllers can only be realized with a very poor performance so that classical two-channel control architectures resulted to be not suitable for these kind of devices. Instead of pure force controllers, local position-based admittance controllers are used and connected to bilateral teleoperation control architectures by exchanging position and force information. The main challenge in parameterizing these controllers turned out to be the fact that human operator and remote environment impedance change significantly over time and thus control parameters have to be found which are able to robustly stabilize the system despite uncertainties. Robust stability of the proposed bilateral control architectures has been evaluated by using the parameter space approach. This method is used in the first step for controller design and in the second step for robustness analysis. The main advantage of this method is that no passive human operator or remote environment have to be assumed, which is necessary when using classical approaches. Moreover a desired dynamic behavior can be specified. As shown, also effects as actuator and sensor dynamics can be easily incorporated in the analysis. The results indicate that the best performance can be achieved by using a position-based admittance control with position-force exchange, as transparency is affected the least. To guarantee robust stability for this architecture, a number of control parameters has to be selected, as indicated by the stability analysis. Much easier to tune because of only two variable control parameters however, is a position-based admittance controller with force-force exchange. This feature is of special importance if control parameters for systems with multiple DOF have to be selected.

While chapter 2 to 4 focused on the optimization of both the mechatronic design and of the implemented control architectures, further improvements can be achieved by incorporating human factors in the development process. Earlier findings in the literature suggested providing only that DOF to the human operator, which are absolutely necessary to perform a certain task, because this would increase task performance. But as it was still unknown how this would affect the feeling of telepresence and whether human movement control is really driven by task performance, chapter 5 investigated effects of varied human movement control on task performance and feeling of telepresence. In contrast to earlier studies, the obtained results indicate that providing all six DOF for movement control led to a better task performance compared to providing a lesser number of DOF. In addition, providing the full range of motion possibilities had a beneficial effect on the feeling of

telepresence as the participants felt more immersed when having the possibility to control all six DOF. This indicates that for high-quality teleoperation systems, as developed in this thesis, all DOF should be provided to the human operator, regardless of the task to be performed. As a side-result of this analysis, it could be further shown that an increasing amount of visual depth cues comprised by a HMD, as opposed to a projection wall, improved human task performance and thus the interaction with the teleoperation system.

If a task that exceeds the abilities of a single person should be performed, e.g. when carrying heavy or bulky objects or performing complex manipulation tasks, we clearly depend on the assistance of other people. While a classical teleoperation system has been found to combine skills such as human adaptability and decision making ability with the advantages of robotic manipulation, collaborative teleoperation systems, as presented in chapter 6, extend these features by the ability to collaborate with other humans by means of a teleoperation system. As in a teleoperation system, the human operator is separated from the environment she/he wants to interact with, different types of collaborative teleoperation architectures can be constructed. Based on a classification into MOMR, SOMR, and MOSR systems, five possible architectures for collaborative teleoperation have been derived and typical application scenarios have been presented. Two different types of possible interactions between the participants have been distinguished, namely unconstrained and constrained interactions, whereby both types of interactions impose different challenges on the control of the corresponding teleoperation system. The most important challenges found in this context are: coordinated motion behavior, collision avoidance, synchronization, robust stability despite of uncertainties, changing kinematic configurations, closed kinematic chains, non-ideal network conditions, and safety issues. With focus on some of these issues three out of the five presented collaborative teleoperation architectures have been implemented by using the developed teleoperation systems. Robust stability for all these architectures could be shown despite changing kinematic configurations and varying human operator and environment impedances. The hereby conducted experiments are worldwide unique, no similar experiments have been presented before.

7.2 Outlook

This thesis covered a variety of design and control issues in the development of a highly integrated, multi-modal, and intuitive teleoperation system. In the following paragraphs, possible extensions of this work and collocated future research directions are pointed out:

In accordance with the concepts developed in this thesis the realization of a mobile haptic interface requires positioning of the mobile platform which carries the two haptic interfaces in such a way that the manipulability of both haptic interfaces is maximized. This can be achieved by using an optimization algorithm which maximizes the manipulability of both haptic interfaces. The implementation of such a holistic control concept that combines haptic interfaces and mobile platform into a common control framework, represents a logical extension of the presented work. Possible solutions for this problem are also subject of our original work [160].

Concerning the developed multi-fingered teleoperation system, improvements are possible by using an advanced robotic gripper with more DOF, as e.g. represented by the SCHUNK Dextrous Hand (SDH) [112] or DLR hand [18]. The closer the kinematics to the human hand, the more dextrous manipulations can be performed and the more intuitive

is the usage of it. More developments are also necessary in providing a better finger force feedback to the human operator, as to date fingers can only pulled and not pushed and force feedback is strongly affected by friction.

The developed multi-modal teleoperation system provides a huge variety of different sensory information the human operator has to integrate. Due to different processing and communication times, a temporal inconsistency in the presented information may result, which might affect transparency of the overall teleoperation system and the integration of multi-modal information. At the moment, no thresholds for still acceptable inconsistencies are known. Thus, more studies on the temporal multi-modal integration capacity of a human operator have to be performed.

While this thesis aimed at realizing an intuitive teleoperation system which requires only few adaptations by the human operator, clear technical limitations are imposed on this ambitious intention. This is mainly due to restrictions of available hardware components or the implemented control architectures, which are not able to realize a really transparent interaction with the remote environment. Thus, manipulations performed by means of a teleoperation system are typically characterized by an increased execution time, failure rate, and stress level of the human operator. To reduce these effects, future teleoperation systems need to be able to assist the human operator in performing the task by still keeping her/him fully in charge of the operation strategy. Some early attempts in designing such systems are described in [116]. More recent developments can be found in [50], where a shared control dextrous telemanipulation system is realized which facilitates grasping of objects. Another approach to assist in teleoperative tasks is proposed by [4], who introduces adaptive virtual fixtures. Some preliminary results of our group on computer assistance concepts for teleoperation systems are reported in [130]; more results will follow in the near future.

Especially in the field of collaborative teleoperation systems, many questions are still unanswered and further research needs to be done. Some of the most promising research directions should be highlighted: Stability and transparency of a collaborative teleoperation system are expected to be improved by introducing new control schemes, which allow transmission of position and force information between all master and slave robots, rather than merely between corresponding units. Hereby, a variety of different interaction possibilities have to be taken into account. Performance of these newly developed architectures needs to be evaluated. New performance criteria for multi-user telepresence systems have to be defined, including transparency and cooperation measures, see e.g. [68] for the definition of such criteria for a typical student-teacher teleoperation scenario. The extension of such concepts to systems with non-ideal network conditions also represents a big challenge. A further improvement of collaborative teleoperation systems can be achieved by extending the already mentioned computer generated assistance functions to support multiple operators in the execution of a collaborative task. Adequate algorithms can hereby be derived from the analysis of the haptic information exchanged between two collaborating humans. Such an analysis may also lead to an interaction model, which can help to artificially increase the feeling of co-presence.

A Hardware Specifications of ViSHaRD7

A.1 Specification of Gears

Table A.1: Specification of gears

Joint#	Series-Version-Size-Ratio	M_R^1 [Nm]	M_A^2 [Nm]	v_{max}^3 [rpm]	<i>slope</i> [m/round]
1	THK KR45H10-D+840L	3.240 N	-	-	0.01
2	CSG-2UH-20-120	113	64	6500	-
3	HFUC-2UH-17-100	54	39	7300	-
4	CPU-M-14A-100	28	11	8500	-
5	HFUC-2A-R-11-100	11	8.9	8500	-
6	HFUC-2A-R-11-100	11	8.9	8500	-
7	HFUC-2A-R-8-100	4.8	3.3	8500	-

¹ limit for repeated peak torque

² limit for average torque

³ maximum input speed

A.2 Specifications of Motors and Encoders

Table A.2: Specification of motors and encoders

Joint	Motor				Encoder		Power amplifier
#	Type	M_H^1 [Nm]	M_c^2 [Nm]	v_{max}^3 [rpm]	Type	I^4	Type
1	Maxon EC60 167132	11.8	0.747	5370	Scancon	7500	maxon DES70/10
2	Maxon RE40 148877	2.5	0.184	7580	MR-Enc. Typ L	1024	Copley 4122Z
3	Maxon RE35 273754	1.07	0.0977	7530	MR-Enc. Typ L	1024	Copley 4122Z
4	Maxon RE35 273754	1.07	0.0977	7530	MR-Enc. Typ L	1024	Copley 4122Z
5	Maxon RE30 310009	1.02	0.0882	8490	MR-Enc. Typ L	1024	Copley 4212Z
6	Maxon RE30 310009	1.02	0.0882	8490	MR-Enc. Typ L	1024	Copley 4212Z
7	Maxon RE-max29	0.268	0.0285	8660	MR-Enc. Typ ML	1024	Copley 4212Z

¹ stall torque ² maximum continuous torque ³ maximum input speed ⁴ impulses per turn

B Dynamic Device Models

In the following sections the dynamic device models for ViSHARD7, ViSHARD10, and the dual arm telemanipulator are reported. Autolev [63] is hereby used as programming language.

B.1 ViSHaRD7 Right Arm

```
%-----
% Problem:  ViSHaRD7 right
%-----
% Newtonian, bodies, frames, points
NEWTONIAN      N
BODIES         B1, B2, B3, B4, B5, B6, B7, BEE
FRAMES         B4H, B5H, B6H, B6HH, BEEH
POINTS         0, S0, S1, S2, S3, S4, S5, S6, S7, SKMS, &
               SEE, STCP  %origins
FRAMES         TCP  %tool center point (HSI rotates around this point)
FRAMES         KMS  %coordinate system attached to middle of FT-sensor

%-----
% Link lengths [m] (lengths from joint to joint)
CONSTANTS L_OX = 0.0    %distance from N to S0
CONSTANTS L_OY = 0.0
%z-direction is generalized coordinate (linear motion)

CONSTANTS L_B1X = 0.0    %distance from S0 to S1 in x-direction ...
CONSTANTS L_B1Y = 0.0
CONSTANTS L_B1Z = 0.0

CONSTANTS L_B2X = 0.350
CONSTANTS L_B2Y = 0.0
CONSTANTS L_B2Z = 0.001

CONSTANTS L_B3X = 0.350
CONSTANTS L_B3Y = 0.0
CONSTANTS L_B3Z = 0.0053

CONSTANTS L_B4X = 0.2025
CONSTANTS L_B4Y = 0.0
CONSTANTS L_B4Z = 0.2828
```

```
CONSTANTS L_B5X = 0.106
CONSTANTS L_B5Y = 0.0
CONSTANTS L_B5Z = -0.2025
```

```
CONSTANTS L_B6X = 0.0654
CONSTANTS L_B6Y = 0.0
CONSTANTS L_B6Z = -0.106
```

```
VARIABLES LEEEX %distance between middle of FT-sensor and
              %EE coordinate system
```

```
VARIABLES LEEY
```

```
VARIABLES LEEZ
```

```
VARIABLES LTCPX %distance between middle of FT-sensor and
              %TCP coordinate system
```

```
VARIABLES LTCPY
```

```
VARIABLES LTCPZ
```

```
%-----
```

```
% Lengths from joint to center of mass of link
```

```
CONSTANTS Off_B1X = -0.04018
```

```
CONSTANTS Off_B1Y = -0.05622
```

```
CONSTANTS Off_B1Z = -0.05499
```

```
CONSTANTS Off_B2X = 0.15264
```

```
CONSTANTS Off_B2Y = 0.01116
```

```
CONSTANTS Off_B2Z = -0.05121
```

```
CONSTANTS Off_B3X = 0.24082
```

```
CONSTANTS Off_B3Y = 0.01094
```

```
CONSTANTS Off_B3Z = -0.04732
```

```
CONSTANTS Off_B4X = 0.20749
```

```
CONSTANTS Off_B4Y = 0
```

```
CONSTANTS Off_B4Z = 0.16518
```

```
CONSTANTS Off_B5X = 0.12819
```

```
CONSTANTS Off_B5Y = 0
```

```
CONSTANTS Off_B5Z = -0.12391
```

```
CONSTANTS Off_B6X = 0.11016
```

```
CONSTANTS Off_B6Y = 0
```

```
CONSTANTS Off_B6Z = -0.07183
```

```
CONSTANTS Off_B7X = -0.0061372
```

```
CONSTANTS Off_B7Y = 0
```

```
CONSTANTS Off_B7Z = 0
```

```
VARIABLES Off_BEEEX
VARIABLES Off_BEEY
VARIABLES Off_BEEZ
```

```
%-----
% Inertia of wavegenerator and motor [kg * m^2]
CONSTANTS J_Ballscrew = 0.0000291 %incl. coupling
CONSTANTS Ballscrew_Radius = 0.01/(2*PI) %[m]
```

```
CONSTANTS J_Wave_HD20 = 0.0000193
CONSTANTS HD20_Ratio = 120
```

```
CONSTANTS J_Wave_HD17 = 0.0000079
CONSTANTS HD17_Ratio = 100
```

```
CONSTANTS J_Wave_HD14 = 0.0000033
CONSTANTS HD14_Ratio = 100
```

```
CONSTANTS J_Wave_HD11 = 0.0000012
CONSTANTS HD11_Ratio = 100
```

```
CONSTANTS J_Wave_HD8 = 0.0000003
CONSTANTS HD8_Ratio = 100
```

```
CONSTANTS J_Rotor_EC60 = 0.0000831
CONSTANTS J_Rotor_RE40 = 0.0000134
CONSTANTS J_Rotor_RE35 = 0.00000696
CONSTANTS J_Rotor_RE30 = 0.00000345
CONSTANTS J_Rotor_REMAX29 = 0.00000119
```

```
%-----
% Link inertia [kg * m^2]
CONSTANTS IB1_11 = 0.00461350154
CONSTANTS IB1_22 = 0.00439990124
CONSTANTS IB1_33 = 0.00271007630
CONSTANTS IB1_12 = 0.00062578871
CONSTANTS IB1_23 = -0.00005991654
CONSTANTS IB1_31 = -0.00013915799
```

```
CONSTANTS IB2_11 = 0.00859838026
CONSTANTS IB2_22 = 0.11011053644
CONSTANTS IB2_33 = 0.10861197902
CONSTANTS IB2_12 = 0.00118366636
CONSTANTS IB2_23 = -0.00053676727
CONSTANTS IB2_31 = 0.00030491157
```

```
CONSTANTS IB3_11 = 0.00459554931
CONSTANTS IB3_22 = 0.04630447801
CONSTANTS IB3_33 = 0.04545162467
CONSTANTS IB3_12 = -0.00346086212
CONSTANTS IB3_23 = -0.00014907434
CONSTANTS IB3_31 = -0.00144417918
```

```
CONSTANTS IB4_11 = 0.02408388538
CONSTANTS IB4_22 = 0.03793209591
CONSTANTS IB4_33 = 0.01480841047
CONSTANTS IB4_12 = 0
CONSTANTS IB4_23 = 0
CONSTANTS IB4_31 = -0.01170709664
```

```
CONSTANTS IB5_11 = 0.00984346200
CONSTANTS IB5_22 = 0.01249259708
CONSTANTS IB5_33 = 0.00304319425
CONSTANTS IB5_12 = 0
CONSTANTS IB5_23 = 0
CONSTANTS IB5_31 = 0.00348378980
```

```
CONSTANTS IB6_11 = 0.00156323252
CONSTANTS IB6_22 = 0.00295963420
CONSTANTS IB6_33 = 0.00166375930
CONSTANTS IB6_12 = 0
CONSTANTS IB6_23 = 0
CONSTANTS IB6_31 = 0.00095308184
```

```
CONSTANTS IB7_11= 0.00010884
CONSTANTS IB7_22= 0.00008217
CONSTANTS IB7_33= 0.00008217
CONSTANTS IB7_12= 0
CONSTANTS IB7_23= 0
CONSTANTS IB7_31= 0
```

```
VARIABLES IBEE_11
VARIABLES IBEE_22
VARIABLES IBEE_33
VARIABLES IBEE_12
VARIABLES IBEE_23
VARIABLES IBEE_31
```

```
% Syntax: I11, I22, I33, I12, I23, I31
```

```
INERTIA      B1,  IB1_11, IB1_22, IB1_33, IB1_12, IB1_23, IB1_31
INERTIA      B2,  IB2_11, IB2_22, IB2_33, IB2_12, IB2_23, IB2_31
INERTIA      B3,  IB3_11, IB3_22, IB3_33, IB3_12, IB3_23, IB3_31
```



```

INERTIA      B4,  IB4_11, IB4_22, IB4_33, IB4_12, IB4_23, IB4_31
INERTIA      B5,  IB5_11, IB5_22, IB5_33, IB5_12, IB5_23, IB5_31
INERTIA      B6,  IB6_11, IB6_22, IB6_33, IB6_12, IB6_23, IB6_31
INERTIA      B7,  IB7_11, IB7_22, IB7_33, IB7_12, IB7_23, IB7_31
INERTIA      BEE, IBEE_11,IBEE_22,IBEE_33,IBEE_12,IBEE_23,IBEE_31

```

```

%-----

```

```

% Link masses [kg]

```

```

CONSTANTS M_B1 = 1.738

```

```

CONSTANTS M_B2 = 4.185

```

```

CONSTANTS M_B3 = 2.497

```

```

CONSTANTS M_B4 = 1.632

```

```

CONSTANTS M_B5 = 1.154

```

```

CONSTANTS M_B6 = 0.807

```

```

CONSTANTS M_B7 = 0.249  %Mass of last link inkl. FT-sensor mass,
                        %without end-effector mass

```

```

VARIABLES M_EE  %Mass inkl. mass of screws and FT-electronics

```

```

MASS B1=M_B1, B2=M_B2, B3=M_B3, B4=M_B4, B5=M_B5, B6=M_B6, &
      B7=M_B7, BEE=M_EE

```

```

%-----

```

```

% Rotation between the coordinate systems starting at Newtonian frame
% CAUTION: The index of the bodydeclaration (Bi) has an offset of +1
% with respect to the declaration of the origins (Si).

```

```

SIMPROT(N    , B1  , 1, 0)

```

```

SIMPROT(B1   , B2  , 3, Q2)

```

```

SIMPROT(B2   , B3  , 3, Q3)

```

```

SIMPROT(B3   , B4  , 3, Q4)

```

```

SIMPROT(B4   , B4H , 2, PI/2)

```

```

SIMPROT(B4H  , B5  , 3, Q5)

```

```

SIMPROT(B5   , B5H , 2, PI/2)

```

```

SIMPROT(B5H  , B6  , 3, Q6)

```

```

SIMPROT(B6   , B6H , 2, PI/2)

```

```

SIMPROT(B6H  , B6HH, 1, PI)

```

```

SIMPROT(B6HH, B7  , 3, Q7)

```

```

%Sensor COS added

```

```

SIMPROT(B7   , KMS, 1, 0)

```

```

%EE COS

```

```

SIMPROT(B7, BEEH , 2, PI/2)

```

```

SIMPROT(BEEH, BEE , 3, PI)

```

```

%TCP COS
SIMPROT(BEE, TCP, 1, 0)

%-----
% Position vectors (from origin "n-1" to origin "n")
P_O_S0> = L_0x * N1> + L_0y * N2> + Q1 * N3>
%linear motion with Q1
P_S0_S1> = L_B1x * B11> + L_B1y * B12> + L_B1z * B13>
P_S1_S2> = L_B2x * B21> + L_B2y * B22> + L_B2z * B23>
P_S2_S3> = L_B3x * B31> + L_B3y * B32> + L_B3z * B33>
P_S3_S4> = L_B4x * B41> + L_B4y * B42> + L_B4z * B43>
P_S4_S5> = L_B5x * B51> + L_B5y * B52> + L_B5z * B53>
P_S5_S6> = L_B6x * B61> + L_B6y * B62> + L_B6z * B63>
P_S6_S7> = 0 * B71> + 0 * B72> + 0 * B73>
P_S6_SKMS> = 0 * KMS1> + 0 * KMS2> + 0 * KMS3>
P_SKMS_SEE> = LEEEX*KMS1> + LEEY*KMS2> + LEEZ*KMS3>
P_SKMS_STCP> = LTCPX*KMS1> + LTCPY*KMS2> + LTCPZ*KMS3>

%-----
% Position vectors (from origin "n-1" to center of mass of "n")
P_S0_B1o> = Off_B1x * B11> + Off_B1y * B12> + Off_B1z * B13>
P_S1_B2o> = Off_B2x * B21> + Off_B2y * B22> + Off_B2z * B23>
P_S2_B3o> = Off_B3x * B31> + Off_B3y * B32> + Off_B3z * B33>
P_S3_B4o> = Off_B4x * B41> + Off_B4y * B42> + Off_B4z * B43>
P_S4_B5o> = Off_B5x * B51> + Off_B5y * B52> + Off_B5z * B53>
P_S5_B6o> = Off_B6x * B61> + Off_B6y * B62> + Off_B6z * B63>
P_S6_B7o> = Off_B7x * B71> + Off_B7y * B72> + Off_B7z * B73>

% Position vector from point SEE to center of gravity of EE
P_SEE_BEEo> = Off_BEEex*BEE1> + Off_BEEey*BEE2> + Off_BEEez*BEE3>

%-----

```

B.2 ViSHaRD7 Left Arm

```

%-----
% Problem:  ViSHaRD7 left
%-----
% Newtonian, bodies, frames, points
NEWTONIAN      N
BODIES         B1, B2, B3, B4, B5, B6, B7, BEE
FRAMES         B4H, B5H, B6H, B6HH, BEEH
POINTS         0, S0, S1, S2, S3, S4, S5, S6, S7, SKMS, &
               SEE, STCP  %origins
FRAMES         TCP  %tool center point (HSI rotates around this point)
FRAMES         KMS  %coordinate system attached to middle of FT-sensor

%-----
% Link lengths [m] (lengths from joint to joint)
CONSTANTS L_OX = 0.0    %distance from N to S0
CONSTANTS L_OY = 0.0
%z-direction is generalized coordinate (linear motion)

CONSTANTS L_B1X = 0.0    %distance from S0 to S1 in x-direction ...
CONSTANTS L_B1Y = 0.0
CONSTANTS L_B1Z = 0.0

CONSTANTS L_B2X = 0.350
CONSTANTS L_B2Y = 0.0
CONSTANTS L_B2Z = 0.001

CONSTANTS L_B3X = 0.350
CONSTANTS L_B3Y = 0.0
CONSTANTS L_B3Z = 0.0053

CONSTANTS L_B4X = 0.2025
CONSTANTS L_B4Y = 0.0
CONSTANTS L_B4Z = 0.2828

CONSTANTS L_B5X = 0.106
CONSTANTS L_B5Y = 0.0
CONSTANTS L_B5Z = -0.2025

CONSTANTS L_B6X = 0.0654
CONSTANTS L_B6Y = 0.0
CONSTANTS L_B6Z = -0.106

VARIABLES LEEEX  %distance between middle of FT-sensor and
               %EE coordinate system
VARIABLES LEEY

```

VARIABLES LEEZ

VARIABLES LTCPX %distance between middle of FT-sensor and
%TCP coordinate system

VARIABLES LTCPY

VARIABLES LTCPZ

%-----

% Lengths from joint to center of mass of link

CONSTANTS Off_B1X = -0.04018

CONSTANTS Off_B1Y = 0.05622

CONSTANTS Off_B1Z = -0.05499

CONSTANTS Off_B2X = 0.15264

CONSTANTS Off_B2Y = -0.0128

CONSTANTS Off_B2Z = -0.05082

CONSTANTS Off_B3X = 0.23981

CONSTANTS Off_B3Y = -0.01094

CONSTANTS Off_B3Z = -0.04481

CONSTANTS Off_B4X = 0.20749

CONSTANTS Off_B4Y = 0

CONSTANTS Off_B4Z = 0.16518

CONSTANTS Off_B5X = 0.12819

CONSTANTS Off_B5Y = 0

CONSTANTS Off_B5Z = -0.12391

CONSTANTS Off_B6X = 0.11016

CONSTANTS Off_B6Y = 0

CONSTANTS Off_B6Z = -0.07183

CONSTANTS Off_B7X = -0.0061372

CONSTANTS Off_B7Y = 0

CONSTANTS Off_B7Z = 0

VARIABLES Off_BEEZ

VARIABLES Off_BEEY

VARIABLES Off_BEEZ

%-----

% Inertia of wavegenerator and motor [kg * m²]

CONSTANTS J_Ballscrew = 0.0000291 %incl. coupling

CONSTANTS Ballscrew_Radius = 0.01/(2*PI) %[m]

```
CONSTANTS J_Wave_HD20    = 0.0000193
CONSTANTS HD20_Ratio     = 120
```

```
CONSTANTS J_Wave_HD17    = 0.0000079
CONSTANTS HD17_Ratio     = 100
```

```
CONSTANTS J_Wave_HD14    = 0.0000033
CONSTANTS HD14_Ratio     = 100
```

```
CONSTANTS J_Wave_HD11    = 0.0000012
CONSTANTS HD11_Ratio     = 100
```

```
CONSTANTS J_Wave_HD8     = 0.0000003
CONSTANTS HD8_Ratio      = 100
```

```
CONSTANTS J_Rotor_EC60   = 0.0000831
CONSTANTS J_Rotor_RE40   = 0.0000134
CONSTANTS J_Rotor_RE35   = 0.00000696
CONSTANTS J_Rotor_RE30   = 0.00000345
CONSTANTS J_Rotor_REMAX29 = 0.00000119
```

```
%-----
```

```
% Link inertia [kg * m^2]
```

```
CONSTANTS IB1_11 = 0.00461350154
CONSTANTS IB1_22 = 0.00439990124
CONSTANTS IB1_33 = 0.00271007630
CONSTANTS IB1_12 = 0.00062578871
CONSTANTS IB1_23 = -0.00005991654
CONSTANTS IB1_31 = -0.00013915799
```

```
CONSTANTS IB2_11 = 0.00859838026
CONSTANTS IB2_22 = 0.11011054
CONSTANTS IB2_33 = 0.10861198
CONSTANTS IB2_12 = 0.00118367
CONSTANTS IB2_23 = -0.00053677
CONSTANTS IB2_31 = 0.00030491
```

```
CONSTANTS IB3_11 = 0.00459555
CONSTANTS IB3_22 = 0.04630448
CONSTANTS IB3_33 = 0.04545162
CONSTANTS IB3_12 = -0.00346086
CONSTANTS IB3_23 = -0.00014907
CONSTANTS IB3_31 = -0.00144418
```

```
CONSTANTS IB4_11 = 0.02408388538
CONSTANTS IB4_22 = 0.03793209591
```

```
CONSTANTS IB4_33 = 0.01480841047
CONSTANTS IB4_12 = 0
CONSTANTS IB4_23 = 0
CONSTANTS IB4_31 = -0.01170709664
```

```
CONSTANTS IB5_11 = 0.00984346200
CONSTANTS IB5_22 = 0.01249259708
CONSTANTS IB5_33 = 0.00304319425
CONSTANTS IB5_12 = 0
CONSTANTS IB5_23 = 0
CONSTANTS IB5_31 = 0.00348378980
```

```
CONSTANTS IB6_11 = 0.00156323252
CONSTANTS IB6_22 = 0.00295963420
CONSTANTS IB6_33 = 0.00166375930
CONSTANTS IB6_12 = 0
CONSTANTS IB6_23 = 0
CONSTANTS IB6_31 = 0.00095308184
```

```
CONSTANTS IB7_11= 0.00010884
CONSTANTS IB7_22= 0.00008217
CONSTANTS IB7_33= 0.00008217
CONSTANTS IB7_12= 0
CONSTANTS IB7_23= 0
CONSTANTS IB7_31= 0
```

```
VARIABLES IBEE_11
VARIABLES IBEE_22
VARIABLES IBEE_33
VARIABLES IBEE_12
VARIABLES IBEE_23
VARIABLES IBEE_31
```

```
% Syntax: I11, I22, I33, I12, I23, I31
```

```
INERTIA      B1,  IB1_11, IB1_22, IB1_33, IB1_12, IB1_23, IB1_31
INERTIA      B2,  IB2_11, IB2_22, IB2_33, IB2_12, IB2_23, IB2_31
INERTIA      B3,  IB3_11, IB3_22, IB3_33, IB3_12, IB3_23, IB3_31
INERTIA      B4,  IB4_11, IB4_22, IB4_33, IB4_12, IB4_23, IB4_31
INERTIA      B5,  IB5_11, IB5_22, IB5_33, IB5_12, IB5_23, IB5_31
INERTIA      B6,  IB6_11, IB6_22, IB6_33, IB6_12, IB6_23, IB6_31
INERTIA      B7,  IB7_11, IB7_22, IB7_33, IB7_12, IB7_23, IB7_31
INERTIA      BEE, IBEE_11, IBEE_22, IBEE_33, IBEE_12, IBEE_23, IBEE_31
```

```
%-----
```

```
% Link masses [kg]
```

```
CONSTANTS M_B1 = 1.738
CONSTANTS M_B2 = 4.185
```

```

CONSTANTS M_B3 = 2.497
CONSTANTS M_B4 = 1.632
CONSTANTS M_B5 = 1.154
CONSTANTS M_B6 = 0.807
CONSTANTS M_B7 = 0.249    %Mass of last link inkl. FT-sensor mass,
                           %without end-effector mass
VARIABLES M_EE    %Mass inkl. mass of screws and FT-electronics

MASS B1=M_B1, B2=M_B2, B3=M_B3, B4=M_B4, B5=M_B5, B6=M_B6, &
      B7=M_B7, BEE=M_EE

%-----
% Rotation between the coordinate systems starting at Newtonian frame
% CAUTION: The index of the bodydeclaration (Bi) has an offset of +1
% with respect to the declaration of the origins (Si).

SIMPROT(N    , B1    , 1, 0)
SIMPROT(B1   , B2   , 3, Q2)
SIMPROT(B2   , B3   , 3, Q3)
SIMPROT(B3   , B4   , 3, Q4)

SIMPROT(B4   , B4H  , 2, PI/2)
SIMPROT(B4H  , B5   , 3, Q5)

SIMPROT(B5   , B5H  , 2, PI/2)
SIMPROT(B5H  , B6   , 3, Q6)

SIMPROT(B6   , B6H  , 2, PI/2)
SIMPROT(B6H  , B6HH, 1, PI)
SIMPROT(B6HH, B7   , 3, Q7)

% Sensor COS added
SIMPROT(B7   , KMS, 1, 0)

% EE COS
SIMPROT(B7, BEEH , 2, PI/2)
SIMPROT(BEEH, BEE , 3, PI)

% TCP COS
SIMPROT(BEE, TCP, 1, 0)

%-----
% Position vectors (from origin "n-1" to origin "n")
P_O_S0>    = L_Ox * N1>    + L_Oy * N2>    + Q1    * N3>
%linear motion with Q1
P_S0_S1>    = L_B1x * B11>    + L_B1y * B12>    + L_B1z * B13>
P_S1_S2>    = L_B2x * B21>    + L_B2y * B22>    + L_B2z * B23>

```

```

P_S2_S3> = L_B3x * B31> + L_B3y * B32> + L_B3z * B33>
P_S3_S4> = L_B4x * B41> + L_B4y * B42> + L_B4z * B43>
P_S4_S5> = L_B5x * B51> + L_B5y * B52> + L_B5z * B53>
P_S5_S6> = L_B6x * B61> + L_B6y * B62> + L_B6z * B63>
P_S6_S7> = 0 * B71> + 0 * B72> + 0 * B73>
P_S6_SKMS> = 0 * KMS1> + 0 * KMS2> + 0 * KMS3>
P_SKMS_SEE> = LEEEX*KMS1> + LEEY*KMS2> + LEEZ*KMS3>
P_SKMS_STCP> = LTCPX*KMS1> + LTCPY*KMS2> + LTCPZ*KMS3>

```

```
%-----
```

```
% Position vectors (from origin "n-1" to center of mass of "n")
```

```

P_S0_B1o> = Off_B1x * B11> + Off_B1y * B12> + Off_B1z * B13>
P_S1_B2o> = Off_B2x * B21> + Off_B2y * B22> + Off_B2z * B23>
P_S2_B3o> = Off_B3x * B31> + Off_B3y * B32> + Off_B3z * B33>
P_S3_B4o> = Off_B4x * B41> + Off_B4y * B42> + Off_B4z * B43>
P_S4_B5o> = Off_B5x * B51> + Off_B5y * B52> + Off_B5z * B53>
P_S5_B6o> = Off_B6x * B61> + Off_B6y * B62> + Off_B6z * B63>
P_S6_B7o> = Off_B7x * B71> + Off_B7y * B72> + Off_B7z * B73>

```

```
% Position vector from point SEE to center of gravity of EE
```

```
P_SEE_BEEo> = Off_BEEx*BEE1> + Off_BEEy*BEE2> + Off_BEEz*BEE3>
```

```
%-----
```


B.3 ViSHaRD10

```

%-----
% Problem:  ViSHaRD7 left
%-----
% Newtonian, bodies, frames, points
NEWTONIAN      N
BODIES         B1, B2, B3, B4, B5, B6, B7, BEE
FRAMES         B4H, B5H, B6H, B6HH, BEEH
POINTS         0, S0, S1, S2, S3, S4, S5, S6, S7, SKMS, &
               SEE, STCP  %origins
FRAMES         TCP  %tool center point (HSI rotates around this point)
FRAMES         KMS  %coordinate system attached to middle of FT-sensor

%-----
% Link lengths [m] (lengths from joint to joint)
CONSTANTS L_OX = 0.0    %distance from N to S0
CONSTANTS L_OY = 0.0
%z-direction is generalized coordinate (linear motion)

CONSTANTS L_B1X = 0.0    %distance from S0 to S1 in x-direction ...
CONSTANTS L_B1Y = 0.0
CONSTANTS L_B1Z = 0.0

CONSTANTS L_B2X = 0.350
CONSTANTS L_B2Y = 0.0
CONSTANTS L_B2Z = 0.001

CONSTANTS L_B3X = 0.350
CONSTANTS L_B3Y = 0.0
CONSTANTS L_B3Z = 0.0053

CONSTANTS L_B4X = 0.2025
CONSTANTS L_B4Y = 0.0
CONSTANTS L_B4Z = 0.2828

CONSTANTS L_B5X = 0.106
CONSTANTS L_B5Y = 0.0
CONSTANTS L_B5Z = -0.2025

CONSTANTS L_B6X = 0.0654
CONSTANTS L_B6Y = 0.0
CONSTANTS L_B6Z = -0.106

VARIABLES LEEEX  %distance between middle of FT-sensor and
               %EE coordinate system
VARIABLES LEEY

```

VARIABLES LEEZ

VARIABLES LTCPX %distance between middle of FT-sensor and
%TCP coordinate system

VARIABLES LTCPY

VARIABLES LTCPZ

%-----

% Lengths from joint to center of mass of link

CONSTANTS Off_B1X = -0.04018

CONSTANTS Off_B1Y = 0.05622

CONSTANTS Off_B1Z = -0.05499

CONSTANTS Off_B2X = 0.15264

CONSTANTS Off_B2Y = -0.0128

CONSTANTS Off_B2Z = -0.05082

CONSTANTS Off_B3X = 0.23981

CONSTANTS Off_B3Y = -0.01094

CONSTANTS Off_B3Z = -0.04481

CONSTANTS Off_B4X = 0.20749

CONSTANTS Off_B4Y = 0

CONSTANTS Off_B4Z = 0.16518

CONSTANTS Off_B5X = 0.12819

CONSTANTS Off_B5Y = 0

CONSTANTS Off_B5Z = -0.12391

CONSTANTS Off_B6X = 0.11016

CONSTANTS Off_B6Y = 0

CONSTANTS Off_B6Z = -0.07183

CONSTANTS Off_B7X = -0.0061372

CONSTANTS Off_B7Y = 0

CONSTANTS Off_B7Z = 0

VARIABLES Off_BEEZ

VARIABLES Off_BEEY

VARIABLES Off_BEEZ

%-----

% Inertia of wavegenerator and motor [kg * m²]

CONSTANTS J_Ballscrew = 0.0000291 %incl. coupling

CONSTANTS Ballscrew_Radius = 0.01/(2*PI) %[m]

```
CONSTANTS J_Wave_HD20    = 0.0000193
CONSTANTS HD20_Ratio     = 120
```

```
CONSTANTS J_Wave_HD17    = 0.0000079
CONSTANTS HD17_Ratio     = 100
```

```
CONSTANTS J_Wave_HD14    = 0.0000033
CONSTANTS HD14_Ratio     = 100
```

```
CONSTANTS J_Wave_HD11    = 0.0000012
CONSTANTS HD11_Ratio     = 100
```

```
CONSTANTS J_Wave_HD8     = 0.0000003
CONSTANTS HD8_Ratio      = 100
```

```
CONSTANTS J_Rotor_EC60   = 0.0000831
CONSTANTS J_Rotor_RE40   = 0.0000134
CONSTANTS J_Rotor_RE35   = 0.00000696
CONSTANTS J_Rotor_RE30   = 0.00000345
CONSTANTS J_Rotor_REMAX29 = 0.00000119
```

```
%-----
```

```
% Link inertia [kg * m^2]
```

```
CONSTANTS IB1_11 = 0.00461350154
CONSTANTS IB1_22 = 0.00439990124
CONSTANTS IB1_33 = 0.00271007630
CONSTANTS IB1_12 = 0.00062578871
CONSTANTS IB1_23 = -0.00005991654
CONSTANTS IB1_31 = -0.00013915799
```

```
CONSTANTS IB2_11 = 0.00859838026
CONSTANTS IB2_22 = 0.11011054
CONSTANTS IB2_33 = 0.10861198
CONSTANTS IB2_12 = 0.00118367
CONSTANTS IB2_23 = -0.00053677
CONSTANTS IB2_31 = 0.00030491
```

```
CONSTANTS IB3_11 = 0.00459555
CONSTANTS IB3_22 = 0.04630448
CONSTANTS IB3_33 = 0.04545162
CONSTANTS IB3_12 = -0.00346086
CONSTANTS IB3_23 = -0.00014907
CONSTANTS IB3_31 = -0.00144418
```

```
CONSTANTS IB4_11 = 0.02408388538
CONSTANTS IB4_22 = 0.03793209591
```

```
CONSTANTS IB4_33 = 0.01480841047
CONSTANTS IB4_12 = 0
CONSTANTS IB4_23 = 0
CONSTANTS IB4_31 = -0.01170709664
```

```
CONSTANTS IB5_11 = 0.00984346200
CONSTANTS IB5_22 = 0.01249259708
CONSTANTS IB5_33 = 0.00304319425
CONSTANTS IB5_12 = 0
CONSTANTS IB5_23 = 0
CONSTANTS IB5_31 = 0.00348378980
```

```
CONSTANTS IB6_11 = 0.00156323252
CONSTANTS IB6_22 = 0.00295963420
CONSTANTS IB6_33 = 0.00166375930
CONSTANTS IB6_12 = 0
CONSTANTS IB6_23 = 0
CONSTANTS IB6_31 = 0.00095308184
```

```
CONSTANTS IB7_11= 0.00010884
CONSTANTS IB7_22= 0.00008217
CONSTANTS IB7_33= 0.00008217
CONSTANTS IB7_12= 0
CONSTANTS IB7_23= 0
CONSTANTS IB7_31= 0
```

```
VARIABLES IBEE_11
VARIABLES IBEE_22
VARIABLES IBEE_33
VARIABLES IBEE_12
VARIABLES IBEE_23
VARIABLES IBEE_31
```

```
% Syntax: I11, I22, I33, I12, I23, I31
```

```
INERTIA      B1,  IB1_11, IB1_22, IB1_33, IB1_12, IB1_23, IB1_31
INERTIA      B2,  IB2_11, IB2_22, IB2_33, IB2_12, IB2_23, IB2_31
INERTIA      B3,  IB3_11, IB3_22, IB3_33, IB3_12, IB3_23, IB3_31
INERTIA      B4,  IB4_11, IB4_22, IB4_33, IB4_12, IB4_23, IB4_31
INERTIA      B5,  IB5_11, IB5_22, IB5_33, IB5_12, IB5_23, IB5_31
INERTIA      B6,  IB6_11, IB6_22, IB6_33, IB6_12, IB6_23, IB6_31
INERTIA      B7,  IB7_11, IB7_22, IB7_33, IB7_12, IB7_23, IB7_31
INERTIA      BEE, IBEE_11, IBEE_22, IBEE_33, IBEE_12, IBEE_23, IBEE_31
```

```
%-----
```

```
% Link masses [kg]
```

```
CONSTANTS M_B1 = 1.738
CONSTANTS M_B2 = 4.185
```

```

CONSTANTS M_B3 = 2.497
CONSTANTS M_B4 = 1.632
CONSTANTS M_B5 = 1.154
CONSTANTS M_B6 = 0.807
CONSTANTS M_B7 = 0.249    %Mass of last link inkl. FT-sensor mass,
                           %without end-effector mass
VARIABLES M_EE    %Mass inkl. mass of screws and FT-electronics

MASS B1=M_B1, B2=M_B2, B3=M_B3, B4=M_B4, B5=M_B5, B6=M_B6, &
      B7=M_B7, BEE=M_EE

%-----
% Rotation between the coordinate systems starting at Newtonian frame
% CAUTION: The index of the bodydeclaration (Bi) has an offset of +1
% with respect to the declaration of the origins (Si).

SIMPROT(N    , B1  , 1, 0)
SIMPROT(B1   , B2  , 3, Q2)
SIMPROT(B2   , B3  , 3, Q3)
SIMPROT(B3   , B4  , 3, Q4)

SIMPROT(B4   , B4H , 2, PI/2)
SIMPROT(B4H  , B5  , 3, Q5)

SIMPROT(B5   , B5H , 2, PI/2)
SIMPROT(B5H  , B6  , 3, Q6)

SIMPROT(B6   , B6H , 2, PI/2)
SIMPROT(B6H  , B6HH, 1, PI)
SIMPROT(B6HH , B7  , 3, Q7)

% Sensor COS added
SIMPROT(B7   , KMS, 1, 0)

% EE COS
SIMPROT(B7, BEEH , 2, PI/2)
SIMPROT(BEEH, BEE , 3, PI)

% TCP COS
SIMPROT(BEE, TCP, 1, 0)

%-----
% Position vectors (from origin "n-1" to origin "n")
P_O_S0>    = L_Ox * N1>    + L_Oy * N2>    + Q1    * N3>
%linear motion with Q1
P_S0_S1>   = L_B1x * B11>   + L_B1y * B12>   + L_B1z * B13>
P_S1_S2>   = L_B2x * B21>   + L_B2y * B22>   + L_B2z * B23>

```

```

P_S2_S3> = L_B3x * B31> + L_B3y * B32> + L_B3z * B33>
P_S3_S4> = L_B4x * B41> + L_B4y * B42> + L_B4z * B43>
P_S4_S5> = L_B5x * B51> + L_B5y * B52> + L_B5z * B53>
P_S5_S6> = L_B6x * B61> + L_B6y * B62> + L_B6z * B63>
P_S6_S7> = 0 * B71> + 0 * B72> + 0 * B73>
P_S6_SKMS> = 0 * KMS1> + 0 * KMS2> + 0 * KMS3>
P_SKMS_SEE> = LEEEX*KMS1> + LEEY*KMS2> + LEEZ*KMS3>
P_SKMS_STCP> = LTCPX*KMS1> + LTCPY*KMS2> + LTCPZ*KMS3>

```

```
%-----
```

```
% Position vectors (from origin "n-1" to center of mass of "n")
```

```

P_S0_B1o> = Off_B1x * B11> + Off_B1y * B12> + Off_B1z * B13>
P_S1_B2o> = Off_B2x * B21> + Off_B2y * B22> + Off_B2z * B23>
P_S2_B3o> = Off_B3x * B31> + Off_B3y * B32> + Off_B3z * B33>
P_S3_B4o> = Off_B4x * B41> + Off_B4y * B42> + Off_B4z * B43>
P_S4_B5o> = Off_B5x * B51> + Off_B5y * B52> + Off_B5z * B53>
P_S5_B6o> = Off_B6x * B61> + Off_B6y * B62> + Off_B6z * B63>
P_S6_B7o> = Off_B7x * B71> + Off_B7y * B72> + Off_B7z * B73>

```

```
% Position vector from point SEE to center of gravity of EE
```

```
P_SEE_BEEo> = Off_BEEx*BEE1> + Off_BEEy*BEE2> + Off_BEEz*BEE3>
```

```
%-----
```

B.4 Dual Arm Telemanipulator

```

%-----
% Problem: Dual arm telemanipulator
%-----
% Newtonian, bodies, frames, points
NEWTONIAN      N
BODIES         B1, B2, B3, B4, B5, B6, B7, BEE
POINTS         0, S0, S1, S2, S3, S4, S5, S6, S7, SKMS, &
               SEE, STCP  %=origins
FRAMES         TMP      %temporary frame,
FRAMES TCP     %tool center point (EE-frames of HSI and TOP are
               %aligned when the devices are in their starting
               %positions)
FRAMES KMS     %coordinate system attached to middle of FT-sensor

%-----
% Gear ratios
CONSTANTS GR1=160, GR2=160, GR3=160, GR4=160, GR5=100, GR6=100, &
GR7=100

%-----
% Link lengths [m] (lengths from joint to joint)
CONSTANTS L1=0.2325  %distance from N to S0
CONSTANTS L2=0.103  %distance from S0 to S1 in x-direction ...
CONSTANTS L3=0.209
CONSTANTS L4=0.103
CONSTANTS L5=0.209
CONSTANTS L6=0.065+0.1695

VARIABLES LEEEX  %distance between middle of FT-sensor and
               %EE coordinate system
CONSTANTS LEEY
CONSTANTS LEEZ

VARIABLES LTCPX %distance between middle of FT-sensor and
               %TCP coordinate system
CONSTANTS LTCPY
CONSTANTS LTCPZ

%-----
% Lengths from joint to center of mass of link
CONSTANTS Off_B1X = 0
CONSTANTS Off_B1Y = 0.00023010
CONSTANTS Off_B1Z = 0.21362435

CONSTANTS Off_B2X = 0.05767568

```

CONSTANTS Off_B2Y = 0.03592568
CONSTANTS Off_B2Z = 0.00050000

CONSTANTS Off_B3X = 0.12636277
CONSTANTS Off_B3Y = 0.00021867
CONSTANTS Off_B3Z = -0.00004087

CONSTANTS Off_B4X = 0.05790828
CONSTANTS Off_B4Y = 0.03590828
CONSTANTS Off_B4Z = 0

CONSTANTS Off_B5X = 0.12642271
CONSTANTS Off_B5Y = -0.00334474
CONSTANTS Off_B5Z = 0

CONSTANTS Off_B6X = 0.03263961
CONSTANTS Off_B6Y = 0.03540350
CONSTANTS Off_B6Z = 0

CONSTANTS Off_B7X = -0.08510251
CONSTANTS Off_B7Y = 0
CONSTANTS Off_B7Z = 0

CONSTANTS Off_BEEY
CONSTANTS Off_BEEZ

%-----
% Inertia of wavegenerator and motor [kg * m²]
CONSTANTS Jwave25=0.413e-4, Jwave20=0.193e-4, Jwave17=0.079e-4
CONSTANTS Jmot=0.0000134

%-----
% Link inertia [kg * m²]
CONSTANTS IB1_11 = 0.00525519
CONSTANTS IB1_22 = 0.00408890
CONSTANTS IB1_33 = 0.00341754 + (Jmot+Jwave25)*GR1²
CONSTANTS IB1_12 = 0
CONSTANTS IB1_23 = -0.00001397
CONSTANTS IB1_31 = 0

CONSTANTS IB2_11 = 0.00074811
CONSTANTS IB2_22 = 0.00155721 + (Jmot+Jwave20)*GR2²
CONSTANTS IB2_33 = 0.00172566
CONSTANTS IB2_12 = 0.00043074
CONSTANTS IB2_23 = 0
CONSTANTS IB2_31 = 0


```

CONSTANTS IB3_11 = 0.00484618 + (Jmot+Jwave20)*GR3^2
CONSTANTS IB3_22 = 0.02985632
CONSTANTS IB3_33 = 0.03101847
CONSTANTS IB3_12 = -0.00008079
CONSTANTS IB3_23 = 0.00000302
CONSTANTS IB3_31 = 0.00001456

```

```

CONSTANTS IB4_11 = 0.00070685
CONSTANTS IB4_22 = 0.00145263 + (Jmot+Jwave20)*GR4^2
CONSTANTS IB4_33 = 0.00160267
CONSTANTS IB4_12 = 0.00040082
CONSTANTS IB4_23 = 0
CONSTANTS IB4_31 = 0

```

```

CONSTANTS IB5_11 = 0.00308813 + (Jmot+Jwave17)*GR5^2
CONSTANTS IB5_22 = 0.02019369
CONSTANTS IB5_33 = 0.02142974
CONSTANTS IB5_12 = 0.00084897
CONSTANTS IB5_23 = 0
CONSTANTS IB5_31 = 0

```

```

CONSTANTS IB6_11 = 0.00017641
CONSTANTS IB6_22 = 0.00020389 + (Jmot+Jwave17)*GR6^2
CONSTANTS IB6_33 = 0.00030587
CONSTANTS IB6_12 = 0.00008539
CONSTANTS IB6_23 = 0
CONSTANTS IB6_31 = 0

```

```

CONSTANTS IB7_11 = 0.00129910 + (Jmot+Jwave17)*GR7^2
CONSTANTS IB7_22 = 0.00751257
CONSTANTS IB7_33 = 0.00751257
CONSTANTS IB7_12 = 0
CONSTANTS IB7_23 = 0
CONSTANTS IB7_31 = 0

```

```

CONSTANTS IBEE_11
CONSTANTS IBEE_22
CONSTANTS IBEE_33
CONSTANTS IBEE_12
CONSTANTS IBEE_23
CONSTANTS IBEE_31

```

```
% Syntax: I11, I22, I33, I12, I23, I31
```

```

INERTIA      B1,  IB1_11, IB1_22, IB1_33, IB1_12, IB1_23, IB1_31
INERTIA      B2,  IB2_11, IB2_22, IB2_33, IB2_12, IB2_23, IB2_31
INERTIA      B3,  IB3_11, IB3_22, IB3_33, IB3_12, IB3_23, IB3_31

```

```

INERTIA      B4,  IB4_11, IB4_22, IB4_33, IB4_12, IB4_23, IB4_31
INERTIA      B5,  IB5_11, IB5_22, IB5_33, IB5_12, IB5_23, IB5_31
INERTIA      B6,  IB6_11, IB6_22, IB6_33, IB6_12, IB6_23, IB6_31
INERTIA      B7,  IB7_11, IB7_22, IB7_33, IB7_12, IB7_23, IB7_31
INERTIA      BEE, IBEE_11,IBEE_22,IBEE_33,IBEE_12,IBEE_23,IBEE_31

```

```

%-----

```

```

% Link masses [kg]

```

```

CONSTANTS M_B1 =2.56318979

```

```

CONSTANTS M_B2 =0.741

```

```

CONSTANTS M_B3 =4.3437

```

```

CONSTANTS M_B4 =0.718

```

```

CONSTANTS M_B5 =6.65078

```

```

CONSTANTS M_B6 =3.19

```

```

CONSTANTS M_B7 =2.187 %Mass of last link inkl. FT-sensor mass,
                    %without end-effector mass

```

```

CONSTANTS M_EE      %Mass inkl. mass of screws and FT-electronics

```

```

MASS B1=M_B1, B2=M_B2, B3=M_B3, B4=M_B4, B5=M_B5, B6=M_B6, &
     B7=M_B7, BEE=M_EE

```

```

%-----

```

```

% Rotation between the coordinate systems starting at Newtonian frame
% CAUTION: The index of the bodydeclaration (Bi) has an offset of +1
% with respect to the declaration of the origins (Si).

```

```

SIMPROT(N,B1,3,Q1)

```

```

SIMPROT(B1,B2,-2,(Q2-pi/2))

```

```

SIMPROT(B2,B3,1,Q3)

```

```

SIMPROT(B3,B4,-2,Q4)

```

```

SIMPROT(B4,B5,1,Q5)

```

```

SIMPROT(B5,B6,2,Q6)

```

```

SIMPROT(B6,B7,1,Q7)

```

```

% Sensor COS added

```

```

SIMPROT(B7, KMS, 1, 0)

```

```

% Rotation of TCP, such that HSI and TOP end-effector coordinate
% systems are aligned when the robots are in their working position

```

```

SIMPROT(KMS,TMP,1,pi)

```

```

SIMPROT(TMP,TCP,2,pi/2)

```

```

% EE COS

```

```

SIMPROT(KMS, BEE, 1, 0)

```

```

%-----

```

```

% Position vectors (from origin "n-1" to origin "n")
P_0_S0>    = 0>
%P_S0_S1>  = L1 * B13> % Right Arm
P_0_S1>    = -L1*B13> % Left Arm
P_S1_S2>    = L2 * B21>
P_S2_S3>    = L3 * B31>
P_S3_S4>    = L4 * B41>
P_S4_S5>    = L5 * B51>
P_S5_S6>    = L6 * B61>
P_S6_SKMS>  = 0*KMS1> + 0*KMS2> + 0*KMS3>
P_SKMS_SEE> = LEEEX*KMS1> + LEEY*KMS2> + LEEZ*KMS3>
P_SKMS_STCP> = LTCPX*KMS1> + LTCPY*KMS2> + LTCPZ*KMS3>

%-----
% Position vectors (from origin "n-1" to center of mass of "n")
P_S0_B1o>  = Off_B1x * B11> + Off_B1y * B12> + Off_B1z * B13>
P_S1_B2o>  = Off_B2x * B21> + Off_B2y * B22> + Off_B2z * B23>
P_S2_B3o>  = Off_B3x * B31> + Off_B3y * B32> + Off_B3z * B33>
P_S3_B4o>  = Off_B4x * B41> + Off_B4y * B42> + Off_B4z * B43>
P_S4_B5o>  = Off_B5x * B51> + Off_B5y * B52> + Off_B5z * B53>
P_S5_B6o>  = Off_B6x * B61> + Off_B6y * B62> + Off_B6z * B63>
P_S6_B7o>  = Off_B7x * B71> + Off_B7y * B72> + Off_B7z * B73>

% Positions vector from point SEE to COG of the EE
P_SEE_BEEo> = Off_BEEex*BEE1> + Off_BEEey*BEE2> + Off_BEEez*BEE3>

%-----

```

C Parameters of Simulation Models

C.1 Haptic Interface ViSHaRD7

Table C.1: Rigid model

parameter	value
m_m	13 kg
b_m	20 Ns/m
m_{em}	0.334 kg
T_f	0.0015 s
T_a	0.003 s
K_{xm}	250
D_{xm}	13,000
K_{xs}	250
D_{xs}	13,000

Table C.2: Compliant model

parameter	value
m_{m1}	6.5 kg
m_{m2}	6.5 kg
b_{m1}	20 Ns/m
b_{m2}	30 Ns/m
c_m	3,0000 N/m
m_{em}	0.334 kg
T_f	0.0015 s
T_a	0.003 s
K_{xm}	250
D_{xm}	13,000
K_{xs}	250
D_{xs}	13,000

C.2 Linear one DOF Teleoperation System

Table C.3: Parameters of linear one DOF teleoperation system

parameter	value
m_m	2.386 kg
b_m	20 Ns/m
m_{em}	0.112 kg
m_s	2.386 kg
b_s	20 Ns/m
m_{es}	0.112 kg
T_f	0.0032 s
T_a	0.00065 s
K_{xm}	132
D_{xm}	530
K_{xs}	132
D_{xs}	530

C.3 Teleoperation System Vishard10 - Dual Arm Telemanipulator

Table C.4: Parameters of teleoperation system formed by ViSHARD10 and dual arm telemanipulator

parameter	value
m_m	23 kg
b_m	20 Ns/m
m_{em}	0.334 kg
m_s	13.5 kg
b_s	20 Ns/m
m_{es}	1.9 kg
T_a	0.0003 s
K_{xm}	250
D_{xm}	23,000
K_{xs}	250
D_{xs}	13,500

C.4 Human Operator Model

Table C.5: Human operator model

parameter	value
b_h	6 Ns/m
m_h	5 kg
c_h	40 N/m

D Descriptive Statistics and Results of the Analysis of Variance

In the following sections the descriptive statistics and the results of the analysis of variance of the experimental evaluation, presented in chapter 5, are reported.

D.1 Descriptive Statistics

D.1.1 Efficiency Measures

Table D.1: Means of efficiency measures for each independent variable

factor	level	efficiency measures				
		mean force [N]	max force [N]	distance [m]	time [s]	quality rating
task phase	1	2.19	9.63	0.84	53.36	7.7
	2	2.19	8.21	0.62	44.83	
number of freed DOF during exp. phase	3	2.73	9.63	0.75	45.25	7.67
	4	2.19	8.57	0.71	49.53	7.83
	6	1.93	8.48	0.73	52.52	7.60
repetition	1	2.20	8.84	0.77	55.34	7.41
	2	2.38	9.00	0.69	42.85	8.00
hand	right	2.34	9.15	0.96	49.1	7.70
	left	2.23	8.68	0.50		
number of freed DOF during training	3	2.71	9.54	0.74	50.54	7.88
	4	2.09	8.76	0.73	49.29	7.19
	6	2.07	8.46	0.71	47.46	8.04
visual feedback	proj. wall	2.75	10.30	0.83	50.16	7.09
	HMD	1.83	7.53	0.63	48.04	8.32

D.1.2 Rotation Measures

Table D.2: Means of rotation measures for each independent variable

factor	level	rotation measures			
		mean torque [Nm]	max torque [Nm]	angle [rad]	axis [rad]
task phase	1	0.46	1.36	0.11	0.02
	2	0.47	1.16	0.16	0.05
number of freed DOF during exp. phase	3	0.56	1.3	0.01	0.00
	4	0.58	1.53	0.18	0.04
	6	0.26	0.95	0.22	0.05
repetition	1	0.46	1.28	0.14	0.03
	2	0.47	1.24	0.13	0.03
hand	right	0.62	1.62	0.18	0.05
	left	0.32	0.89	0.08	0.02
number of freed DOF during training	3	0.48	1.16	0.12	0.02
	4	0.47	1.32	0.14	0.03
	6	0.45	1.30	0.15	0.04
visual feedback	projection wall HMD	0.44 0.49	1.34 1.18	0.15 0.12	0.04 0.03

D.1.3 Telepresence Measures

Table D.3: Means of telepresence measures for each independent variable

factor	level	transparency measures		
		rating 1	rating 2	rating 3
task phase	1	4.39	4.36	4.93
	2			
number of freed DOF during exp. phase	3	3.85	3.93	4.60
	4	4.54	4.53	5.1
	6	4.78	4.61	5.1
repetition	1	4.25	4.19	4.89
	2	4.53	4.52	4.97
hand	right	4.39	4.36	4.93
	left			
number of freed DOF during training	3	5.06	4.64	5.39
	4	4.36	4.56	5.44
	6	3.75	3.88	3.96
visual feedback	projection wall HMD	4.49 4.29	4.50 4.21	5.11 4.75

D.2 Results of the Analysis of Variance

D.2.1 Factor freed DOF during Experimental Session

Table D.4: Main effects of the factor freed DOF during the experimental session (3, 4 vs. 6)

<i>factor</i>		<i>source</i>	<i>df</i>	<i>F</i>	η^2	<i>p</i>
within subjects						
number of freed DOF during exp. session	task performance measures	mean force	2.2	10.01*	0.500	0.001
		max force	2.2	3.29	0.248	0.058
		distance	2.2	0.14	0.013	0.875
		time	2.2	0.79	0.073	0.467
		quality rating	2.2	0.58	0.055	0.568
	rotation measures	mean torque	2.2	45.00*	0.818	<0.000
		max torque	2.2	28.26*	0.739	<0.000
		angle	2.2	117.39*	0.921	<0.000
		axis	2.2	43.52*	0.813	<0.000
	telepresence measures	rating 1	2.2	3.90*	0.281	0.037
		rating 2	2.2	2.00	0.167	0.161
		rating 3	2.2	3.65*	0.267	0.045
	strategy	strategy	2.2	18.46*	0.649	0.001

*significant ($\alpha=5\%$)

D.2.2 Factor Visual Feedback

Table D.5: Main effects of the factor visual feedback (projection wall vs. HMD)

<i>factor</i>		<i>source</i>	<i>df</i>	<i>F</i>	η^2	<i>p</i>
between subjects						
visual feedback	task performance measures	mean force	1.1	5.86*	0.37	0.036
		max force	1.1	9.3*	0.482	0.012
		distance	1.1	10.89*	0.521	0.008
		time	1.1	0.07	0.007	0.795
		quality rating	1.1	7.56*	0.430	0.021
	rotation measures	mean torque	1.1	1.86	0.156	0.203
		max torque	1.1	2.89	0.224	0.120
		angle	1.1	2.27	0.185	0.163
		axis	1.1	1.00	0.091	0.342
	telepresence measures	rating 1	1.1	0.20*	0.020	0.065
		rating 2	1.1	0.57	0.054	0.467
		rating 3	1.1	0.42	0.040	0.531
	strategy	strategy	1.1	4.82	0.325	0.053

*significant ($\alpha=5\%$)

D.2.3 Factor Task Phase

Table D.6: Main effects of the factor task phase (phase 1 vs. phase 2)

<i>factor</i>		<i>source</i>	<i>df</i>	<i>F</i>	η^2	<i>p</i>
			within subjects			
task phase	task performance measures	mean force	1.1	0.94	0.086	0.356
		max force	1.1	8.37*	0.456	0.016
		distance	1.1	9.93*	0.498	0.010
		time	1.1	1.32	0.116	0.278
	rotation measures	mean torque	1.1	0.22	0.021	0.650
		max torque	1.1	11.74*	0.540	0.006
		angle	1.1	2.49	0.199	0.146
		axis	1.1	11.92*	0.544	0.006
	strategy	strategy	1.1	1.54	0.133	0.244

*significant ($\alpha=5\%$)

D.2.4 Factor Hand

Table D.7: Main effects of the factor hand (left vs. right)

<i>factor</i>		<i>source</i>	<i>df</i>	<i>F</i>	η^2	<i>p</i>
			within subjects			
hand	task performance measures	mean force	1.1	0.10	0.010	0.757
		max force	1.1	1.27	0.286	0.113
		distance	1.1	257.43*	0.963	<0.000
	rotation measures	mean torque	1.1	39.46*	0.798	<0.000
		max torque	1.1	80.30*	0.889	<0.000
		angle	1.1	21.49*	0.682	0.001
		axis	1.1	14.13*	0.586	0.004

*significant ($\alpha=5\%$)

D.2.5 Factor Number of Freed DOF during Training

Table D.8: Main effects of the factor number of freed DOF during training (3, 4 vs. 6)

<i>factor</i>	<i>source</i>	<i>df</i>	<i>F</i>	η^2	<i>p</i>	
between subjects						
number of freed DOF during training	task performance measures	mean force	2.1	1.33	0.210	0.308
		max force	2.1	0.52	0.094	0.610
		distance	2.1	0.07	0.014	0.933
		time	2.1	0.05	0.009	0.954
		quality rating	2.1	1.42	0.221	0.287
	rotation measures	mean torque	2.1	0.17	0.033	0.846
		max torque	2.1	1.31	0.208	0.312
		angle	2.1	1.07	0.176	0.380
		axis	2.1	1.58	0.240	0.253
	telepresence measures	rating 1	2.1	2.62	0.344	0.122
		rating 2	2.1	1.43	0.222	0.285
		rating 3	2.1	2.68	0.349	0.117
	strategy	strategy	2.1	0.08	0.015	0.927

*significant ($\alpha=5\%$)

D.2.6 Factor Repetition

Table D.9: Main effects of the factor repetition (2 levels)

<i>factor</i>	<i>source</i>	<i>df</i>	<i>F</i>	η^2	<i>p</i>	
within subjects						
repetition	task performance measures	mean force	1.1	2.36	0.191	0.156
		max force	1.1	0.12	0.012	0.735
		distance	1.1	3.28	0.247	0.100
		time	1.1	10.61*	0.515	0.009
		quality rating	1.1	12.89*	0.563	0.005
	rotation measures	mean torque	1.1	1.36	0.119	0.271
		max torque	1.1	0.47	0.045	0.507
		angle	1.1	0.43	0.041	0.526
		axis	1.1	0.36	0.035	0.561
	telepresence measures	rating 1	1.1	1.06	0.096	0.327
		rating 2	1.1	1.69	0.144	0.223
		rating 3	1.1	0.21	0.020	0.659
	strategy	strategy	1.1	0.88	0.081	0.371

*significant ($\alpha=5\%$)

E Presence and Immersive Tendency Questionnaire

Fragebogen zur Präsenz und immersiven Tendenz

VpNr. _____

Fragebogen zur Person

Die folgenden Antworten werden vertraulich behandelt und anonym ausgewertet.

Alter: _____

Geschlecht: _____

Händigkeit: _____

Wie viel Erfahrung haben Sie mit virtuellen Realitäten? (Bitte ankreuzen.)

<i>keine</i>	<i>wenig</i>	<i>mittel</i>	<i>viel</i>	<i>sehr viel</i>
--------------	--------------	---------------	-------------	------------------

Wie viele Stunden pro Monat verbringen Sie mit Computerspielen mit 3D-Graphik? _____

Fragebogen zur Präsenz und immersiven Tendenz

VpNr.

**Fragebogen zu Präsenz und
Immersiven Tendenz in virtuellen Realitäten**

Die folgenden Fragen erkundigen sich nach der Qualität Ihres Erlebnisses einer virtuellen Realität. Abhängig von der Technik, die zur Darstellung und Steuerung der virtuellen Umgebung benutzt wird sowie anderen Faktoren, erleben verschiedene Personen virtuelle Umgebungen als unterschiedlich realistisch. Dieser Fragebogen misst den Einfluss verschiedener Faktoren auf Ihr Erleben der virtuellen Umgebung.

Bitte denken Sie bei der Beantwortung der Fragen an alle Aufgaben, die Sie während des gesamten Experiments durchlaufen haben.

Immersive Tendenz
2/4

Mit den folgenden Fragen soll ermittelt werden, wie stark Sie sich im Allgemeinen in Ereignisse hineinversetzen (*immersive tendency*).

1. Lassen Sie sich leicht tief in Spiel- oder Fernsehfilme hineinziehen?

1	2	3	4	5	6	7
Nein			weder noch			Ja

2. Sind Sie manchmal so sehr in eine Fernsehsendung oder in ein Buch vertieft, dass andere Menschen nur schwer Ihre Aufmerksamkeit auf sich ziehen können?

1	2	3	4	5	6	7
nie			weder noch			sehr oft

3. Wie oft identifizieren Sie sich stark mit den Charakteren einer Geschichte?

1	2	3	4	5	6	7
nie			weder noch			sehr oft

4. Fühlten Sie sich jemals so sehr in ein Computerspiel verwickelt, dass Sie eher das Gefühl hatten, Sie seien Teil des Spiels, als dass Sie nur einen Joystick bewegen und einen Bildschirm beobachten?

1	2	3	4	5	6	7
Nein, nie			weder noch			Ja, sehr oft

5. Wenn sie sich Sportübertragungen ansehen: Sind Sie bisweilen so sehr in ein Spiel vertieft, dass Sie wie einer der Spieler handeln?

1	2	3	4	5	6	7
Nein, nie			weder noch			Ja, sehr oft

Fragebogen zur Präsenz und immersiven Tendenz

VpNr. _____

6. Werden Sie manchmal so sehr in einen Tagtraum hineingezogen, dass Sie sich der Dinge um Sie herum nicht mehr bewusst sind?

1	2	3	4	5	6	7
Nein, nie			weder noch			Ja, sehr oft

7. Haben Sie manchmal Träume, die so real sind, dass Sie sich beim Erwachen desorientiert fühlen?

1	2	3	4	5	6	7
Nein, nie			weder noch			Ja, sehr oft

8. Hat jemals eine Jagd- oder Kampfszene in Film oder Fernsehen Aufregung bei Ihnen ausgelöst?

1	2	3	4	5	6	7
Nein, nie			weder noch			Ja, sehr oft

9. Hat Sie jemals etwas in einer Fernsehsendung oder in einem Spielfilm geängstigt?

1	2	3	4	5	6	7
Nein, nie			weder noch			Ja, sehr oft

10. Ist es Ihnen jemals passiert, dass Sie nach einem beängstigenden Film lange Zeit besorgt oder verängstigt waren?

1	2	3	4	5	6	7
Nein, nie			weder noch			Ja, sehr oft

11. Sind Sie manchmal so mit einer Sache beschäftigt, dass Sie die Zeit vergessen?

1	2	3	4	5	6	7
Nein, nie			weder noch			Ja, sehr oft

Bibliography

- [1] Barrett Technology Inc . BarrettHand.
<http://www.barrett.com/robot/products-hand.htm>, April 2008.
- [2] Immersion Corp . CyberGrasp Exoskeleton.
http://www.immersion.com/3d/products/cyber_grasp.php, April 2008.
- [3] Immersion Corp . CyberGlove II Wireless Data Glove.
http://www.immersion.com/3d/products/cyber_glove.php, April 2008.
- [4] D. K. E. Aarno. *Intention Recognition in Human Machine Collaborative Systems*. PhD thesis, KTH School of Computer Science and Communication, Stockholm, Sweden, March 2007.
- [5] J. Ackermann. *Robust Control, The Parameter Space Approach*. Springer, London, 2nd edition, 2002.
- [6] R. J. Adams and B. Hannaford. Stable Haptic Interaction with Virtual Environments. *IEEE Trans. on Robotics and Automation*, 14(3):465–474, 1999.
- [7] J. Aleotti and S. Caselli. Grasp Recognition in Virtual Reality for Robot Pregrasp Planning by Demonstration. In *Proc. of IEEE International Conference on Robotics and Automation*, pages 2801–2806, May 15-19, 2006.
- [8] R. Anderson and M. Spong. Bilateral Control of Teleoperators with Time Delay. *IEEE Trans. on Robotics and Automation*, 34(5):494 – 501, 1989.
- [9] J. Artigas, J. Vilanova, C. Preusche, and G. Hirzinger. Time Domain Passivity Control-based Telepresence with Time Delay. In *Proc. of the IEEE/RSJ International Conference on Intelligent Robots and Systems*, Beijing, China, October 2006.
- [10] P. G. Backes. Generalized Compliant Motion with Sensor Fusion. In *Proc. of Fifth International Conference on Advanced Robotics, 'Robots in Unstructured Environments'*, pages 1281–1286, Pisa, Italy, 1991.
- [11] P. G. Backes. Dual-arm Supervisory and Shared Control Task Description and Execution. *Robotics and Autonomous Systems*, 12(1–2):29–54, 1994.
- [12] P. G. Backes and K. S. Tso. UMI: An Interactive Supervisory and Shared Control System for Telerobotics. In *Proc. of the IEEE International Conference on Robotics and Automation*, volume 2, pages 1096–1101, Cincinnati, OH, May 1990.
- [13] H. Baier, F. Freyberger, and G. Schmidt. A High Fidelity Interactive Stereo Vision System and its Application to Teleoperation Tasks. In *Proc. of the Workshop on Advances in Interactive Multimodal Telepresence Systems*, pages 33–42, Munich, Germany, 2001.

- [14] Barrett Technology Inc. *BarrettHand BH8-Series User Manual, Firmware Version 4.3x*, February 2002.
- [15] S. Berman, J. Friedman, and T. Flash. Object-action Abstraction for Teleoperation. In *Proc. of the IEEE International Conference on Systems, Man and Cybernetics*, volume 3, pages 2631–2636, October 2005.
- [16] N. A. Bernstein. *The Coordination and Regulation of Movements*. Pergamon Press, Oxford, 1967.
- [17] R. G. Bonitz and T. C. Hsia. Internal Force-based Impedance Control for Cooperating Manipulators. *IEEE Trans. on Robotics and Automation*, 12(1):78–89, 1995.
- [18] C. Borst, M. Fischer, S. Haidacher, H. Liu, and G. Hirzinger. DLR Hand II: Experiments and Experiences with an Anthropomorphic Hand. In *Proc. of the IEEE International Conference on Robotics and Automation*, Taipei, Taiwan, September 2003.
- [19] G. Burdea. *Force and Touch Feedback for Virtual Reality*. John Wiley & Sons, 1996.
- [20] F. Caccavale and B. Siciliano. Quaternion-based Kinematic Control of Redundant Spacecraft/Manipulator Systems. In *Proc. of the IEEE International Conference on Robotics and Automation*, volume 1, pages 435–440, Seoul, 2001.
- [21] D. G. Caldwell, A. Wardle, O. Kocak, and M. Goodwin. Telepresence Feedback and Input Systems for a Twin Armed Mobile Robot. *IEEE Robotics and Automation Magazine*, 3:29–38, 1996.
- [22] G. Campion and V. Hayward. Fundamental Limits in The Rendering of Virtual Haptic Textures. In *Proc. of the First Joint Eurohaptics Conference and Symposium on Haptic Interfaces for Virtual Environments and Teleoperator Systems*, pages 263–270, 2005.
- [23] M. C. Cavusoglu, W. Williams, F. Tendick, and S. S. Sastry. Robotics for Telesurgery: Second Generation Berkeley/UCSF Laparoscopic Telesurgical Workstation and Looking towards the Future Applications. *Industrial Robot, Special Issue on Medical Robotics*, 30(1):22–29, 2003.
- [24] S. Chang, J. Kim, J. H. Borm, and C. Lee. KIST Teleoperation System for Humanoid Robot. In *Proc. of the IEEE/RSJ International Conference on Intelligent Robots and Systems*, pages 1198–1203, 1999.
- [25] H. C. Cho and J. H. Park. Impedance Controller Design of Internet-Based Teleoperation Using Absolute Stability Concept. In *IEEE/RSJ International Conf. on Intelligent Robots and Systems*, pages 2256–2261, October 2002.
- [26] H. C. Cho and J. H. Park. Impedance Control with Variable Damping for Bilateral Teleoperation under Time Delay. *JSME International Journal*, 48(4):695–703, 2005.
- [27] N. Y. Chong, S. Kawabata, K. Ohba, T. Kotoku, K. Komoriya, K. Takase, and K. Tanie. Multioperator Teleoperation of Multirobot Systems with Time-Delay: Part 2 - Testbed Description. *Presence*, 11(3):292–303, 2002.

-
- [28] N. Chopra, M.W. Spong, S. Hirche, and M. Buss. Bilateral Teleoperation over the Internet: The Time Varying Delay Problem. In *Proc. of the American Control Conference*, pages 155–160, 2003.
- [29] C. L. Clover, G. R. Luecke, J. J. Troy, and W. A. McNeely. Dynamic Simulation of Virtual Mechanisms With Haptic Feedback Using Industrial Robotics Equipment. In *Proc. of the IEEE International Conference on Robotics and Automation*, pages 724–730, 1997.
- [30] E. Colgate and N. Hogan. An Analysis of Contact Instability in Terms of Passive Physical Equivalents. In *Proc. of the IEEE International Conference on Robotics and Automation*, pages 404–409, 1989.
- [31] Shadow Robot Company. Shadow Hand. <http://www.shadowrobot.com/>, April 2008.
- [32] M. R. Cutkosky. On Grasp Choice, Grasp Models, and the Design of Hands for Manufacturing Tasks. *IEEE Trans. on Robotics and Automation*, 5(3):269–279, June 1989.
- [33] R. P. Darken. Spatial Orientation and Wayfinding in Large-Scale Virtual Spaces II. *Presence*, 8(6):3–6, 1999.
- [34] B. Deml. *Telepräsenzsysteme: Gestaltung der Mensch-System-Schnittstelle*. PhD thesis, Universität der Bundeswehr München, 2004.
- [35] F. Dorsch, H. Häcker, and H. K. Stapf. *Dorsch Psychologisches Wörterbuch*. Huber, Bern, 1998.
- [36] C. Droste and M. von Planta. *Memorix, Edition Medizin*. Wiley-VCH, Weinheim, 2nd edition, 1989.
- [37] M. Ehrenmann, R. Zollner, O. Rogalla, and R. Dillmann. Programming Service Tasks in Household Environments by Human Demonstration. In *Proc. of the 11th IEEE International Workshop on Robot and Human Interactive Communication*, pages 460–467, September 2002.
- [38] S. Einenkel. Kalibrierung und Abbildung der menschlichen Hand auf einen dreifingrigen Greifer zur mehrfingrigen Telemanipulation. Master’s thesis, Technische Universität München, 2006, *in german*.
- [39] S. Ekvall and D. Kragic. Interactive Grasp Learning Based on Human Demonstration. In *Proc. of the IEEE International Conference on Robotics and Automation*, volume 4, pages 3519–3524, April, May 2004.
- [40] I. H. Elhaji, A. Goradia, N. Xi, C. M. Kit, Y. H. Liu, and T. Fukuda. Design and Analysis of Internet-based Tele-coordinated Multi-Robot Systems. *Autonomous Robots*, 15:237–254, 2003.
- [41] D. C. Ellson. The Independence of Tracking in Two and Three Dimensions with the B-29 Pedestal Sight. Technical Report TSEAA-694-2G, Aero Medical Laboratory, 1947.

- [42] S. Eppinger and W. Seering. Understanding bandwidth limitations in robot force control. In *Proceedings of the IEEE International Conference on Robotics and Automation*, pages 904–909, 1987.
- [43] M. O. Ernst. A Bayesian View on Multimodal Cue Integration. In G. Knoblich, M. Grosjean, I. Thornton, and M. Shiffrar, editors, *Human Body Perception From The Inside Out*, pages 105–131. Oxford University Press, New York, NY, USA, 2005.
- [44] M. Fischer, P. van der Smagt, and G. Hirzinger. Learning Techniques in a Dataglove Based Telemanipulation System for the DLR Hand. In *Proc. of the IEEE International Conference on Robotics and Automation*, volume 2, pages 1603–1608, May 1998.
- [45] A. Formaglio, A. Giannitrapani, M. Franzini, D. Prattichizzo, and F. Barbagli. Performance of Mobile Haptic Interfaces. In *Proc. of the 44th IEEE European Control Conference on Decision and Control*, pages 8343–8348, December 2005.
- [46] R. Frazer and W. Duncan. On the Criteria for the Stability of Small Motions. In *Proc. of the Royal Society, Series A*, volume 124, pages 642–654, 1929.
- [47] J. F. Gardner. Direction of Pointer Motion in Relation to the Movement of Flight Controls. Technical Report 6016, Air Material Command, Wright-Patterson, AFB, OH, 1950.
- [48] J. Glassmire, M. OMalley, W. Bluethmann, and R. Ambrose. Cooperative Manipulation between Humans and Teleoperated Agents. In *Proc. of the 12th International Symposium on Haptic Interfaces for Virtual Environment and Teleoperator Systems*, pages 114–120, Los Alamitos, CA, USA, 2004. IEEE Computer Society.
- [49] S. Grange, F. Conti, P. Rouiller, P. Helmer, and C. Baur. Overview of the Delta Haptic Device. In *Eurohaptics*, 2001.
- [50] W. B. Griffin. *Shared Control for Dexterous Telemanipulation with Haptic Feedback*. PhD thesis, Stanford University, Palo Alto, USA, June 2003.
- [51] B. Hannaford. A Design Framework for Teleoperators with Kinesthetic Feedback. *IEEE Trans. on Robotics and Automation*, 5(4):426–434, 1989.
- [52] K. Hashtrudi-Zaad and S. E. Salcudean. Analysis of Control Architectures for Teleoperation Systems with Impedance/Admittance Master and Slave Devices. *The International Journal of Robotics Research*, 20(6):419–445, June 2001.
- [53] H. Hasunuma, H.i Kagaya, M. Takatori, J. Fujimori, F. Mifune, S. Shikoda, M. Kobayasi, T. Itoko, and S. Tachi. Development of Teleoperation Master System with a Kinesthetic Sensation of Presence. In *Proc. of the International Conference on Artificial Reality and Telexistence*, Waseda University, December 1999.
- [54] S. Hayati, T. Lee, K. Tso, and P. Backes. A Testbed for a Unified Teleoperated-Autonomous Dual-Arm Robotic System. *IEEE Trans. on Robotics and Automation*, 2:1090–1095, 1990.

-
- [55] V. Hayward and O.R. Astley. Performance measures for haptic interfaces. In *Robotics Research: The 7th International Symposium*, pages 195–207. Springer, 1996.
- [56] R. Held and N. Durlach. Telepresence. *Presence: Teleoperators and Virtual Environments*, 1(1):109–112, 1992.
- [57] S. Hirche, M. Ferre, J. Barrio, C. Melchiorri, and M. Buss. Bilateral Control Architectures for Telerobotics. In M. Ferre, M. Buss, R. Aracil, C. Melchiorri, and C. Balaguer, editors, *Advances in Telerobotics*. Springer STAR series, Berlin, 2007.
- [58] J. M. Hollerbach. Locomotion Interfaces. In K.M. Stanney, editor, *Handbook of Virtual Environments: Design, Implementation, and Applications*, pages 239–254. Lawrence Erlbaum Associates, Inc., 2002.
- [59] J. Hong and X. Tan. Calibrating a VPL DataGlove for Teleoperating the Utah/MIT Hand. In *Proc. of the IEEE International Conference on Robotics and Automation*, volume 3, pages 1752–1757, May 1989.
- [60] K. Hong and J. G. Kim. Manipulability Analysis of a Parallel Machine Tool: Application to Optimal Link Length Design. *Journal of Robotic Systems*, 17(8):403–415, 2000.
- [61] B. E. Insko. Measuring Presence: Subjective, Behavioral and Physiological Methods. In G. Riva, F. Davide, and W. A. IJsselsteijn, editors, *Being There: Concepts, Effects and Measurement of User Presence in Synthetic Environments*. Ios Press, Amsterdam, The Netherlands, 2003.
- [62] S. C. Jacobsen, E. K. Iverson, D. F. Knutti, R. T. Johnson, and K. B. Biggers. Design of the Utah/MIT Dexterous Hand. In *Proc. of the IEEE International Conference on Robotics and Automation*, pages 1520–1532, San Francisco, April 1986.
- [63] T. Kane and D. Levinson. *Autolev User's Manual*. Online Dynamics, Inc., 1605 Honfleur Drive, Sunnyvale, CA 94087, USA, 2001.
- [64] K. Kaneko, F. Kanehiro, S. Kajita, H. Hirukawa, T. Kawasaki, M. Hirata, K. Akachi, and T. Isozumi. Humanoid Robot HRP-2. In *Proc. of the IEEE International Conference on Robotics and Automation*, 2004.
- [65] S. B. Kang and K. Ikeuchi. Toward Automatic Robot Instruction from Perception-Mapping Human Grasps to Manipulator Grasps. *IEEE Trans. on Robotics and Automation*, 13(1):81–95, February 1997.
- [66] F. Keyrouz and K. Diepold. Binaural Source Localization and Spatial Audio Reproduction for Telepresence Applications. *Presence Journal: Teleoperators and Virtual Environments, Special Issue on High Fidelity Telepresence II*, 16:509–522, 2007.
- [67] F. Keyrouz and K. Diepold. A New HRTF Interpolation Approach for Fast Synthesis of Dynamic Environmental Interaction. *Audio Engineering Society (AES) Journal*, 56 (1/2), February 2008.

- [68] B. Khademian and K. Hashtrudi-Zaad. A Four-Channel Multilateral Shared Control Architecture for Dual-User Teleoperation Systems. In *IEEE/RSJ International Conf. on Intelligent Robots and Systems*, pages 2660–2666, 2007.
- [69] O. Khatib, K. Yokoi, K. Chan, R. Ruspini, D. an Holmberg, A. Casal, and A. Baader. Force Strategies for Cooperative Tasks in Multiple Mobile Manipulation Systems. In *International Symposium of Robotics Research*, 1995.
- [70] P. K. Khosla and T. Kanade. Real-Time Implementation of the Computed-Torque Scheme. *IEEE Trans. on Robotics and Automation*, 5(2):245–253, 1989.
- [71] J. Kim, P. Chang, and H. Park. Transparent Teleoperation Using Two-Channel Control Architectures. In *Proc. of the IEEE/RSJ International Conference on Robots and Systems*, pages 2824–2831, 2005.
- [72] K. Kinugawa and H. Noborio. A Shared Autonomy of Multiple Mobile Robots in Teleoperation. In *Proc. of the IEEE International Workshop on Robot and Human Interactive Communication*, pages 319–325, 2001.
- [73] N. Klopčar and J. Lenarčič. Kinematic Model for Determination of Human Arm Reachable Workspace. *Meccanica*, 40:203–219, 2005.
- [74] A. Kron. *Beiträge zur bimanuellen und mehrfingerigen haptischen Informationsvermittlung in Telepräsenzsystemen*. PhD thesis, Technische Universität München, 2004, in german.
- [75] A. Kron and G. Schmidt. Stability and Performance Analysis of Kinesthetic Control Architectures for Bimanual Telepresence Systems. *Journal of Intelligent Robotic Systems*, 46:1–26, May 2006.
- [76] K. J. Kyriakopoulos, J. Van Riper, A. Zink, and H. E. Stephanou. Kinematic Analysis and Position/Force Control of the Anthrobot Dextrous Hand. *IEEE Trans. on Systems, Man and Cybernetics*, 27(1):95–104, February 1997.
- [77] D. Lawrence. Stability and Transparency in Bilateral Teleoperation. *IEEE Trans. on Robotics and Automation*, 9(5):624–637, 1993.
- [78] D. Lawrence and J. Chapel. Performance Trade-Offs for Hand Controller Design. In *Proc. of the IEEE International Conference on Robotics and Automation*, pages 3211–3216, 1994.
- [79] D. A. Lawrence, L. Y. Pao, A. M. Dougherty, M. A. Salada, and Y. Pavlou. Rate-Hardness: A New Performance Metric for Haptic Interfaces. *IEEE Trans. on Robotics and Automation*, 16:357–371, 2000.
- [80] D. Lee, O. Martinez-Palafox, and M.W. Spong. Bilateral Teleoperation of a Wheeled Mobile Robot over Delayed Communication Network. In *Proc. of the IEEE International Conference on Robotics and Automation*, pages 3298 –3303, Orlando, Florida, May 2006.

-
- [81] D. Lee and Spong M.W. Bilateral Teleoperation of Multiple Cooperative Robots with Delayed Communication: Theory. In *Proc. of the IEEE International Conference on Robotics and Automation*, pages 360–365, April 2005.
- [82] D. Lee and M.W. Spong. Passive Bilateral Teleoperation With Constant Time Delay. *IEEE Trans. on Robotics and Automation*, 22(2):269–281, 2006.
- [83] D.J. Lee and P.Y. Li. Passive Bilateral Control and Tool Dynamics Rendering for Nonlinear Mechanical Teleoperators. *IEEE Trans. on Robotics and Automation*, 21(5):936–951, 2001.
- [84] A. Liégeois. Automatic Supervisory Control of the Configuration and Behaviour of Multibody Mechanisms. *IEEE Trans. on Systems, Man and Cybernetics*, 7(12):868–871, 1977.
- [85] F. B. Llewellyn. Some Fundamental Properties of Transmission Systems. In *Proc. of the IRE*, volume 40, pages 271–283, March 1952.
- [86] R. S. Marken. Degrees of Freedom in Behaviour. *Psychological Science*, 2(2):92–100, 1991.
- [87] J. Martin and J. Savall. Mechanisms for Haptic Torque Feedback. In *Proc. of the First Joint Eurohaptics Conference and Symposium on Haptic Interfaces for Virtual Environment and Teleoperator Systems*, pages 611–614, 2005.
- [88] L. E. Masliah and P. Milgram. Measuring the Allocation of Control in a 6 Degree-of-Freedom Docking Experiment. In *Proc. of the Conference on Human Factors in Computing Systems*, pages 25–32, The Hague, Netherlands, April 2000.
- [89] T. Massie and J. Salisbury. The PHANTOM Haptic Interface: A Device for Probing Virtual Objects. In *Proc. of the ASME Winter Annual Meeting: Dynamic Systems and Control Division*, volume 55, pages 295–301, 1994.
- [90] Y. Nakamura. *Advanced Robotics: Redundancy and Optimization*. Addison-Wesley Publishing Company, 1991.
- [91] E. Nash, G. Edwards, J. Thompson, and W. Barfield. A Review of Presence and Performance in Virtual Environments. *International Journal of Human-Computer Interaction*, 12(1):1–41, 2000.
- [92] E. S. Neo, K. Yokoi, S. Kajita, and K. Tanie. Whole-Body Motion Generation Integrating Operator’s Intention and Robot’s Autonomy in Controlling Humanoid Robots. *IEEE Transactions on Robotics*, 23(4):763–775, August 2007.
- [93] G. Niemeyer and J. J. E. Slotine. Telemanipulation with Time Delays. *International Journal of Robotics Research*, 23(9):873–890, 2004.
- [94] N. Nitzsche. *Weiträumige Telepräsenz: Unbeschränkte Fortbewegung und haptische Interaktion*. PhD thesis, Technische Universität München, 2006, *in german*.
- [95] N. Nitzsche, U. Hanebeck, and G. Schmidt. Design Issues of Mobile Haptic Interfaces. *Journal of Robotic Systems*, 20(9):549–556, 2003.

- [96] N. Nitzsche and G. Schmidt. A Mobile Haptic Interface Mastering a Mobile Teleoperator. In *Proc. of the IEEE/RSJ International Conference on Intelligent Robots and Systems*, Sendai, Japan, 2004.
- [97] T. Ortmaier, H. Weiss, and G. Hirzinger. Telepresence and Teleaction in Minimally Invasive Surgery. In *Proc. of the Robotik 2004, VDI-Berichte 1841*. VDI-Verlag, Munich, 2004.
- [98] L. Pao and T.H. Speeter. Transformation of Human Hand Positions for Robotic Hand Control. In *Proc. of the IEEE International Conference on Robotics and Automation*, volume 3, pages 1758–1763, May 1989.
- [99] M. de Pascale, A. Formaglio, and D. Prattichizzo. A Mobile Platform for Haptic Grasping in Large Environments. *Virtual Reality Journal*, 10:11–23, 2006.
- [100] G. Raisbeck. A Definition of Passive Linear Networks in Terms of Time and Energy. *Journal of Applied Physics*, 25:1510–1514, 1954.
- [101] G. Reinhart, S. Clarke, B. Petzold, and J. Schilp. Telepresence as a Solution to Manual Micro-Assembly. *CIRP Annals*, 53(1):21–24, 2004.
- [102] D. Reintsema, K. Landzettel, and G. Hirzinger. DLR’s Advanced Telerobotic Concepts and Experiments for On-Orbit Servicing. In M. Ferre, M. Buss, R. Aracil, C. Melchiorri, and C. Balaguer, editors, *Advances in Telerobotics: Human System Interfaces, Control, and Applications*, pages 324–345. Springer, STAR series, 2007.
- [103] P. Ridao, M. Carreras, E. Hernandez, and N. Palomeras. Underwater Telerobotics for Collaborative Research. In M. Ferre, M. Buss, R. Aracil, C. Melchiorri, and C. Balaguer, editors, *Advances in Telerobotics: Human System Interfaces, Control, and Applications*, pages 347–359. Springer, STAR series, 2007.
- [104] R. N. Rohling and J. M. Hollerbach. Optimized Fingertip Mapping for Teleoperation of Dextrous Robot Hands. In *Proc. of the IEEE International Conference on Robotics and Automation*, volume 3, pages 769–775, May 1993.
- [105] W. Sadowski and K. Stanney. Measuring and Managing Presence in Virtual Environments. In K. Stanney, editor, *Handbook of Virtual Environments*. Lawrence Erlbaum Associates, Inc., 2002.
- [106] J. K. Salisbury and M. T. Mason. *Robot Hands and the Mechanics of Manipulation*. MIT press, Cambridge, 1985.
- [107] T. Schauß. Entwicklung einer beidarmigen mobilen haptischen Schnittstelle. Studienarbeit, Lehrstuhl für Steuerungs und Regelungstechnik, Technische Universität München, 2007, *in german*.
- [108] R. Scheuchenpflug. Measuring Presence in Virtual Environments. In M. Smith, G. Salvendy, and M. Kasdorf, editors, *HCI International 2001*, pages 56–58, 2001.
- [109] A. Schiele and G. Visentin. The ESA Human Arm Exoskeleton for Space Robotics. In *Proc. of the 7th International Symposium on Artificial Intelligence, Robotics and Automation in Space*, Nara, Japan, 2003.

-
- [110] T. Schilling, editor. *Telerobotic Applications*. WILEY Publishers, 1999.
- [111] S. A. Schneider and R. H. Cannon. Object Impedance Control for Cooperative Manipulation: Theory and Experimental Results. *IEEE Trans. on Robotics and Automation*, 8(3):383–394, 1992.
- [112] Schunk. SCHUNK Dextrous Hand (SDH). <http://www.schunk.com>, April 2008.
- [113] M. Schwaiger, T. Thümmel, and H. Ulbrich. A 2D-Motion Platform: The Cybercarpet. In *Proc. of the World Haptics Conference*, pages 415–420, Tsukuba, Japan, 2007.
- [114] J. W. Senders, J. M. Christensen, and R. Sabe. Comparison of Single Operator’s Performance with Team Performance in a Tracking Task. Technical Report TN-55-362, Aero Medical Laboratory, Wright Air Development Center, 1955.
- [115] P. Setoodeh, S. Sirouspour, and A. Shahdi. Discrete-Time Multi-Model Control for Cooperative Teleoperation under Time Delay. In *IEEE International Conf. on Robotics and Automation*, pages 2921–2926, Orlando, Florida, May 2006.
- [116] T. B. Sheridan. *Telerobotics, Automation, and Human Supervisory Control*. The MIT Press, 1992.
- [117] S. Sirouspour. Modeling and Control of Cooperative Teleoperation Systems. *IEEE Trans. on Robotics*, 21(6):1220–1225, 2005.
- [118] S. Sirouspour. Robust Control Design for Cooperative Teleoperation. In *Proc. of the IEEE International Conference on Robotics and Automation*, pages 1145–1150, 2005.
- [119] S. Sirouspour and P. Setoodeh. Multi-operator/Multi-robot Teleoperation: An Adaptive Nonlinear Control Approach. In *Proc. of the IEEE/RSJ International Conference on Intelligent Robots and Systems*, pages 2506–2511, 2005.
- [120] B. Stanczyk. *Development and Control of an Anthropomorphic Teleoperator*. PhD thesis, Technische Universität München, Lehrstuhl für Steuerungs- und Regelungstechnik, 2006.
- [121] B. Stanczyk and M. Buss. Development of a Telerobotic System for Exploration of Hazardous Environments. In *Proc. of the IEEE/RSJ International Conference on Intelligent Robots and Systems*, pages 2532–2537, Sendai, Japan, 2004.
- [122] T. Suzuki, T. Sekine, T. Fujii, H. Asama, and I. Endo. Cooperative Formation among Multiple Mobile Robot Teleoperation in Inspection Task. In *Proc. of the IEEE Conference on Decision and Control*, pages 358–363, 2000.
- [123] S. Tachi, K. Komoriya, K. Sawada, T. Nishiyama, T. Itoko, M. Kobayashi, and K. Inoue. Teleexistence Cockpit for Humanoid Robot Control. *Advanced Robotics*, 17(3):199–217, 2003.

- [124] M. Tomasello, M. Carpenter, J. Call, T. Behne, and H. Moll. Understanding and Sharing Intentions: The Origins of Cultural Cognition. *Behavioral and brain sciences*, 28:675–735, 2005.
- [125] M. T. Turvey, H. L. Fitch, and B. Tuller. The Bernstein Perspective I. The Problems of Degrees of Freedom and Context-Conditioned Variability. In J. A. S. Kelso, editor, *Human Motor Behavior. An Introduction.*, pages 239–252. NJ: Lawrence Erlbaum Associates, 1982.
- [126] C. W. Tyler. Sensory Processing of Binocular Disparity. In C. M. Schorr and K. J. Cioffreda, editors, *Vergence Eye Movements: Basic and Clinical Aspects*. Boston: Butterworths, 1983.
- [127] M. Ueberle. *Design, Control, and Evaluation of a Family of Kinesthetic Haptic Interfaces*. PhD thesis, Technische Universität München, Lehrstuhl für Steuerungs- und Regelungstechnik, 2006.
- [128] M. Ueberle and M. Buss. Control of Kinesthetic Haptic Interfaces. In *Proc. of the IEEE/RSJ International Conference on Intelligent Robots and Systems, Workshop on Touch and Haptics*, 2004.
- [129] M. Ueberle, N. Mock, and M. Buss. Design, Control, and Evaluation of a Hyper-Redundant Haptic Interface. In M. Ferre, M. Buss, R. Aracil, C. Melchiorri, and C. Balaguer, editors, *Advances in Telerobotics: Human System Interfaces, Control, and Applications*. Springer, STAR series, 2007.
- [130] U. Unterhinninghofen, F. K. B. Freyberger, and M. Buss. Study on Computer Assistance for Telepresent Reaching Movements. In *Proc. of the EuroHaptics*, Madrid, Spain, 2008.
- [131] R. Q. Van der Linde, P. Lammertse, E. Frederiksen, and B. Ruiters. The HapticMaster, a New High-Performance Haptic Interface. In *Proc. of the EuroHaptics*, pages 1–5, 2002.
- [132] J. Wang, S. Dodds, and W. Bailey. Coordinated Control of Multiple Robotic Manipulators Handling a Common Object – Theory and Experiments. *IEE Proceedings, Control Theory and Applications*, 144(1):73–84, 1997.
- [133] X. G. Wang, M. Moallem, and R. V. Patel. An Internet-Based Distributed Multiple-Telerobot System. *IEEE Trans. on Systems, Man, and Cybernetics - Part A: Systems and Humans*, 33(5):627–633, 2003.
- [134] C. Ware and J. Rose. Rotating Virtual Objects with Real Handles. *Computer-Human Interaction*, 6(2):162–180, 1999.
- [135] J. T. Wen and K. Kreutz-Delgado. Motion and Force Control of Multiple Robotic Manipulators. *Automatica*, 28(4):729–743, 1992.
- [136] B. G. Witmer and M. J. Singer. Measuring Presence in Virtual Environments: A Presence Questionnaire. *Presence*, 7(3):225–240, 1998.

-
- [137] T. Wojtara and K. Nonami. Hand Posture Detection by Neural Network and Grasp Mapping for a Master Slave Hand System. In *Proc. of the IEEE/RSJ International Conference on Intelligent Robots and Systems*, volume 1, pages 866–871, Sept., Oct. 2004.
- [138] A. K. Wright and M. M. Stanisic. Kinematic Mapping between the EXOS Hand-master Exoskeleton and the Utah-MIT Dextrous Hand. In *Proc. of the IEEE International Conference on Systems Engineering*, pages 809–811, 1990.
- [139] Y. Yokokohji and T. Yoshikawa. Bilateral Control of Master-Slave Manipulators for Ideal Kinesthetic Coupling-Formulation and Experiment. *IEEE Trans. on Robotics and Automation*, 10(5):605 – 620, 1994.
- [140] W. K. Yoon, Y. Tsumaki, and M. Uchiyama. An Experimental Teleoperation System for Dual-Arm Space Robotics. *Journal of Robotics and Mechatronics*, 12(4):378–383, 2000.
- [141] T. Yoshikawa. *Foundations of Robotics: Analysis and Control*. MIT Press, Cambridge, 1990.
- [142] T. Yoshikawa. Translational and Rotational Manipulability of Robotic Manipulators. In *Proc. of the International Conference on Industrial Electronics, Control and Instrumentation*, 1991.
- [143] S. Zhai and P. Milgram. Quantifying Coordination in Multiple DOF Movement and its Application to Evaluating 6 DOF Input Devices. In *Proc. of the Conference on Human Factors in Computing Systems*, pages 320–327, Los Angeles, CA, April 1998.
- [144] S. Zhai and J. W. Senders. Investigating Coordination in Multidegree of Freedom Control I: Time-on-target Analysis of 6DOF Tracking. In *Proc. of the Human Factors and Ergonomics Society 41st Annual Meeting*, pages 1249–1254, Santa Monica, CA, September 1997.
- [145] S. Zhai and J. W. Senders. Investigating Coordination in Multidegree of Freedom Control II: Correlation Analysis in 6DOF Tracking. In *Proc. of the Human Factors and Ergonomics Society 41st Annual Meeting*, pages 1254–1258, Santa Monica, CA, September 1997.
- [146] W. H. Zhu and S. Salcudean. Stability Guaranteed Teleoperation: An Adaptive Motion/Force Control Approach. *IEEE Trans. on Automatic Control*, 45(11):1951–1969, 2000.

Own related publications and reports

- [147] M. Buss, M. Kuschel, K. K. Lee, A. Peer, B. Stanczyk, and U. Unterhinninghofen. High Fidelity Telepresence Systems: Design, Control, and Evaluation. In *Proc. of the Joint International COE/HAM SFB-453 Workshop on Human Adaptive Mechatronics and High-Fidelity Telepresence*, pages 53–58, Tokyo, Japan, 2006.

- [148] M. Buss, K. K. Lee, N. Nitzsche, A. Peer, B. Stanczyk, and U. Unterhinninghofen. Advanced Telerobotics: Dual-Handed and Mobile Remote Manipulation. In M. Ferre, M. Buss, R. Aracil, C. Melchiorri, and C. Balaguer, editors, *Advances in Telerobotics: Human System Interfaces, Control, and Applications*, pages 471–497. Springer, STAR series, 2007.
- [149] Y. Komoguchi, A. Peer, and M. Buss. Control and Performance Evaluation of a New Redundant Haptic Interface. In *SICE Annual Conference*, pages 2671–2676, Kagawa University, Japan, 2007.
- [150] Y. Komoguchi, K. Yano, A. Peer, and M. Buss. Redundancy Resolution of a 7 DOF Haptic Interface Considering Collision and Singularity Avoidance. In *Proc. of the IEEE International Conference on Intelligent Robots and Systems*, 2008.
- [151] A. Peer. Classification and Control of Collaborative Telemanipulation Systems. Technical Report TR-LSR-2005-11-1, Institute of Automatic Control Engineering, Technische Universität München, 2005.
- [152] A. Peer. A New Haptic Interface for Bimanual Manipulations - Design, Control, and Evaluation. Technical Report TR-LSR-2007-06-2, Institute of Automatic Control Engineering, Technische Universität München, 2007.
- [153] A. Peer and M. Buss. A New Admittance Type Haptic Interface for Bimanual Manipulations. *IEEE/ASME Transactions on Mechatronics*, 13(4):416–428, 2008.
- [154] A. Peer and M. Buss. Robust Stability Analysis of a Bilateral Teleoperation System Using the Parameter Space Approach. In *Proc. of the IEEE/RSJ International Conference on Intelligent Robots and Systems*, 2008.
- [155] A. Peer and M. Buss. Robust Stability Analysis of Bilateral Teleoperation Architectures for Admittance-Type Devices. In *Proc. of the IEEE International Conference on Robotics and Automation, Workshop New Vistas and Challenges in Telerobotics*, 2008.
- [156] A. Peer and M. Buss. Robust Stability Analysis of Bilateral Teleoperation Systems Using Admittance-Type Devices. In *Proc. of the International Conference on Instrumentation, Control, and Information Technology*, 2008.
- [157] A. Peer, S. Einenkel, and M. Buss. Multi-fingered Telemanipulation – Mapping of a Human Hand to a Three Finger Gripper. In *Proc. of the 17th International Symposium on Robot and Human Interactive Communication*, pages 465–470, 2008.
- [158] A. Peer, S. Hirche, C. Weber, I. Krause, M. Buss, S. Miossec, P. Evrard, O. Stasse, E. S. Neo, A. Kheddar, and K. Yokoi. Intercontinental Cooperative Telemanipulation between Germany and Japan. In *Proc. of the IEEE/RSJ International Conference on Intelligent Robots and Systems*, 2008.
- [159] A. Peer, Y. Komoguchi, and M. Buss. Towards a Mobile Haptic Interface for Bimanual Manipulations. In *Proc. of the IEEE/RSJ International Conference on Intelligent Robots and Systems*, pages 384–391, 2007.

-
- [160] A. Peer, T. Schauß, U. Unterhinninghofen, and M. Buss. A Mobile Haptic Interface for Bimanual Manipulations in Extended Remote/Virtual Environments. In *Robotics Research Trends*. Nova Publishers, 2008.
- [161] A. Peer, B. Stanczyk, and M. Buss. Haptic Telemanipulation with Dissimilar Kinematics. In *Proc. of the IEEE/RSJ International Conference on Intelligent Robots and Systems*, pages 3493 – 3498, Edmonton, Canada, 2005.
- [162] A. Peer, U. Unterhinninghofen, and M. Buss. Tele-Assembly in Wide Remote Environments. In *Proc. of the 2nd International Workshop on Human-Centered Robotic Systems*, Munich, Germany, 2006.
- [163] A. Peer, U. Unterhinninghofen, and M. Buss. Tele-Assembly in Wide Remote Environments. *Robotics Today*, 20(4), 2008.
- [164] A. Peer, U. Unterhinninghofen, K.K. Lee, B. Stanczyk, and M. Buss. Haptic Telemanipulation in Extensive Remote Environments. In *Proc. of the Joint International COE/HAM SFB-453 Workshop on Human Adaptive Mechatronics and High-Fidelity Telepresence*, pages 57–62, Tokyo, Japan, 2005.
- [165] H. Pongrac, A. Peer, B. Färber, and M. Buss. Effects of Varied Human Movement Control on Task Performance and Feeling of Telepresence. In *Proc. of the EuroHaptics, LNCS 5024*, pages 755–765, Heidelberg, 2008. Springer.
- [166] A. Rafael, M. Buss, M. Ferre, S. Cobos, S. Hirche, M. Kuschel, and A. Peer. The Human Role in Telerobotics. In M. Ferre, M. Buss, R. Aracil, C. Melchiorri, and C. Balaguer, editors, *Advances in Telerobotics: Human System Interfaces, Control, and Applications*, pages 11–24. Springer, STAR series, 2007.
- [167] B. Stanczyk, A. Peer, and M. Buss. Development of a High Performance Haptic Telemanipulation System with Dissimilar Kinematics. *Advanced Robotics*, 20(11):1303–1320, 2006.
- [168] M. Ueberle, H. Esen, A. Peer, U. Unterhinninghofen, and M. Buss. Haptic Feedback Systems for Virtual Reality and Telepresence Applications. In *Proc. of the Harmonic Drive International Symposium*, pages 99–107, Matsumoto, Nagano, Japan, 2006.
- [169] M. Ueberle, N. Mock, A. Peer, C. Michas, and M. Buss. Design and Control Concepts of a Hyper Redundant Haptic Interface for Interaction with Virtual Environments. In *Proc. of the IEEE/RSJ International Conference on Intelligent Robots and Systems, Workshop on Touch and Haptics*, Sendai, Japan, 2004.